Dental microwear textures differ in pigs with overall similar diets but fed with different seeds

Margot Louail, Stéphane Ferchaud, Antoine Souron, Axelle E.C. Walker, Gildas Merceron

Dental microwear textures differ in pigs with overall similar diets but fed with different seeds

Margot Louail[1*], Stéphane Ferchaud[2], Antoine Souron[3], Axelle E.C. Walker[1], Gildas Merceron[1]

1. PALEVOPRIM, UMR 7262 CNRS and University of Poitiers, 86073 Poitiers Cedex 9, France

2. GenESI, UE 1372 INRAE, 86480 Rouillé, France

3. PACEA, UMR 5199 CNRS and University of Bordeaux, 33615 Pessac Cedex, France

*Corresponding author

Email address:

*margot.louail@univ-poitiers.fr

stephane.ferchaud@inrae.fr

antoine.souron@u-bordeaux.fr

axelle.walker@univ-poitiers.fr

gildas.merceron@univ-poitiers.fr

16 Abstract

17 The thick-enameled, bunodont dentition shared by most early hominins has traditionally
18 been interpreted as reflecting durophagy, especially in the robust genus *Paranthropus*.
19 However, subsequent works on dental microwear textures (DMT) and biogeochemical
20 compositions have challenged this hypothesis. Some authors argued that their robust
21 morphology might have been driven by the consumption of mechanically challenging
22 resources during periods of food scarcity. An experimental baseline using a model taxon with
23 bunodont, thick-enameled cheek teeth, could help better interpret DMT and test hypotheses
24 regarding the consumption of mechanically challenging foods that could be fallback foods.
25 Besides, earlier studies have shown that DMT can track subtle dietary variations in extant taxa.
26 This study aims at testing the hypothesis that the consumption of various seeds has an impact
27 on DMT of bunodont mammals despite similar overall diets. Trials were conducted on four
28 groups of domestic pigs (*Sus scrofa*) all fed on mixed cereal and soy flours: the control group
29 received only flours (n = 12), and the three others were supplemented with either 20 % corn
30 kernels (n = 6), 30 % barley seeds (n = 5), or 10 hazelnuts in shell per day (n = 6). We studied
31 phases I and II facets on first molars and on fourth deciduous premolars, and applied a
32 subsampling surface strategy to identify discriminative parameters among dietary groups.
33 Principal Component Analyses show that DMT differ between pigs fed on different types of
34 seeds. Our results also demonstrate that combining both crushing and shearing facets into
35 analyses improves dietary discriminations. This study shows that variables that contribute most
36 to dietary discriminations as selected from the subsampling strategy are mainly height
37 parameters. These results thus support the idea that the consumption of seeds has an impact
38 on the relief of surface textures.

39

40 Keywords: suids, bunodont, omnivorous, feeding experiments

1. Introduction

Ecological constraints associated with feeding and foraging can exert key selective pressures among animals, leading to physiological, morphological, and/or behavioral adaptations (e.g., Bels and Herrel, 2019). Thus, investigating the diets of extinct species contributes to a better understanding of how their morphological diversity can be related to feeding adaptive traits (Codron et al., 2008; Cerling et al., 2011; Winkler et al., 2013). Dietary inferences have primarily been based on functional interpretations of craniomandibular and dental morphologies (Anthony and Kay, 1993; Ungar, 2002; Damuth and Janis, 2011). However, if trophic morphology may help us to identify gross dietary habits, it tells us more about what an extinct species was capable to eat than the precise composition of its diet (Lister, 2013; Tütken et al., 2013; Gailer et al., 2016; van Casteren et al., 2019). Dietary habits and feeding adaptations are not equivalent, and it has been shown that some species do not actually, or very rarely, eat items to which their trophic morphology seems to be adapted. Some apparently specialized feeders have in fact a more diversified diet than expected given their morphology. This phenomenon, known as “Liem’s Paradox”, was first demonstrated (Liem, 1980) for cichlid fish. It has been proposed as well among other taxa, notably primates (Remis, 2002; Lambert et al., 2004; Norconk and Veres, 2011; Sayers, 2013; Grine and Daegling, 2017). A mismatch between craniomandibular and dental morphology and dietary habits has also been described among extant and extinct suids (Harris and Cerling, 2002; Souron, 2017; Lazagabaster, 2019). To explain some apparent discrepancies between dental morphologies and diets, notably in some primate species, resources now commonly referred as “fallback foods” (FBFs) have received considerable attention (Robinson and Wilson, 1998; Yamashita, 1998; Lambert et al., 2004; Marshall and Wrangham, 2007). FBFs are defined as resources that are particularly consumed during periods of food scarcity, when preferred items are scarce or unavailable (Marshall et al., 2009). Such items, generally mechanically challenging, have been recognized as potential selective drivers of trophic morphologies or behaviors, notably among primates (MacArthur and Pianka, 1966; Robinson and Wilson, 1998; Potts, 2004). They

received much more attention in recent years (Altmann, 2009; Constantino and Wright, 2009; Constantino et al., 2009; Lucas et al., 2009; Marshall et al., 2009; Wrangham et al., 2009).

Numerous studies advocated for the importance of FBFs as key selective agents in the evolution of early hominins, particularly to understand the discrepancy between dietary habits inferred from dental microwear and dental morphologies (Laden and Wrangham, 2005; Scott et al., 2005; Dominy et al., 2008; Ungar et al., 2008; Constantino et al., 2009; Strait et al., 2009). The thick-enameled, bunodont cheek teeth shared by most early hominins has traditionally been considered as reflecting durophagy, especially in the robust genus *Paranthropus* whose diet was thought to be mainly composed of hard foods such as nuts and seeds (Robinson, 1954). This interpretation based on craniomandibular and dental morphology have led to the vision that *Paranthropus* were specialized feeders. However, later works focusing on enamel biogeochemical compositions and dental microwear textures have challenged this hypothesis. Notably, they show contrasting patterns between eastern and southern African *Paranthropus* and overlapping diets between some hominins (e.g., Ungar and Sponheimer, 2011; Martin et al., 2020). Some authors have suggested robust morphologies might have been driven by the consumption of mechanically challenging foods during “fallback” episodes of resource stress (e.g., Ungar and Daegling, 2013). However, without an experimental baseline using model taxa with similar bunodont, thick-enameled dentition, it has proven difficult to interpret DMT of early hominins and to test hypotheses regarding their fallback strategies. Moreover, such an experimental baseline would also be helpful to test hypotheses regarding the relationship between craniomandibular and dental morphologies and the consumption of FBFs among suids with seasonal/opportunistic feeding behaviors (Lazagabaster, 2019).

Besides enamel biogeochemical composition, dental microwear texture analysis (DMTA) is one of the few proxies that inform us about what was actually eaten by an extinct species. Indeed, microscopic marks on enamel surfaces are highly dependent on the mechanical properties and inner biosilica content of the masticated foods, although exogenous

abrasive particles may also contribute to toothwear (Teaford and Oyen, 1989; Lucas, 2004; Hua et al., 2015; Xia et al., 2015; Daegling et al., 2016; Merceron et al., 2016; Teaford et al., 2017; Winkler et al., 2020; see also Lucas et al., 2013; van Casteren et al., 2018). Microwear textures have a fast turnover rate so that DMTA records the diet of an animal a few weeks or months before death (Teaford and Oyen, 1989; Romero et al., 2012; Winkler et al., this volume). DMTA has proved its efficiency in assessing the diets of extant primate species (Scott et al., 2006, 2012; Krueger et al., 2008; Percher et al., 2017) and has been widely used for paleodietary reconstructions (Scott et al., 2005; Merceron et al., 2006, 2009, this volume; Ungar et al., 2008; Martin et al., 2018; Peterson et al., 2018). DMTA can then provide insights into ecological niche partitioning and dietary overlap between sympatric species, thus contributing to a better understanding of inter- and intraspecific competition (Teaford and Runestad, 1992; Ramdarshan et al., 2011; Merceron et al., 2014; Hofman-Kamińska et al., 2018; Martin et al., 2018; Percher et al., 2017; Aiba et al., 2019). Moreover, studies have shown that DMTA can reflect subtle dietary variations within species or populations, such as seasonal, social or sexual differences (Teaford and Robinson, 1989; Merceron et al., 2010; Berlioz et al., 2017; Percher et al., 2017). However, the mechanisms of dental microwear formation are still highly debated (Lucas et al., 2013, 2014; Xia et al., 2015; van Casteren et al., 2018, 2020; Teaford et al., 2020; Winkler et al., 2020) and little is known about whether microwear patterns can reflect small proportions of foods such as FBFs in an individual's diet. These limitations are crucial elements that need to be investigated to better interpret microwear textures of extinct species, notably among early hominins. Controlled-food experiments are assumed to reduce the dietary variability and thus enable targeting the effect of specific resources on dental microwear textures. In recent years, there have been an increasing number of studies with controlled feeding experiments (Teaford and Oyen, 1989; Hoffman et al., 2015; Calandra et al., 2016; Merceron et al., 2016; Ramdarshan et al., 2016, 2017; Ackermans et al., 2018, 2020; Zykov et al., 2018; Martin et al., 2019, this volume; Winkler et al., 2019, this volume; Schulz-Kornas et al., 2020). Most studies focused on herbivorous mammals and there is no work focusing on DMT variations of controlled-fed omnivorous mammals with bunodont, thick-

123 enameled dentition and similar overall diets (but see Teaford and Oyen, 1989; Teaford et al.,
124 2017, this volume). Few works analyzed DMT variations among extant and extinct suids that
125 exhibit this morphology, but they all point to the need of further studies for a better
126 understanding of the relationship between dental microwear patterns and feeding behaviors
127 (Ward and Mainland, 1999; Souron et al., 2015; Ungar et al., 2017; Yamada et al., 2018;
128 Lazagabaster, 2019). Thus, such a controlled-feeding study is particularly interesting for
129 helping the interpretation of DMT patterns among extant and extinct suids, as well as among
130 early hominins and for a better understanding of niche partitioning between them.

131 In the present study, we investigate DMT variations on 29 domestic pigs (*Sus scrofa*),
132 issued from controlled feeding experiments. We aim to test the hypothesis that the
133 consumption of various types of seeds leads to significant differences of DMT despite similar
134 overall diets. Recent in vivo and in vitro experimental studies have shown contrasting results
135 about whether the consumption of hard seeds impacts dental microwear but none focused on
136 standard measures of overall microwear textures (Teaford et al., 2020; van Casteren et al.,
137 2020). Because high texture complexity (*Asfc*) has been related to the consumption of hard
138 and/or brittle items, such as seeds, nuts, woody browse, hard fruits or bones (Scott et al., 2006,
139 2012; Schubert et al., 2010; Daegling et al., 2011), we expect that pigs fed on the hardest
140 seeds would show more complex textures than pigs fed on softer seeds, and even more than
141 pigs fed only on flours. Besides, because pigs had a large part of their diet in common, and
142 considering previous studies by Francisco et al. (2018a, 2018b), we expect that using the
143 whole set of discriminative texture parameters selected from their surface sampling strategy
144 will highlight dietary discriminations depending on the type of seeds consumed. Moreover, we
145 hypothesize that combining both phase I (shearing) and phase II (crushing) facets will improve
146 these discriminations.

147

148 **2. Material and methods**

149 **2.1. Controlled-food trials**

150 The controlled-food experiments were carried out at the experimental unit UE1372
151 GenESI (Pigs innovative breeding experimental Facility, Vienne, France; DOI:
152 10.15454/1.5572415481185847E12) of the INRAE (*Institut national de recherche pour*
153 *l'agriculture, l'alimentation et l'environnement*). Trials were conducted on domestic pigs (*Sus*
154 *scrofa*; large-white cross breed Piétrain) and were designed by G.M. and S.F (agreement
155 number: APAFiS 155/2015012117162897, *Ministère de l'Enseignement Supérieur et de la*
156 *Recherche*). We considered a total of 29 juvenile pigs fed with four different diets *ad libitum*
157 (Figure 1). Pigs were weaned about 28 days old and were raised on concrete floors. Each
158 animal had access to an individual trough. They were kept together in groups of five to six pigs
159 according to their dedicated diet. Before they were given their dedicated diets, they were all
160 fed daily with a dry base diet (manufactured by ALICOOP) composed of 90 % of wheat
161 (*Triticum* ssp.*)*, barley (*Hordeum vulgare*), and triticale (x *Triticosecale*) flour, and 10 % of
162 soybean (*Glycine max*) flour. This period of homogenization of surface textures lasted at least
163 48 days. The control group (n = 12) was then fed exclusively with the same base diet described
164 above for at least another 30 days before death. This base diet, composed of ground cereal
165 and soy seeds (Table 1), is expected to have little impact on dental microwear textures and
166 represents a baseline for comparing dietary signals among the experimental groups. However,
167 these base flours contain the outer parts of the grains and therefore imply higher abrasivity
168 than finer flours. The three other groups then received seeds of different size and hardness
169 (Table 2) in addition to the base diet. A 4-day period of adaptation to the new diet (with a
170 progressive intake of seeds) was carried out on these three groups just before the dietary
171 switch. The corn group (n = 6) was fed with 60 % of the base diet and 20 % of corn (*Zea mays*)
172 flour, supplemented with 20 % (as dry matter weight) of corn kernels. The barley group (n = 5)
173 was fed with 30 % of barley seeds and 70 % of the base diet. These two groups of pigs received
174 their dedicated diet for at least another 95 days before death. The hazelnut group (n = 6) was
175 fed with the same amount of flours than the control group and received 10 hazelnuts in shell

(*Corylus avellana*; endosperm and shell used but leafy involucre removed, Figure 1) per pig each day for another 30 days, during the month before slaughter. Due to a lack of homogeneity in hardness measurements in literature, we considered the mean force required for cracking the seed as an indicator for seed hardness (rupture force decreasing from hazelnuts to barley seeds; Table 2). Indeed, hardness is frequently defined as the resistance of a surface to deforming under indentation, and is usually measured as the ratio of rupture force to indented area (Lucas, 2004); rupture force thus helps estimate the hardness of the seeds. Each flour (including the base diet) was sieved through mesh of 1.25 mm and 0.5 mm diameter. The wheat, barley and triticale flour is composed of approximately 25 % particles above 1.25 mm diameter and 35 % below 0.5 mm. The soybean flour is composed of approximately 60 % particles above 1.25 mm diameter and less than 10 % below 0.5 mm (Table 2). Consequently, because the base diet is composed of an important amount of particles above 1.25 mm, it would be inapproriate to consider the pigs fed only on flours as a model for soft-food eaters. The corn flour, only given to the corn group, is composed of less than 20 % particles above 1.25 mm diameter and 43 % below 0.5 mm (Table 2). Each group was approximately sex-balanced (Table S1). None of the pigs lost weight during the experiments. As planned by the experimental unit, pigs were slaughtered from six and a half months to nine and a half months old when they reached their target weight (about 150–200 kg; females slaughtered a month after males) and were all sold for meat (Figure 1; see Table S1 for details). Pig skulls were then boiled for 4 hours in water to remove the flesh, and dried in an oven for 24 hours at 40 °C.

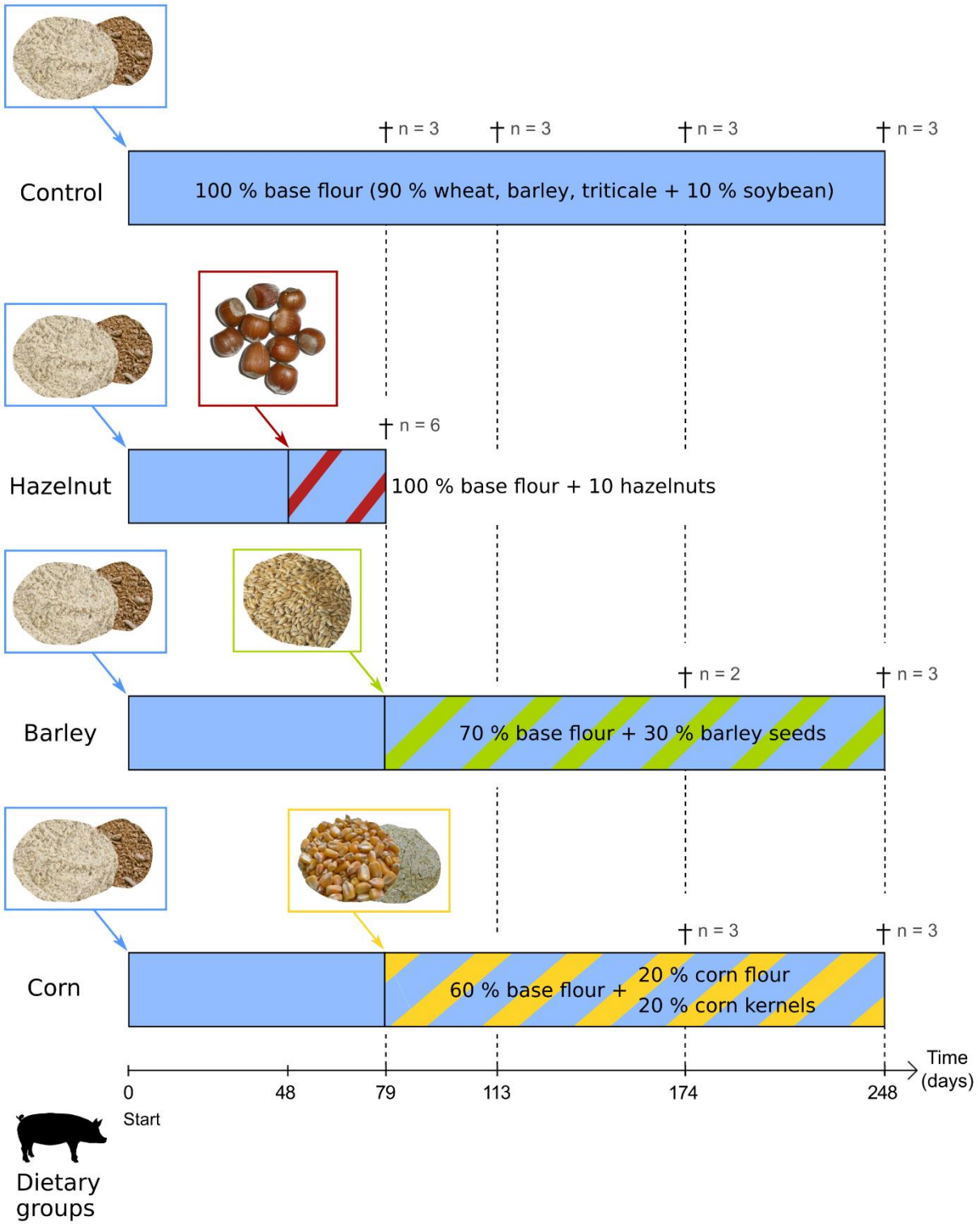

Figure 1. Graphical representation of the controlled-feeding experimental design conducted on domestic pigs (*Sus scrofa*). Food items given to pigs are represented in blue (base diet: 90 % wheat, barley and triticale flour + 10 % soybean flour), red and blue (100 % base diet + 10 hazelnuts in shell per day), green and blue (70 % base diet + 30 % barley seeds), and yellow and blue (60 % base diet + 20 % corn flour + 20 % corn kernels). Period of homogenization of surface textures lasted at least 48 days. A 4-day period of adaptation to the new diet (not

represented on the figure) was carried out just before the dietary switch. Each time point specified by † indicate feeding duration before slaughter (and number of pigs slaughtered).

Table 1. Particle size distribution within the flours given to pigs. The base diet given to all dietary groups is composed of 90 % wheat, barley, and triticale flour and 10 % of soybean flour. The corn flour is only given to the corn group (20 % of the diet).

Flour	Total sieved weight	< 0.5 mm	0.5 mm – 1.25 mm	> 1.25 mm
Wheat, barley, triticale (g)	1024	383	391	250
Wheat, barley, triticale (%)	**100**	**37.4**	**38.2**	**24.4**
Soybean (g)	840	75	255	510
Soybean (%)	**100**	**8.9**	**30.4**	**60.7**
Corn (g)	955	411	376	168
Corn (%)	**100**	**43**	**39.4**	**17.6**

Table 2. Summary statistics (mean and standard deviation SD) for dimensions (length of major and minor axes), density and hardness index of each seed type. Dimensions are averaged from 30 measured seeds. Densities are estimated from weights of 30 seeds for corn kernels and hazelnuts, and from number of seeds in 20 g for barley. Mean rupture forces are averaged from two studies for each type of seeds: hazelnut (Ercisli et al., 2011; Delprete and Sesana, 2014), corn (Tran et al., 1981; Kalkan et al., 2011), and barley (Markowski et al., 2010; Nouri Jangi et al., 2011).

Seed	Major axis (mm)		Minor axis (mm)		Density (seeds/kg)	Rupture force (N)
	Mean	SD	Mean	SD		
Barley	8.93	0.89	3.64	0.31	22,500	140.51
Corn	12.75	0.91	8.18	0.53	3,333	164.42
Hazelnut	20.56	1.51	19.22	0.72	375	331.26

2.2. Molding, scanning, and processing of the surfaces

This study focused on lower and upper first molars (Figure 2) because molars are the most studied teeth when analyzing dental microwear in paleodietary investigations. We considered the first ones as the second molars were not fully erupted by the end of the experiments. None of the molars showed dentin exposure, or only slightly on some buccal cusp apices, corresponding to early stages of wear (stages b-c following Rolett and Chiu, 1994). We also analyzed deciduous upper fourth premolars (Figure 2) because they are more

worn than molars and are thus expected to be more functional, and consequently to carry a more pronounced dietary signal than molars. Moreover, deciduous fourth premolars are molariform (see Figure 2) and display the same wear pattern, including phase I and phase II dental facets. All crushing and shearing facets were visible on premolars, islets of dentin were visible and wear facets on mesial cusps tended to coalesce (stages d-e following Rolett and Chiu, 1994). We did not analyze lower fourth deciduous premolars because they are heavily worn. Each tooth surface was cleaned with cotton swabs soaked with a 3 % bleach solution (NaOCl) to remove organic matter, dust, and dirt, and then generously rinsed with distilled water. Once dry, occlusal surfaces were molded with polyvinylsiloxane (Regular Body President, ref. 6015 - ISO 4823, medium consistency, polyvinylsiloxane addition-type, Coltene Whaledent). We studied both one shearing (phase I) and one crushing (phase II) facet of the same tooth (Figure 2). Each facet was carefully cut on the silicon impression (negative replica) and scanned as flat as possible using “TRIDENT”, a white-light confocal profilometer Leica DCM8 with a 100x objective housed at the PALEVOPRIM lab, CNRS and University of Poitiers, France (Numerical aperture = 0.90; Working distance = 0.9 mm; Leica Microsystems). Each scanned surface was pre-processed using LeicaMap v8.0 (Leica Microsystems; MountainsMap, Digital Surf). Surfaces were inverted along the z-axis and non-measured points (< 3 %) were filled with a smooth shape (Laplacian filter) calculated from neighboring points. A morphological filter was applied to remove artifacts such as aberrant peaks (Merceron et al., 2016) and surfaces were then leveled. A 200 × 200 µm (1551 × 1551 pixels) leveled area was automatically generated at the center of each surface. In case of adhering dirt particles, the extracted area was shifted aside to get the particles out of the field of selection. In the worst case, the particles were manually erased using a user-defined contour on few scans and replaced with a smooth shape calculated from neighboring points. If adhering dirt particles exceed 10 µm, the specimen was cleaned and scanned again until there was no dirt on the surface.

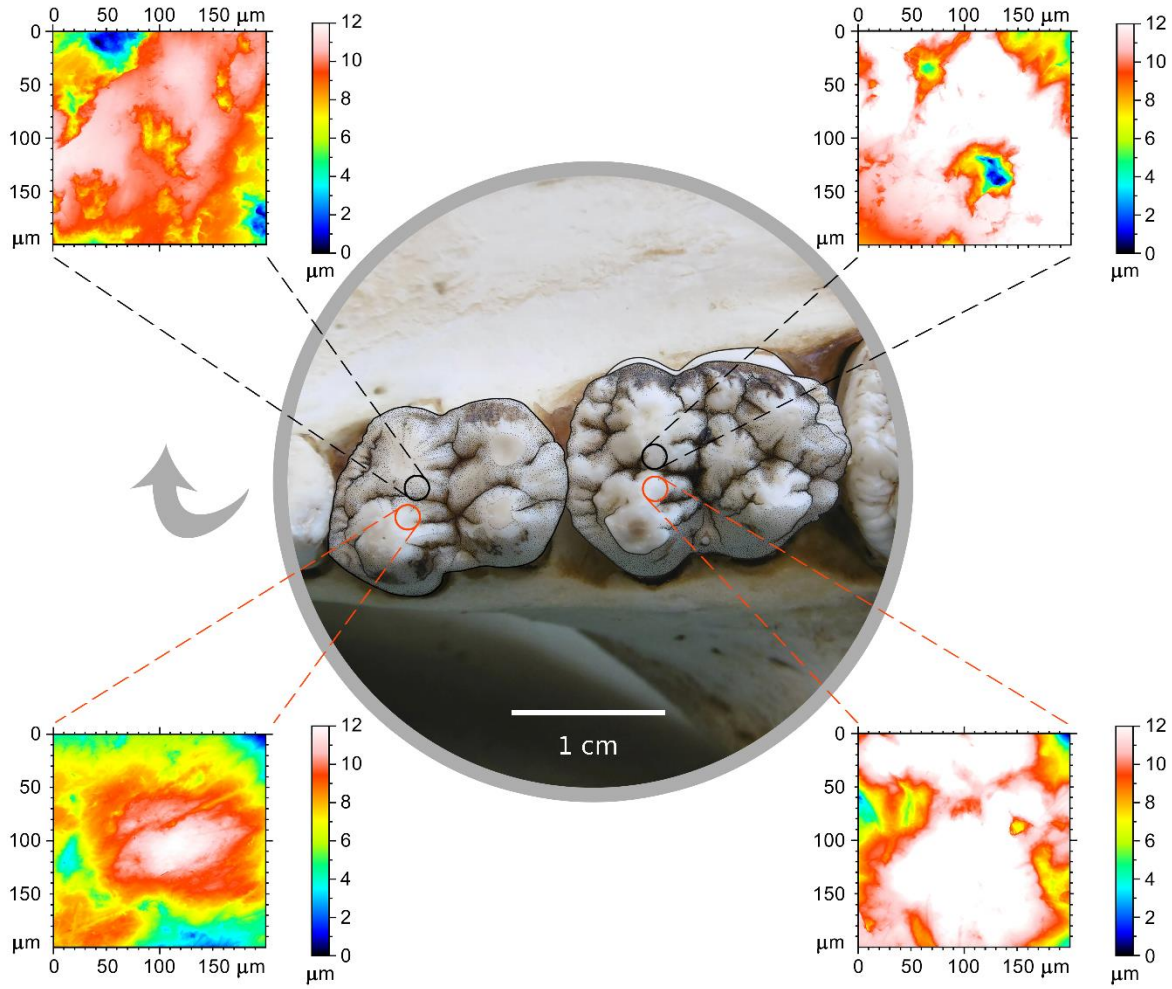

Figure 2. Exemplary occlusal views of right upper first molar (right) and fourth deciduous premolar (left) and topography (false color elevation map) of one individual for each scanned crushing and shearing facet. Localizations of one shearing and one crushing facet are depicted in red and black circles, respectively. The arrow is oriented mesio-lingually.

2.3. Acquisition of textural parameters

We generated two sets of data for each scanned surface: 1) Scale-Sensitive Fractal Analysis parameters (SSFA; Scott et al., 2006); 2) parameters obtained using a statistical routine introduced by Francisco et al. (2018a, 2018b), including most parameters (some modified) from the international standard ISO 25178. Prior to the calculation of SSFA-parameters, a second-order least square polynomial surface (PS2) was subtracted from each surface to remove the concavity of dental facets in order to better visualize the relief due to microwear. Parameters obtained with the statistical routine are measured on surfaces

subtracted from an eighth-order least square polynomial surface (PS8) because it enhances roughness clarity (Francisco et al., 2018b).

1) SSFA-parameters were calculated using LeicaMap v. 8.0. We considered four texture variables for this study: Area-scale fractal complexity (*Asfc*), exact proportion of Length-scale anisotropy of relief (*epLsar (Sfrax)* in LeicaMap v8.0), Scale of maximum fractal complexity (*Smfc*), Heterogeneity of Area-scale fractal complexity (*HAsfc*, calculated through 36 cells). Complexity (*Asfc*) measures the surface roughness at a given scale. Anisotropy (*epLsar*) quantifies the orientation concentration of surface roughness. *Smfc* estimates the scale at which maximal complexity is calculated. *HAsfc* measures the variation of complexity of subsampled parts of the surface (6 × 6 blocks in this study). Detailed descriptions of these parameters can be found in Scott et al. (2006).

2) The sampling method described by Francisco et al. (2018a, 2018b) generates 256 sub-surfaces of 256 × 256 pixels per scanned surface. It produces one global value (on the whole 200 × 200 µm surface) per parameter and different statistics per parameter from the 256 sub-surfaces batch. Sixteen height, spatial, and topological parameters are generated (Table S2). Nine statistics per parameter and per surface (composed of 256 sub-surfaces) are extracted: mean and median, skewness and kurtosis, standard deviation, means of the *n* values above and below the first and third quartiles, means of the 25 % lowest and highest values (Table S3). It thus generates a set of 160 variables (combination of statistics and parameters plus the global value). Francisco et al.'s routine (2018a, 2018b) is run independently for each of the two types of facets (crushing and shearing) to target the most discriminative variables among samples (Tables S4, S9, S14). The routine starts with a Box-Cox transformation and ends with the extraction of the three best discriminative variables after running Fisher's LSD tests (Figure S1A). We followed here Merceron et al.'s (this volume) implementation (Figure S1B): after LSD tests, each set (for crushing and shearing facets) of discriminative variables is ordered by decreasing number of significant differences between the four feeding groups of pigs (Figure S1B, Box 1). Then, we computed the geometric mean,

294 rather than the arithmetic one, of significant p-values ($p < 0.05$) per variable because the
295 arithmetic mean can be overly influenced by high values (Figure S1B, Box 2). We extracted
296 the variable with the lowest mean p-value for each parameter for each of the two sets on
297 crushing and shearing facets (Figure S1B, Box 4). Finally, 8 and 14 variables are extracted on
298 lower molars (respectively on crushing and shearing facets; Table S5), 13 and 12 variables
299 are extracted on upper molars (respectively on crushing and shearing facets; Table S10) and
300 15 and 3 variables are extracted on upper deciduous premolars (respectively on crushing and
301 shearing facets; Table S15).

302 **2.4. Statistical analyses**

303 All statistical analyses were conducted in the R statistical environment (R Core Team,
304 2019, v3.6.2). Using the discriminative variables gathered from the sampling method, we
305 performed six Principal Component Analyses (PCA; packages “FactoMineR”, “ggplot2” and
306 “factoextra”) on each of the two types of facets on lower molars, upper molars, and upper
307 deciduous premolars. Additionally, three PCA were produced combining both crushing and
308 shearing facets on lower molars, upper molars, and upper deciduous premolars (Figure S1B,
309 Box 5). SSFA-parameters (*Asfc*, *epLsar*, *HAsfc,* and *Smfc*) on each of the two types of facets
310 were then inserted into PCA as supplementary variables (Figure S1B, Box 6). Contrary to
311 variables gathered from the sampling method, SSFA-parameters had no influence on the PC
312 computations but they were used to help interpret the distributions.

313 Analyses of variance (one-way ANOVAs) were performed on the PC coordinates to
314 detect significant differences among the four controlled-fed groups. PC coordinates were Box-
315 Cox transformed to meet the ANOVA assumptions of homoscedasticity and normality of the
316 residual errors. Then, we conducted two post-hoc tests (package “agricolae”) to detect
317 significant differences between dietary groups (Tables S6-S8, S11-S13, S16-S18): Tukey’s
318 Honest Significant Difference test (HSD) and Fisher’s Least Significant Difference test (LSD;

less conservative than Tukey's HSD). In case of violation of the assumptions, an alternative Kruskal-Wallis test was run followed with a post-hoc Dunn's test.

3. Results

3.1. Lower molars

When combining crushing and shearing lower molar facets in the PCA, the most contributing variables along PC1 are from shearing facets and represent in majority dispersion statistics of height parameters (Figure S2). Along PC2, the most contributing variables are equally issued from crushing and shearing facets. They mainly represent dispersion statistics but also central (contributing about 20 % to PC2) and distribution (about 10 %) of height parameters. PC1 is twice as informative as PC2: PC1 and PC2 explain respectively 35.6 % and 18.1 % of the variance (Figure S2). Significant differences between dietary groups are observed only on PC1 and PC2 axes (Table S6). Added as supplementary variables, *Asfc* (SSFA-parameter) of shearing facets is positively correlated with PC1 values, and *Asfc* of crushing facets is positively correlated with PC2 values (Figure 3).

Pigs fed with barley seeds show the highest PC1 values. Hazelnut-fed pigs and the control group exhibit significantly lower PC1 values, meaning they show less complex enamel surfaces on molar shearing facets than the barley-fed pigs ($p < 0.002$ and $p < 0.004$, respectively; Figure 3, Table S6). Dispersion statistics of the absolute value of the smallest height *Sv* and median height *Smd*, and percentage of nearly horizontal faces *Sh,* all on shearing facets, contribute to pull these two groups toward low PC1 values (Figure 3, Figure S2). Pigs fed with corn kernels tend to express intermediate PC1 values. Barley-fed pigs display higher values of complexity *Asfc* on shearing facets (supplementary variable) compared to all other groups (Figure 3).

Along PC2, corn kernel-fed pigs show high values whereas the three other groups all display lower values (Figure 3). They tend to show high values of complexity *Asfc* on crushing facets, as reflected by the positive correlation of this supplementary to PC2 (Figure 3). The corn group is significantly different from the control one ($p < 0.03$, Table S6), and from the two other groups of seed-eaters according to LSD ($p < 0.02$; but $p < 0.10$ according to HSD, Table S6). The control group and hazelnut-fed pigs are overlapping along both PCs.

When considering only one type of facets, the discriminations between the DMT of lower molars of three groups of seed-eating pigs are weaker than when combining both types of facets (Figure 3). Using parameters on crushing facets only, the barley-fed group slightly overlaps with the two other groups of seed-eaters but significant differences are observed (along PC1, $p < 0.05$ between barley-fed and corn-fed pigs, and along PC2, $p < 0.04$ between barley-fed and hazelnut-fed pigs; Table S7). The hazelnut-fed and the corn-fed groups seem well distinct but significant difference is only observed with LSD (along PC1, $p = 0.04$; Table S7). Control pigs overlap with the three groups of seed-eaters but tend to be distinct from barley-fed pigs ($p = 0.04$ with LSD along PC2; Table S7). Parameters on shearing facets only allow to discriminate barley-fed pigs from the other groups (along PC1: $p < 0.004$ between barley-fed and hazelnut-fed pigs, $p < 0.005$ between barley-fed and control pigs; along PC2: $p < 0.02$ between barley-fed and corn-fed pigs according to Dunn's test; Table S8). Indeed, four out of five individuals of the barley group display high values along PC1 whereas the other groups show lower values along PC1 (except for one individual of the control group). Corn-fed pigs and hazelnut-fed pigs are slightly overlapping along both PCs. The control group tends to show the lowest values along PC2 and is significantly different from the hazelnut group ($p = 0.01$, Dunn's test; Table S8) and from the corn group ($p = 0.002$, Dunn's test; Table S8).

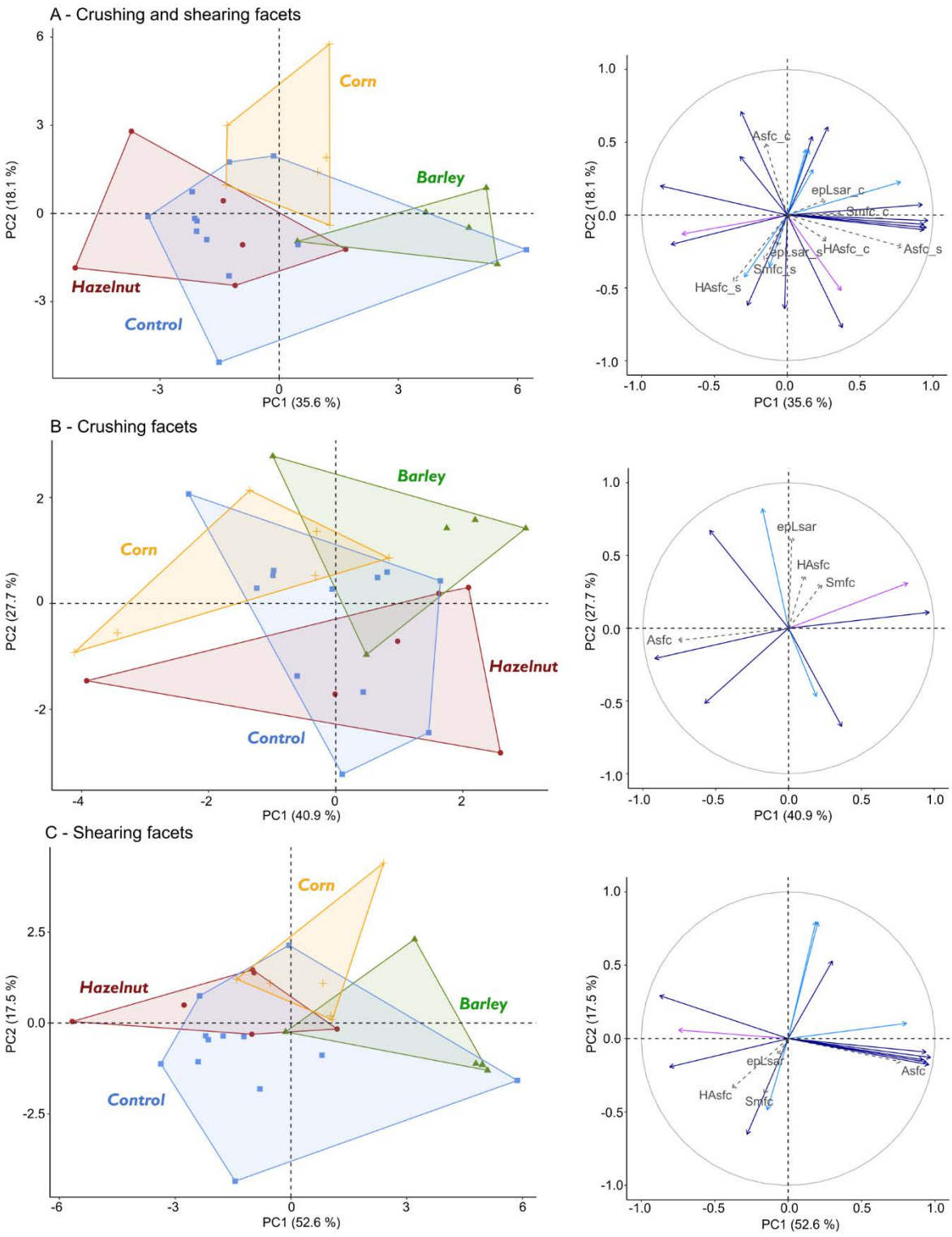

Figure 3. Distributions of individuals (left) and correlation circle (right) along PC1 and PC2 of the four dietary groups based on dental wear parameters from both crushing and shearing lower first molar facets (A), on crushing facets alone (B) and on shearing facets alone (C). Dietary groups: ●: 100 % base flours + 10 hazelnuts in shell a day, ▲: 70 % base flours + 30 % barley seeds, +: 60 % base flours + 20 % corn flour + 20 % corn kernels, ■: 100 % base flours. Active variables (filled arrows): height (dark blue), spatial (light blue), and topological (purple) parameters. SSFA-parameters added as supplementary variables (gray dotted

arrows). Suffixes "_c": crushing facets, "_s": shearing facets. See Figure S7 to visualize the distributions using sexes as another grouping factor.

3.2. Upper molars

When combining crushing and shearing facets on upper molars, PC1 explains about 30 % of the variance, PC2 about 20 % (Figure S3). Along PC1, the most contributing variables are mainly issued from shearing facets and mainly represent dispersion statistics of height parameters. Along PC2, parameters on crushing facets are the most contributing variables. They represent central and dispersion statistics of height parameters, but the median of the percentage of nearly horizontal faces (*Sh*), a topological parameter, contributes almost 10 % to the observed variance. No significant differences are observed on other PCs (Table S11). Added as supplementary variables, the anisotropy of crushing facets (*epLsar_c*) is positively correlated with PC1 values, and *Asfc* of crushing facets is positively correlated with PC2 values (Figure 4).

Along PC1, hazelnut fed-pigs show low values, and barley-fed pigs display on average low values but with a large inter-individual dispersion (Figure 4). Corn-fed pigs display the highest PC1 values and are strongly distinct from hazelnut-fed pigs ($p < 0.002$, Table S11), and well distinct from the two other groups as well ($p < 0.03$, Table S11). This reflects more complex molar shearing surfaces among corn kernel fed-pigs. The anisotropy SSFA-parameter *epLsar* of crushing facets tends to reflect a trend toward textures with more parallel striations associated with high values along PC1, whereas the most contributing variables to this PC are from shearing facets. Numerous SSFA-parameters, notably related to complexity, are also positively associated to PC1. Control pigs are highly variable along PC1 but do not show extreme values along PC2, suggesting low complexity on crushing upper molar facets, similarly to lower molars. Hazelnut-fed pigs show the highest PC2 values but with high inter-individual dispersion (Figure 4). Notably, first quartiles of arithmetic mean of the absolute value of the height *Sa* and of height standard deviation *Sq*, and the median of the relative area *Sdar* (developed area/projected area), all compiled on crushing facets, contribute to pull the

hazelnut-fed group toward high PC2 values (Figure 4, Figure S3). *Asfc* on crushing facets, positively associated with PC2, reflects a tendency to more complex surfaces on pigs fed with hazelnuts (Figure 4). Barley-fed pigs show intermediate to low values along PC2 and are significantly different from hazelnut-fed pigs along this component ($p < 0.03$, Table S11).

When considering one type of facets, the dietary discrimination is weaker than when considering both types (Figure 4). However, regarding parameters on crushing facets only, the three groups of seed-eating pigs tend to exhibit different microwear patterns. Hazelnut-fed pigs display complex surfaces and tend to be discriminated from the two other groups fed with seeds, especially from the corn-fed group. However, significant differences are only observed with LSD between hazelnut-fed and corn-fed pigs (both $p < 0.02$; Table S12). Barley-fed pigs exhibit low values on both PCs and are well discriminated from the hazelnut-fed group along PC1 ($p < 0.02$; Table S12) and from corn-fed pigs along PC2 ($p < 0.02$; Table S12). Regarding shearing facets only, only pigs fed with corn kernels are well distinct from the three other groups (along PC1: $p < 0.02$ between corn-fed and hazelnut-fed pigs, $p < 0.03$ between corn-fed and barley-fed pigs, and $p = 0.01$ between corn fed and control pigs with LSD but $p = 0.05$ with HSD; Table S13).

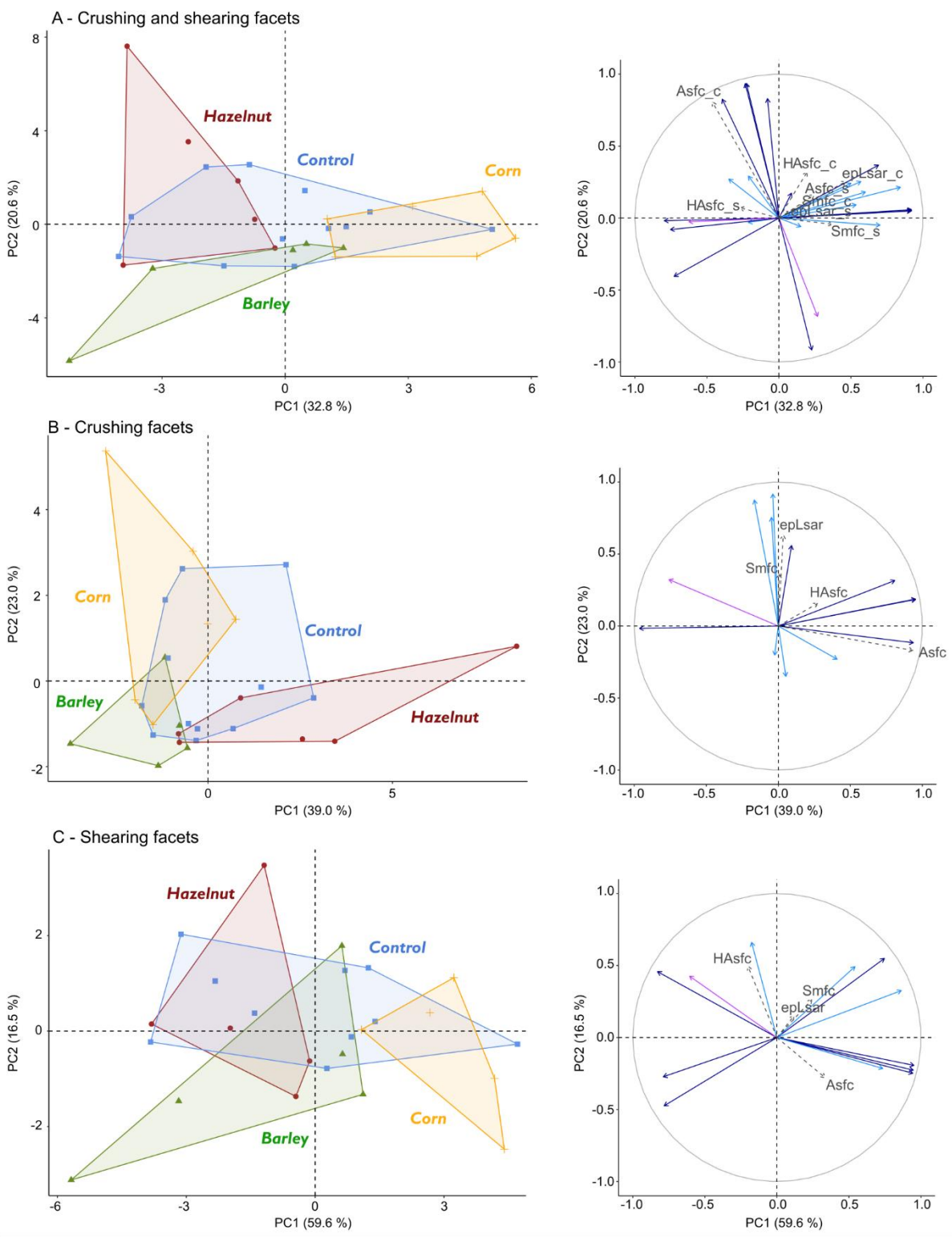

Figure 4. Distributions of individuals (left) and correlation circle (right) along PC1 and PC2 of the four dietary groups on both crushing and shearing upper first molar facets (A), on crushing facets alone (B), and on shearing facets alone (C). Dietary groups: ●: 100 % base flours + 10 hazelnuts in shell a day, ▲: 70 % base flours + 30 % barley seeds, +: 60 % base flours + 20 % corn flour + 20 % corn kernels, ■: 100 % base flours. Active variables (filled arrows): height (dark blue), spatial (light blue), and topological (purple) parameters. SSFA-parameters added

as supplementary variables (gray dotted arrows). Suffixes "_c": crushing facets, "_s": shearing facets. See Figure S8 to visualize the distributions using sexes as another grouping factor.

3.3. Upper deciduous premolars

Principal component analysis on upper fourth deciduous premolars shows that parameters on crushing facets contribute the most to both PC1 and PC2 (Figure S4). Significant differences between dietary groups are observed on PC1 and PC2, as well as on PC3 (Table S16). PC1 explains 33.7 % of the variance observed and is twice as informative as PC2 (Figure S4). No parameter on shearing facets substantially contributes to PC1. The most contributing variables along PC1 are dispersion statistics of height parameters on crushing facets, but the mean percentage of nearly horizontal faces *Sh* (on crushing facets), a topological parameter, contributes almost 10 % to PC1. Added as supplementary variable, *Asfc* of crushing facets is positively correlated with PC1 (Figure 5). Along this PC, barley-fed pigs are well distinct from control and corn-fed pigs (both $p < 0.002$, Table S16). Barley-fed pigs show the lowest PC1 values and corn-fed pigs exhibit the highest PC1 values (Figure 5). Specifically, the 25 % highest values of absolute smallest height *Sv* as well as the mean percentage of nearly horizontal faces *Sh*, both measured on crushing facets, contribute to pull barley-fed pigs toward low PC1 values (Figure S4). Dispersion statistics of the arithmetic mean of the absolute of the heights *Sa* and height standard deviation *Sq* of crushing facets contribute to pull the corn group toward high PC1 values.

PC2 explains 17 % of the variance and provides complementary information to PC1. The most contributing variables to PC2 mainly represent dispersion statistics of spatial parameters on crushing facets. Although no parameter on shearing facet substantially contributes to PC2, *epLsar* on shearing facets is positively associated to this component. The relative area *Sdar* (height parameter) and percentage of nearly horizontal faces *Sh,* both on crushing facets, contribute as well, albeit to a lesser extent. Along PC2, hazelnut-fed pigs show the lowest values and are well distinct from the three other groups ($p < 0.03$, Table S16).

Dispersion statistics of spatial parameters contribute to pull the control, the barley-fed, and the corn-fed groups toward high PC2 values. Control pigs and corn-fed pigs show similar values along both PC1 and PC2 axes (Figure 5). PC3 (Figure S5), which explains 12.8 % of the variance, provides few complementary discriminative information, but only for distinguishing the control group from the corn-fed group ($p < 0.02$, Table S16). However, control pigs still overlap with corn-fed pigs, as well as with hazelnut-fed pigs.

When considering only one type of facets, the PCA using parameters on crushing facets provides highly similar results (most contributing variables to PCs and distribution of individuals) to the PCA using both types of facets (Figure 5; see also Figures S5 and S6). Along PC1, barley-fed pigs differ from corn-fed ($p < 0.002$) and control pigs ($p < 0.003$), and from hazelnut-fed pigs along PC2 ($p < 0.04$; Table S17). The hazelnut and the corn groups differ significantly along PC2 ($p < 0.04$; Table S17). On shearing facets, only PC1 tends to show differences between dietary groups ($p = 0.08$; Table S18). No differences are observed on PC2 ($p > 0.3$) or PC3 ($p > 0.1$). The PCA biplot on shearing facets shows that all groups are strongly overlapping. The hazelnut-fed pigs differ from corn-fed pigs along PC1 but only according to LSD ($p = 0.02$). In contrast to molars, the combination of facets on upper fourth deciduous premolars does not improve the dietary discrimination compared to analyses that consider only crushing facets. However, combining both types of facets does not mask the discriminations.

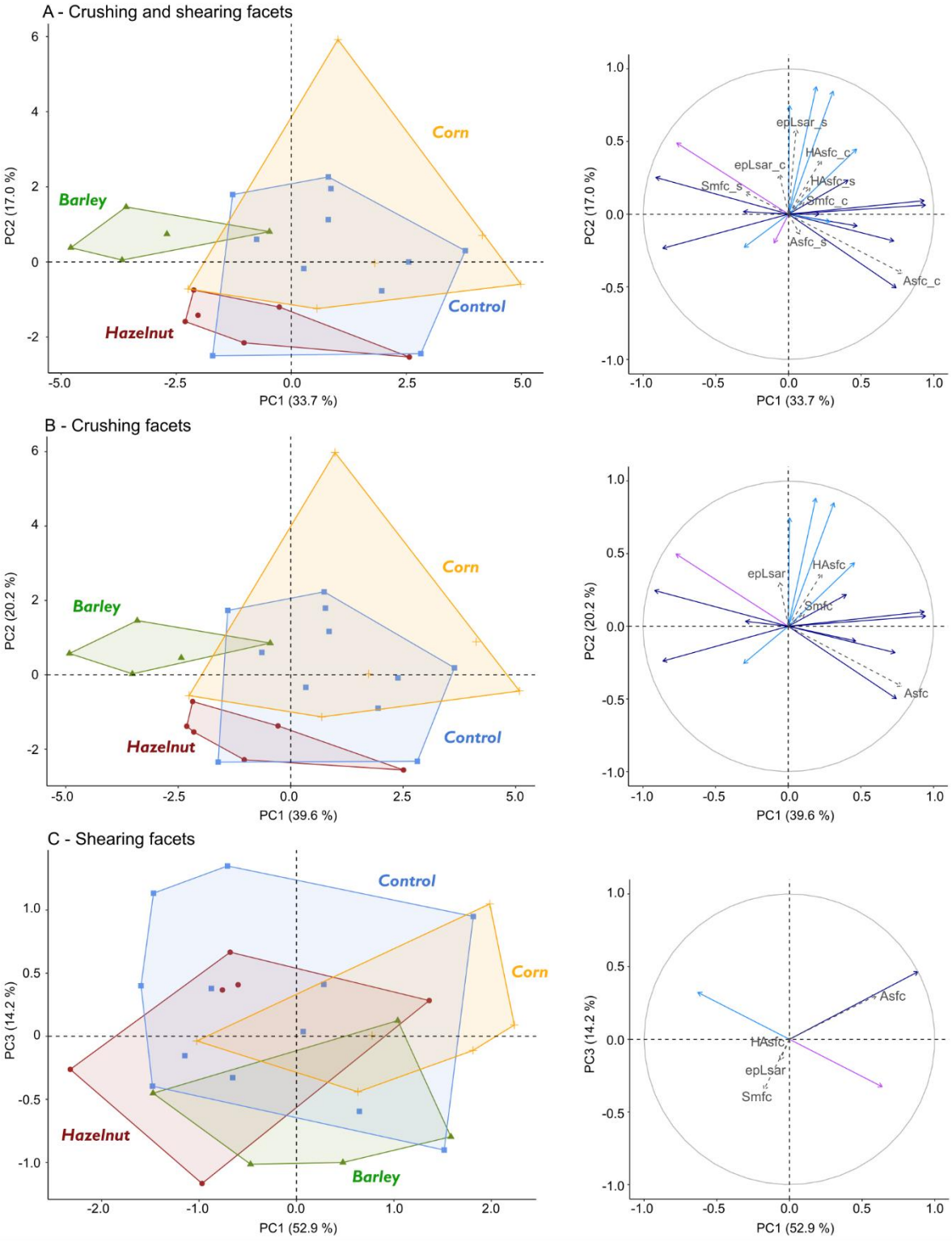

Figure 5. Distributions of individuals (left) and correlation circle (right) of the four dietary groups along PC1 and PC2 on both crushing and shearing upper fourth deciduous premolar facets (A), along PC1 and PC2 on crushing facets alone (B) and along PC1 and PC4 on shearing facets alone (C). Dietary groups: ●: 100 % base flours + 10 hazelnuts in shell a day, ▲: 70 % base flours + 30 % barley seeds, +: 60 % base flours + 20 % corn flour + 20 % corn kernels, ■: 100 % base flours. Active variables (filled arrows): height (dark blue), spatial (light blue) and topological (purple) parameters. SSFA-parameters added as supplementary variables (gray

dotted arrows). Suffixes "_c": crushing facets, "_s": shearing facets. See Figure S9 to visualize the distributions using sexes as another grouping factor.

4. Discussion

4.1. DMT in controlled-fed pigs and dietary overlapping among hominins

The present study analyzed DMT variations of controlled-fed pigs characterized by bunodont, thick-enameled cheek teeth. To our knowledge, this is the first work proposing an experimental baseline with a model taxon for interpreting DMT variations among extinct taxa with bunodont dentition and similar tooth wear pattern, such as suids or primates. We focused here on four dietary groups: pigs were all fed with the same flours (at least 60 % of the diet), supplemented with different types of seeds for three groups. While those pigs had overall similar diets, our results highlight significant differences in their DMT. In line with several studies on wild caught specimens (Teaford and Robinson, 1989; Merceron et al., 2010; Berlioz et al., 2017; Percher et al., 2017), this work strongly supports that DMT reflect intra-specific and even intra-population minor variations in dietary habits. Moreover, although van Casteren et al. (2020) recently argued that "hard plant tissues barely influence dental microwear textures", we show that controlled-fed pigs exhibit significant differences in DMT depending on the type of seeds consumed. Nonetheless, our results have some limitations, notably because the feeding groups were given different concentrations of seeds so we cannot disentangle the respective impacts of seed structure and seed concentrations on DMT.

This work is of particular interest for reconstructing dietary habits of early hominins, for whom several studies have suggested overlapping diets that may have differed mainly regarding fallback foods consumed during periods of food scarcity (Ungar, 2004; Scott et al., 2005; Ungar and Sponheimer, 2011; Ungar et al., 2012; Ungar and Daegling, 2013). Works based on enamel stable carbon isotopes and dental microwear textures have challenged the hypothesis of durophagy and specialized diets within the *Paranthropus* genus as driving the selection of their robust craniomandibular and dental morphology (see references below),

conversely to their “gracile” contemporaneous early *Homo* considered as generalists (e.g., Wood and Strait, 2004). In addition to highlighting overlapping diets between some early hominins, these works show strongly different patterns between the eastern and the southern African species of *Paranthropus* (e.g., Sponheimer et al., 2006; Ungar et al., 2008; Ungar and Sponheimer, 2011; Martin et al., 2020). On the one hand, eastern African *P. boisei* exhibit stable carbon isotope compositions indicative of a dominant C_4 diet, most likely composed of grasses and/or sedges (Cerling et al., 2011, 2013; Wynn et al., 2020). Analyses of their dental microwear show low texture complexity, providing no evidence that they regularly consumed hard foods and would rather advocate for an abrasive diet composed of silica-bearing herbaceous monocots, *i.e.*, grasses, sedges (Ungar et al., 2008, 2012). Among alternative hypotheses, the ingestion of dust and grit with foods has been proposed as severely impacting the enamel surface and as driving the selection of robust morphologies (Madden, 2014). Southern African *P. robustus*, on the other hand, exhibit stable carbon isotopic compositions consistent with a mixed or dominant C_3 diet (Lee-Thorp et al., 1994; Sponheimer et al., 2006; Caley et al., 2018; Lüdecke et al., 2018; see also Balter et al., 2012). They show the highest average value of texture complexity compared to other early hominins, as well as a broad range of individual variation (Scott et al., 2005; Peterson et al., 2018). This distribution has been suggested to be more comparable to extant primates that occasionally rely on hard items as FBFs (Ungar and Sponheimer, 2011). Consequently, these studies suggest that robust craniomandibular and dental morphologies might have been favored by an occasional consumption of mechanically challenging FBFs critical for survival.

The present controlled-food experiments are not directly comparable with data from wild populations (either past or present-day species) as diets in the wild are much more diverse than controlled diets in experimental settings. Those experiments nevertheless highlight our understanding of the relations between dietary variations and dental microwear textures, and consequently improve our interpretations on the role of feeding habits upon niche partitioning among early hominins.

4.2. Improving dietary discriminations using a surface sampling strategy and combining phase I and phase II facets

The surface sampling strategy used in this study exploits different statistics for a whole set of standard texture parameters measured on 256 sub-surfaces per scanned surface and allows detection of the most discriminative parameters among several dietary groups (Francisco et al., 2018a, 2018b). Rather than considering variables independently, we performed Principal Component Analyses with the most discriminative variables selected from the sampling strategy (see Material and Methods and Figure S1). Our results show that this approach allows detection of significant differences in dental microwear textures among different groups of controlled-fed pigs with overall similar diets. In every analysis, we show that most discriminative variables are dispersion and distribution statistics of surface texture parameters, rather than central tendency statistics (mean or median). Dispersion statistics are the most contributing variables to PCs (Figures S1, S2, S3), which thus have the potential to discriminate groups with slight differences in diet. Several data analysis (not only in DMTA) have pointed out that quantiles, distribution or dispersion among samples may yield more significant differences than central tendencies (Plavcan and Cope, 2001; Ragni et al., 2017; Merceron et al., this volume; see also Lambrechtsen et al., 1999; Brewer and Pickle, 2002; Phillips et al., 2005; Cox et al., 2013; Krzywinski and Altman, 2014). We suggest that dispersion statistics of standard parameters, and not only central tendencies, are of particular interest for DMTA studies focusing on taxa with subtle dietary variations. It is also worth noting that some of the observed dietary discriminations are not mirrored by the global value of SSFA-parameters added as supplementary variables into PCAs. Notably, the distinction on upper molars of pigs fed with barley seeds is not reflected by any SSFA-parameter, and that is also the case for the distinction of hazelnut-fed pigs on upper deciduous premolars. These observations thus reinforce the relevance of using a wider set of texture parameters to target significant differences among animals with overall similar diets. In the same way that earlier studies using 2D dental microwear methods were able to discriminate a species from others

561 by the frequency of the occurrence of few large pits per surface (e.g., Solounias and
562 Semprebon, 2002; Merceron et al., 2005), the sampling strategy chosen here may allow to
563 discriminate the species not by the central tendency values of a given parameter, but by its
564 distribution shape or its value at the quartile Q_n.

565 PCAs highlight that parameters measured on both crushing and shearing facets bear
566 discriminant dietary signals. Considering only one type of facets on upper or lower molars
567 allows discriminating one group of seed-eaters from another (or from the two others), but does
568 not reveal significant differences (observed with both HSD and LSD) among all three groups
569 of seed-eaters. In contrast, when combining the two types of facets, the differences among the
570 three groups of seed-eaters are even stronger and are significant with both post-hoc tests.
571 Consequently, combining data from crushing and shearing facets on molars leads to a better
572 discrimination among all three groups of seed-eaters. When considering the upper deciduous
573 premolars, the combination of two dental facet types does not lead to a better discrimination
574 than when considering only crushing facets. Nevertheless, including shearing facets in the
575 analysis does not mask the dietary signal on upper deciduous premolars. Thus, this study
576 supports recent results showing that the combination of facet types may improve the resolution
577 of dietary reconstructions (Arman et al., 2019; Merceron et al., this volume). While crushing
578 facets are mostly considered in DMT analyses on early hominins because they are thought to
579 be more discriminant than shearing ones among primates (Krueger et al., 2008), we argue that
580 both types of facets should be considered for future studies (see Martin et al., 2019; Merceron
581 et al., this volume).

582

583 **4.3. DMT variations depending on the presence and type of seeds consumed**

584 Because high texture complexity has been related to hard food consumption (Scott et
585 al., 2006, 2012; Schubert et al., 2010; Daegling et al., 2011), we expected that the highest
586 complexity values would correspond to the harder dietary item consumed (but see

587 Ramdarshan et al., 2016). Thus, pigs fed on hazelnuts in shell should exhibit more complex
588 textures than corn and barley-fed pigs (Table 2), and even more in comparison to control pigs.
589 However, earlier works have pointed out that surface complexity alone might not be a strong
590 indicator for the hardness of seeds consumed, because their consumption does not
591 necessarily generate the expected complex surfaces on enamel (Ramdarshan et al., 2016;
592 van Casteren et al., 2020). Our results on lower molars, indeed, show that pigs fed on
593 hazelnuts exhibit facets that appear to be about as complex as those of pigs fed only on flours,
594 and pigs fed on barley (the less resistant seeds) show more complex shearing facets than the
595 other dietary groups. However, on upper molars, barley-fed pigs do not show the most complex
596 facets. Thus, the complexity of enamel surfaces does not seem associated with seed hardness
597 in this study. Besides the hardness of the seeds consumed, other factors should also be
598 considered to better understand the relationships between seed consumption and texture
599 complexity (e.g., seed size, particle size after mastication, number of seeds in one bolus, seed
600 digestibility; see Lucas, 2004). For example, it has been suggested that food resources of
601 smaller particle size might require higher bite force for oral processing than larger ones (Lucas,
602 2004), as well as bolus containing high amount of small resources (van Casteren et al., 2020).
603 In the present study, we did not control for these factors, and we used seeds of different
604 hardness and size, and representing different proportions of the diet depending on the feeding
605 groups. Thus, we cannot identify which factor predominantly influences the differences among
606 the groups. Nevertheless, we show overall that DMT are impacted by seed consumption and
607 that they differ between the three groups of seed-eating pigs.

608 PCAs and ANOVAs on PC coordinates show significant differences in DMT of the three
609 groups of pigs fed on seeds. The dietary discrimination is, however, weaker on both upper and
610 lower molars than on upper deciduous premolars. Wear facets on upper and lower molars
611 were barely developed and not all crushing and shearing facets were developed, although
612 every individual showed distinct facets at their early stages of formation, notably on mesial
613 cusps. Molars of pigs are erupted between 4 to 6 months old (Legge, 2013) and were thus

614 probably in full occlusion only a few weeks before death, particularly among pigs fed with
615 hazelnuts (slaughtered at 195 days old). This could explain that, contrary to what is found on
616 deciduous premolars, there is no difference in dental microwear complexity between crushing
617 and shearing facets on molars. This would have been expected because of their different
618 implications in mastication with more occlusal pitting on phase II homologous facets involved
619 into grinding and crushing of foods, conversely to phase I facets involved in slicing food items
620 with lateral movements. This difference between facets is observed on upper deciduous
621 premolars because, being erupted at about 25 days old (Tucker and Widowski, 2009), they
622 were fully functional at the time pigs received their dedicated diet. To sum up, our results show
623 a stronger dietary discrimination among the three groups of seed-eaters on the worn upper
624 deciduous premolars than on the barely worn molars.

625 While the present study shows significant differences in DMT between pigs fed on
626 different seeds, we observe that control pigs fed only on flours are highly overlapping with one
627 or two groups of seed-eaters. This is actually not surprising because, in addition to the high
628 proportion of diet these groups have in common, the flours contained an important number of
629 particles above 1.25 mm in diameter (24 % for the wheat flour, 61 % for the soy flour; Table
630 2). Indeed, feeding pigs with finely ground flours is not possible because it would lead to gastric
631 damages, such as ulcers, that would affect animal well-being. These flours, rich in millimetric
632 seed fragments, explain why the texture complexity is overall high, even in the control group.
633 Moreover, Winkler et al. (2020) recently showed that angular quartz particles lead to complex
634 surfaces. Although it is not clear if this also applies on softer seed particles, such as corn
635 fragments, it is likely that numerous particles in the flours are angular. This might contribute to
636 the overall complexity among pigs in this study.

637 Altogether, our results are in line with a recent in vivo experiment on captive capuchin
638 monkeys (*Sapajus apella*; Teaford et al., 2020), which demonstrates that hard food
639 consumption impacts tooth wear by generating new features on wear facet in a very short
640 period of time (3-4 hours). We here provide novel information that complements their study as

we considered texture parameters. We show overall that dispersion statistics of height parameters are, in majority, the variables that most contribute to PCs. This is congruent with Schulz-Kornas et al.'s (2019) study on Western chimpanzees who showed that some height parameters (on crushing and shearing facets) differ depending on nut consumption. Our results thus support the hypothesis that the consumption of different seeds generates differences on DMT highlighted by parameters related to surface height profiles.

5. Conclusions

The present study aimed at testing the hypothesis that the consumption of various types of seeds has an impact on dental microwear textures despite overall similar diets. Controlled feeding trials were conducted on four dietary groups of domestic pigs which exhibit thick-enameled, bunodont cheek teeth. Such an experimental baseline might help the interpretation of DMT patterns among extinct bunodont species of suids or primates with overlapping dietary signals. This could greatly contribute to discussions regarding the consumption of mechanically challenging resources that could be fallback foods for early hominins.

We used a subsampling surface strategy that measures different statistics for a whole set of texture parameters. We performed Principal Component Analyses on shearing (phase I) and crushing (phase II) facets independently, as well as by combining the two types of facets. Our results show that controlled-fed pigs exhibit significant differences in their DMT patterns depending on the type of seeds consumed. This study shows that both phase I and II facets bear discriminant dietary signals and that considering both types of facets in the analyses improves dietary discriminations. These discriminations are not mirrored by standard Scale Sensitive Fractal Analysis (SSFA) parameters in every case when added as supplementary variables, substantiating the efficiency of the subsampling surface strategy to detect significant differences among groups with a high proportion of diet in common. The variables selected from the subsampling strategy that most contribute to dietary discriminations represent in

majority dispersion statistics of height parameters. Thus, these results show that dispersion statistics have the potential to distinguish DMT among groups with overall similar diets, and support the hypothesis that the consumption of seeds has an impact on texture parameters related to surface relief.

Acknowledgments

The authors thank R. Marquet, notably for preparing pigs' crania and mandibles after slaughter, and the staff from the GenESI experimental unit. We also thank S. Riffaut for drawing Figure 2. This study was funded by the ANR project Diet-Scratches (ANR-17-CE27-0002-02, PIs: G. Merceron and S. Ferchaud; French Agency for Research), the ALIHOM project (project n°210389, *Nouvelle-Aquitaine* region, France, PI: G. Merceron) and the *Ministère de l'Enseignement supérieur, de la Recherche et de l'Innovation* (France). The authors thank G. Reynaud and L. Painault (PALEVOPRIM, Poitiers, France) for administrative guidance, and G. Thiery (PALEVOPRIM, Poitiers, France) and X. Milhet (Pprime institute, Poitiers, France) for discussion. We thank two anonymous reviewers and the editors whose comments greatly improved the initial version of the manuscript.

References

Ackermans, N.L., Winkler, D.E., Schulz-Kornas, E., Kaiser, T.M., Müller, D.W.H., Kircher, P.R., Hummel, J., Clauss, M., Hatt, J.-M., 2018. Controlled feeding experiments with diets of different abrasiveness reveal slow development of mesowear signal in goats (*Capra aegagrus hircus*). Journal of Experimental Biology 221, jeb186411. https://doi.org/10.1242/jeb.186411

Ackermans, N.L., Winkler, D.E., Martin, L.F., Kaiser, T.M., Clauss, M., Hatt, J.-M., 2020. Dust and grit matter: abrasives of different size lead to opposing dental microwear textures in experimentally fed sheep (*Ovis aries*). Journal of Experimental Biology 223, jeb220442. https://doi.org/10.1242/jeb.220442

Aiba, K., Miura, S., Kubo, M.O., 2019. Dental microwear texture analysis in two ruminants, Japanese serow (*Capricornis crispus*) and sika deer (*Cervus nippon*), from Central Japan. Mammal Study 44, 183–192. https://doi.org/10.3106/ms2018-0081

Altmann, S.A., 2009. Fallback foods, eclectic omnivores, and the packaging problem. American Journal of Physical Anthropology 140, 615–629. https://doi.org/10.1002/ajpa.21097

Anthony, M.R.L., Kay, R.F., 1993. Tooth form and diet in ateline and alouattine primates; reflections on the comparative method. American Journal of Science 293, 356–382. https://doi.org/10.2475/ajs.293.A.356

Arman, S.D., Prowse, T.A.A., Couzens, A.M.C., Ungar, P.S., Prideaux, G.J., 2019. Incorporating intraspecific variation into dental microwear texture analysis. Journal of the Royal Society Interface 16, 20180957. https://doi.org/10.1098/rsif.2018.0957

Balter, V., Braga, J., Télouk, P., Thackeray, J.F., 2012. Evidence for dietary change but not landscape use in South African early hominins. Nature 489, 558–560. https://doi.org/10.1038/nature11349

Bels, V., Herrel, A., 2019. Feeding, a Tool to Understand Vertebrate Evolution Introduction to "Feeding in Vertebrates," in: Bels, V., Whishaw, I.Q. (Eds.), Feeding in Vertebrates: Evolution, Morphology, Behavior, Biomechanics, Fascinating Life Sciences. Springer International Publishing, Cham, pp. 1–18. https://doi.org/10.1007/978-3-030-13739-7_1

Berlioz, E., Azorit, C., Blondel, C., Ruiz, M.S.T., Merceron, G., 2017. Deer in an arid habitat: dental microwear textures track feeding adaptability. Hystrix, the Italian Journal of Mammalogy 28, 222–230. https://doi.org/10.4404/hystrix-28.2-12048

Brewer, C.A., Pickle, L., 2002. Evaluation of Methods for Classifying Epidemiological Data on Choropleth Maps in Series. Annals of the Association of American Geographers 92, 662–681. https://doi.org/10.1111/1467-8306.00310

Calandra, I., Zub, K., Szafrańska, P.A., Zalewski, A., Merceron, G., 2016. Silicon-based plant defences, tooth wear and voles. Journal of Experimental Biology 219, 501–507. https://doi.org/10.1242/jeb.134890

Caley, T., Extier, T., Collins, J.A., Schefuß, E., Dupont, L., Malaizé, B., Rossignol, L., Souron, A., McClymont, E.L., Jimenez-Espejo, F.J., García-Comas, C., Eynaud, F., Martinez, P., Roche, D.M., Jorry, S.J., Charlier, K., Wary, M., Gourves, P.-Y., Billy, I., Giraudeau, J., 2018. A two-million-year-long hydroclimatic context for hominin evolution in southeastern Africa. Nature 560, 76–79. https://doi.org/10.1038/s41586-018-0309-6

Cerling, T.E., Mbua, E., Kirera, F.M., Manthi, F.K., Grine, F.E., Leakey, M.G., Sponheimer, M., Uno, K.T., 2011. Diet of *Paranthropus boisei* in the early Pleistocene of East Africa. Proceedings of the National Academy of Sciences 108, 9337–9341. https://doi.org/10.1073/pnas.1104627108

Cerling, T.E., Manthi, F.K., Mbua, E.N., Leakey, L.N., Leakey, M.G., Leakey, R.E., Brown, F.H., Grine, F.E., Hart, J.A., Kaleme, P., Roche, H., Uno, K.T., Wood, B.A., 2013. Stable isotope-based diet reconstructions of Turkana Basin hominins. Proceedings of the National Academy of Sciences 110, 10501–10506. https://doi.org/10.1073/pnas.1222568110

738 Codron, D., Brink, J.S., Rossouw, L., Clauss, M., Codron, J., Lee-Thorp, J.A., Sponheimer, M.,
739 2008. Functional differentiation of African grazing ruminants: an example of specialized
740 adaptations to very small changes in diet. Biological Journal of the Linnean Society 94,
741 755–764. https://doi.org/10.1111/j.1095-8312.2008.01028.x
742 Constantino, P.J., Wright, B.W., 2009. The importance of fallback foods in primate ecology and
743 evolution. American Journal of Physical Anthropology 140, 599–602.
744 https://doi.org/10.1002/ajpa.20978
745 Constantino, P.J., Lucas, P.W., Lee, J.J.-W., Lawn, B.R., 2009. The influence of fallback foods
746 on great ape tooth enamel. American Journal of Physical Anthropology 140, 653–660.
747 https://doi.org/10.1002/ajpa.21096
748 Cox, C., Schneider, M.F., Muñoz, A., 2013. Quantiles of Residual Survival, in: Lee, M.-L.T.,
749 Gail, M., Pfeiffer, R., Satten, G., Cai, T., Gandy, A. (Eds.), Risk Assessment and
750 Evaluation of Predictions, Lecture Notes in Statistics. Springer, New York, NY, pp. 87–
751 103. https://doi.org/10.1007/978-1-4614-8981-8_6
752 Daegling, D.J., McGraw, W.S., Ungar, P.S., Pampush, J.D., Vick, A.E., Bitty, E.A., 2011. Hard-
753 object feeding in sooty mangabeys (*Cercocebus atys*) and interpretation of early
754 hominin feeding ecology. PLoS ONE 6, e23095.
755 https://doi.org/10.1371/journal.pone.0023095
756 Daegling, D.J., Hua, L.-C., Ungar, P.S., 2016. The role of food stiffness in dental microwear
757 feature formation. Archives of Oral Biology 71, 16–23.
758 https://doi.org/10.1016/j.archoralbio.2016.06.018
759 Damuth, J., Janis, C.M., 2011. On the relationship between hypsodonty and feeding ecology
760 in ungulate mammals, and its utility in palaeoecology. Biological Reviews 86, 733–758.
761 https://doi.org/10.1111/j.1469-185X.2011.00176.x
762 Delprete, C., Sesana, R., 2014. Mechanical characterization of kernel and shell of hazelnuts:
763 proposal of an experimental procedure. Journal of Food Engineering 124, 28–34.
764 https://doi.org/10.1016/j.jfoodeng.2013.09.027

765 Dominy, N.J., Vogel, E.R., Yeakel, J.D., Constantino, P., Lucas, P.W., 2008. Mechanical
766 properties of plant underground storage organs and implications for dietary models of
767 early hominins. Evolutionary Biology 35, 159–175. https://doi.org/10.1007/s11692-008-
768 9026-7
769 Ercisli, S., Ozturk, I., Kara, M., Kalkan, F., Seker, H., Duyar, O., Erturk, Y., 2011. Physical
770 properties of hazelnuts. International Agrophysics 25, 115–121.
771 Francisco, A., Blondel, C., Brunetière, N., Ramdarshan, A., Merceron, G., 2018a. Enamel
772 surface topography analysis for diet discrimination. A methodology to enhance and
773 select discriminative parameters. Surface Topography: Metrology and Properties 6,
774 015002. https://doi.org/10.1088/2051-672X/aa9dd3
775 Francisco, A., Brunetière, N., Merceron, G., 2018b. Gathering and analyzing surface
776 parameters for diet identification purposes. Technologies 6, 75.
777 https://doi.org/10.3390/technologies6030075
778 Gailer, J.P., Calandra, I., Schulz-Kornas, E., Kaiser, T.M., 2016. Morphology is not destiny:
779 discrepancy between form, function and dietary adaptation in bovid cheek teeth.
780 Journal of Mammalian Evolution 23, 369–383. https://doi.org/10.1007/s10914-016-
781 9325-1
782 Grine, F.E., Daegling, D.J., 2017. Functional morphology, biomechanics and the retrodiction
783 of early hominin diets. Comptes Rendus Palevol 16, 613–631.
784 https://doi.org/10.1016/j.crpv.2017.01.005
785 Harris, J.M., Cerling, T.E., 2002. Dietary adaptations of extant and Neogene African suids.
786 Journal of Zoology 256, 45–54. https://doi.org/10.1017/S0952836902000067
787 Hoffman, J.M., Fraser, D., Clementz, M.T., 2015. Controlled feeding trials with ungulates: a
788 new application of in vivo dental molding to assess the abrasive factors of microwear.
789 Journal of Experimental Biology 218, 1538–1547. https://doi.org/10.1242/jeb.118406
790 Hofman-Kamińska, E., Merceron, G., Bocherens, H., Makowiecki, D., Piličiauskienė, G.,
791 Ramdarshan, A., Berlioz, E., Kowalczyk, R., 2018. Foraging habitats and niche
792 partitioning of European large herbivores during the Holocene – Insights from 3D dental

microwear texture analysis. Palaeogeography, Palaeoclimatology, Palaeoecology 506, 183–195. https://doi.org/10.1016/j.palaeo.2018.05.050

Hua, L.-C., Brandt, E.T., Meullenet, J.-F., Zhou, Z.-R., Ungar, P.S., 2015. Technical note: An in vitro study of dental microwear formation using the BITE Master II chewing machine. American Journal of Physical Anthropology 158, 769–775. https://doi.org/10.1002/ajpa.22823

Kalkan, F., Kara, M., Bastaban, S., Turgut, N., 2011. Strength and frictional properties of popcorn kernel as affected by moisture content. International Journal of Food Properties 14, 1197–1207. https://doi.org/10.1080/10942911003637319

Krueger, K.L., Scott, J.R., Kay, R.F., Ungar, P.S., 2008. Technical note: Dental microwear textures of “Phase I” and “Phase II” facets. American Journal of Physical Anthropology 137, 485–490. https://doi.org/10.1002/ajpa.20928

Krzywinski, M., Altman, N., 2014. Visualizing samples with box plots. Nature Methods 11, 119–120. https://doi.org/10.1038/nmeth.2813

Laden, G., Wrangham, R., 2005. The rise of the hominids as an adaptive shift in fallback foods: Plant underground storage organs (USOs) and australopith origins. Journal of Human Evolution 49, 482–498. https://doi.org/10.1016/j.jhevol.2005.05.007

Lambert, J.E., Chapman, C.A., Wrangham, R.W., Conklin-Brittain, N.L., 2004. Hardness of cercopithecine foods: Implications for the critical function of enamel thickness in exploiting fallback foods. American Journal of Physical Anthropology 125, 363–368. https://doi.org/10.1002/ajpa.10403

Lambrechtsen, J., Rasmussen, F., Hansen, H., Jacobsen, I., 1999. Tracking and factors predicting rising in ‘tracking quartile’ in blood pressure from childhood to adulthood: Odense Schoolchild Study. Journal of Human Hypertension 13, 385–391. https://doi.org/10.1038/sj.jhh.1000836

Lazagabaster, I.A., 2019. Dental microwear texture analysis of Pliocene Suidae from Hadar and Kanapoi in the context of early hominin dietary breadth expansion. Journal of Human Evolution 132, 80–100. https://doi.org/10.1016/j.jhevol.2019.04.010

821 Lee-Thorp, J.A., van der Merwe, N.J., Brain, C.K., 1994. Diet of *Australopithecus robustus* at
822 Swartkrans from stable carbon isotopic analysis. Journal of Human Evolution 27, 361–
823 372. https://doi.org/10.1006/jhev.1994.1050
824 Legge, A.J., 2013. 'Practice with Science': Molar Tooth Eruption Ages in Domestic, Feral and
825 Wild Pigs (*Sus scrofa*). International Journal of Osteoarchaeology.
826 https://onlinelibrary.wiley.com/pb-
827 assets/assets/10991212/Anthony_Legge_Final_Paper.pdf (accessed 16 September
828 2020)
829 Liem, K.F., 1980. Adaptive significance of intra- and interspecific differences in the feeding
830 repertoires of cichlid fishes. American Zoologist 20, 295–314.
831 https://doi.org/10.1093/icb/20.1.295
832 Lister, A.M., 2013. The role of behaviour in adaptive morphological evolution of African
833 proboscideans. Nature 500, 331–334. https://doi.org/10.1038/nature12275
834 Lucas, P.W., 2004. Dental Functional Morphology: How Teeth Work, 1st ed. Cambridge
835 University Press. https://doi.org/10.1017/CBO9780511735011
836 Lucas, P.W., Constantino, P.J., Chalk, J., Ziscovici, C., Wright, B.W., Fragaszy, D.M., Hill,
837 D.A., Lee, J.J.-W., Chai, H., Darvell, B.W., Lee, P.K.D., Yuen, T.D.B., 2009. Indentation
838 as a technique to assess the mechanical properties of fallback foods. American Journal
839 of Physical Anthropology 140, 643–652. https://doi.org/10.1002/ajpa.21026
840 Lucas, P.W., Omar, R., Al-Fadhalah, K., Almusallam, A.S., Henry, A.G., Michael, S., Thai, L.A.,
841 Watzke, J., Strait, D.S., Atkins, A.G., 2013. Mechanisms and causes of wear in tooth
842 enamel: implications for hominin diets. Journal of The Royal Society Interface 10,
843 20120923. https://doi.org/10.1098/rsif.2012.0923
844 Lucas, P.W., Casteren, A. van, Al-Fadhalah, K., Almusallam, A.S., Henry, A.G., Michael, S.,
845 Watzke, J., Reed, D.A., Diekwisch, T.G.H., Strait, D.S., Atkins, A.G., 2014. The role of
846 dust, grit and phytoliths in tooth wear. Annals Zoologici Fennici 51, 143–152.
847 https://doi.org/10.5735/086.051.0215

Lüdecke, T., Kullmer, O., Wacker, U., Sandrock, O., Fiebig, J., Schrenk, F., Mulch, A., 2018. Dietary versatility of Early Pleistocene hominins. Proceedings of the National Academy of Sciences USA 115, 13330–13335. https://doi.org/10.1073/pnas.1809439115

MacArthur, R.H., Pianka, E.R., 1966. On optimal use of a patchy environment. The American Naturalist 100, 603–609. https://doi.org/10.1086/282454

Madden, R.H., 2014. Hypsodonty in Mammals: Evolution, Geomorphology and the Role of Earth Surface Processes. Cambridge University Press, Cambridge. https://doi.org/10.1017/CBO9781139003384

Markowski, M., Majewska, K., Kwiatkowski, D., Malkowski, M., Burdylo, G., 2010. Selected geometric and mechanical properties of barley (*Hordeum vulgare* L.) grain. International Journal of Food Properties 13, 890–903. https://doi.org/10.1080/10942910902908888

Marshall, A.J., Wrangham, R.W., 2007. Evolutionary consequences of fallback foods. International Journal of Primatology 28, 1219–1235. https://doi.org/10.1007/s10764-007-9218-5

Marshall, A.J., Boyko, C.M., Feilen, K.L., Boyko, R.H., Leighton, M., 2009. Defining fallback foods and assessing their importance in primate ecology and evolution. American Journal of Physical Anthropology 140, 603–614. https://doi.org/10.1002/ajpa.21082

Martin, F., Plastiras, C.-A., Merceron, G., Souron, A., Boisserie, J.-R., 2018. Dietary niches of terrestrial cercopithecines from the Plio-Pleistocene Shungura Formation, Ethiopia: evidence from Dental Microwear Texture Analysis. Scientific Reports 8, 14052. https://doi.org/10.1038/s41598-018-32092-z

Martin, J.E., Tacail, T., Braga, J., Cerling, T.E., Balter, V., 2020. Calcium isotopic ecology of Turkana Basin hominins. Nature Communications 11, 3587. https://doi.org/10.1038/s41467-020-17427-7

Martin, L.F., Winkler, D., Tütken, T., Codron, D., De Cuyper, A., Hatt, J.-M., Clauss, M., 2019. The way wear goes: phytolith-based wear on the dentine–enamel system in guinea

875 pigs (*Cavia porcellus*). Proceedings of the Royal Society B: Biological Sciences 286,
876 20191921. https://doi.org/10.1098/rspb.2019.1921
877 Martin, L.F., Krause, L., Ulbricht, A., Winkler, D.E., Codron, D., Kaiser, T.M., Müller, J.,
878 Hummel, J., Clauss, M., Hatt, J.-M., Schulz-Kornas, E., this volume. Dental wear at
879 macro- and microscopic scale in rabbits fed diets of different abrasiveness.
880 Palaeogeography, Palaeoclimatology, Palaeoecology.
881 Merceron, G., Blondel, C., De Bonis, L., Koufos, G.D., Viriot, L., 2005. A new method of dental
882 microwear analysis: Application to extant primates and *Ouranopithecus macedoniensis*
883 (Late Miocene of Greece). Palaios 20, 551–561.
884 https://doi.org/10.2110/palo.2004.p04-17
885 Merceron, G., Taylor, S., Scott, R., Chaimanee, Y., Jaeger, J.-J., 2006. Dietary
886 characterization of the hominoid *Khoratpithecus* (Miocene of Thailand): evidence from
887 dental topographic and microwear texture analyses. Naturwissenschaften 93, 329–
888 333. https://doi.org/10.1007/s00114-006-0107-0
889 Merceron, G., Scott, J., Scott, R.S., Geraads, D., Spassov, N., Ungar, P.S., 2009. Folivory or
890 fruit/seed predation for *Mesopithecus*, an earliest colobine from the Late Miocene of
891 Eurasia? Journal of Human Evolution 57, 732–738.
892 https://doi.org/10.1016/j.jhevol.2009.06.009
893 Merceron, G., Escarguel, G., Angibault, J.-M., Verheyden-Tixier, H., 2010. Can dental
894 microwear textures record inter-individual dietary variations? PLoS ONE 5, e9542.
895 https://doi.org/10.1371/journal.pone.0009542
896 Merceron, G., Hofman-Kamińska, E., Kowalczyk, R., 2014. 3D dental microwear texture
897 analysis of feeding habits of sympatric ruminants in the Białowieża Primeval Forest,
898 Poland. Forest Ecology and Management 328, 262–269.
899 https://doi.org/10.1016/j.foreco.2014.05.041
900 Merceron, G., Ramdarshan, A., Blondel, C., Boisserie, J.-R., Brunetiere, N., Francisco, A.,
901 Gautier, D., Milhet, X., Novello, A., Pret, D., 2016. Untangling the environmental from

902 the dietary: dust does not matter. Proceedings of the Royal Society B: Biological
903 Sciences 283, 20161032. https://doi.org/10.1098/rspb.2016.1032
904 Merceron, G., Kallend, A., Francisco, A., Louail, M., Martin, F., Plastiras, C.-F., Thiery, G.,
905 Noûs, C., Boisserie, J.-R., this volume. Further away with dental microwear analysis:
906 food resource partitioning among Plio-Pleistocene monkeys from the Shungura
907 Formation, Ethiopia. Palaeogeography, Palaeoclimatology, Palaeoecology.
908 Norconk, M.A., Veres, M., 2011. Physical properties of fruit and seeds ingested by primate
909 seed predators with emphasis on sakis and bearded sakis. The Anatomical Record
910 294, 2092–2111. https://doi.org/10.1002/ar.21506
911 Nouri Jangi, A., Mortazavi, S.A., Tavakoli, M., Ghanbari, A., Tavakolipour, H., Haghayegh,
912 G.H., 2011. Comparison of mechanical and thermal properties between two varieties
913 of barley (*Hordeum vulgare* L.) grains. Australian Journal of Agricultural Engineering 2,
914 132–139.
915 Percher, A.M., Merceron, G., Nsi Akoue, G., Galbany, J., Romero, A., Charpentier, M.J., 2017.
916 Dental microwear textural analysis as an analytical tool to depict individual traits and
917 reconstruct the diet of a primate. American Journal of Physical Anthropology 165, 123–
918 138. https://doi.org/10.1002/ajpa.23337
919 Peterson, A., Abella, E.F., Grine, F.E., Teaford, M.F., Ungar, P.S., 2018. Microwear textures
920 of *Australopithecus africanus* and *Paranthropus robustus* molars in relation to
921 paleoenvironment and diet. Journal of Human Evolution 119, 42–63.
922 https://doi.org/10.1016/j.jhevol.2018.02.004
923 Phillips, B.D., Metz, W.C., Nieves, L.A., 2005. Disaster threat: Preparedness and potential
924 response of the lowest income quartile. Global Environmental Change Part B:
925 Environmental Hazards 6, 123–133. https://doi.org/10.1016/j.hazards.2006.05.001
926 Plavcan, J.M., Cope, D.A., 2001. Metric variation and species recognition in the fossil record.
927 Evolutionary Anthropology 10, 204–222. https://doi.org/10.1002/evan.20001
928 Potts, R., 2004. Paleoenvironmental basis of cognitive evolution in great apes. American
929 Journal of Primatology 62, 209–228. https://doi.org/10.1002/ajp.20016

930 Ragni, A.J., Teaford, M.F., Ungar, P.S., 2017. A molar microwear texture analysis of pitheciid
931 primates. American Journal of Primatology 79, e22697.
932 https://doi.org/10.1002/ajp.22697
933 Ramdarshan, A., Alloing-Séguier, T., Merceron, G., Marivaux, L., 2011. The primate
934 community of Cachoeira (Brazilian Amazonia): A model to decipher ecological
935 partitioning among extinct species. PLoS ONE 6, e27392.
936 https://doi.org/10.1371/journal.pone.0027392
937 Ramdarshan, A., Blondel, C., Brunetière, N., Francisco, A., Gautier, D., Surault, J., Merceron,
938 G., 2016. Seeds, browse, and tooth wear: a sheep perspective. Ecology and Evolution
939 6, 5559–5569. https://doi.org/10.1002/ece3.2241
940 Ramdarshan, A., Blondel, C., Gautier, D., Surault, J., Merceron, G., 2017. Overcoming
941 sampling issues in dental tribology: Insights from an experimentation on sheep.
942 Palaeontologia Electronica 20, 1–19. https://doi.org/10.26879/762
943 Remis, M.J., 2002. Food preferences among captive western gorillas (*Gorilla gorilla gorilla*)
944 and chimpanzees (*Pan troglodytes*). International Journal of Primatology 23, 231–249.
945 https://doi.org/10.1023/A:1013837426426
946 Robinson, B.W., Wilson, D.S., 1998. Optimal foraging, specialization, and a solution to Liem's
947 paradox. The American Naturalist 151, 223–235. https://doi.org/10.1086/286113
948 Robinson, J.T., 1954. Prehominid dentition and hominid evolution. Evolution 8, 324–334.
949 https://doi.org/10.1111/j.1558-5646.1954.tb01499.x
950 Rolett, B.V., Chiu, M., 1994. Age estimation of prehistoric pigs (*Sus scrofa*) by molar eruption
951 and attrition. Journal of Archaeological Science 21, 377–386.
952 https://doi.org/10.1006/jasc.1994.1036
953 Romero, A., Galbany, J., Juan, J.D., Pérez-Pérez, A., 2012. Brief communication: Short- and
954 long-term in vivo human buccal–dental microwear turnover. American Journal of
955 Physical Anthropology 148, 467–472. https://doi.org/10.1002/ajpa.22054

Sayers, K., 2013. On folivory, competition, and intelligence: generalisms, overgeneralizations, and models of primate evolution. Primates 54, 111–124. https://doi.org/10.1007/s10329-012-0335-1

Schubert, B.W., Ungar, P.S., DeSantis, L.R.G., 2010. Carnassial microwear and dietary behaviour in large carnivorans: Carnivoran dental microwear. Journal of Zoology 280, 257–263. https://doi.org/10.1111/j.1469-7998.2009.00656.x

Schulz-Kornas, E., Stuhlträger, J., Clauss, M., Wittig, R.M., Kupczik, K., 2019. Dust affects chewing efficiency and tooth wear in forest dwelling Western chimpanzees (*Pan troglodytes verus*). American Journal of Physical Anthropology 169, 66–77. https://doi.org/10.1002/ajpa.23808

Schulz-Kornas, E., Winkler, D.E., Clauss, M., Carlsson, J., Ackermans, N.L., Martin, L.F., Hummel, J., Müller, D.W.H., Hatt, J.-M., Kaiser, T.M., 2020. Everything matters: Molar microwear texture in goats (*Capra aegagrus hircus*) fed diets of different abrasiveness. Palaeogeography, Palaeoclimatology, Palaeoecology 552, 109783. https://doi.org/10.1016/j.palaeo.2020.109783

Scott, R.S., Ungar, P.S., Bergstrom, T.S., Brown, C.A., Grine, F.E., Teaford, M.F., Walker, A., 2005. Dental microwear texture analysis shows within-species diet variability in fossil hominins. Nature 436, 693–695. https://doi.org/10.1038/nature03822

Scott, R.S., Ungar, P.S., Bergstrom, T.S., Brown, C.A., Childs, B.E., Teaford, M.F., Walker, A., 2006. Dental microwear texture analysis: technical considerations. Journal of Human Evolution 51, 339–349. https://doi.org/10.1016/j.jhevol.2006.04.006

Scott, R.S., Teaford, M.F., Ungar, P.S., 2012. Dental microwear texture and anthropoid diets. American Journal of Physical Anthropology 147, 551–579. https://doi.org/10.1002/ajpa.22007

Solounias, N., Semprebon, G., 2002. Advances in the reconstruction of ungulate ecomorphology with application to early fossil equids. American Museum Novitates 3366, 1–49

983 Souron, A., 2017. Diet and Ecology of Extant and Fossil Wild Pigs, in: Melletti, M., Meijaard,
984 E. (Eds.), Ecology, Conservation and Management of Wild Pigs and Peccaries.
985 Cambridge University Press, pp. 29–38. https://doi.org/10.1017/9781316941232.005
986 Souron, A., Merceron, G., Blondel, C., Brunetière, N., Colyn, M., Hofman-Kamińska, E.,
987 Boisserie, J.-R., 2015. Three-dimensional dental microwear texture analysis and diet
988 in extant Suidae (Mammalia: Cetartiodactyla). Mammalia 79, 279–291.
989 https://doi.org/10.1515/mammalia-2014-0023
990 Sponheimer, M., Passey, B.H., de Ruiter, D.J., Guatelli-Steinberg, D., Cerling, T.E., Lee-
991 Thorp, J.A., 2006. Isotopic evidence for dietary variability in the early hominin
992 *Paranthropus robustus*. Science 314, 980–982.
993 https://doi.org/10.1126/science.1133827
994 Strait, D.S., Weber, G.W., Neubauer, S., Chalk, J., Richmond, B.G., Lucas, P.W., Spencer,
995 M.A., Schrein, C., Dechow, P.C., Ross, C.F., Grosse, I.R., Wright, B.W., Constantino,
996 P., Wood, B.A., Lawn, B., Hylander, W.L., Wang, Q., Byron, C., Slice, D.E., Smith, A.L.,
997 2009. The feeding biomechanics and dietary ecology of *Australopithecus africanus*.
998 Proceedings of the National Academy of Sciences 106, 2124–2129.
999 https://doi.org/10.1073/pnas.0808730106
1000 Teaford, M.F., Oyen, O.J., 1989. In vivo and in vitro turnover in dental microwear. American
1001 Journal of Physical Anthropology 80, 447–460.
1002 https://doi.org/10.1002/ajpa.1330800405
1003 Teaford, M.F., Robinson, J.G., 1989. Seasonal or ecological differences in diet and molar
1004 microwear in *Cebus nigrivittatus*. American Journal of Physical Anthropology 80, 391–
1005 401. https://doi.org/10.1002/ajpa.1330800312
1006 Teaford, M.F., Runestad, J.A., 1992. Dental microwear and diet in Venezuelan primates.
1007 American Journal of Physical Anthropology 88, 347–364.
1008 https://doi.org/10.1002/ajpa.1330880308

1009 Teaford, M.F., Ungar, P.S., Taylor, A.B., Ross, C.F., Vinyard, C.J., 2017. In vivo rates of dental
1010 microwear formation in laboratory primates fed different food items. Biosurface and
1011 Biotribology 3, 166–173. https://doi.org/10.1016/j.bsbt.2017.11.005
1012 Teaford, M.F., Ungar, P.S., Taylor, A.B., Ross, C.F., Vinyard, C.J., 2020. The dental microwear
1013 of hard-object feeding in laboratory *Sapajus apella* and its implications for dental
1014 microwear formation. American Journal of Physical Anthropology 171, 439–455.
1015 https://doi.org/10.1002/ajpa.24000
1016 Tran, T.L., deMan, J.M., Rasper, V.F., 1981. Measurement of corn kernel hardness. Canadian
1017 Institute of Food Science and Technology Journal 14, 42–48.
1018 https://doi.org/10.1016/S0315-5463(81)72675-0
1019 Tucker, A.L., Widowski, T.M., 2009. Normal profiles for deciduous dental eruption in domestic
1020 piglets: Effect of sow, litter, and piglet characteristics. Journal of Animal Science 87,
1021 2274–2281. https://doi.org/10.2527/jas.2008-1498
1022 Tütken, T., Kaiser, T.M., Vennemann, T., Merceron, G., 2013. Opportunistic feeding strategy
1023 for the earliest Old World hypsodont equids: Evidence from stable isotope and dental
1024 wear proxies. PLoS ONE 8, e74463. https://doi.org/10.1371/journal.pone.0074463
1025 Ungar, P., 2002. Reconstructing the Diets of Fossil Primates, in: Plavcan, J.M., Kay, R.F.,
1026 Jungers, W.L., van Schaik, C.P. (Eds.), Reconstructing Behavior in the Primate Fossil
1027 Record. Springer US, Boston, MA, pp. 261–296. https://doi.org/10.1007/978-1-4615-
1028 1343-8_7
1029 Ungar, P., 2004. Dental topography and diets of *Australopithecus afarensis* and early *Homo*.
1030 Journal of Human Evolution 46, 605–622. https://doi.org/10.1016/j.jhevol.2004.03.004
1031 Ungar, P.S., Daegling, D.J., 2013. The Functional Morphology of Jaws and Teeth: Implications
1032 for Understanding Early Hominin Dietary Adaptations, in: Sponheimer, M., Lee-Thorp,
1033 J.A., Reed, K.E., Ungar, P. (Eds.), Early Hominin Paleoecology. University Press of
1034 Colorado, pp. 203–250. https://doi.org/10.5876/9781607322252:c060
1035 Ungar, P.S., Sponheimer, M., 2011. The diets of early hominins. Science 334, 190–193.
1036 https://doi.org/10.1126/science.1207701

1037 Ungar, P.S., Grine, F.E., Teaford, M.F., 2008. Dental microwear and diet of the Plio-
1038 Pleistocene hominin *Paranthropus boisei*. PLoS ONE 3, e2044.
1039 https://doi.org/10.1371/journal.pone.0002044
1040 Ungar, P.S., Krueger, K.L., Blumenschine, R.J., Njau, J., Scott, R.S., 2012. Dental microwear
1041 texture analysis of hominins recovered by the Olduvai Landscape Paleoanthropology
1042 Project, 1995–2007. Journal of Human Evolution 63, 429–437.
1043 https://doi.org/10.1016/j.jhevol.2011.04.006
1044 Ungar, P.S., Abella, E.F., Burgman, J.H.E., Lazagabaster, I.A., Scott, J.R., Delezene, L.K.,
1045 Manthi, F.K., Plavcan, J.M., Ward, C.V., 2017. Dental microwear and Pliocene
1046 paleocommunity ecology of bovids, primates, rodents, and suids at Kanapoi. Journal
1047 of Human Evolution 140, 102315. https://doi.org/10.1016/j.jhevol.2017.03.005
1048 van Casteren, A., Lucas, P.W., Strait, D.S., Michael, S., Bierwisch, N., Schwarzer, N., Al-
1049 Fadhalah, K.J., Almusallam, A.S., Thai, L.A., Saji, S., Shekeban, A., Swain, M.V., 2018.
1050 Evidence that metallic proxies are unsuitable for assessing the mechanics of microwear
1051 formation and a new theory of the meaning of microwear. Royal Society Open Science
1052 5, 171699. https://doi.org/10.1098/rsos.171699
1053 van Casteren, A. van, Wright, E., Kupczik, K., Robbins, M.M., 2019. Unexpected hard-object
1054 feeding in Western lowland gorillas. American Journal of Physical Anthropology 170,
1055 433–438. https://doi.org/10.1002/ajpa.23911
1056 van Casteren, A., Strait, D.S., Swain, M.V., Michael, S., Thai, L.A., Philip, S.M., Saji, S., Al-
1057 Fadhalah, K., Almusallam, A.S., Shekeban, A., McGraw, W.S., Kane, E.E., Wright,
1058 B.W., Lucas, P.W., 2020. Hard plant tissues do not contribute meaningfully to dental
1059 microwear: evolutionary implications. Scientific Reports 10, 582.
1060 https://doi.org/10.1038/s41598-019-57403-w
1061 Ward, J., Mainland, I.L., 1999. Microwear in modern rooting and stall-fed pigs: the potential of
1062 dental microwear analysis for exploring pig diet and management in the past.
1063 Environmental Archaeology 4, 25–32. https://doi.org/10.1179/env.1999.4.1.25

1064 Winkler, D.E., Schulz, E., Calandra, I., Gailer, J.-P., Landwehr, C., Kaiser, T.M., 2013.
1065 Indications for a dietary change in the extinct Bovid genus *Myotragus* (Plio-Holocene,
1066 Mallorca, Spain). Geobios 46, 143–150. https://doi.org/10.1016/j.geobios.2012.10.010
1067 Winkler, D.E., Andrianasolo, T.H., Andriamandimbiarisoa, L., Ganzhorn, J.U.,
1068 Rakotondranary, S.J., Kaiser, T.M., Schulz-Kornas, E., 2016. Tooth wear patterns in
1069 black rats (*Rattus rattus*) of Madagascar differ more in relation to human impact than
1070 to differences in natural habitats. Ecology and Evolution 6, 2205–2215.
1071 https://doi.org/10.1002/ece3.2048
1072 Winkler, D.E., Schulz-Kornas, E., Kaiser, T.M., De Cuyper, A., Clauss, M., Tütken, T., 2019.
1073 Forage silica and water content control dental surface texture in guinea pigs and
1074 provide implications for dietary reconstruction. Proceedings of the National Academy
1075 of Sciences USA 116, 1325–1330. https://doi.org/10.1073/pnas.1814081116
1076 Winkler, D.E., Tütken, T., Schulz-Kornas, E., Kaiser, T.M., Müller, J., Leichliter, J., Weber, K.,
1077 Hatt, J.-M., Clauss, M., 2020. Shape, size, and quantity of ingested external abrasives
1078 influence dental microwear texture formation in guinea pigs. Proceedings of the
1079 National Academy of Sciences USA 117, 22264–22273.
1080 https://doi.org/10.1073/pnas.2008149117
1081 Winkler, D.E., Schulz-Kornas, E., Kaiser, T.M., Codron, D., Leichliter, J., Hummel, J., Martin,
1082 L.F., Clauss, M., Tütken, T., this volume. The turnover of dental microwear texture:
1083 Testing the “last supper” effect in small mammals in a controlled feeding experiment.
1084 Palaeogeography, Palaeoclimatology, Palaeoecology.
1085 Wood, B., Strait, D., 2004. Patterns of resource use in early *Homo* and *Paranthropus*. Journal
1086 of Human Evolution 46, 119–162. https://doi.org/10.1016/j.jhevol.2003.11.004
1087 Wrangham, R., Cheney, D., Seyfarth, R., Sarmiento, E., 2009. Shallow-water habitats as
1088 sources of fallback foods for hominins. American Journal of Physical Anthropology 140,
1089 630–642. https://doi.org/10.1002/ajpa.21122
1090 Wynn, J.G., Alemseged, Z., Bobe, R., Grine, F.E., Negash, E.W., Sponheimer, M., 2020.
1091 Isotopic evidence for the timing of the dietary shift toward C4 foods in eastern African

Paranthropus. Proceeding of the National Academy of Sciences USA 117, 21978–21984. https://doi.org/10.1073/pnas.2006221117

Xia, J., Zheng, J., Huang, D., Tian, Z.R., Chen, L., Zhou, Z., Ungar, P.S., Qian, L., 2015. New model to explain tooth wear with implications for microwear formation and diet reconstruction. Proceedings of the National Academy of Sciences USA 112, 10669–10672. https://doi.org/10.1073/pnas.1509491112

Yamada, E., Kubo, M.O., Kubo, T., Kohno, N., 2018. Three-dimensional tooth surface texture analysis on stall-fed and wild boars (*Sus scrofa*). PLoS ONE 13, e0204719. https://doi.org/10.1371/journal.pone.0204719

Yamashita, N., 1998. Functional dental correlates of food properties in five Malagasy lemur species. American Journal of Physical Anthropology 106, 169–188. https://doi.org/10.1002/(SICI)1096-8644(199806)106:2<169::AID-AJPA5>3.0.CO;2-L

Zykov, S.V., Kropacheva, Yu.E., Smirnov, N.G., Dimitrova, Yu.V., 2018. Molar microwear of narrow-headed vole (*Microtus gregalis* Pall., 1779) depending on the feed abrasiveness. Doklady Biological Sciences 478, 16–18. https://doi.org/10.1134/S0012496618010052

Table S1. Detailed description of the controlled-feeding experiments per individual. 1: female, 2: uncastrated male, 3: castrated male.

Dietary group	Specimen number	Birth date	Sex	Start of trial (date)	Age at dietary switch (days)	Age at slaughter (days)	Total feeding duration (days)	Feeding duration after dietary switch (days)
Hazelnut	870601	13/12/2018	2	08/04/2019	163	194	78	30
	870603	13/12/2018	2	08/04/2019	163	194	78	30
	870609	13/12/2018	2	08/04/2019	163	194	78	30
	870610	13/12/2018	1	08/04/2019	163	194	78	30
	870645	12/12/2018	1	08/04/2019	164	195	78	30
	870649	12/12/2018	1	08/04/2019	164	195	78	30
Barley	812073	17/06/2018	1	28/07/2018	120	215	174	95
	811925	13/06/2018	3	28/07/2018	124	293	248	169
	812003	15/06/2018	1	28/07/2018	122	291	248	169
	812078	17/06/2018	3	28/07/2018	120	289	248	169
	812031	14/06/2018	3	28/07/2018	123	218	174	95
Corn	812046	14/06/2018	3	28/07/2018	123	218	174	95
	812049	14/06/2018	3	28/07/2018	123	218	174	95
	812068	17/06/2018	1	28/07/2018	120	215	174	95
	811916	13/06/2018	1	28/07/2018	124	293	248	169
	811958	14/06/2018	3	28/07/2018	123	292	248	169
	812020	14/06/2018	1	28/07/2018	123	292	248	169
Base	811924	13/06/2018	3	28/07/2018		219	174	
	812004	15/06/2018	3	28/07/2018		217	174	
	812074	17/06/2018	3	28/07/2018		215	174	
	811949	14/06/2018	1	28/07/2018		292	248	
	812026	14/06/2018	1	28/07/2018		292	248	
	812036	14/06/2018	1	28/07/2018		292	248	
	870614	13/12/2018	2	08/04/2019		194	78	
	870619	13/12/2018	2	08/04/2019		194	78	
	870641	12/12/2018	2	08/04/2019		195	78	
	870623	13/12/2018	1	08/04/2019		229	113	
	870638	12/12/2018	1	08/04/2019		230	113	
	870640	12/12/2018	1	08/04/2019		230	113	

Table S2. Discriminative parameters considered in this study for surface analysis using the routine described in Francisco et al. (2018a, 2018b) (see supplementary materials for detailed descriptions of the parameters).

Parameter	Description	Type
Sa	Arithmetic mean height[1]	Height
Sp	Maximum peak height[1]	
Sq	Root-mean-square-height[1]	
Sv	Maximum pit height[1]	
Ssk	Skewness[1]	
Sku	Kurtosis[1]	
Sdar	Relative area (developed area/projected area, Sdar = Sdr - 1)	
Sm	Mean height	
Smd	Median height	
Rmax	Semi-major axis of the f_{ACF} ellipsis[2]	Spatial
Sal	Autocorrelation length, semi-minor axis of the f_{ACF} ellipsis[1, 2]	
Stri	Rmax/Sal ratio[1, 2]	
b.sl	Highest slope of f_{ACF} at the distance r_s from the origin	
r.sl	b.sl/s.sl ratio	
s.sl	Smallest slope of f_{ACF} at the distance r_s from the origin	
Sh	Percentage of quasi-horizontal faces	Topological

[1]ISO 25178 parameters in their more or less modified form. [2]Because some surfaces exhibit long wavelengths, the default value s = 0.2 is a bit low and the parameter is redefined as the average for s = 0.3, 0.4, and 0.5.

Table S3. Statistics considered in this study for surface analysis using the routine described in Francisco et al. (2018a, 2018b).

Statistic	Description	Statistic category
G	One value per surface	Global
Mean	Mean of *n* values	Central
Median	Median of *n* values	Central
Skw	Skewness of *n* values	Distribution
Kurt	Kurtosis of *n* values	Distribution
min.25	Mean of the 25 % lowest values among *n* values	Dispersion
max.25	Mean of the 25 % highest values among *n* values	Dispersion
fst.25	Value at the first quartile of the distribution of *n* values	Dispersion
lst.25	Value at the third quartile of the distribution of *n* values	Dispersion

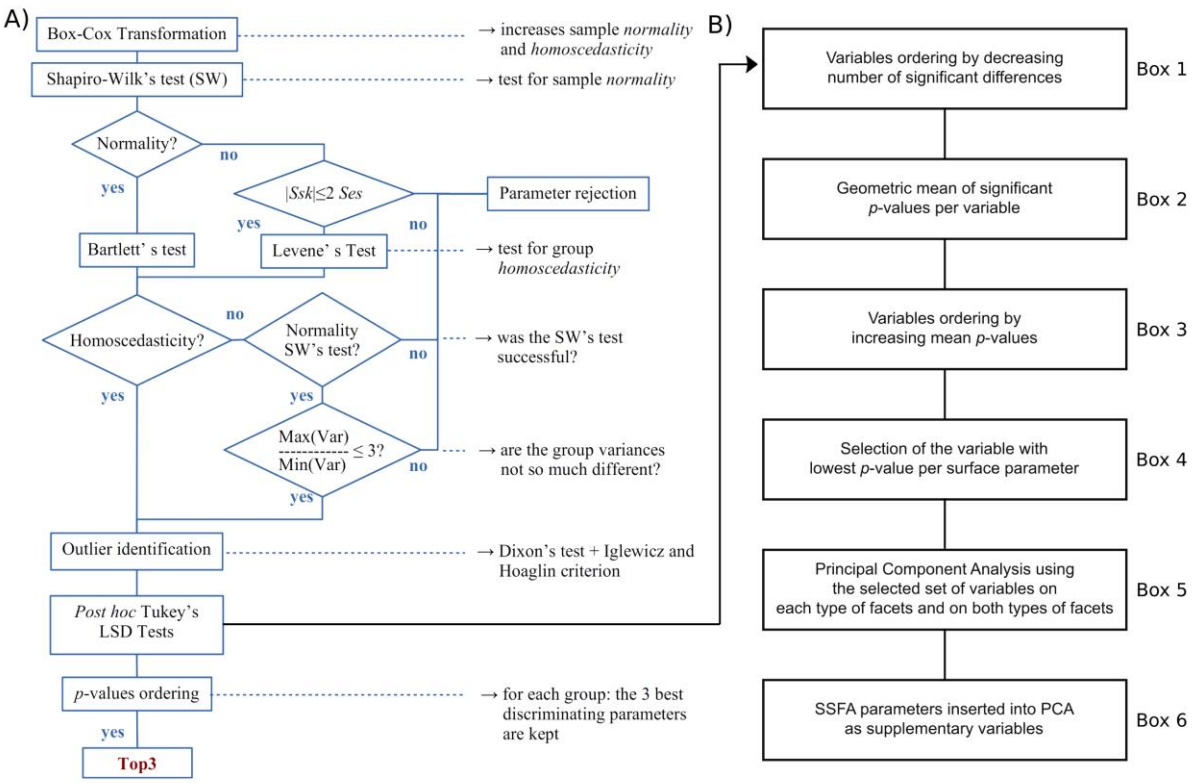

Figure S1. Steps of the procedure developed by Francisco et al. (2018a, 2018b) and implementation (B) made by Merceron et al. (this volume) and in this study. Modified from Francisco et al. (2018b) and Merceron et al. (this volume).

Table S4. Variables per parameter recognized as discriminative among the four lots on lower first molar facets (crushing and shearing) using the routine shown in Francisco et al. (2018a, 2018b).

Phase II (crushing) lower molar facets			Phase I (shearing) lower molar facets		
fst.25_Sh	max.25_Sh	SdaG	fst.25_Sh	max.25_Sku	min.25_Smd
fst.25_Sdar	max.25_Sv	skw_r.sl	fst.25_r.sl	max.25_Sm	min.25_Sp
fst.25_Sku	mea_Sh	skw_Sal	fst.25_Rmax	max.25_Sp	min.25_Sq
ShG	med_Sh	skw_Sp	fst.25_Sa	max.25_Sq	min.25_Stri
kurt_r.sl	med_Sdar	SpG	fst.25_Sal	max.25_Stri	min.25_Sv
kurt_Sp	med_Sv	std_Sh	fst.25_Sdar	max.25_Sv	RmaG
lst.25_Sh	min.25_Sdar	std_r.sl	fst.25_Sm	mea_Sh	SaG
lst.25_Smd	min.25_Sku	std_Sp	fst.25_Smd	mea_r.sl	SalG
lst.25_Sv			fst.25_Sp	mea_Rmax	SdaG
			fst.25_Sq	mea_Sa	SkuG
			fst.25_Stri	mea_Sdar	skw_Sh
			fst.25_Sv	mea_Sp	skw_Rmax
			ShG	mea_Sq	skw_Sa
			kurt_Sh	mea_Stri	skw_Sdar
			kurt_r.sl	mea_Sv	skw_Smd
			kurt_Rmax	med_Sh	skw_Sq
			kurt_Sa	med_r.sl	skw_Ssk
			kurt_Sdar	med_Rmax	skw_Stri
			kurt_Sq	med_Sa	SqG
			kurt_Stri	med_Sal	std_Sh
			lst.25_Sh	med_Sdar	std_Rmax
			lst.25_r.sl	med_Sp	std_Sa
			lst.25_Sa	med_Sq	std_Sal
			lst.25_Sdar	med_Stri	std_Sdar
			lst.25_Sm	med_Sv	std_Sku
			lst.25_Sp	min.25_Sh	std_Sm
			lst.25_Sq	min.25_r.sl	std_Smd
			lst.25_Stri	min.25_Rmax	std_Sp
			lst.25_Sv	min.25_Sa	std_Sq
			max.25_Sh	min.25_Sal	std_Ssk
			max.25_Rmax	min.25_Sdar	std_Stri
			max.25_Sa	min.25_Sm	
			max.25_Sdar		

Table S5. The most discriminative variables per parameters selected from the whole set of variables showing at least one significant difference among the four lots on lower first molar facets (crushing and shearing).

Facet	Variable	Parameter	Type	Statistic	Statistic category
Crushing	SpG	Sp	Height	global	Global
	med_Sh	Sh	Topological	median	Central
	min.25_Sku	Sku	Height	min.25	Dispersion
	min.25_Sdar	Sdar	Height	min.25	Dispersion
	lst.25_Sv	Sv	Height	lst.25	Dispersion
	std_r.sl	r.sl	Spatial	std	Dispersion
	skw_Sal	Sal	Spatial	skewness	Distribution
	lst.25_Smd	Smd	Height	lst.25	Dispersion
Shearing	max.25_Sa	Sa	Height	max.25	Dispersion
	max.25_Sq	Sq	Height	max.25	Dispersion
	fst.25_Sdar	Sdar	Height	fst.25	Dispersion
	max.25_Sp	Sp	Height	max.25	Dispersion
	lst.25_Sh	Sh	Topological	lst.25	Dispersion
	fst.25_Sv	Sv	Height	fst.25	Dispersion
	max.25_Sm	Sm	Height	max.25	Dispersion
	min.25_r.sl	r.sl	Spatial	min.25	Dispersion
	std_Rmax	Rmax	Spatial	standard deviation	Dispersion
	std_Sal	Sal	Spatial	standard deviation	Dispersion
	min.25_Smd	Smd	Height	min.25	Dispersion
	std_Stri	Stri	Spatial	standard deviation	Dispersion
	SkuG	Sku	Height	global	Dispersion
	skw_Ssk	Ssk	Height	skewness	Distribution

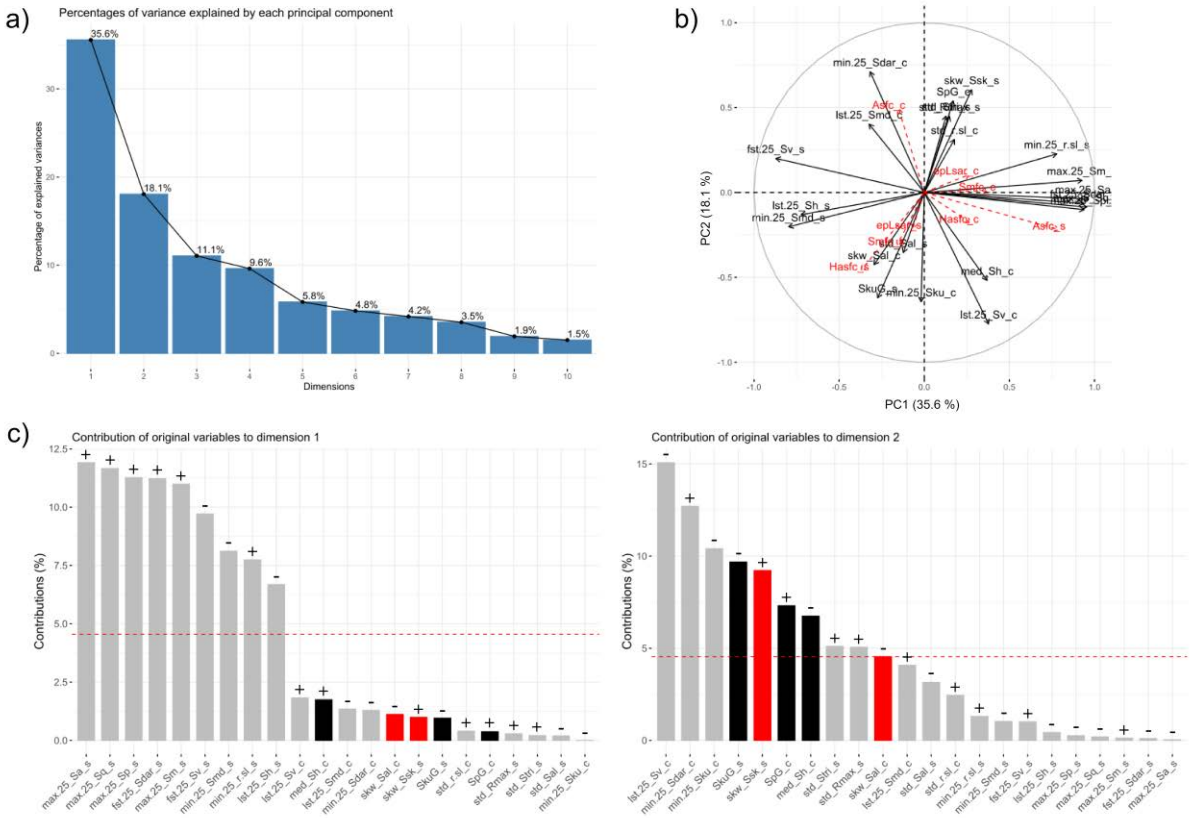

Figure S2. Principal Component Analysis based on the 23 most discriminative variables issued from both crushing (phase II) and shearing (phase I) facets on lower first molars. a) Percentage of variance explained by each principal component. b) Correlation circle between PC1 and PC2 with SSFA-parameters as supplementary variables (dotted red arrows). c) Contribution of each variable to PC1 (left) and PC2 (right) in percentage and direction (positive: +, negative: -). Suffixes "_c" and "_s" refer to crushing and shearing facets, respectively. Black columns: central/global statistic, gray: dispersion statistics, red: distribution statistics. Dotted red line: expected average value if the contributions were uniform; any variable below this line could be considered negligible in contributing to the dimension.

Table S6. Analysis of variances on PC coordinates from PCA on crushing and shearing facets of lower first molars and combined HSD (above diagonal) and LSD (below diagonal) post hoc tests. Only p-values below a 10 % level of significance are given for post hoc tests.

		Df	SS	MS	*F*	*p*
PC1	Effect	3	24.09	8.031	6.95	0.0015
	Residuals	25	28.89	1.156		
PC2	Effect	3	49.23	16.410	3.547	0.0288
	Residuals	25	115.67	4.627		
PC3	Effect	3	0.401	0.1338	0.392	0.76
	Residuals	25	8.535	0.3414		
PC4	Effect	3	8.66	2.886	1.896	0.156
	Residuals	25	38.05	1.522		
PC5	Effect	3	0.768	0.2559	0.223	0.879
	Residuals	25	28.643	1.1457		

HSD / LSD		Hazelnut	Barley	Control	Corn
PC1	Hazelnut		0.0015		
	Barley	0.0003		0.0035	
	Control		0.0007		
	Corn	0.0638	0.0262		
PC2	Hazelnut				0.0691
	Barley				
	Control				0.0275
	Corn	0.0155	0.0245	0.0057	

Table S7. Analysis of variances on PC coordinates from PCA on crushing facets of lower first molars and combined HSD (above diagonal) and LSD (below diagonal) post hoc tests. Only p-values below a 10 % level of significance are given for post hoc tests.

		Df	SS	MS	*F*	*p*
PC1	Effect	3	152.9	50.95	3.014	0.0489
	Residuals	25	422.7	16.91		
PC2	Effect	3	53.37	17.79	3.277	0.0376
	Residuals	25	135.74	5.43		

HSD / LSD		Hazelnut	Barley	Control	Corn
PC1	Hazelnut				
	Barley				0.0489
	Control		0.0805		
	Corn	0.0370	0.0106		
PC2	Hazelnut		0.0370		
	Barley	0.0079			
	Control		0.0361		
	Corn	0.0519			

Table S8. Analysis of variances on PC coordinates from PCA on shearing facets of lower first molars and combined HSD (above diagonal) and LSD (below diagonal) post hoc tests. A Kruskal-Wallis is run on PC2 followed with a Dunn's test. Only p-values below a 10 % level of significance are given for post hoc tests.

ANOVA		Df	SS	MS	*F*	*p*
PC1	Effect	3	43.11	14.37	6.303	0.0025
	Residuals	25	56.99	2.28		

Kruskal-Wallis	Df	χ^2	*p*
PC2	3	10.898	0.0123

HSD / LSD		Hazelnut	Barley	Control	Corn
PC1	Hazelnut		0.0031		
	Barley	0.0006		0.0049	
	Control		0.0009		
	Corn	0.0696	0.0435		

Dunn		Hazelnut	Barley	Control	Corn
PC2	Hazelnut				
	Barley				
	Control	0.0135			
	Corn		0.0190	0.0020	

1167

1168 **Table S9** Variables per parameter recognized as discriminative among the four lots on upper first molar
1169 facets (crushing and shearing) using the routine shown in Francisco et al. (2018a, 2018b).

Phase II (crushing) upper molar facets			**Phase I (shearing) upper molar facets**		
fst.25_Sh	max.25_Sq	min.25_Stri	fst.25_Rmax	max.25_Sku	min.25_Sku
fst.25_Sdar	mea_Sh	min.25_Sv	fst.25_Sa	max.25_Sv	min.25_Smd
fst.25_Stri	mea_r.sl	RmaG	fst.25_Sal	mea_Sa	min.25_Sp
fst.25_Sv	mea_Sa	SaG	fst.25_Sku	mea_Sal	min.25_Sq
ShG	mea_Sdar	SdaG	fst.25_Smd	mea_Sku	min.25_Ssk
kurt_s.sl	mea_Sp	skw_b.sl	fst.25_Sp	mea_Ssk	SaG
lst.25_Sh	mea_Sq	skw_s.sl	fst.25_Sq	med_r.sl	SalG
lst.25_Rmax	mea_Sv	skw_Sa	fst.25_Ssk	med_Rmax	SkuG
lst.25_Sa	med_Sh	skw_Sal	kurt_s.sl	med_Sa	skw_s.sl
lst.25_Sdar	med_Rmax	skw_Sm	kurt_Sa	med_Sal	skw_Sa
lst.25_Sp	med_Sa	SpG	kurt_Sq	med_Sku	skw_Sq
lst.25_Sq	med_Sdar	SqG	lst.25_Rmax	med_Sp	SskG
lst.25_Stri	med_Sp	std_r.sl	lst.25_Sa	med_Sq	std_Sh
lst.25_Sv	med_Sq	std_Sdar	lst.25_Sku	med_Ssk	std_Sal
max.25_r.sl	med_Stri	std_Sp	lst.25_Sq	min.25_Sa	std_Sku
max.25_S	med_Sv	std_Sv	max.25_Sal	min.25_Sal	std_Ssk
max.25_Sdar	min.25_Sh	StrG			
max.25_Sp	min.25_Sdar				

1170

1171

Table S10. The most discriminative variables per parameter are selected from the whole set of variables showing at least one significant difference among the four lots on upper first molar facets (crushing and shearing).

Facet	Variable	Parameter	Type	Statistic	Statistic category
Crushing	med_Stri	Stri	Spatial	median	central
	skw_Sal	Sal	Spatial	skewness	distribution
	skw_b.sl	b.sl	Spatial	skewness	distribution
	skw_s.sl	s.sl	Spatial	skewness	distribution
	med_Sh	Sh	Topological	median	central
	med_Sdar	Sdar	Height	median	central
	RmaG	Rmax	Spatial	global	global
	std_r.sl	r.sl	Spatial	standard deviation	dispersion
	SpG	Sp	Height	global	global
	med_Sv	Sv	Height	median	central
	lst.25_Sq	Sq	Height	lst.25	dispersion
	lst.25_Sa	Sa	Height	lst.25	dispersion
	skw_Sm	Sm	Height	skewness	distribution
Shearing	min.25_Sp	Sp	Height	min.25	dispersion
	min.25_Sq	Sq	Height	min.25	dispersion
	med_Sku	Sku	Height	median	central
	min.25_Sa	Sa	Height	min.25	dispersion
	max.25_Sv	Sv	Height	max.25	dispersion
	fst.25_Rmax	Rmax	Spatial	fst.25	dispersion
	med_Ssk	Ssk	Height	median	central
	SalG	Sal	Spatial	global	global
	skw_s.sl	s.sl	Spatial	skewness	distribution
	med_r.sl	r.sl	Spatial	median	central
	fst.25_Smd	Smd	Height	fst.25	dispersion
	std_Sh	Sh	Topological	standard deviation	dispersion

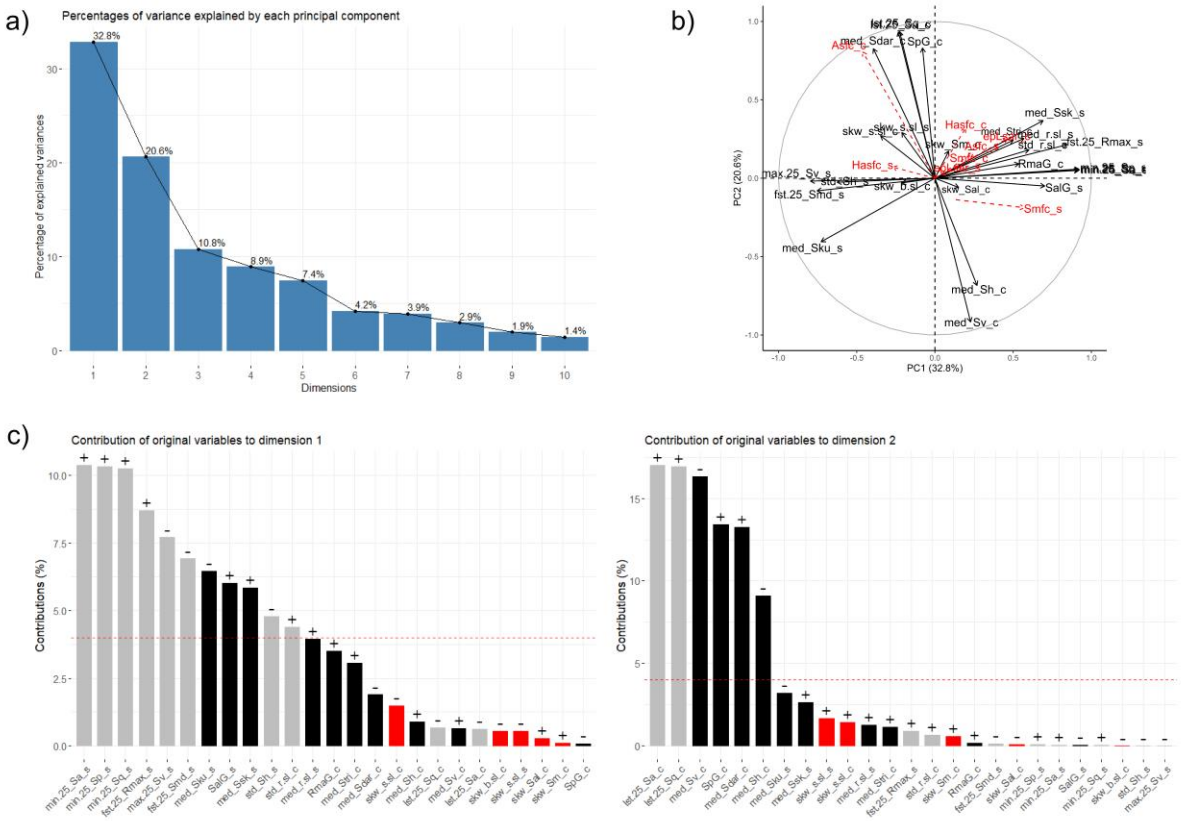

1176

1177 **Figure S3.** Principal Component Analysis based on the 25 most discriminative variables issued from
1178 both crushing (phase II) and shearing (phase I) facets on upper first molars. a) Percentage of variance
1179 explained by each principal component. b) Correlation circle between PC1 and PC2 with SSFA-
1180 parameters as supplementary variables (red dotted arrows). c) Contribution of each variable to PC1
1181 (left) and PC2 (right) in percentage and direction (positive: +, negative: -). Suffixes "_c" and "_s" refer to
1182 crushing and shearing facets, respectively. Black columns: central/global statistic, gray: dispersion
1183 statistics, red: distribution statistics. Dotted red line: expected average value if the contributions were
1184 uniform; any variable below this line could be considered negligible in contributing to the dimension.

1185

1186 **Table S11.** Analysis of variances on PC coordinates from PCA on upper first molars and combined HSD
1187 (above diagonal) and LSD (below diagonal) post hoc tests. Only p-values below a 10 % level of
1188 significance are given for post hoc tests.

		Df	SS	MS	*F*	*p*
PC1	Effect	3	103.3	34.44	6.406	0.0023
	Residuals	25	134.4	5.38		
PC2	Effect	3	19.73	6.577	3.299	0.0368
	Residuals	25	49.84	1.994		
PC3	Effect	3	0.782	0.2607	0.69	0.567
	Residuals	25	9.449	0.3779		
PC4	Effect	3	0.6138	0.2046	1.86	0.162
	Residuals	25	2.7507	0.1100		
PC5	Effect	3	17.92	5.973	1.01	0.405
	Residuals	25	147.84	5.914		

1189

1190

1191

LSD \ HSD		Hazelnut	Barley	Control	Corn
PC1	Hazelnut				0.0022
	Barley				0.0133
	Control				0.0246
	Corn	0.0004	0.0027	0.0051	
PC2	Hazelnut		0.0215		
	Barley	0.0044			
	Control		0.0389		
	Corn		0.0982		

Table S12. Analysis of variances on PC coordinates from PCA on crushing facets of upper first molars and combined HSD (above diagonal) and LSD (below diagonal) post hoc tests. Only p-values below a 10 % level of significance are given for post hoc tests.

		Df	SS	MS	*F*	*p*
PC1	Effect	3	4.829	1.6096	4.15	0.0162
	Residuals	25	9.696	03878		
PC2	Effect	3	0.9605	03202	4.13	0.0165
	Residuals	25	1.9379	00775		

LSD \ HSD		Hazelnut	Barley	Control	Corn
PC1	Hazelnut		0.0160		0.0570
	Barley	0.0032			
	Control	0.0639	0.0714		
	Corn	0.0126			
PC2	Hazelnut				0.0771
	Barley				0.0171
	Control		0.0377		
	Corn	0.0175	0.0035		

Table S13. Analysis of variances on PC coordinates from PCA on shearing facets of upper first molars and combined HSD (above diagonal) and LSD (below diagonal) post hoc tests. Only p-values below a 10 % level of significance are given for post hoc tests.

		Df	SS	MS	*F*	*p*
PC1	Effect	3	219.2	73.05	4.851	0.0102
	Residuals	21	316.2	15.06		
PC2	Effect	3	6.248	2.083	1.39	0.274
	Residuals	21	31.478	1.499		

LSD \ HSD		Hazelnut	Barley	Control	Corn
PC1	Hazelnut				0.0129
	Barley				0.0231
	Control				0.0500
	Corn	0.0026	0.0048	0.0110	

Table S14. Variables per parameter recognized as discriminative among the four lots on upper fourth deciduous premolar facets (crushing and shearing) using the routine shown in Francisco et al. (2018a, 2018b).

Phase II (crushing) upper premolar facets			Phase I (shearing) upper premolar facets		
fst.25_Sh	max.25_Rmax	min.25_Sm	lst.25_Smd	skw_Sh	skw_Sal
fst.25_r.sl	max.25_Sa	min.25_Smd			
fst.25_Sa	max.25_Sdar	min.25_Sp			
fst.25_Sdar	max.25_Sm	min.25_Sq			
fst.25_Sm	max.25_Smd	min.25_Sv			
fst.25_Sp	max.25_Sp	r.sG			
fst.25_Sq	max.25_Sq	SaG			
fst.25_Sv	max.25_Stri	SdaG			
ShG	max.25_Sv	skw_b.sl			
kurt_b.sl	mea_Sh	skw_Rmax			
kurt_Rmax	mea_r.sl	skw_Sdar			
kurt_Sa	mea_Rmax	skw_Sku			
kurt_Sdar	mea_Sa	skw_Sp			
kurt_Sku	mea_Sdar	skw_Sq			
kurt_Smd	mea_Smd	skw_Stri			
kurt_Sp	mea_Sp	skw_Sv			
kurt_Sq	mea_Sq	SqG			
kurt_Ssk	mea_Stri	std_Sh			
kurt_Stri	mea_Sv	std_r.sl			
lst.25_Sh	med_Sh	std_Rmax			
lst.25_r.sl	med_r.sl	std_Sa			
lst.25_Rmax	med_Sa	std_Sal			
lst.25_Sa	med_Sdar	std_Sdar			
lst.25_Sdar	med_Sp	std_Sm			
lst.25_Sm	med_Sq	std_Smd			
lst.25_Smd	med_Sv	std_Sp			
lst.25_Sp	min.25_Sh	std_Sq			
lst.25_Sq	min.25_r.sl	std_Stri			
lst.25_Stri	min.25_Sa	std_Sv			
lst.25_Sv	min.25_Sal	SvG			
max.25_Sh	min.25_Sdar				
max.25_r.sl					

Table S15. The most discriminative variables per parameter are selected from the whole set of variables showing at least one significant difference among the four lots on fourth upper deciduous premolar facets (crushing and shearing).

Facet	Variable	Parameter	Type	Statistic	Statistic category
Crushing	min.25_Sdar	Sdar	Height	min.25	dispersion
	mea_Sh	Sh	Topological	mean	central
	kurt_Sp	Sp	Height	kurtosis	distribution
	max.25_Sv	Sv	Height	max.25	dispersion
	lst.25_r.sl	r.sl	Spatial	lst.25	dispersion
	fst.25_Sq	Sq	Height	fst.25	dispersion
	fst.25_Sa	Sa	Height	fst.25	dispersion
	std_Sal	Sal	Spatial	standard deviation	dispersion
	lst.25_Stri	Stri	Spatial	lst.25	dispersion
	fst.25_Sm	Sm	Height	fst.25	dispersion
	kurt_Sku	Sku	Height	kurtosis	distribution
	lst.25_Smd	Smd	Height	lst.25	dispersion
	max.25_Rmax	Rmax	Spatial	max.25	dispersion
	kurt_b.sl	b.sl	Spatial	kurtosis	distribution
	kurt_Ssk	Ssk	Height	kurtosis	distribution
Shearing	skw_Sal	Sal	Spatial	skewness	distribution
	lst.25_Smd	Smd	Height	lst.25	dispersion
	skw_Sh	Sh	Topological	skewness	distribution

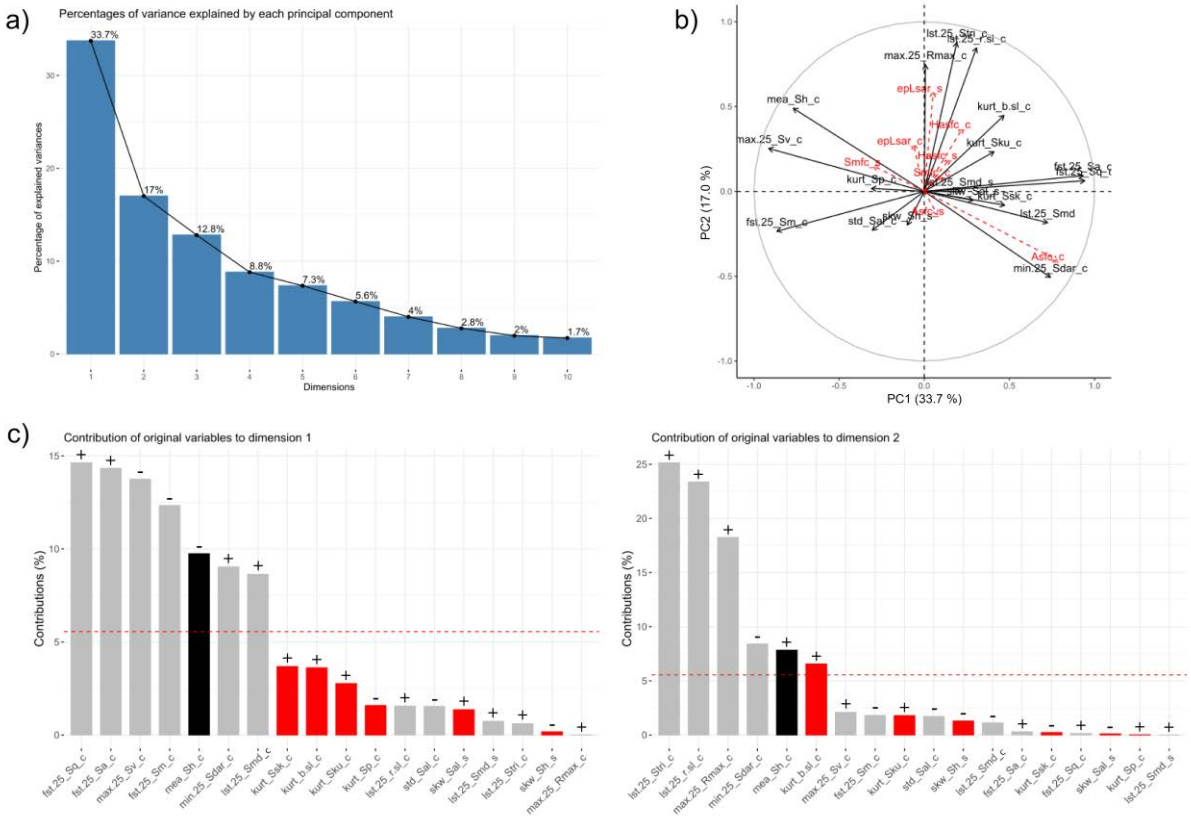

Figure S4. Principal Component Analysis based on the 19 most discriminative variables issued from both crushing (phase II) and shearing (phase I) facets on upper fourth deciduous premolars. a) Percentage of variance explained by each principal component. b) Correlation circle between PC1 and PC2 with SSFA-parameters as supplementary variables (red dotted arrows). c) Contribution of each variable to PC1 (left) and PC2 (right) in percentage and direction (positive: +, negative: -). Suffixes "_c" and "_s" refer to crushing and shearing facets, respectively. Black columns: central/global statistic, gray: dispersion statistics, red: distribution statistics. Dotted red line: expected average value if the contributions were uniform; any variable below this line could be considered negligible in contributing to the dimension.

Table S16. Analysis of variances on PC coordinates from PCA on upper fourth deciduous premolars and combined HSD (above diagonal) and LSD (below diagonal) post hoc tests. A Kruskal-Wallis is run on PC3 followed with a Dunn's test. Only p-values below a 10 % level of significance are given for post hoc tests.

ANOVA		Df	SS	MS	*F*	*p*
PC1	Effect	3	16.92	5.640	8.247	0.0006
	Residuals	24	16.41	0.684		
PC4	Effect	3	1.662	0.5539	0.498	0.687
	Residuals	24	26.708	1.1128		
PC5	Effect	3	2.862	0.9542	1.142	0.352
	Residuals	24	20.052	0.8355		

Kruskal-Wallis	Df	χ^2	*p*
PC2	3	9.8919	0.0195
PC3	3	13.903	0.0030

HSD / LSD		Hazelnut	Barley	Control	Corn
PC1	Hazelnut				
	Barley	0.0267		0.0012	0.0010
	Control	0.0840	0.0002		
	Corn	0.0432	0.0002		

Dunn		Hazelnut	Barley	Control	Corn
PC2	Hazelnut				
	Barley	0.0018			
	Control	0.0055			
	Corn	0.0209			
PC3	Hazelnut				
	Barley	0.0017			
	Control		0.0130		
	Corn	0.0014		0.0119	

Table S17. Analysis of variances on PC coordinates from PCA on crushing facets of upper fourth deciduous premolars and combined HSD (above diagonal) and LSD (below diagonal) post hoc tests. Only p-values below a 10 % level of significance are given for post hoc tests.

		Df	SS	MS	*F*	*p*
PC1	Effect	3	21.25	7.082	7.539	0.0010

	Residuals	24	22.55	0.939		
PC2	Effect	3	3.836	1.2785	3.999	0.0192
	Residuals	24	7.673	0.3197		
PC3	Effect	3	4.48	1.4935	2.641	0.0724
	Residuals	24	13.57	0.5654		

1236

LSD \ HSD		Hazelnut	Barley	Control	Corn
PC1	Hazelnut				
	Barley	0.0476		0.0023	0.0017
	Control	0.0785	0.0004		
	Corn	0.0358	0.0003		
PC2	Hazelnut		0.0302	0.0691	0.0373
	Barley	0.0064			
	Control	0.0156			
	Corn	0.0080			
PC3	Hazelnut				
	Barley				
	Control				0.0875
	Corn	0.0592		0.0202	

1237

1238 **Table S18.** Analysis of variances on PC coordinates from PCA on shearing facets of upper fourth
1239 deciduous premolars and combined HSD (above diagonal) and LSD (below diagonal) post hoc tests.
1240 Only p-values below a 10 % level of significance are given for post hoc tests.

		Df	SS	MS	*F*	*p*
PC1	Effect	3	5.242	1.7473	2.481	0.0843
	Residuals	25	17.607	0.7043		
PC3	Effect	3	1.437	0.4789	2.202	0.1130
	Residuals	25	5.438	0.2175		

1241

1242

LSD \ HSD		Hazelnut	Barley	Control	Corn
PC1	Hazelnut				0.0847
	Barley				
	Control				
	Corn	0.0194		0.0346	
PC3	Hazelnut				
	Barley	0.0798		0.0852	
	Control		0.0195		
	Corn		0.0563		

1243

1244

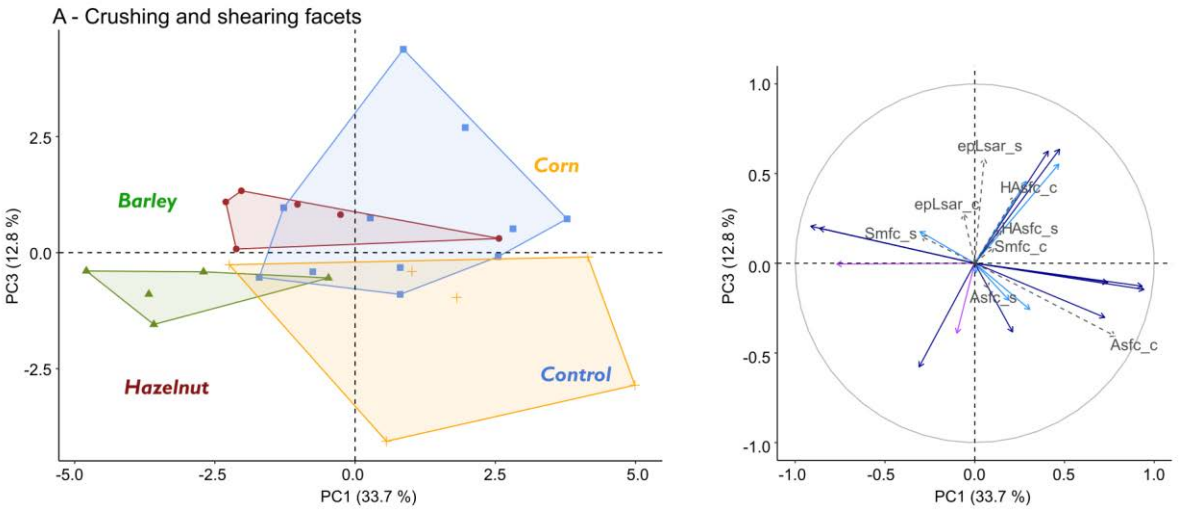

Figure S5. Distribution of individuals (left) and correlation circle (right) along PC1 and PC3 of the four dietary groups on both crushing and shearing facets of upper deciduous premolars. Dietary groups: ●: 100 % base flours +10 hazelnuts in shell a day, ▲: 70 % base flours + 30 % barley seeds, +: 60 % base flours + 20 % corn flour + 20 % corn kernels, ■: 100 % base flours. Active variables (filled arrows): height (dark blue), spatial (light blue), and topological (purple) parameters. SSFA parameters added as supplementary variables (gray dotted arrows). Suffixes "_c": crushing facets, "_s": shearing facets.

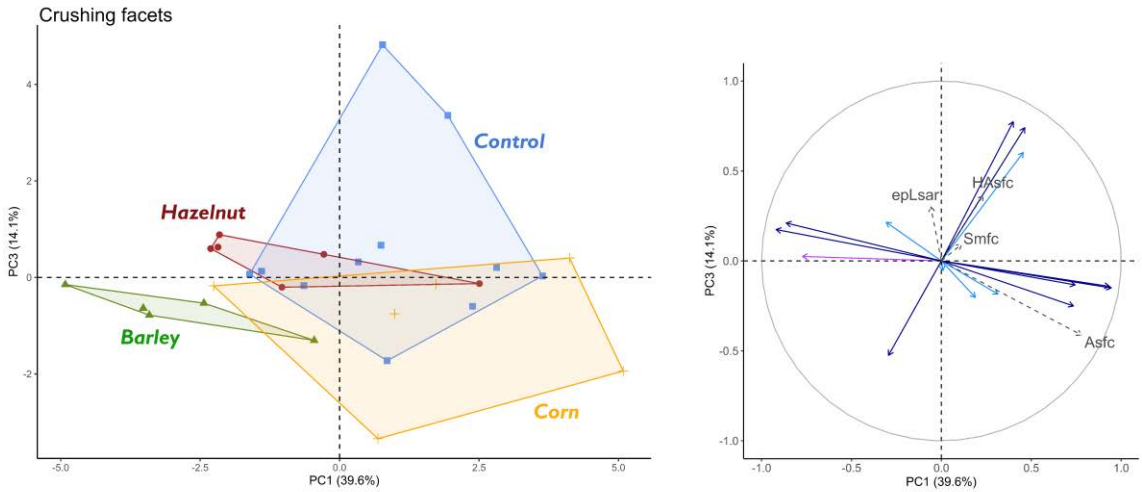

Figure S6. Distribution of individuals (left) and correlation circle (right) along PC1 and PC3 of the four dietary groups on crushing facets of upper deciduous premolars. Dietary groups: ●: 100 % base flours +10 hazelnuts in shell a day, ▲: 70 % base flours + 30 % barley seeds, +: 60 % base flours + 20 % corn flour + 20 % corn kernels, ■: 100 % base flours. Active variables (filled arrows): height (dark blue), spatial (light blue) and topological (purple) parameters. SSFA parameters added as supplementary variables (gray dotted arrows).

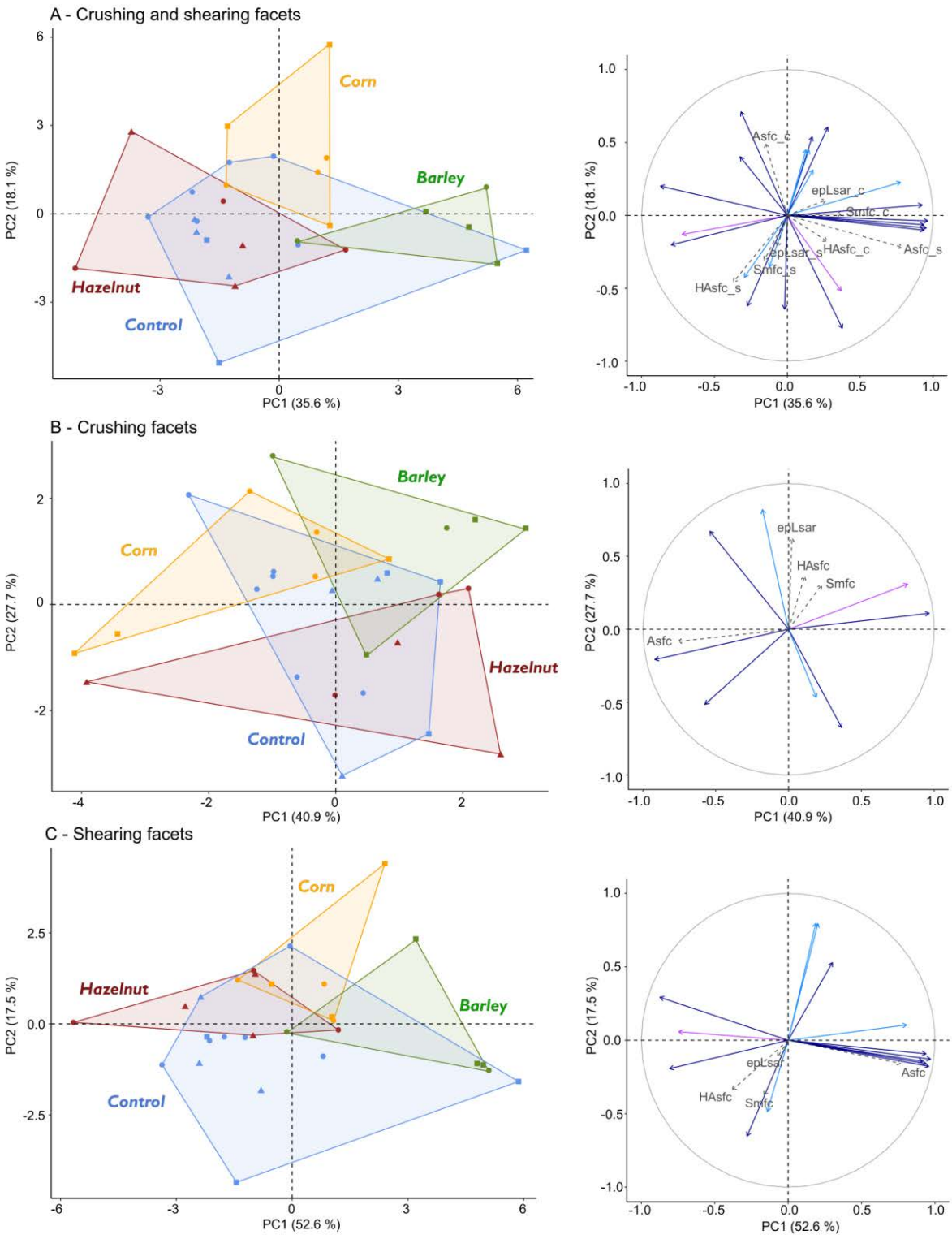

Figure **S7**. Distributions of individuals (left) and correlation circle (right) along PC1 and PC2 of the four dietary groups on both crushing and shearing lower first molar facets (A), on crushing facets alone (B), and on shearing facets alone (C). Dietary groups: 100 % base flours + 10 hazelnuts in shell a day (red), 70 % base flours + 30 % barley seeds (green), 60 % base flours + 20 % corn flour + 20 % corn kernels (yellow), 100 % base flours (blue). Sexes: ●: females, ▲: uncastrated males, ■: castrated males. Active variables (filled arrows): height (dark blue), spatial (light blue), and topological (purple) parameters. SSFA-parameters added as supplementary variables (gray dotted arrows). Suffixes "_c": crushing facets, "_s": shearing facets.

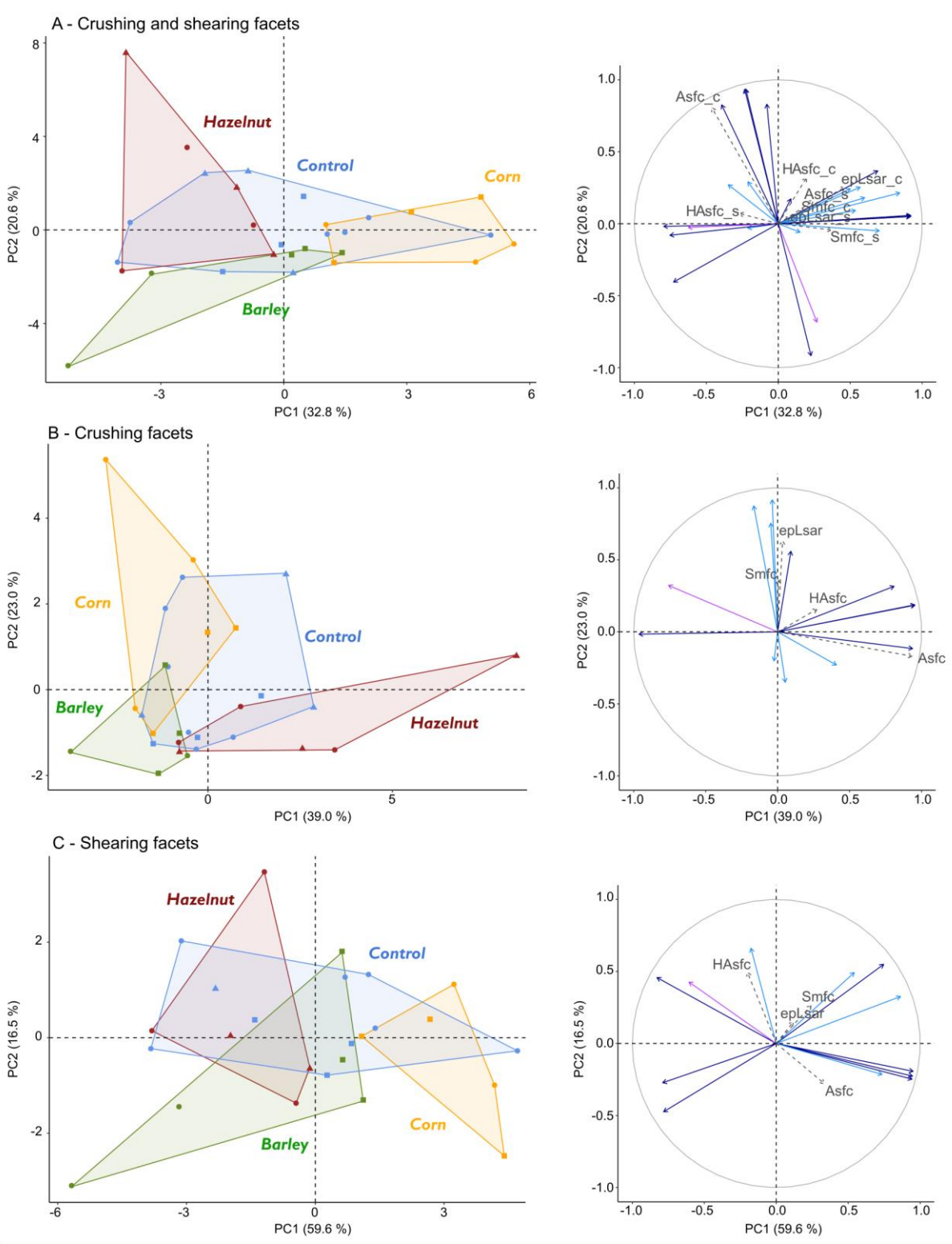

Figure **S8**. Distributions of individuals (left) and correlation circle (right) along PC1 and PC2 of the four dietary groups on both crushing and shearing upper first molar facets (A), on crushing facets alone (B), and on shearing facets alone (C). Dietary groups: 100 % base flours + 10 hazelnuts in shell a day (red), 70 % base flours + 30 % barley seeds (green), 60 % base flours + 20 % corn flour + 20 % corn kernels (yellow), 100 % base flours (blue). Sexes: ●: females, ▲: uncastrated males, ■: castrated males. Active variables (filled arrows): height (dark blue), spatial (light blue), and topological (purple) parameters. SSFA-parameters added as supplementary variables (gray dotted arrows). Suffixes "_c": crushing facets, "_s": shearing facets.

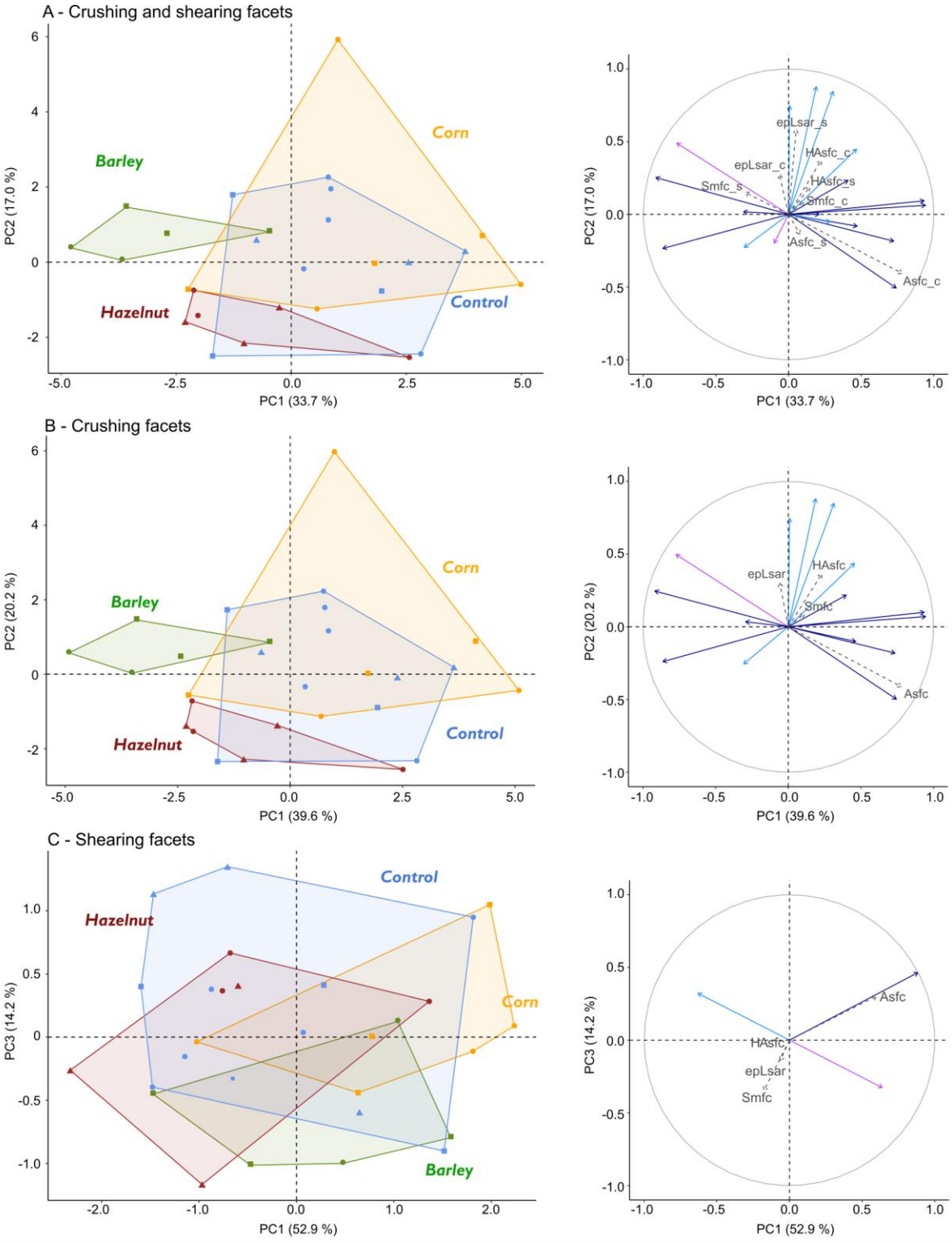

Figure **S9**. Distributions of individuals (left) and correlation circle (right) along PC1 and PC2 of the four dietary groups on both crushing and shearing upper fourth deciduous premolar facets (A), on crushing facets alone (B), and on shearing facets alone (C). Dietary groups: 100 % base flours + 10 hazelnuts in shell a day (red), 70 % base flours + 30 % barley seeds (green), 60 % base flours + 20 % corn flour + 20 % corn kernels (yellow), 100 % base flours (blue). Sexes: ●: females, ▲: uncastrated males, ■: castrated males. Active variables (filled arrows): height (dark blue), spatial (light blue), and topological (purple) parameters. SSFA-parameters added as supplementary variables (gray dotted arrows). Suffixes "_c": crushing facets, "_s": shearing facets.

Appendix 1

Photosimulations and false color elevation maps of scanned shearing and crushing facets on first lower and upper molars and on upper fourth deciduous premolars of the four dietary groups: control, hazelnut, barley and corn.

Photosimulations and false color elevation maps of scanned shearing and crushing facets on molars and deciduous premolars of the **control group** (100% flours)

scanned at the PALEVOPRIM lab by M. Louail, University of Poitiers, France with "TRIDENT", white light confocal microscope Leica DCM8 - April 2020
ALIHOM Project (Région Nouvelle Aquitaine, France), ANR Diet-Scratches

DIET-SCRATCHES

ANR-17-CE27-0002
PIs: G. Merceron & S. Ferchaud

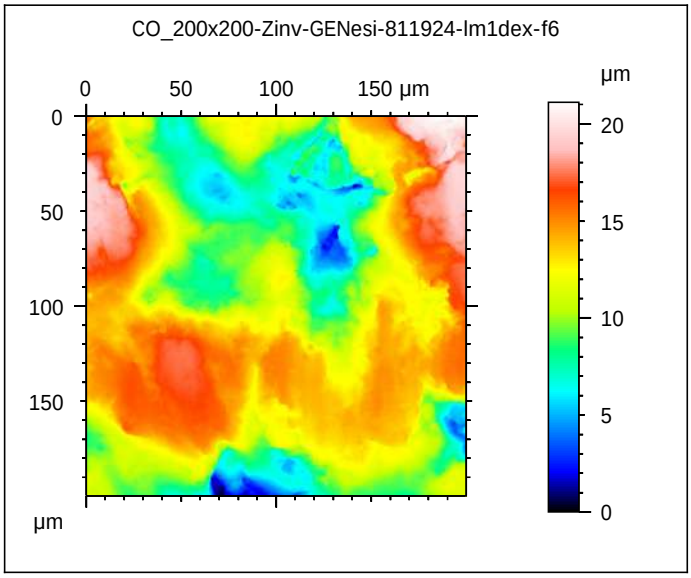

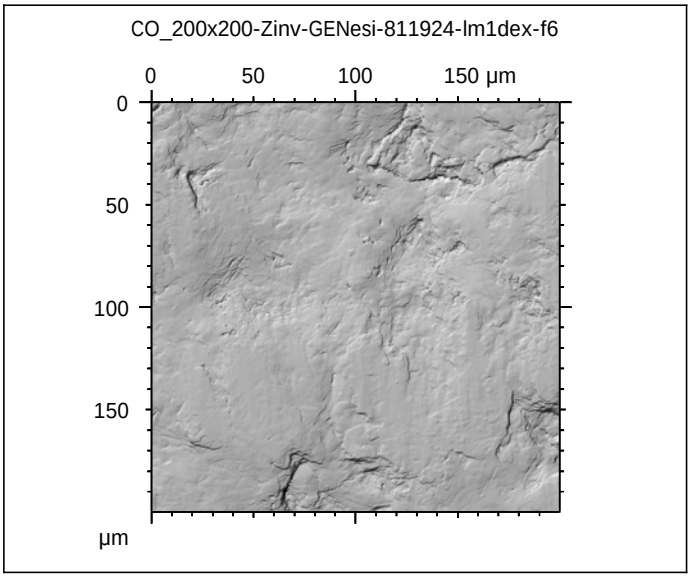

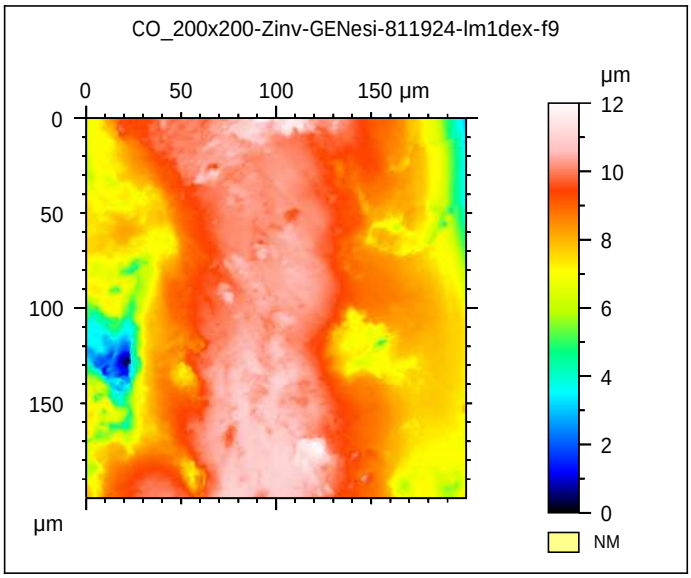

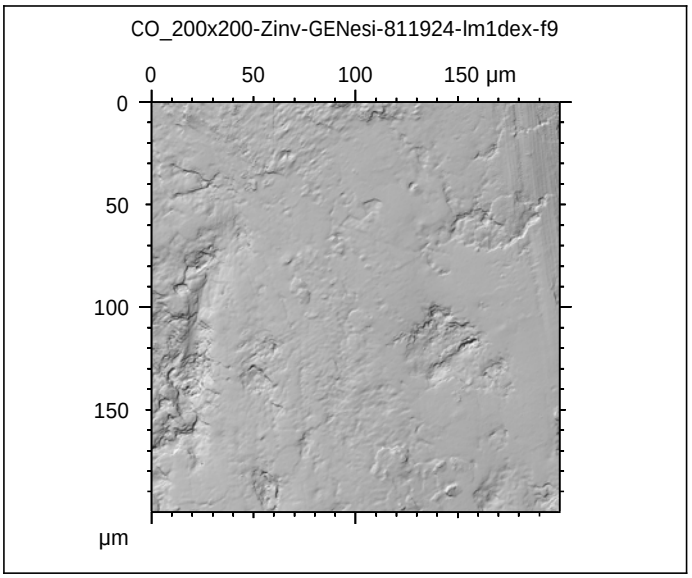

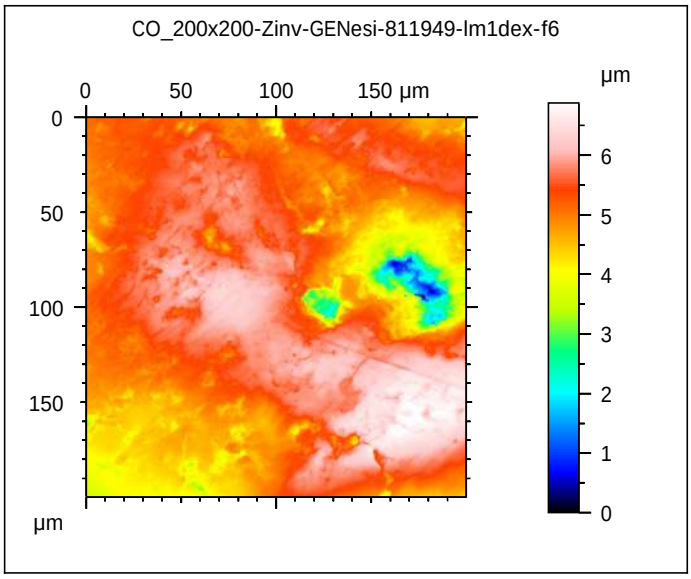

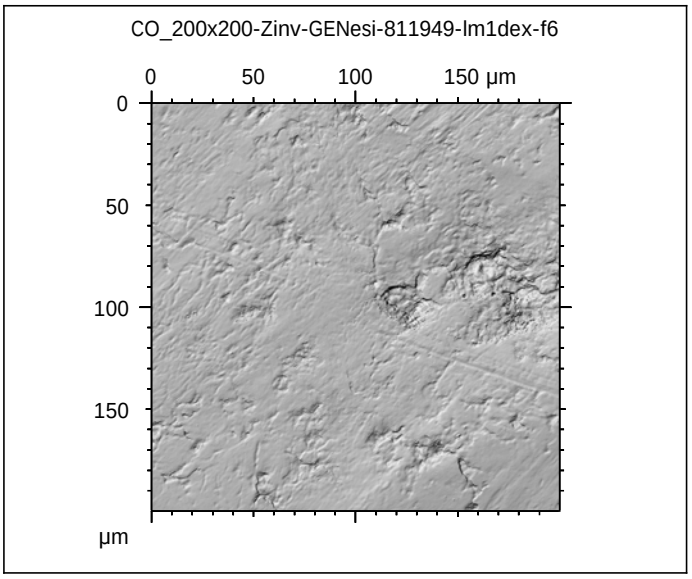

Leica Map Premium 8.0.9173

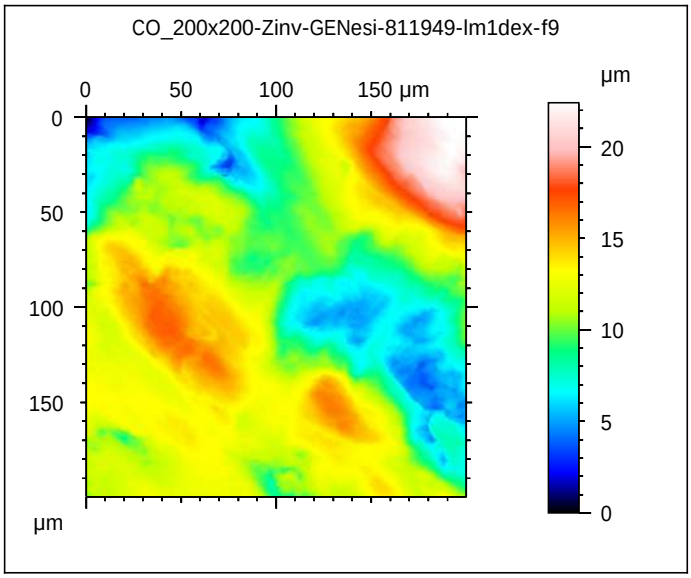
CO_200x200-Zinv-GENesi-811949-lm1dex-f9
0
50
100
150 µm
µm
20
15
10
5
0

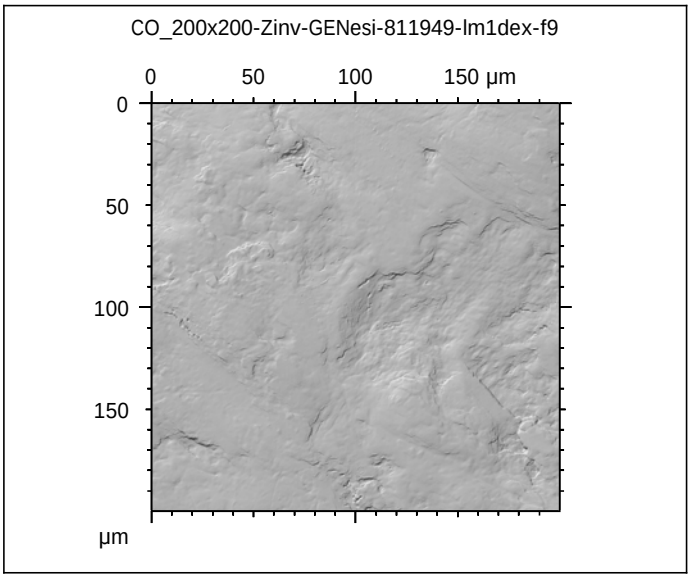
CO_200x200-Zinv-GENesi-811949-lm1dex-f9
0
50
100
150 µm
µm

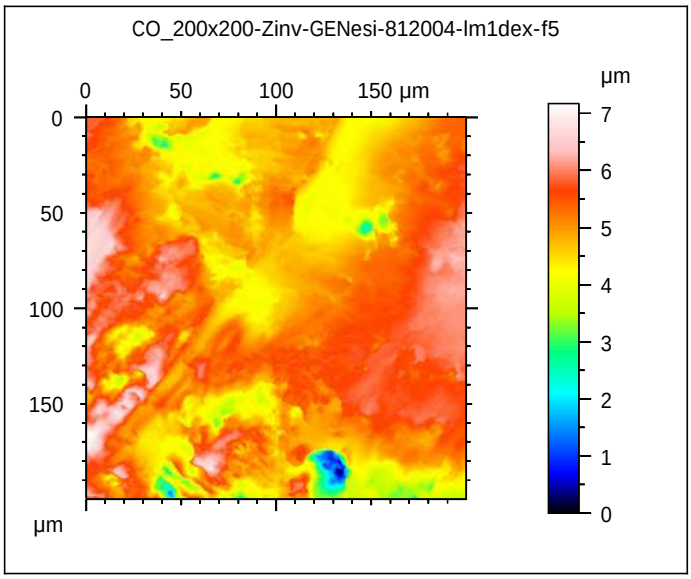
CO_200x200-Zinv-GENesi-812004-lm1dex-f5
0
50
100
150 µm
µm
7
6
5
4
3
2
1
0

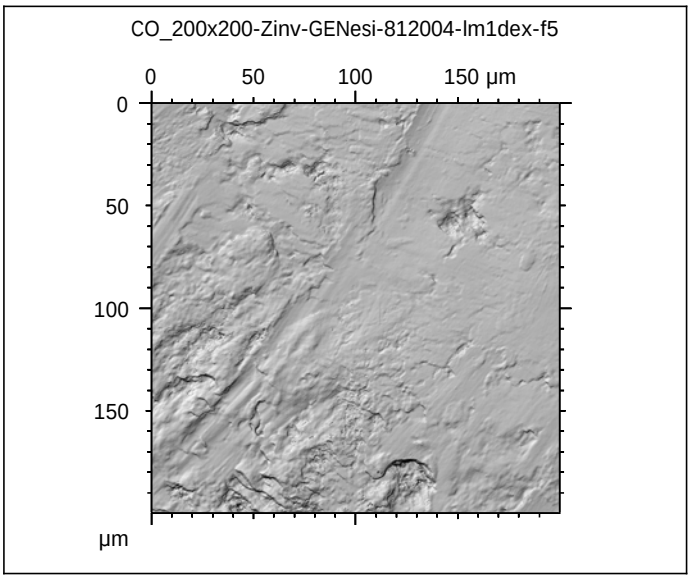
CO_200x200-Zinv-GENesi-812004-lm1dex-f5
0
50
100
150 µm
µm

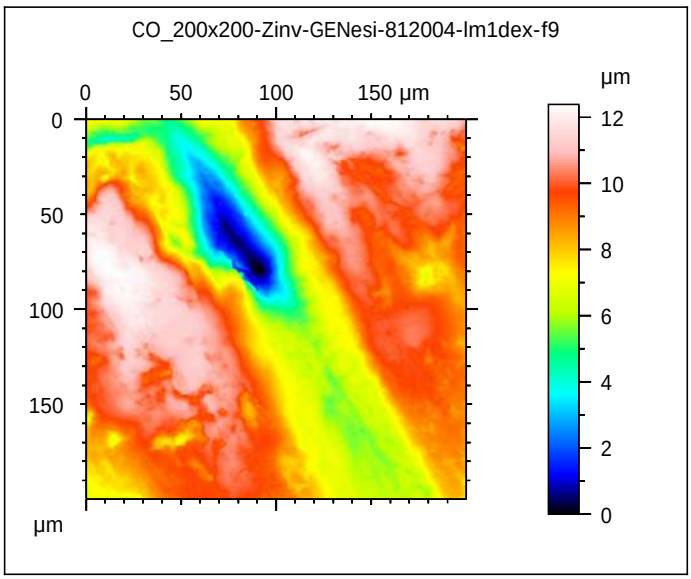
CO_200x200-Zinv-GENesi-812004-lm1dex-f9
0
50
100
150 µm
µm
12
10
8
6
4
2
0

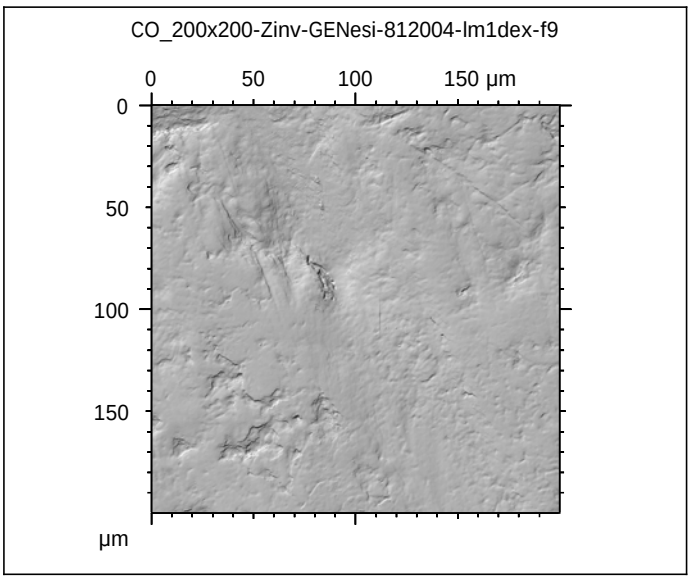
CO_200x200-Zinv-GENesi-812004-lm1dex-f9
0
50
100
150 µm
µm

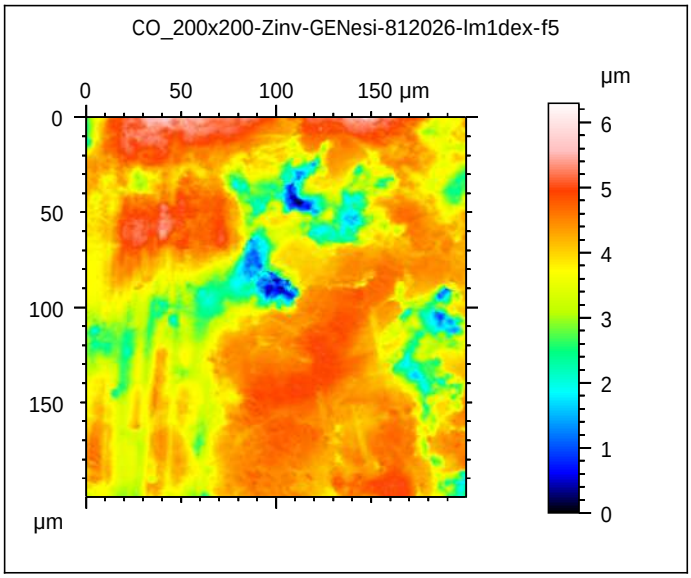
CO_200x200-Zinv-GENesi-812026-lm1dex-f5
0
50
100
150 µm
µm
0
50
100
150
µm
6
5
4
3
2
1
0

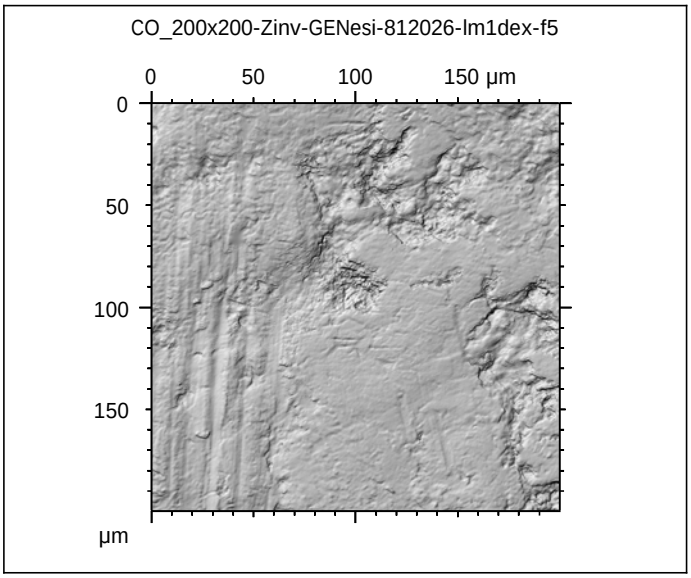
CO_200x200-Zinv-GENesi-812026-lm1dex-f5
0
50
100
150 µm
0
50
100
150
µm

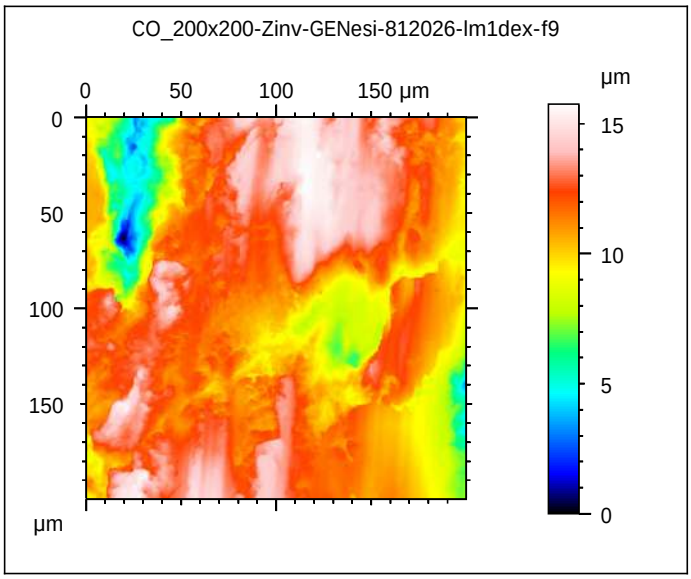
CO_200x200-Zinv-GENesi-812026-lm1dex-f9
0
50
100
150 µm
µm
0
50
100
150
µm
15
10
5
0

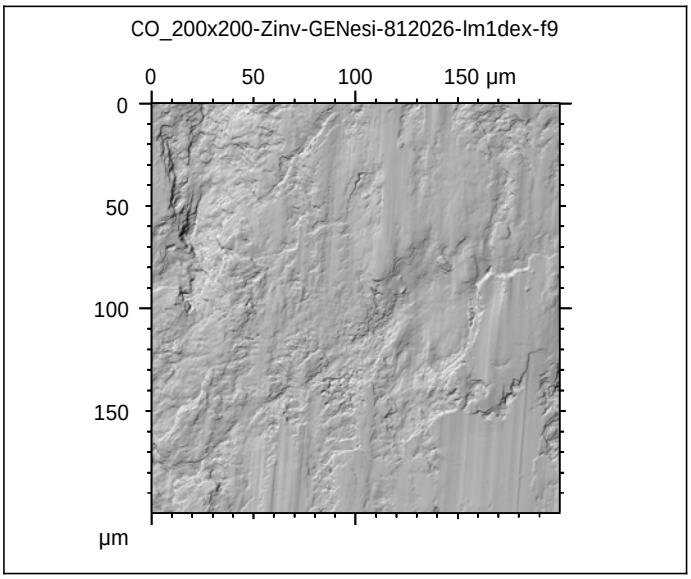
CO_200x200-Zinv-GENesi-812026-lm1dex-f9
0
50
100
150 µm
0
50
100
150
µm

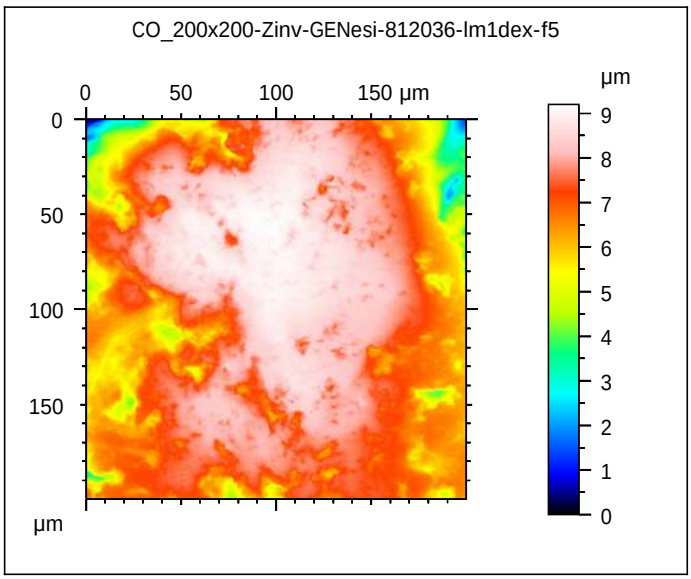
CO_200x200-Zinv-GENesi-812036-lm1dex-f5
0
50
100
150 µm
µm
0
50
100
150
µm
9
8
7
6
5
4
3
2
1
0

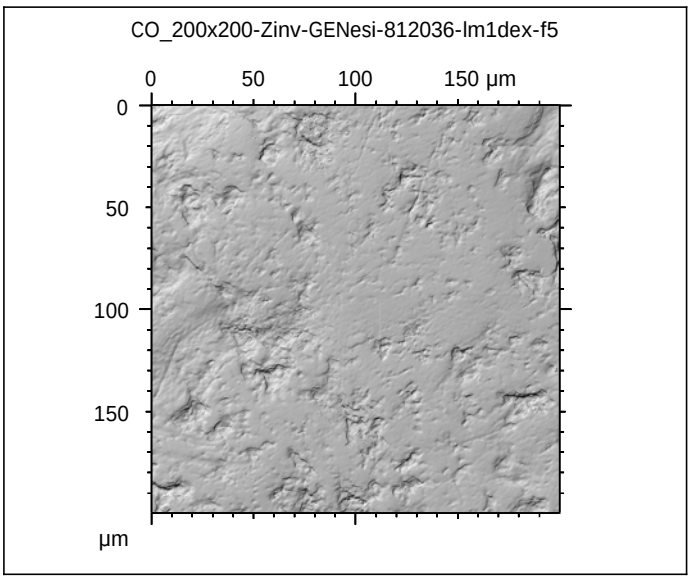
CO_200x200-Zinv-GENesi-812036-lm1dex-f5
0
50
100
150 µm
0
50
100
150
µm

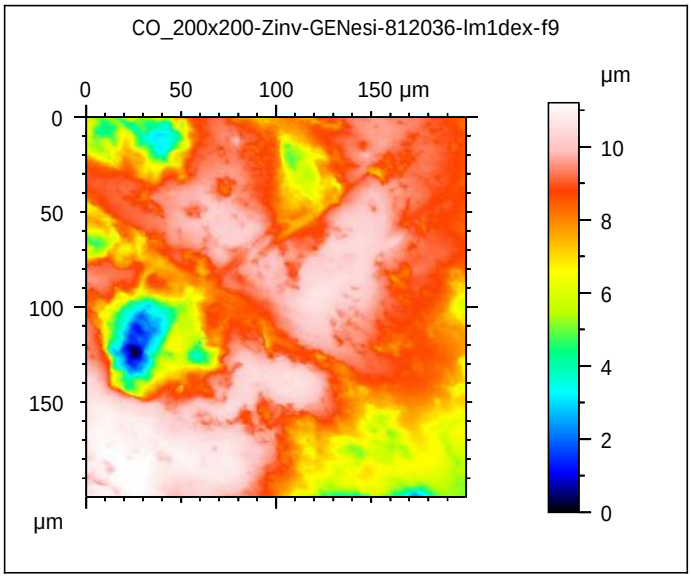
CO_200x200-Zinv-GENesi-812036-lm1dex-f9
0
50
100
150 µm
µm
0
50
100
150
µm
10
8
6
4
2
0

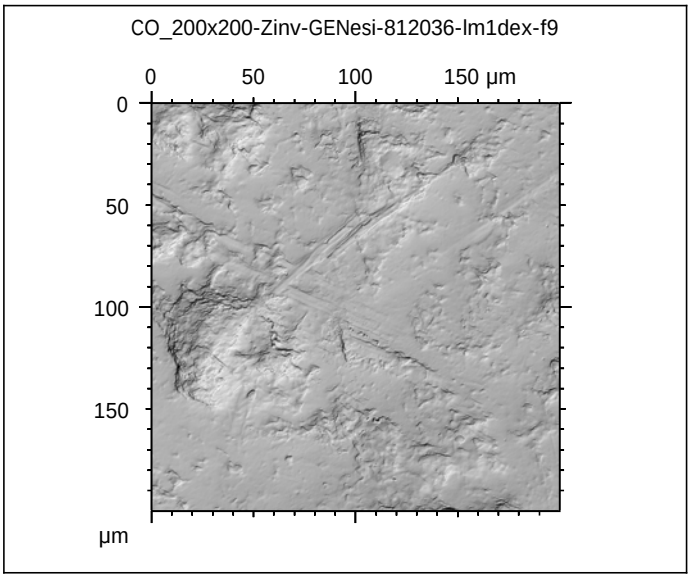
CO_200x200-Zinv-GENesi-812036-lm1dex-f9
0
50
100
150 µm
0
50
100
150
µm

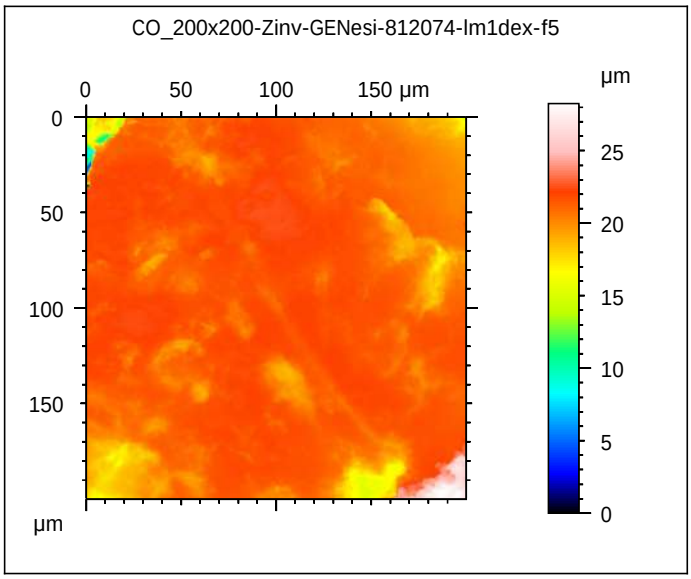
CO_200x200-Zinv-GENesi-812074-lm1dex-f5
0
50
100
150 µm
µm
0
50
100
150
µm
25
20
15
10
5
0

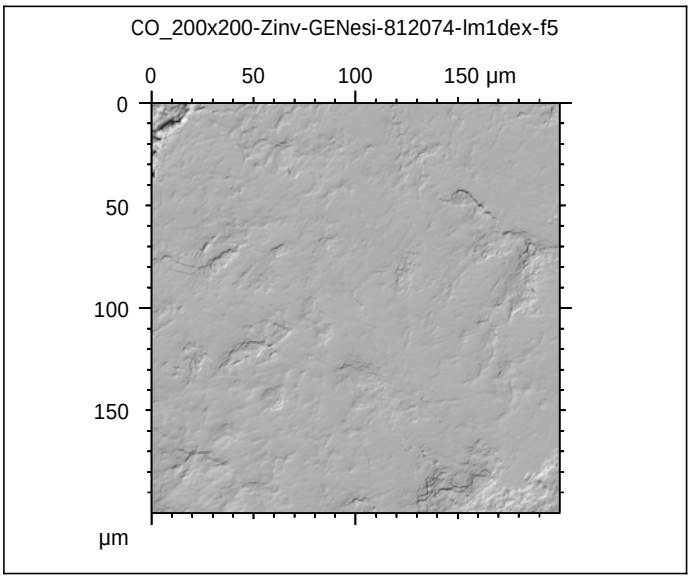
CO_200x200-Zinv-GENesi-812074-lm1dex-f5
0
50
100
150 µm
0
50
100
150
µm

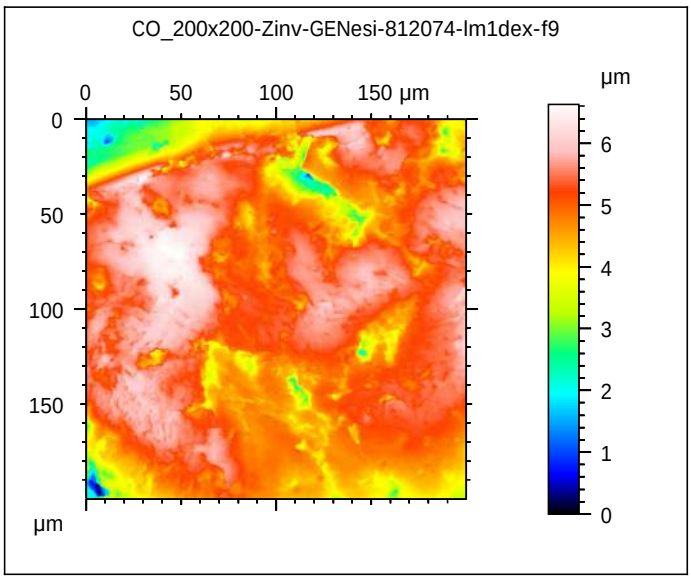
CO_200x200-Zinv-GENesi-812074-lm1dex-f9
0
50
100
150 µm
µm
0
50
100
150
µm
6
5
4
3
2
1
0

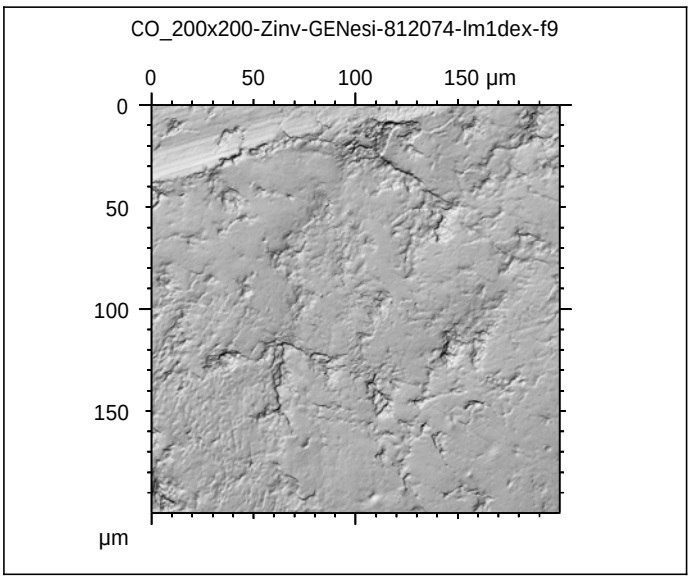
CO_200x200-Zinv-GENesi-812074-lm1dex-f9
0
50
100
150 µm
0
50
100
150
µm

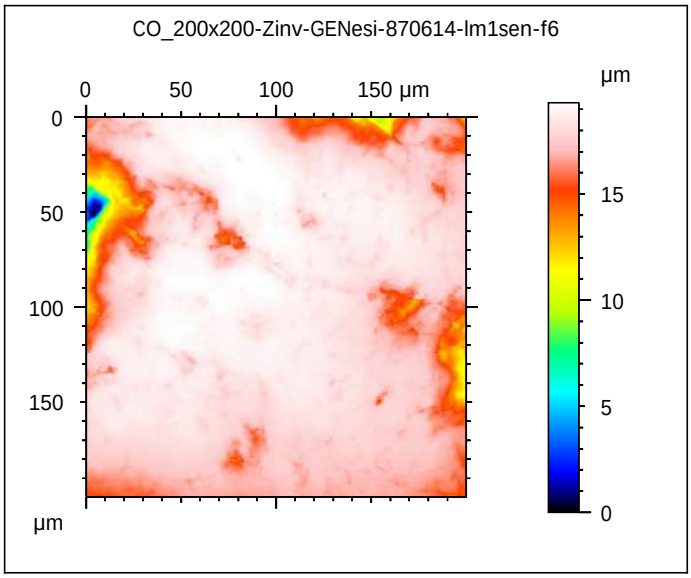
CO_200x200-Zinv-GENesi-870614-lm1sen-f6
0
50
100
150 µm
µm
0
50
100
150
µm
15
10
5
0

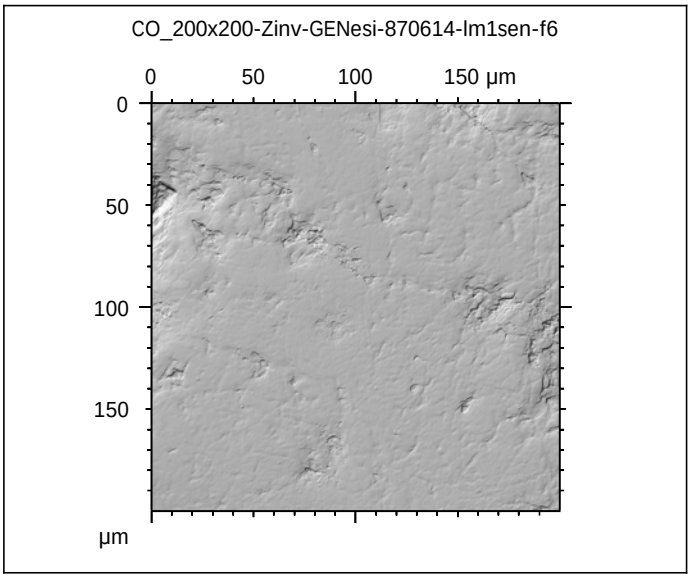
CO_200x200-Zinv-GENesi-870614-lm1sen-f6
0
50
100
150 µm
0
50
100
150
µm

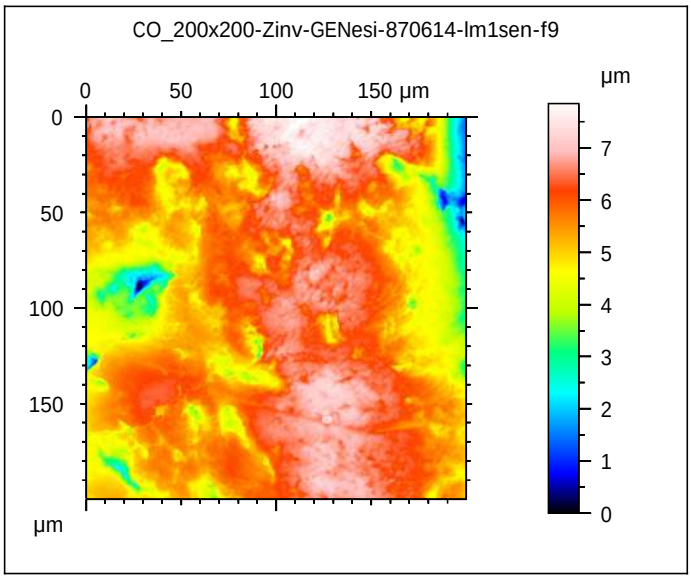
CO_200x200-Zinv-GENesi-870614-lm1sen-f9
0
50
100
150 µm
µm
0
50
100
150
µm
7
6
5
4
3
2
1
0

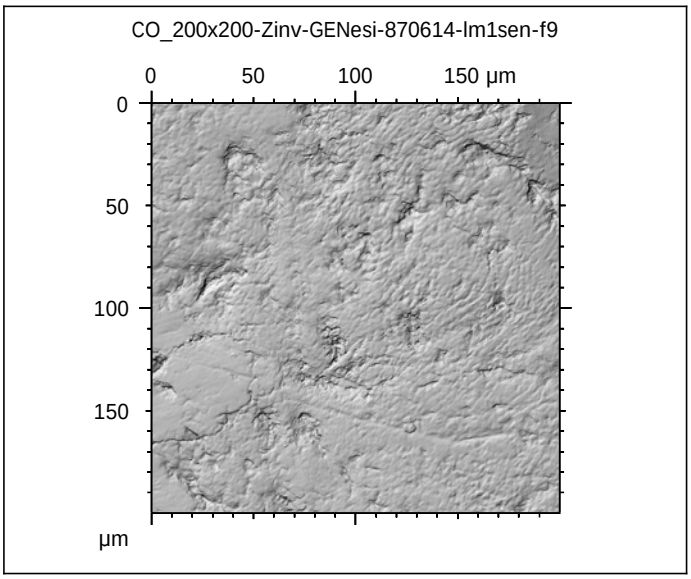
CO_200x200-Zinv-GENesi-870614-lm1sen-f9
0
50
100
150 µm
0
50
100
150
µm

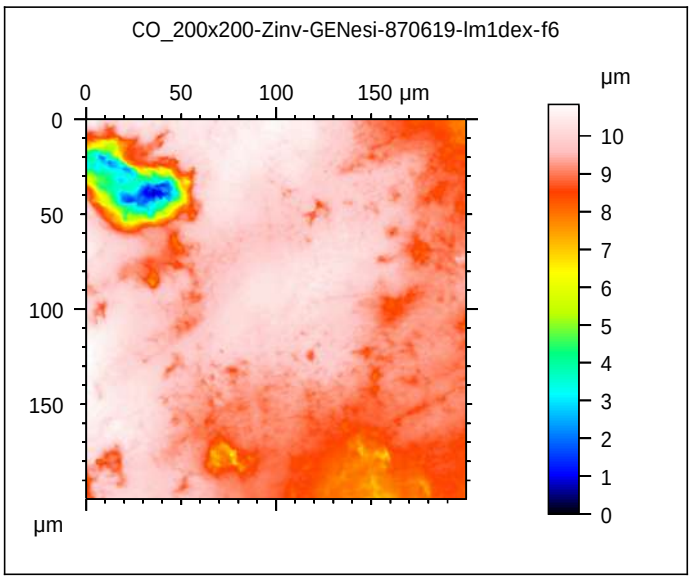
CO_200x200-Zinv-GENesi-870619-lm1dex-f6
0
50
100
150 µm
µm
0
50
100
150
µm
10
9
8
7
6
5
4
3
2
1
0

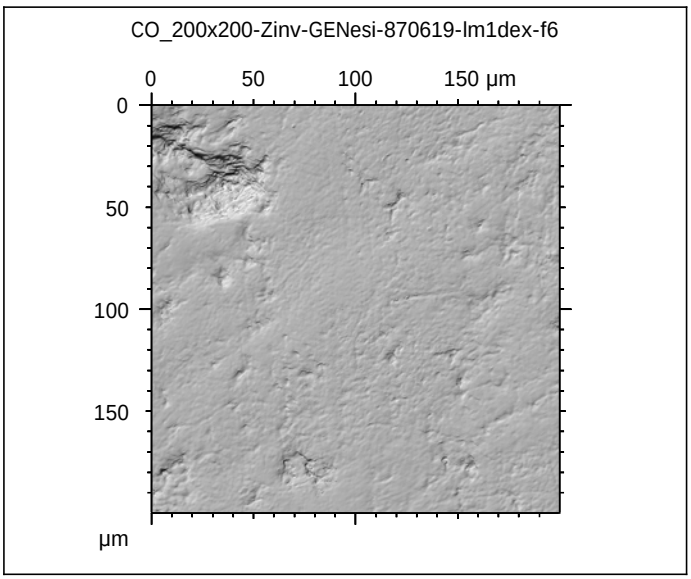
CO_200x200-Zinv-GENesi-870619-lm1dex-f6
0
50
100
150 µm
0
50
100
150
µm

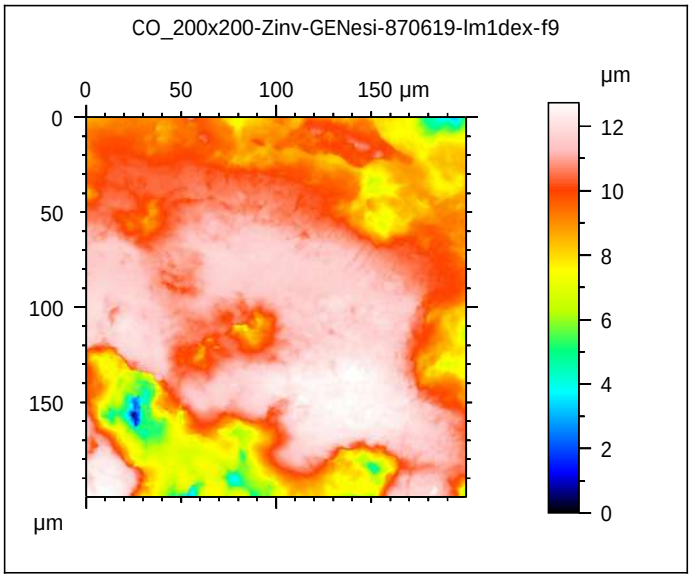
CO_200x200-Zinv-GENesi-870619-lm1dex-f9
0
50
100
150 µm
µm
12
10
8
6
4
2
0

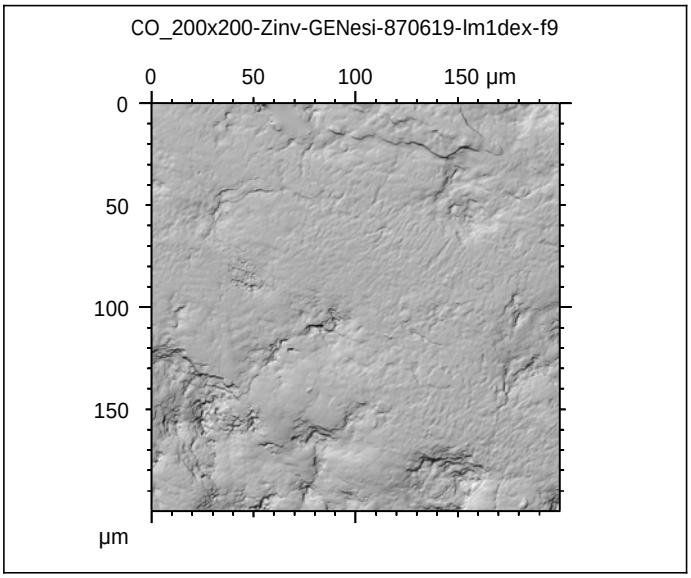
CO_200x200-Zinv-GENesi-870619-lm1dex-f9
0
50
100
150 µm
µm

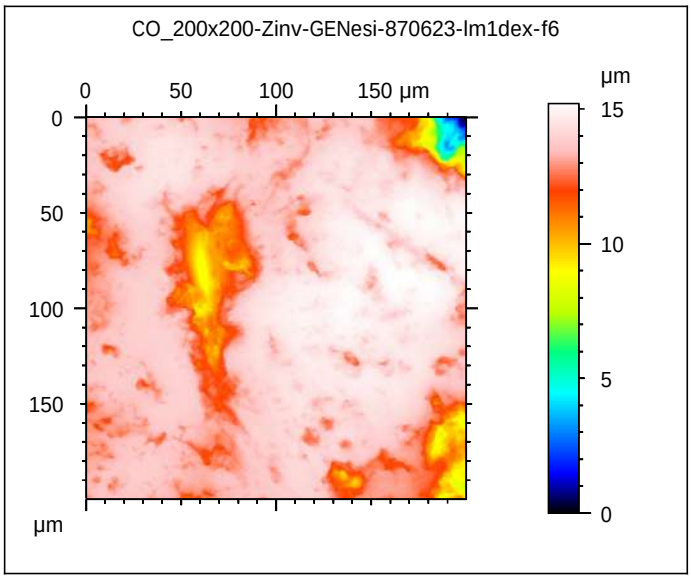
CO_200x200-Zinv-GENesi-870623-lm1dex-f6
0
50
100
150 µm
µm
15
10
5
0

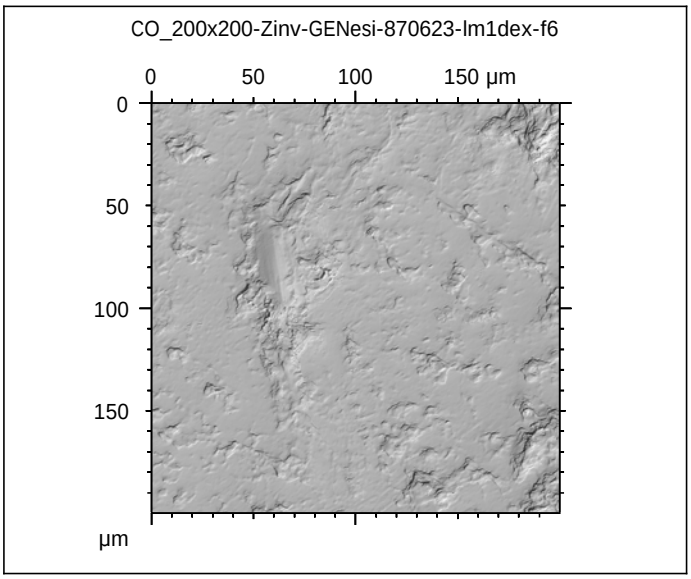
CO_200x200-Zinv-GENesi-870623-lm1dex-f6
0
50
100
150 µm
µm

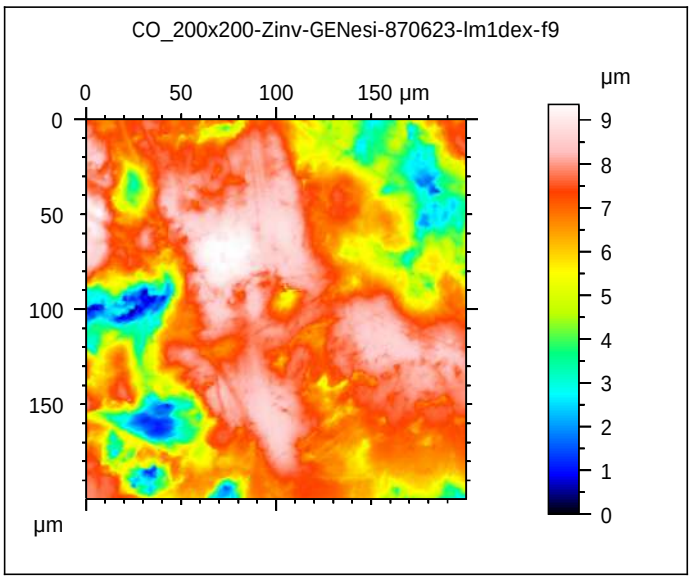
CO_200x200-Zinv-GENesi-870623-lm1dex-f9
0
50
100
150 µm
µm
9
8
7
6
5
4
3
2
1
0

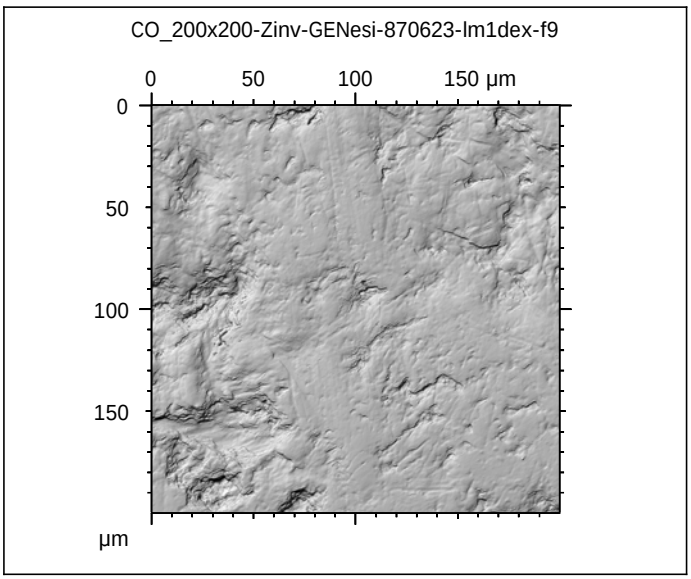
CO_200x200-Zinv-GENesi-870623-lm1dex-f9
0
50
100
150 µm
µm

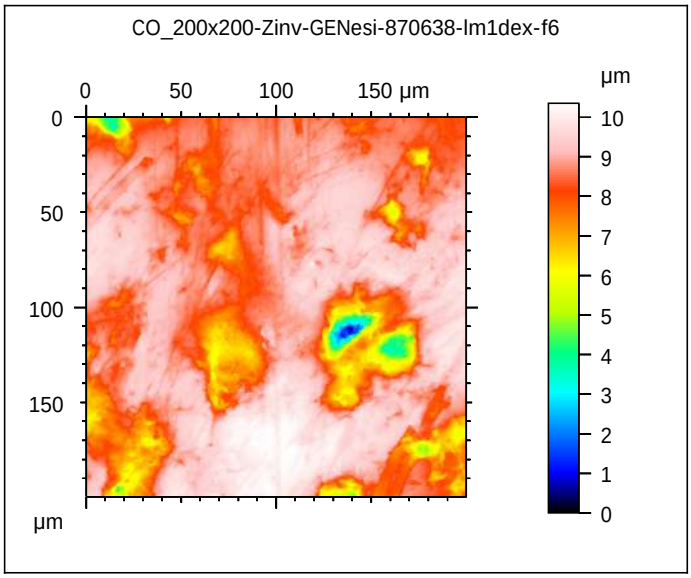
CO_200x200-Zinv-GENesi-870638-lm1dex-f6
0
50
100
150 µm
µm
10
9
8
7
6
5
4
3
2
1
0

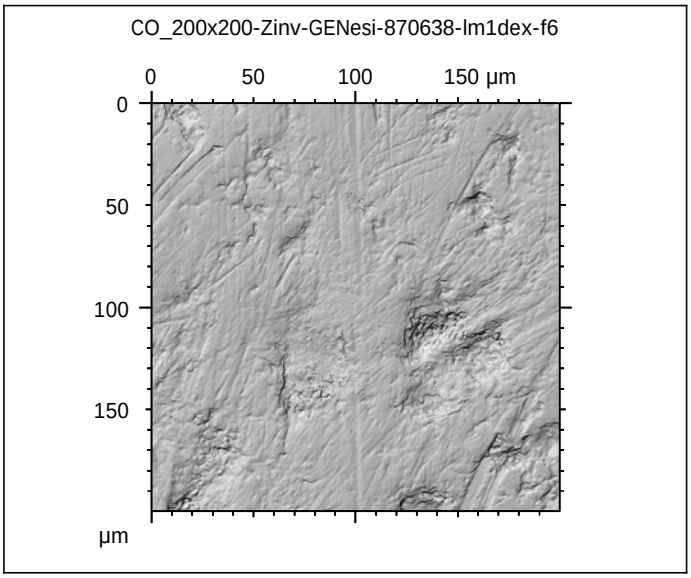
CO_200x200-Zinv-GENesi-870638-lm1dex-f6
0
50
100
150 µm
µm

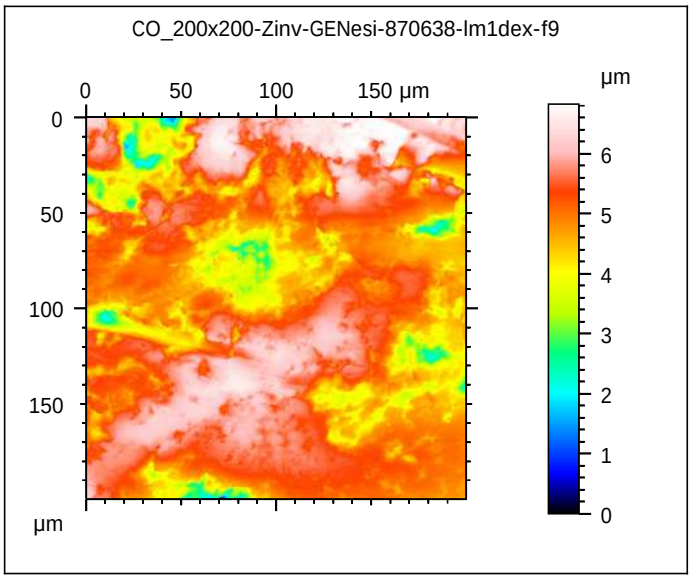
CO_200x200-Zinv-GENesi-870638-lm1dex-f9
0
50
100
150 µm
µm
6
5
4
3
2
1
0

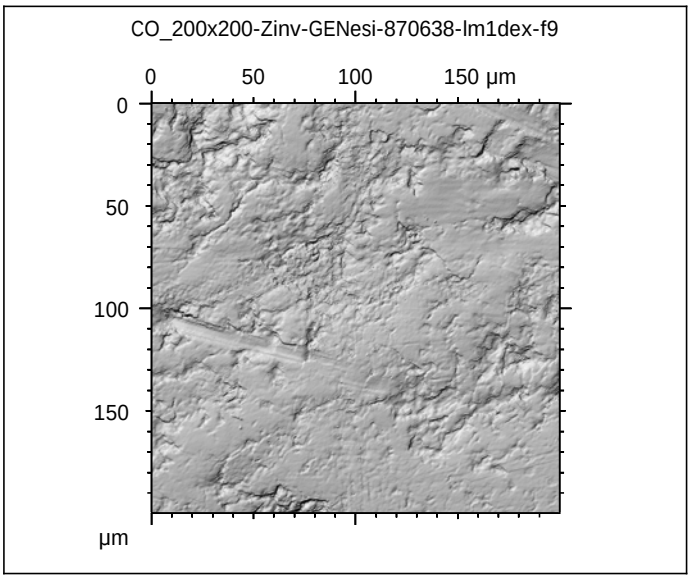
CO_200x200-Zinv-GENesi-870638-lm1dex-f9
0
50
100
150 µm
µm

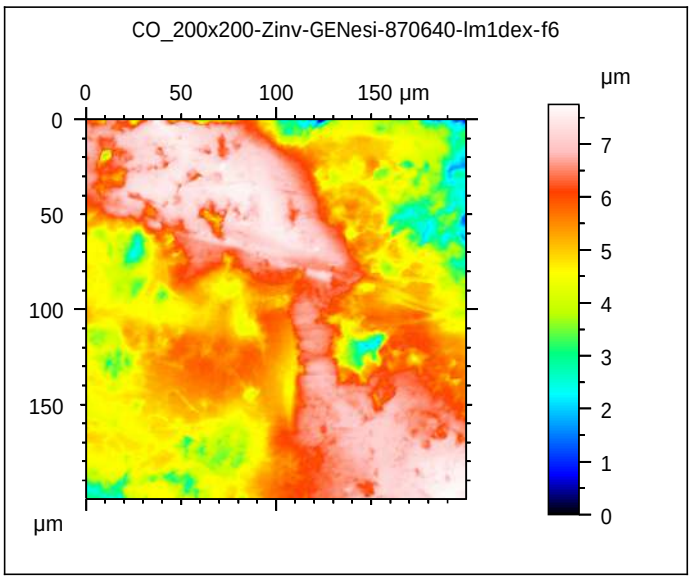
CO_200x200-Zinv-GENesi-870640-lm1dex-f6
0
50
100
150 µm
µm
7
6
5
4
3
2
1
0

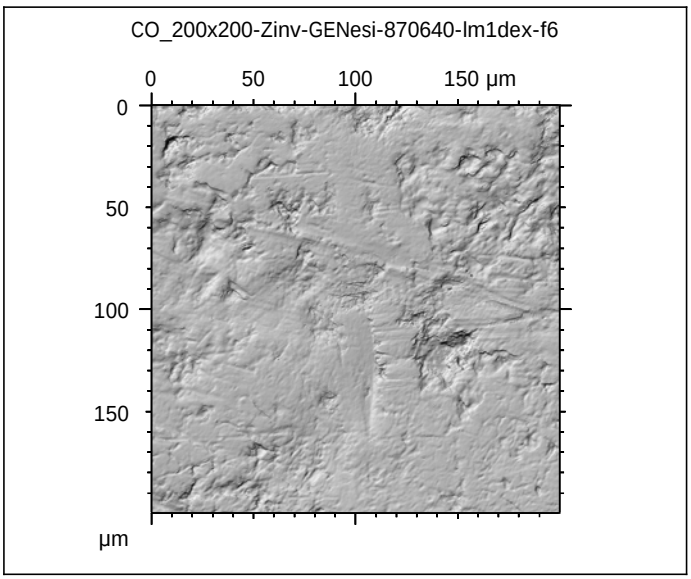
CO_200x200-Zinv-GENesi-870640-lm1dex-f6
0
50
100
150 µm
µm

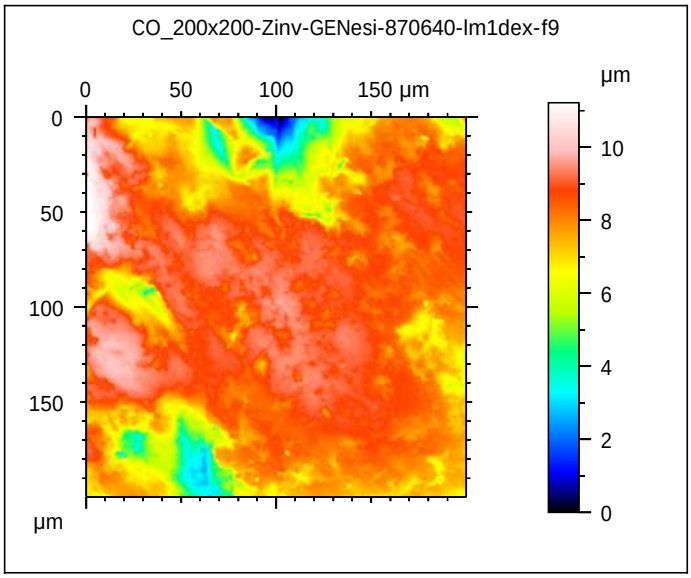
CO_200x200-Zinv-GENesi-870640-lm1dex-f9
0
50
100
150 µm
µm
10
8
6
4
2
0

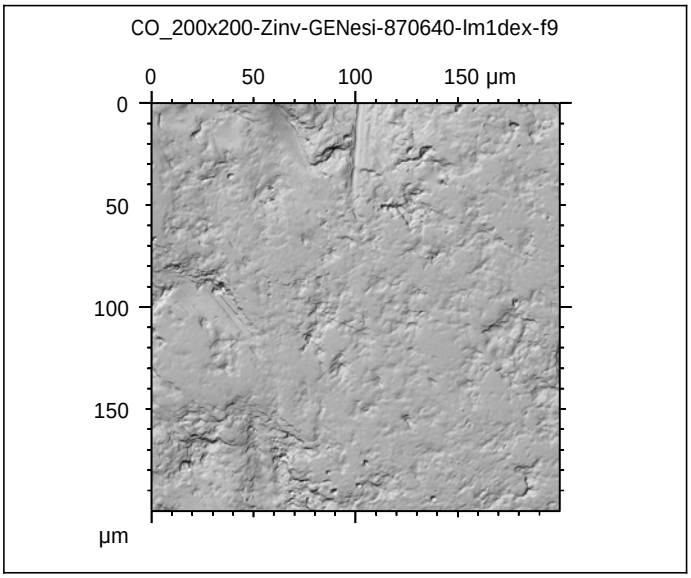
CO_200x200-Zinv-GENesi-870640-lm1dex-f9
0
50
100
150 µm
µm

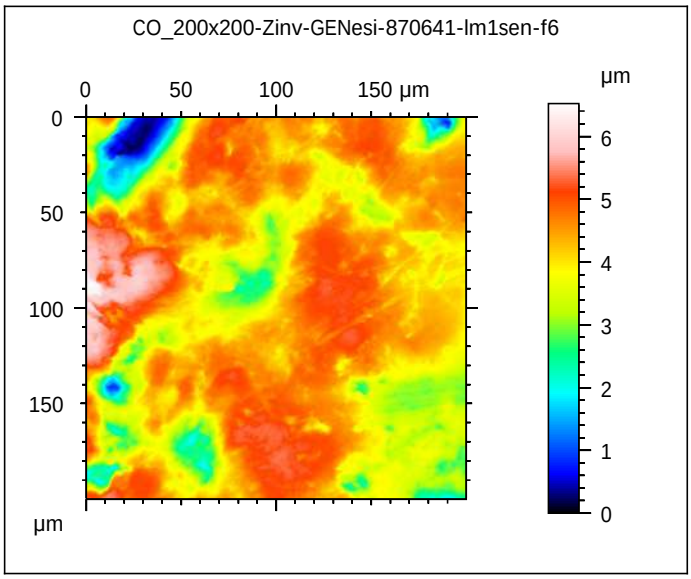
CO_200x200-Zinv-GENesi-870641-lm1sen-f6
0
50
100
150 µm
µm
6
5
4
3
2
1
0

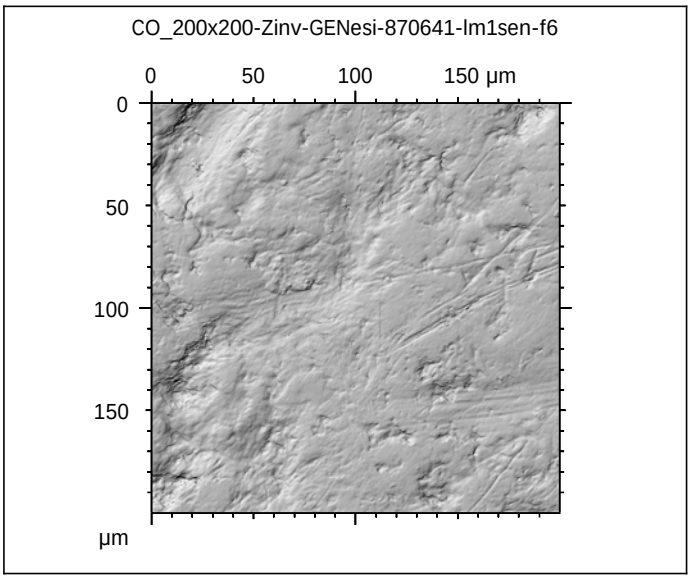
CO_200x200-Zinv-GENesi-870641-lm1sen-f6
0
50
100
150 µm
µm

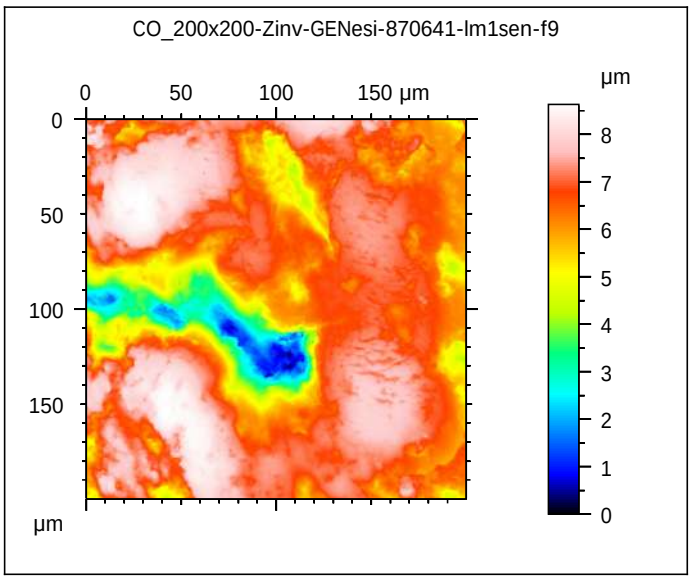
CO_200x200-Zinv-GENesi-870641-lm1sen-f9
0
50
100
150 µm
µm
8
7
6
5
4
3
2
1
0

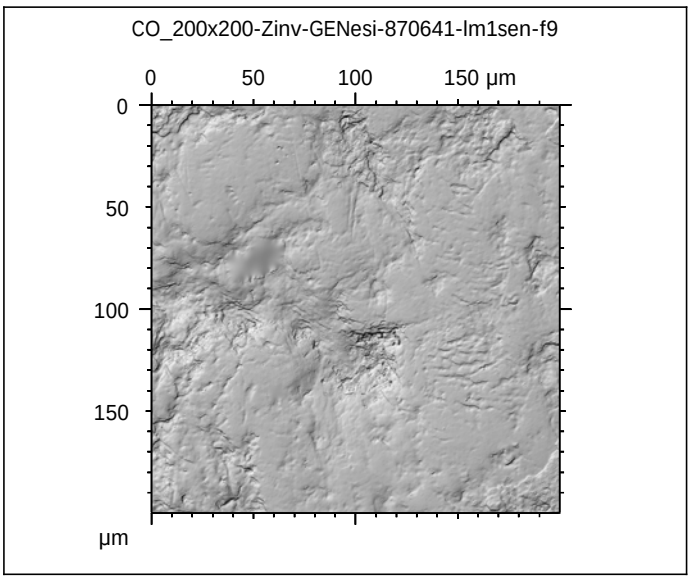
CO_200x200-Zinv-GENesi-870641-lm1sen-f9
0
50
100
150 µm
µm

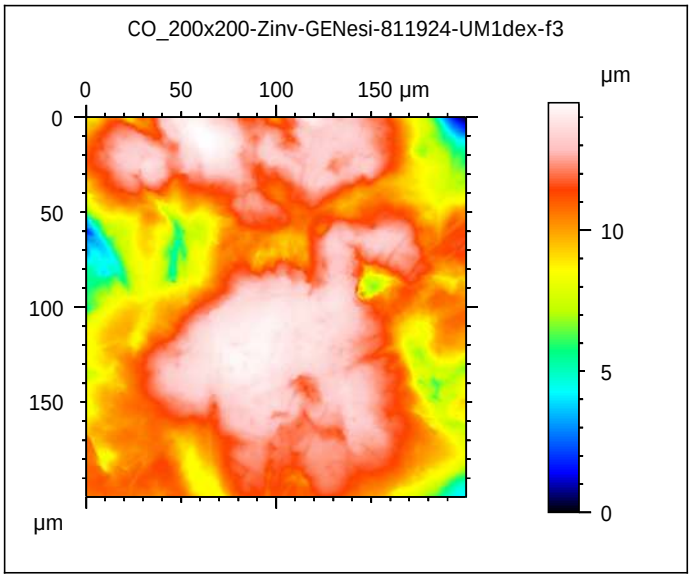
CO_200x200-Zinv-GENesi-811924-UM1dex-f3
0
50
100
150 µm
µm
0
50
100
150
µm
µm
10
5
0

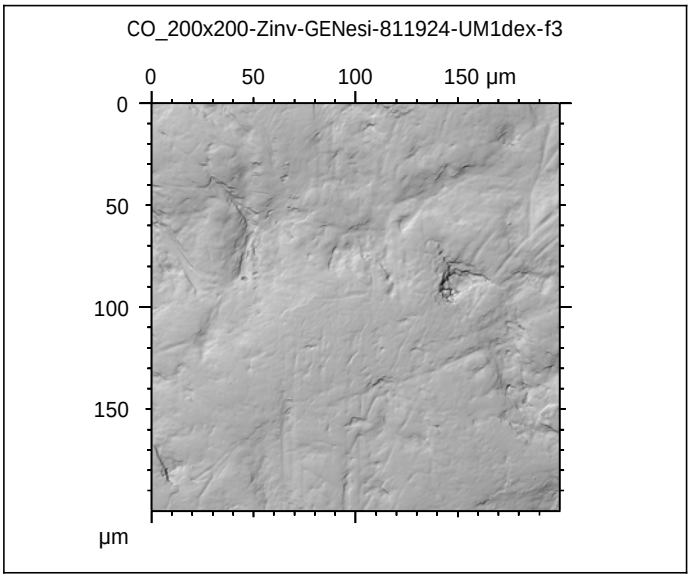
CO_200x200-Zinv-GENesi-811924-UM1dex-f3
0
50
100
150 µm
0
50
100
150
µm

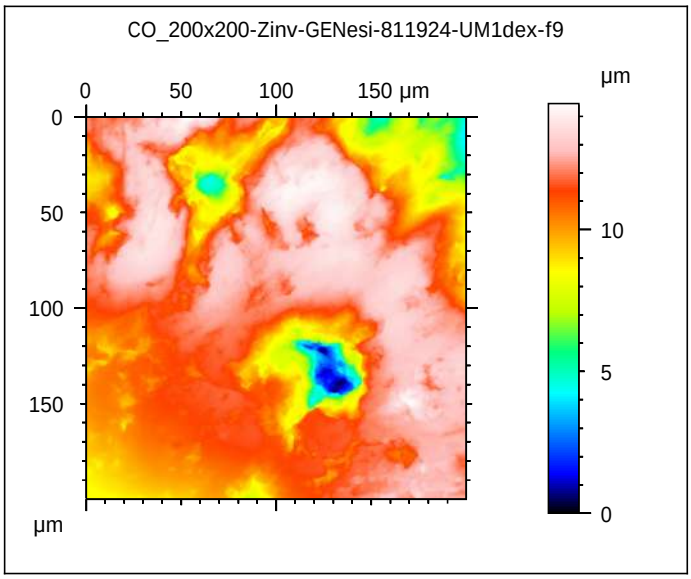
CO_200x200-Zinv-GENesi-811924-UM1dex-f9
0
50
100
150 µm
µm
0
50
100
150
µm
µm
10
5
0

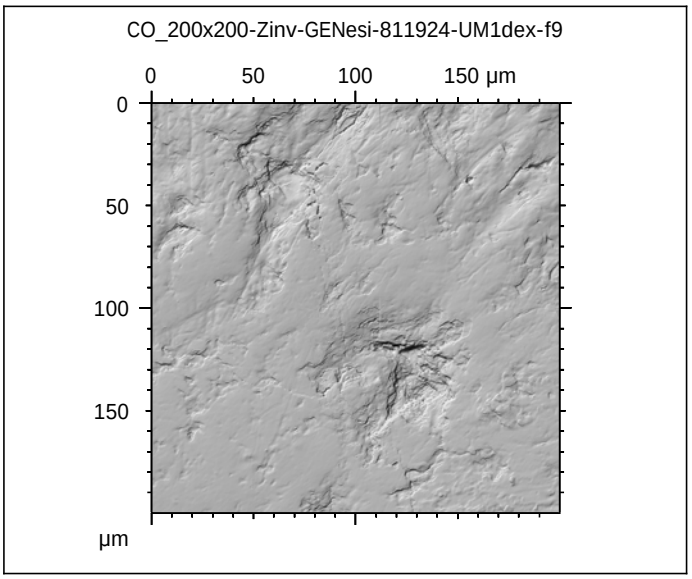
CO_200x200-Zinv-GENesi-811924-UM1dex-f9
0
50
100
150 µm
0
50
100
150
µm

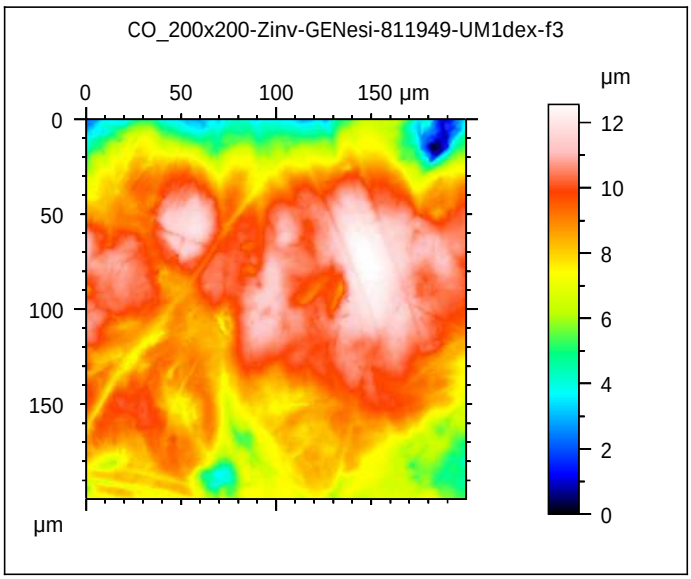
CO_200x200-Zinv-GENesi-811949-UM1dex-f3
0
50
100
150 µm
µm
0
50
100
150
µm
µm
12
10
8
6
4
2
0

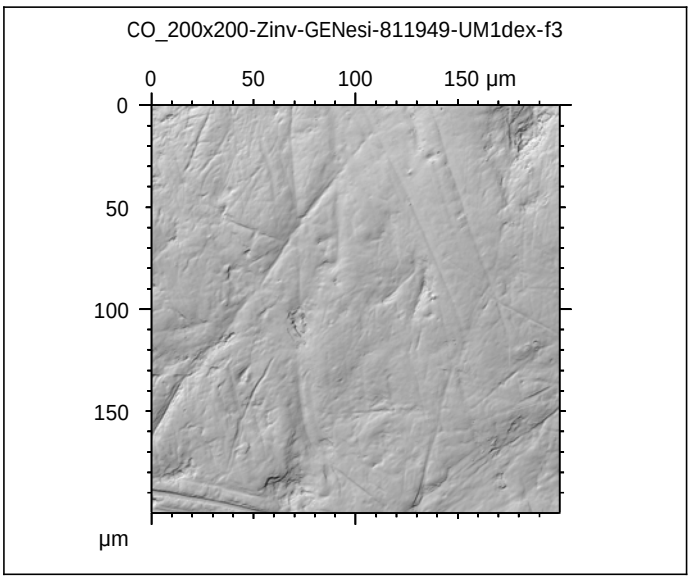
CO_200x200-Zinv-GENesi-811949-UM1dex-f3
0
50
100
150 µm
0
50
100
150
µm

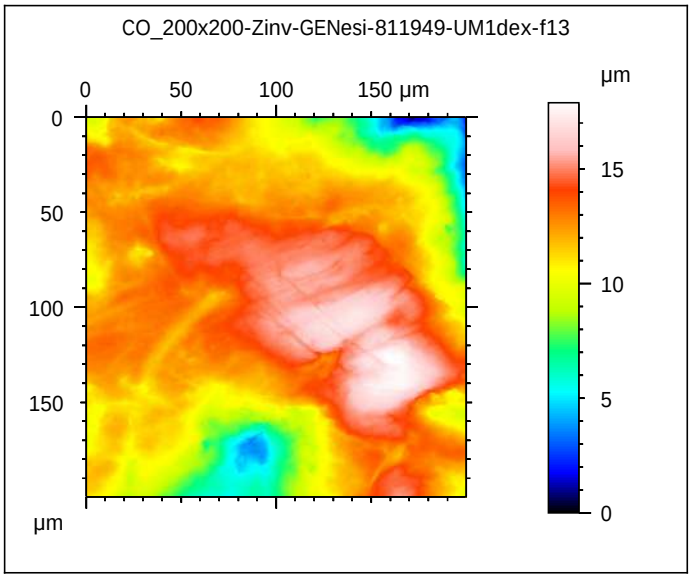
CO_200x200-Zinv-GENesi-811949-UM1dex-f13
0
50
100
150 µm
µm
0
50
100
150
µm
15
10
5
0

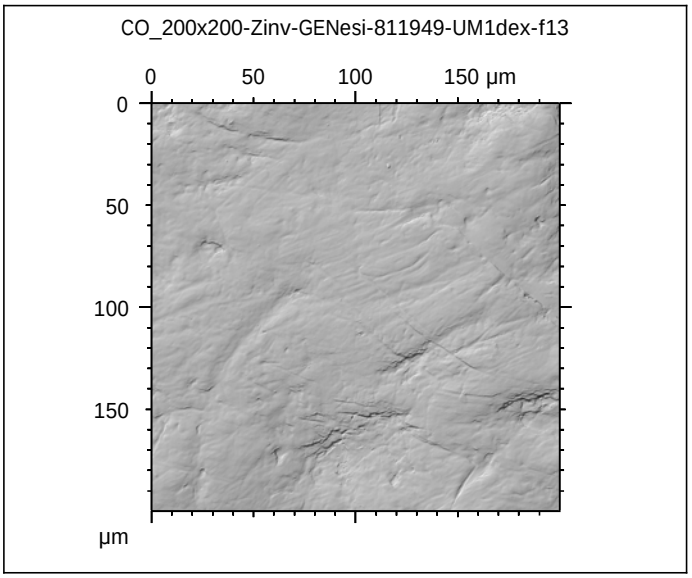
CO_200x200-Zinv-GENesi-811949-UM1dex-f13
0
50
100
150 µm
0
50
100
150
µm

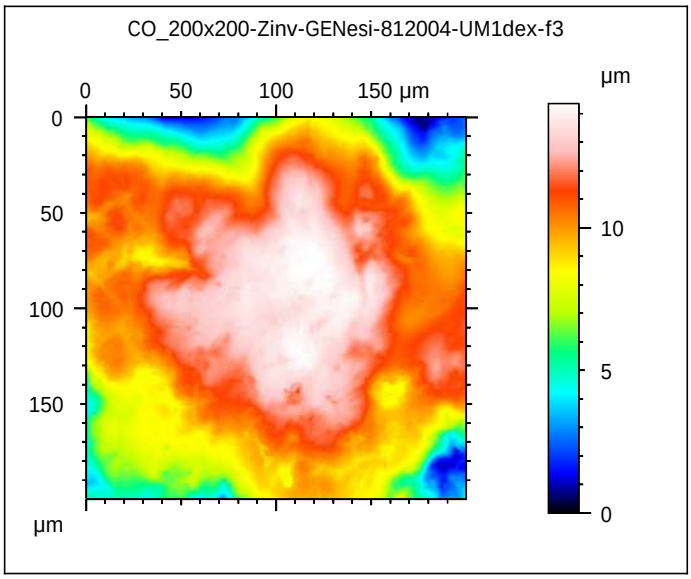
CO_200x200-Zinv-GENesi-812004-UM1dex-f3
0
50
100
150 µm
µm
0
50
100
150
µm
10
5
0

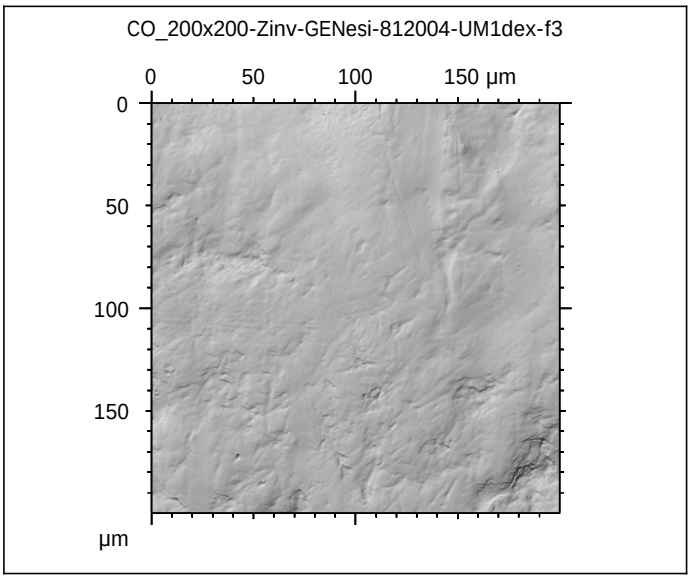
CO_200x200-Zinv-GENesi-812004-UM1dex-f3
0
50
100
150 µm
0
50
100
150
µm

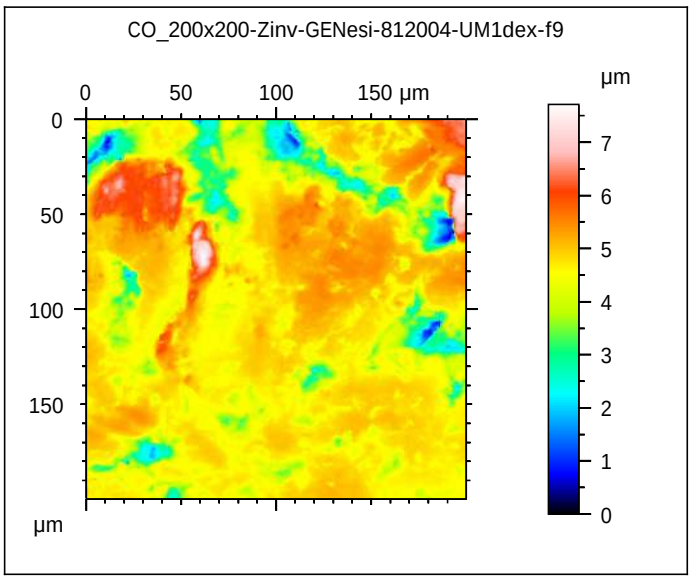
CO_200x200-Zinv-GENesi-812004-UM1dex-f9
0
50
100
150 µm
µm
0
50
100
150
µm
7
6
5
4
3
2
1
0

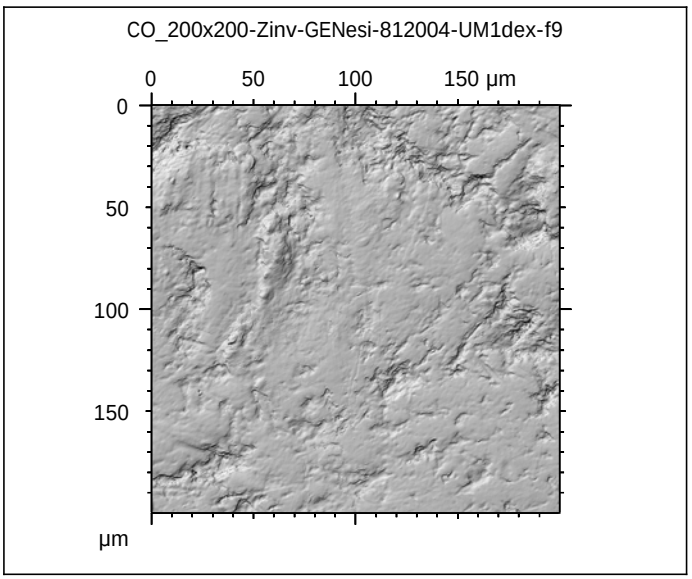
CO_200x200-Zinv-GENesi-812004-UM1dex-f9
0
50
100
150 µm
0
50
100
150
µm

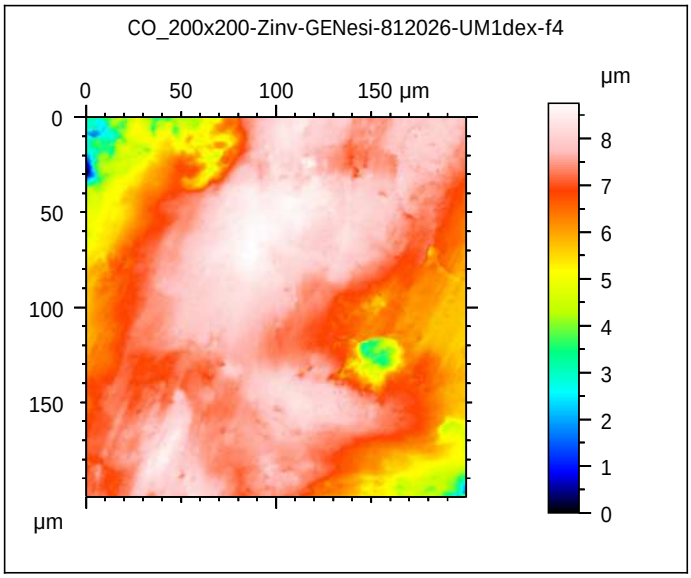
CO_200x200-Zinv-GENesi-812026-UM1dex-f4
0
50
100
150 µm
µm
0
50
100
150
µm
8
7
6
5
4
3
2
1
0

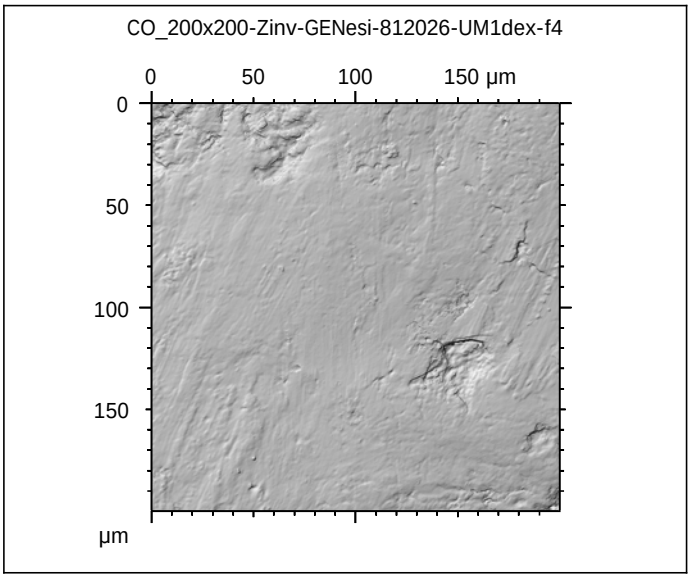
CO_200x200-Zinv-GENesi-812026-UM1dex-f4
0
50
100
150 µm
0
50
100
150
µm

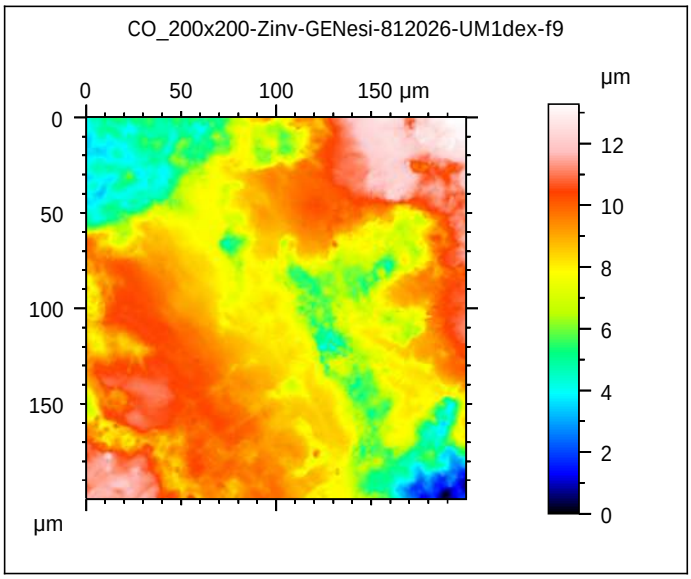
CO_200x200-Zinv-GENesi-812026-UM1dex-f9
0
50
100
150 µm
µm
0
50
100
150
µm
12
10
8
6
4
2
0

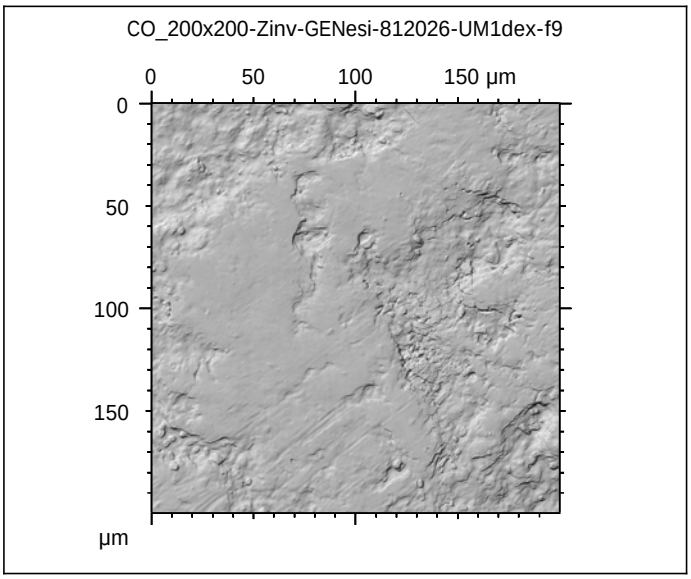
CO_200x200-Zinv-GENesi-812026-UM1dex-f9
0
50
100
150 µm
0
50
100
150
µm

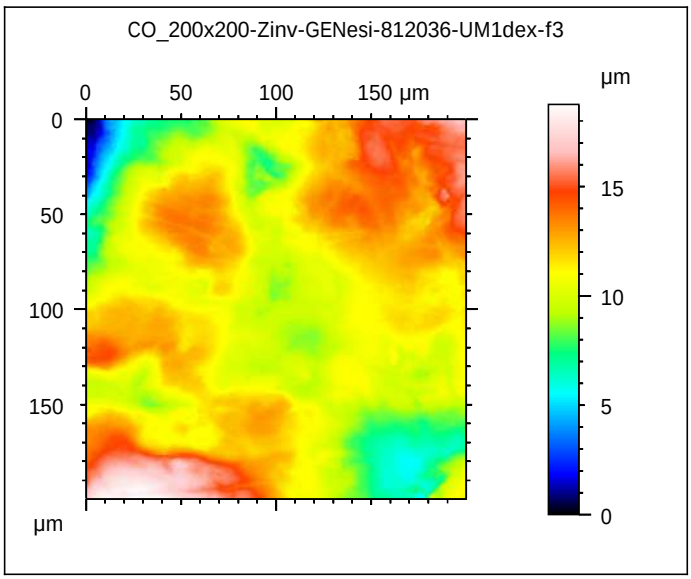
CO_200x200-Zinv-GENesi-812036-UM1dex-f3
0
50
100
150 µm
µm
0
50
100
150
µm
15
10
5
0

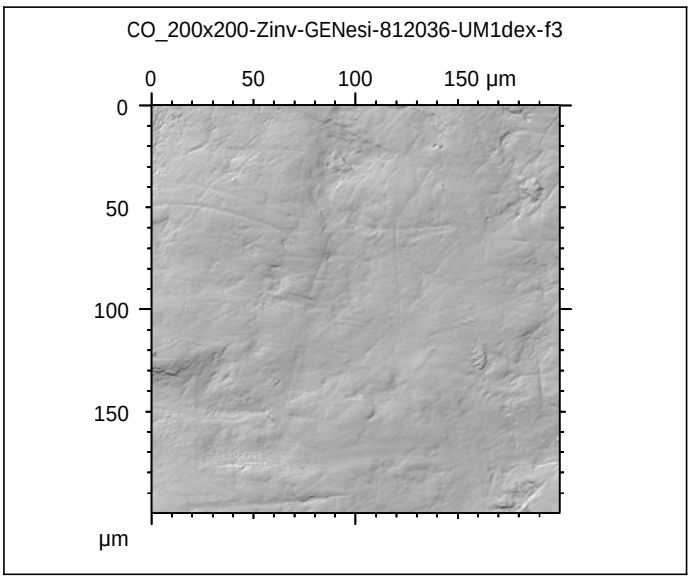
CO_200x200-Zinv-GENesi-812036-UM1dex-f3
0
50
100
150 µm
0
50
100
150
µm

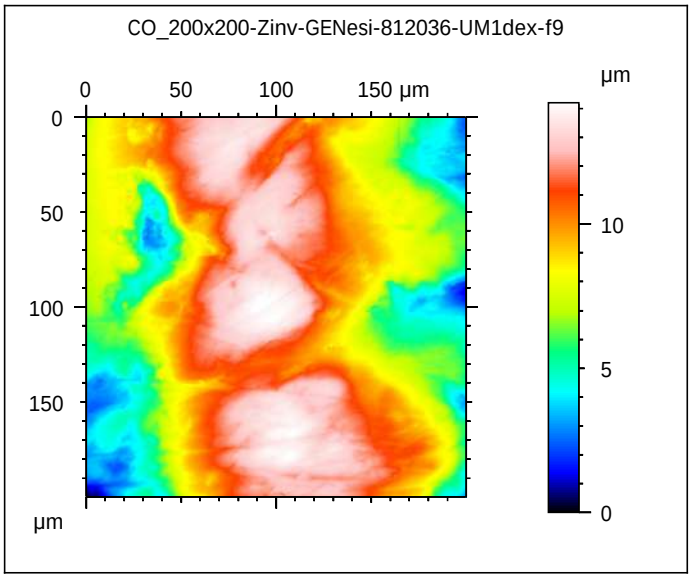
CO_200x200-Zinv-GENesi-812036-UM1dex-f9
0
50
100
150 µm
µm
0
50
100
150
µm
10
5
0

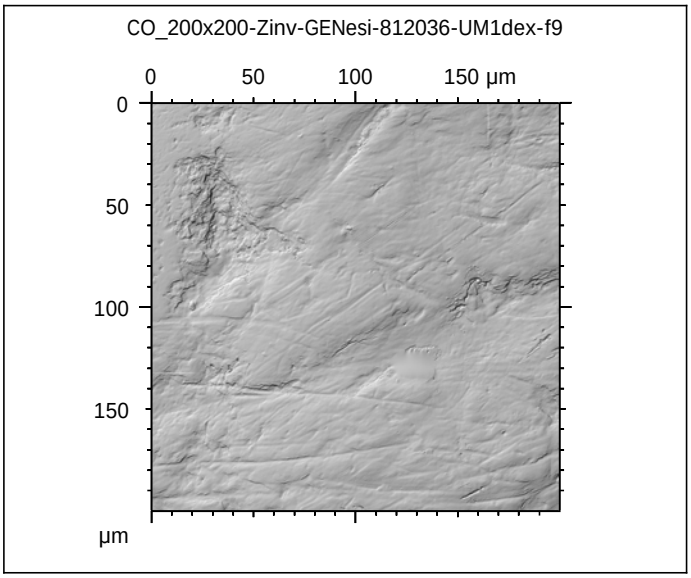
CO_200x200-Zinv-GENesi-812036-UM1dex-f9
0
50
100
150 µm
0
50
100
150
µm

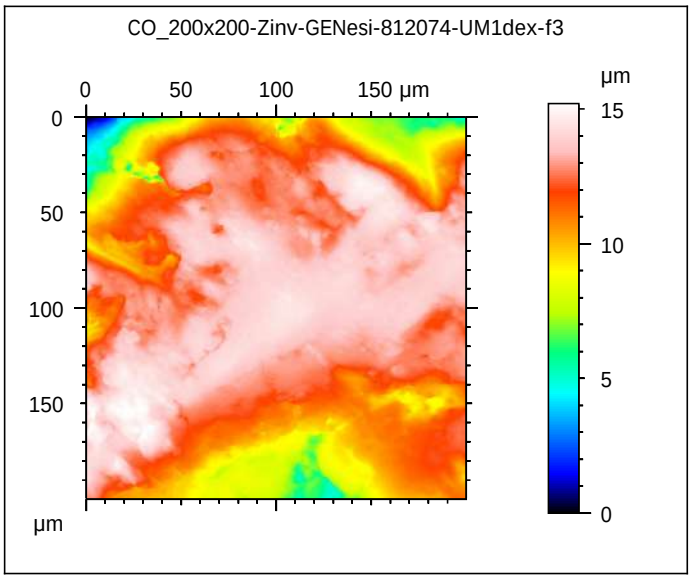
CO_200x200-Zinv-GENesi-812074-UM1dex-f3
0
50
100
150 µm
µm
0
50
100
150
µm
15
10
5
0

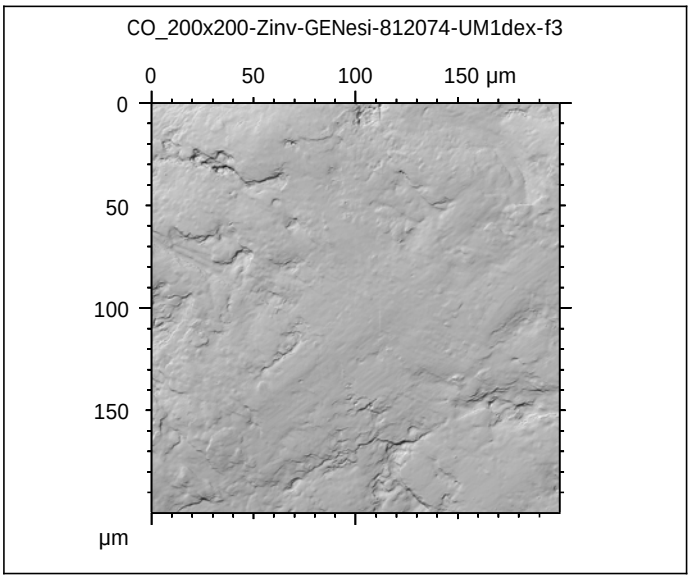
CO_200x200-Zinv-GENesi-812074-UM1dex-f3
0
50
100
150 µm
0
50
100
150
µm

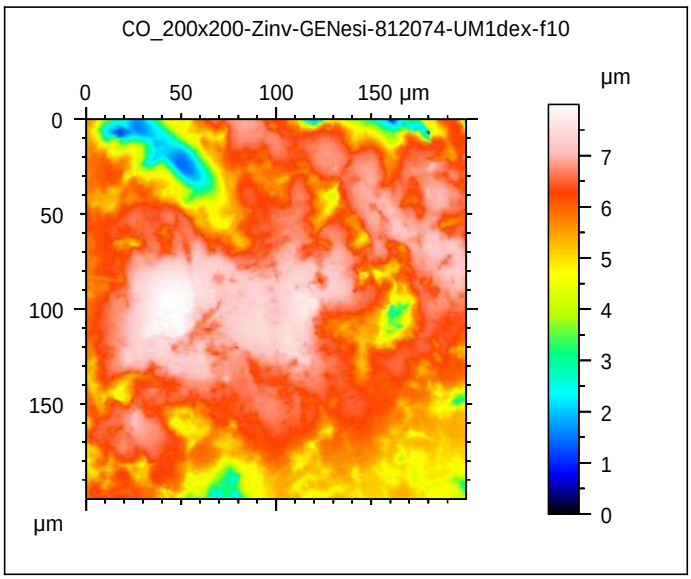
CO_200x200-Zinv-GENesi-812074-UM1dex-f10
0
50
100
150 µm
µm
0
50
100
150
µm
7
6
5
4
3
2
1
0

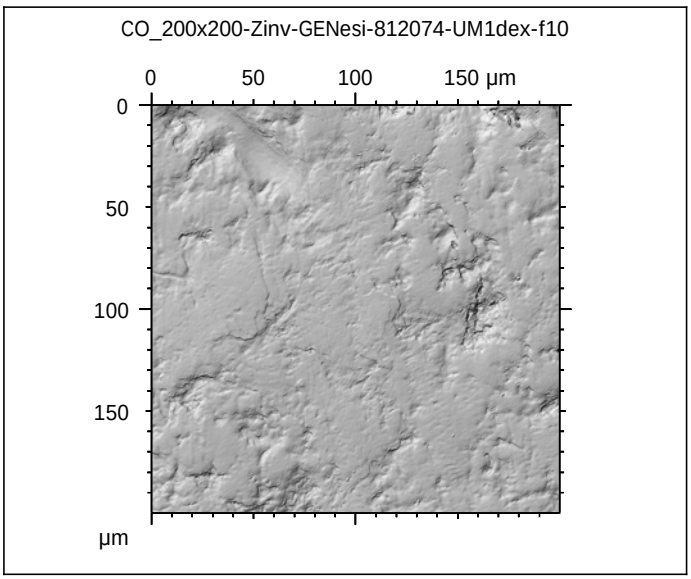
CO_200x200-Zinv-GENesi-812074-UM1dex-f10
0
50
100
150 µm
0
50
100
150
µm

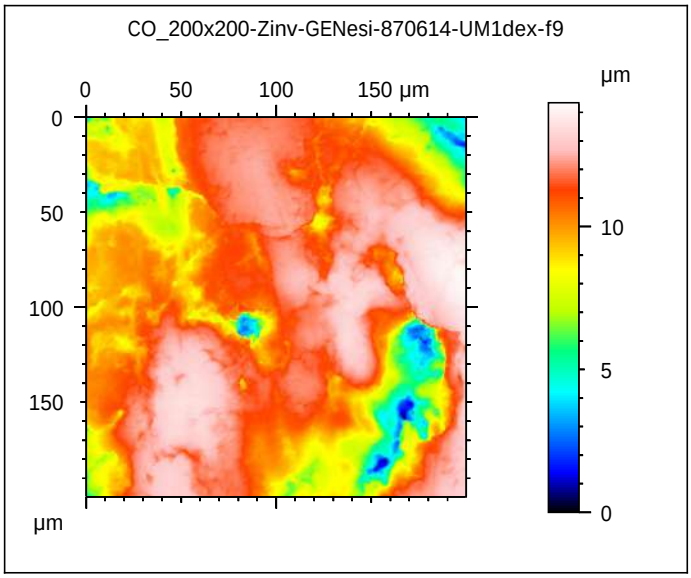
CO_200x200-Zinv-GENesi-870614-UM1dex-f9
0
50
100
150 µm
µm
0
50
100
150
µm
10
5
0

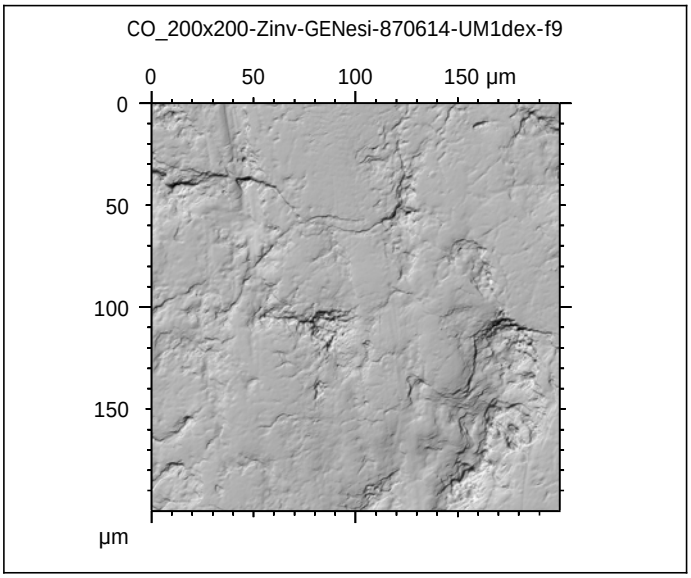
CO_200x200-Zinv-GENesi-870614-UM1dex-f9
0
50
100
150 µm
0
50
100
150
µm

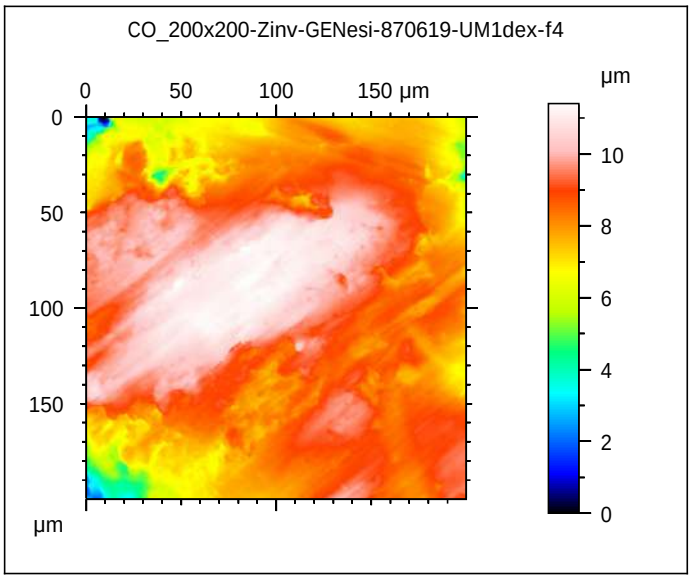
CO_200x200-Zinv-GENesi-870619-UM1dex-f4
0
50
100
150 µm
µm
0
50
100
150
µm
10
8
6
4
2
0

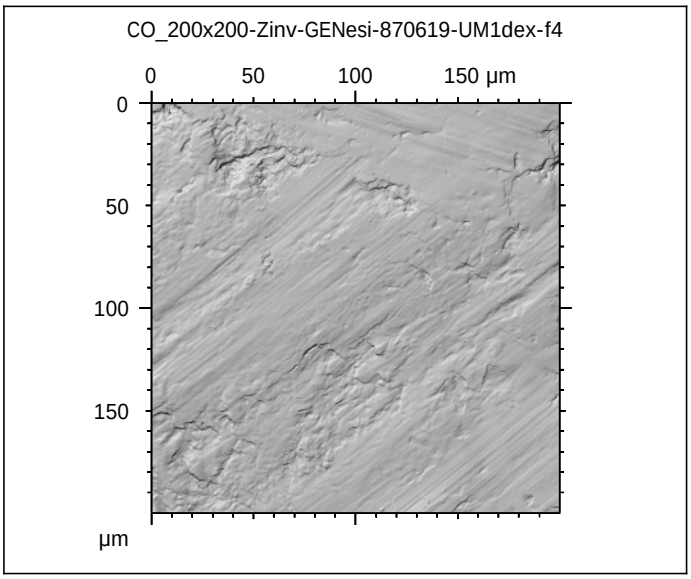
CO_200x200-Zinv-GENesi-870619-UM1dex-f4
0
50
100
150 µm
0
50
100
150
µm

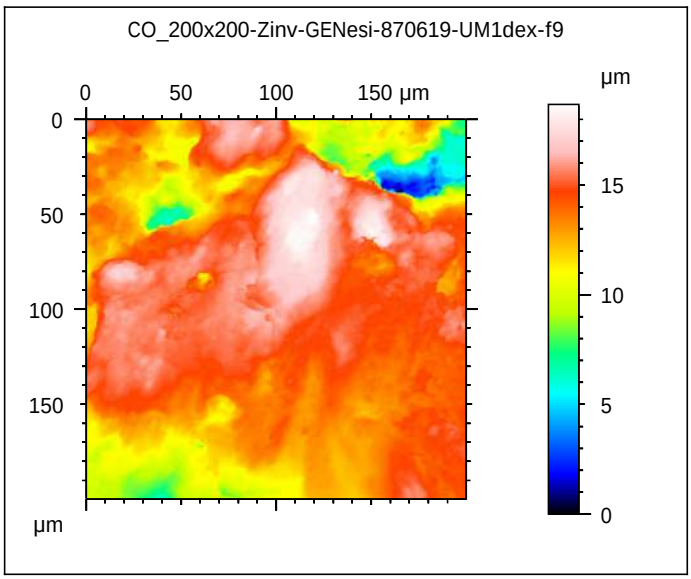
CO_200x200-Zinv-GENesi-870619-UM1dex-f9
0
50
100
150 µm
µm
0
50
100
150
µm
15
10
5
0

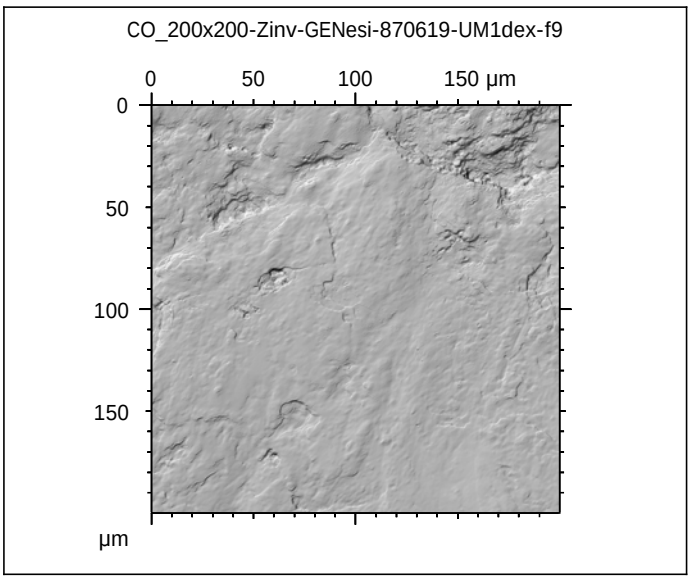
CO_200x200-Zinv-GENesi-870619-UM1dex-f9
0
50
100
150 µm
0
50
100
150
µm

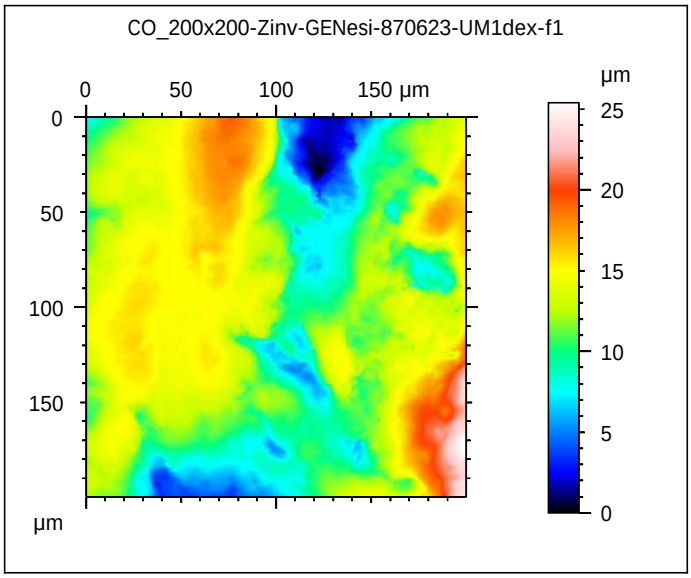
CO_200x200-Zinv-GENesi-870623-UM1dex-f1
0
50
100
150 µm
µm
25
20
15
10
5
0

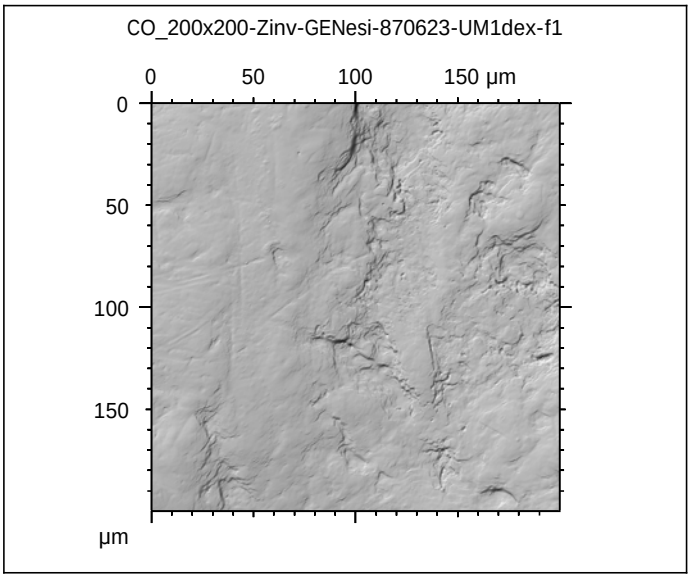
CO_200x200-Zinv-GENesi-870623-UM1dex-f1
0
50
100
150 µm
µm

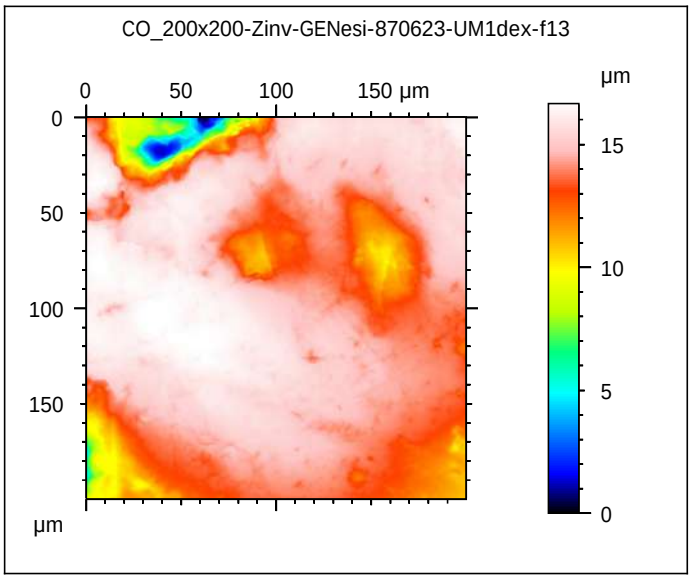
CO_200x200-Zinv-GENesi-870623-UM1dex-f13
0
50
100
150 µm
µm
15
10
5
0

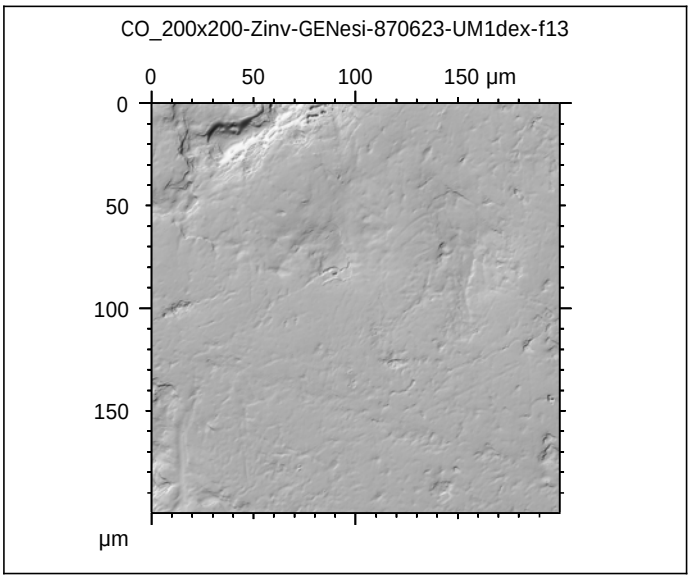
CO_200x200-Zinv-GENesi-870623-UM1dex-f13
0
50
100
150 µm
µm

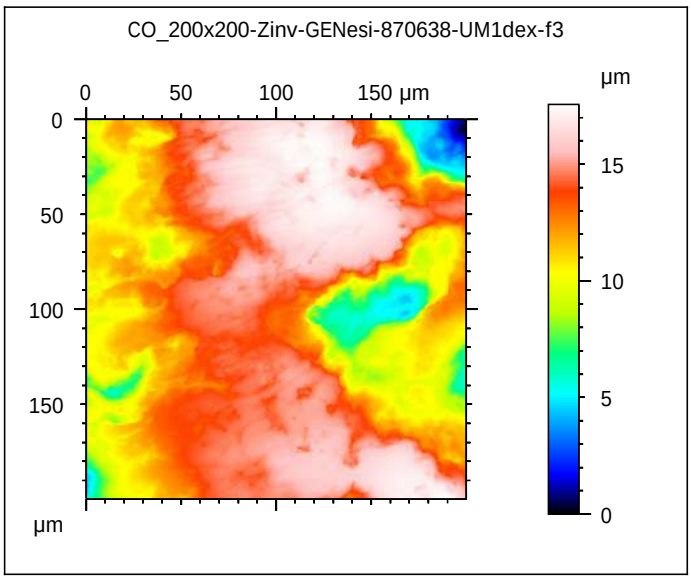
CO_200x200-Zinv-GENesi-870638-UM1dex-f3
0
50
100
150 µm
µm
15
10
5
0

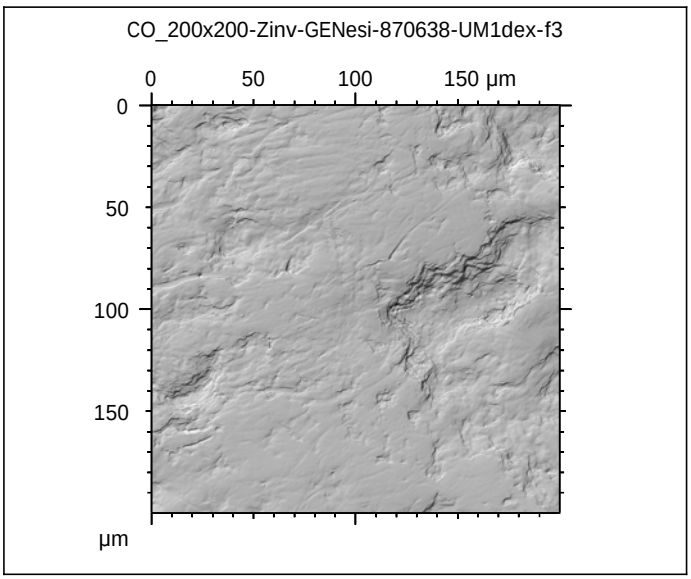
CO_200x200-Zinv-GENesi-870638-UM1dex-f3
0
50
100
150 µm
µm

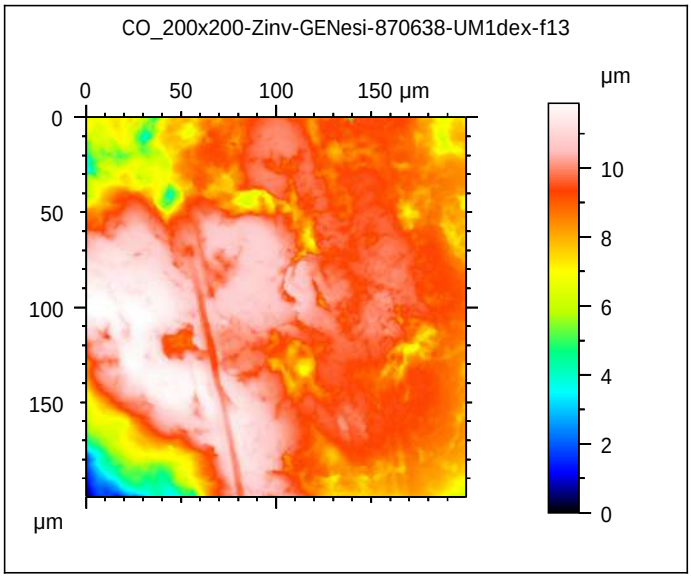
CO_200x200-Zinv-GENesi-870638-UM1dex-f13
0
50
100
150 µm
µm
0
50
100
150
µm
µm
10
8
6
4
2
0

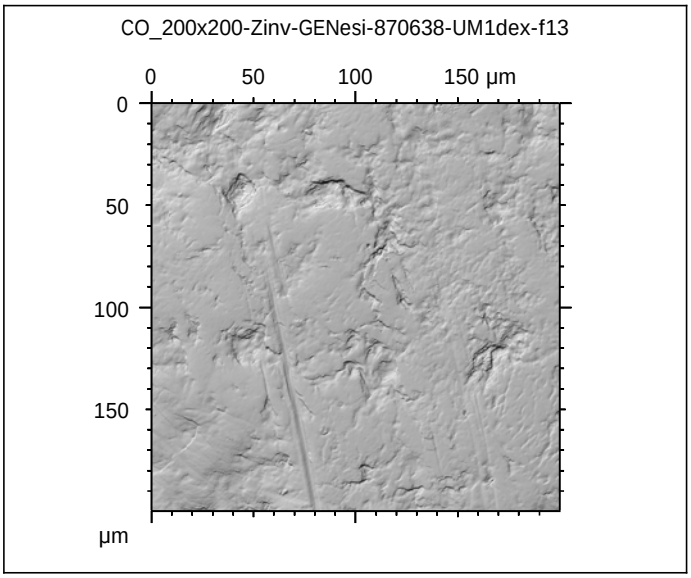
CO_200x200-Zinv-GENesi-870638-UM1dex-f13
0
50
100
150 µm
0
50
100
150
µm

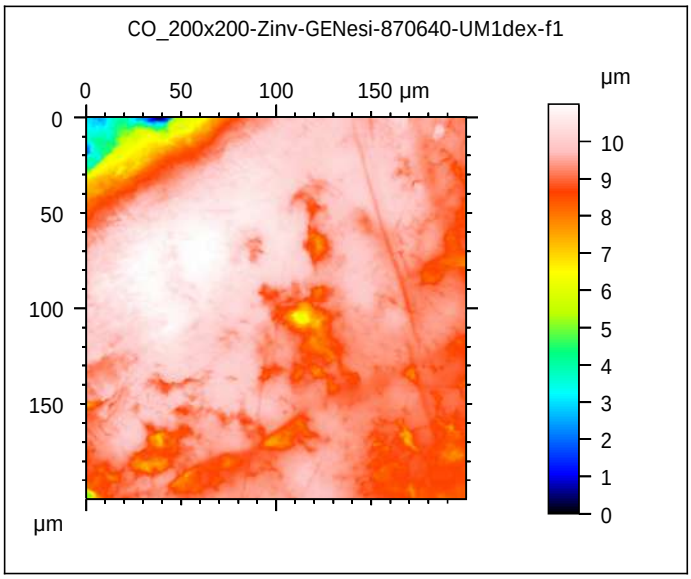
CO_200x200-Zinv-GENesi-870640-UM1dex-f1
0
50
100
150 µm
µm
0
50
100
150
µm
µm
10
9
8
7
6
5
4
3
2
1
0

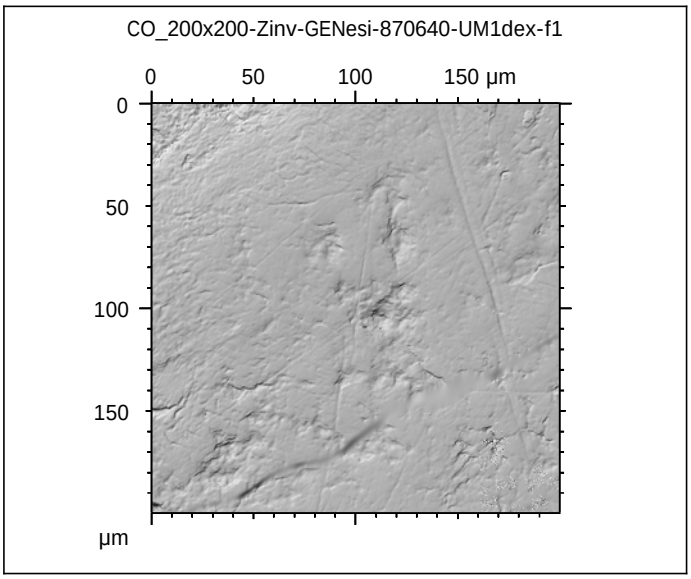
CO_200x200-Zinv-GENesi-870640-UM1dex-f1
0
50
100
150 µm
0
50
100
150
µm

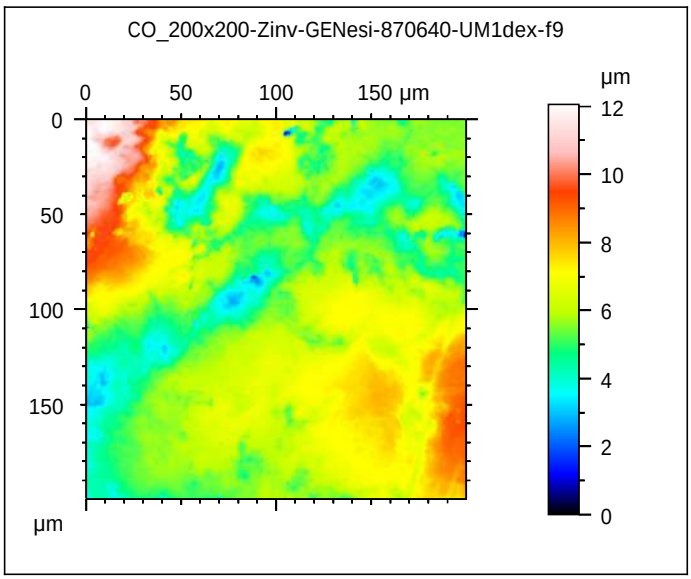
CO_200x200-Zinv-GENesi-870640-UM1dex-f9
0
50
100
150 µm
µm
0
50
100
150
µm
µm
12
10
8
6
4
2
0

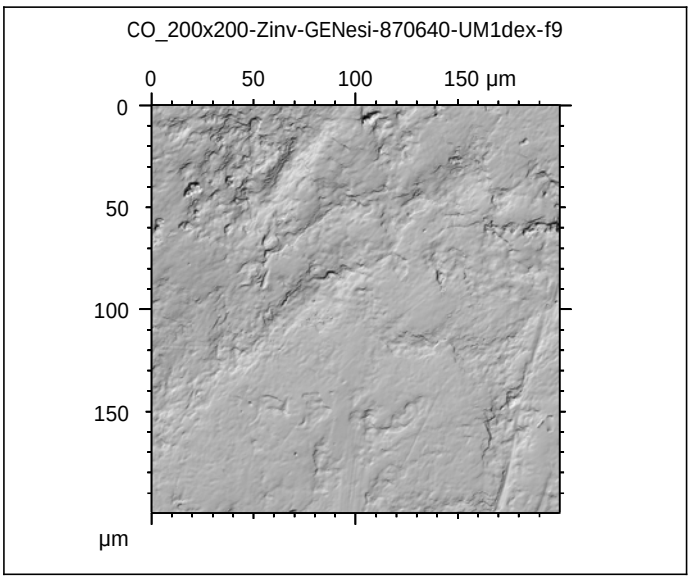
CO_200x200-Zinv-GENesi-870640-UM1dex-f9
0
50
100
150 µm
0
50
100
150
µm

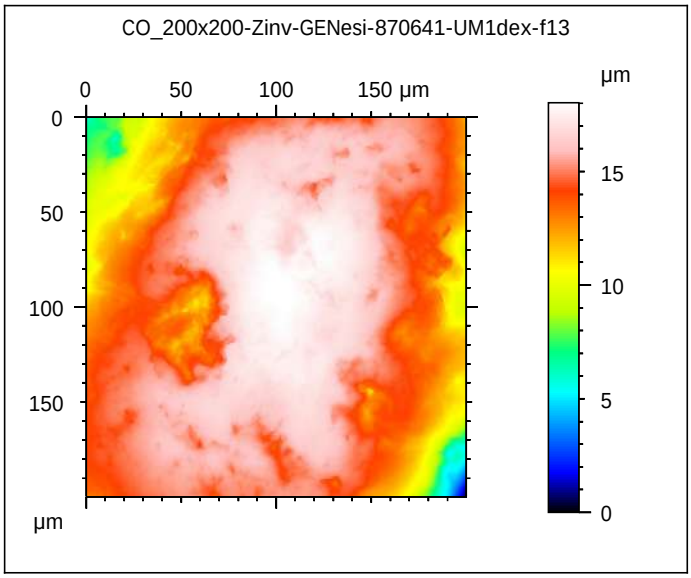
CO_200x200-Zinv-GENesi-870641-UM1dex-f13
0
50
100
150 µm
µm
15
10
5
0

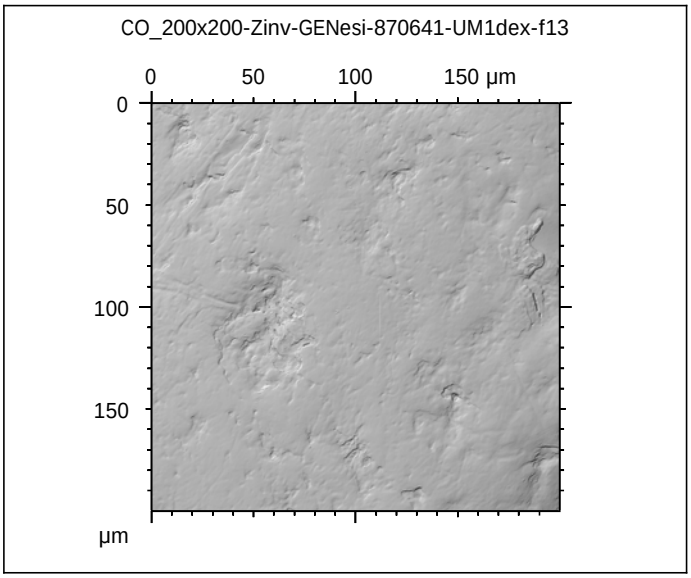
CO_200x200-Zinv-GENesi-870641-UM1dex-f13
0
50
100
150 µm
µm

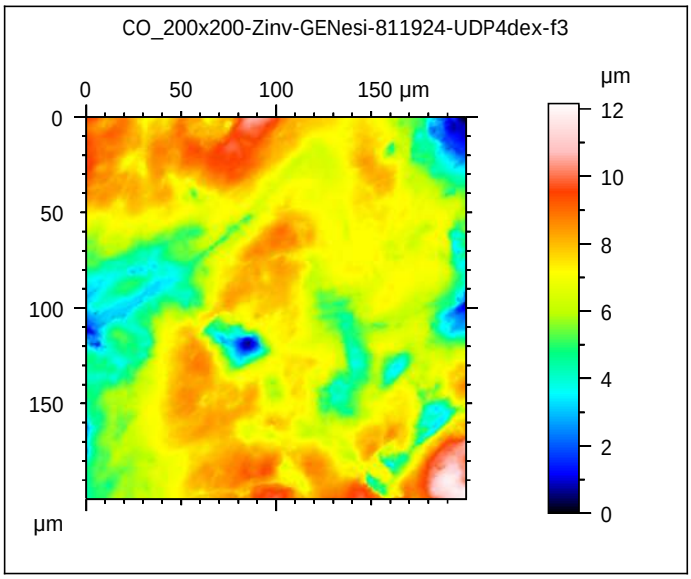
CO_200x200-Zinv-GENesi-811924-UDP4dex-f3
0
50
100
150 µm
µm
12
10
8
6
4
2
0

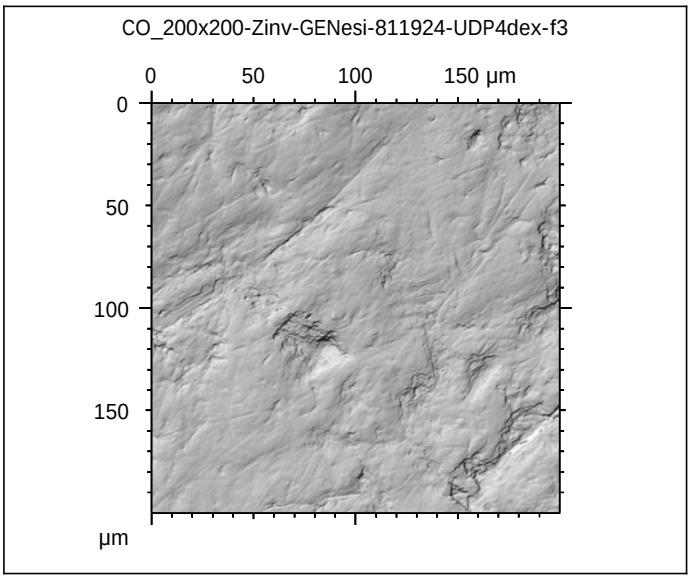
CO_200x200-Zinv-GENesi-811924-UDP4dex-f3
0
50
100
150 µm
µm

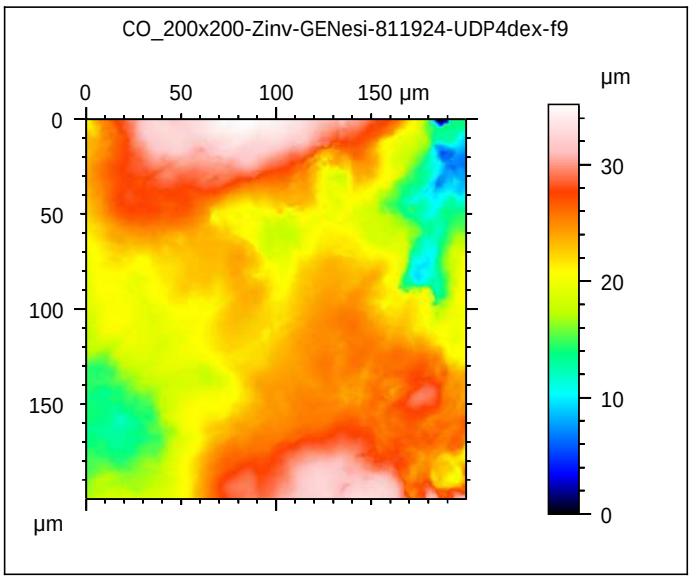
CO_200x200-Zinv-GENesi-811924-UDP4dex-f9
0
50
100
150 µm
µm
30
20
10
0

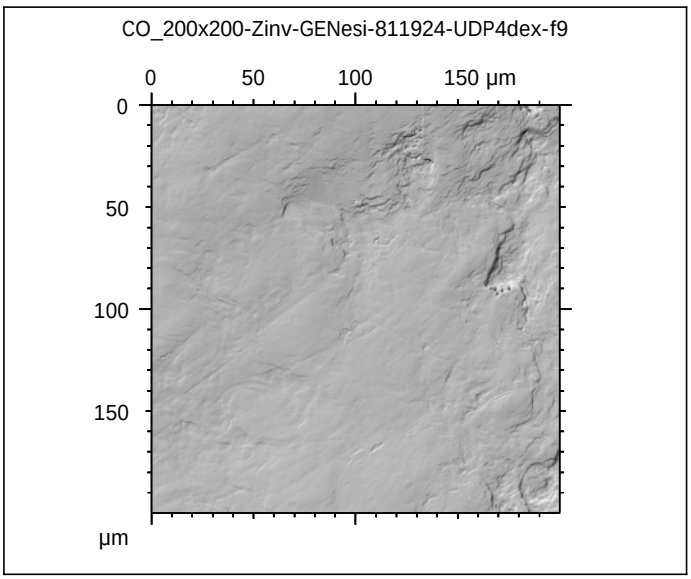
CO_200x200-Zinv-GENesi-811924-UDP4dex-f9
0
50
100
150 µm
µm

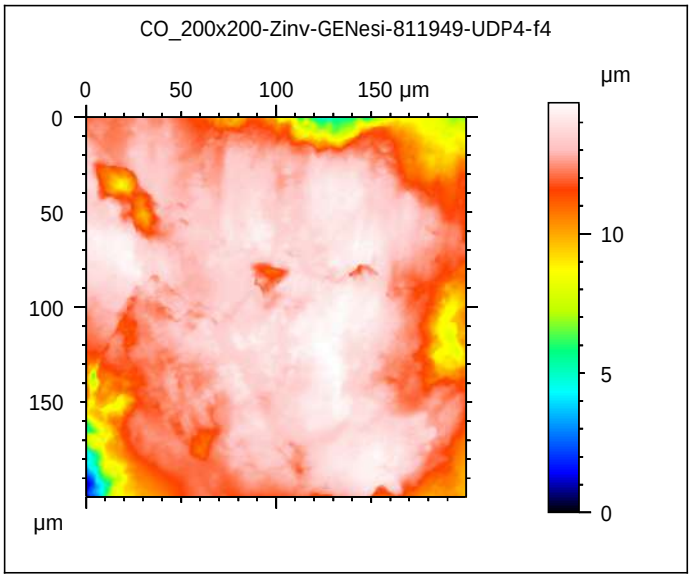
CO_200x200-Zinv-GENesi-811949-UDP4-f4
0
50
100
150 µm
µm
0
50
100
150
µm
µm
10
5
0

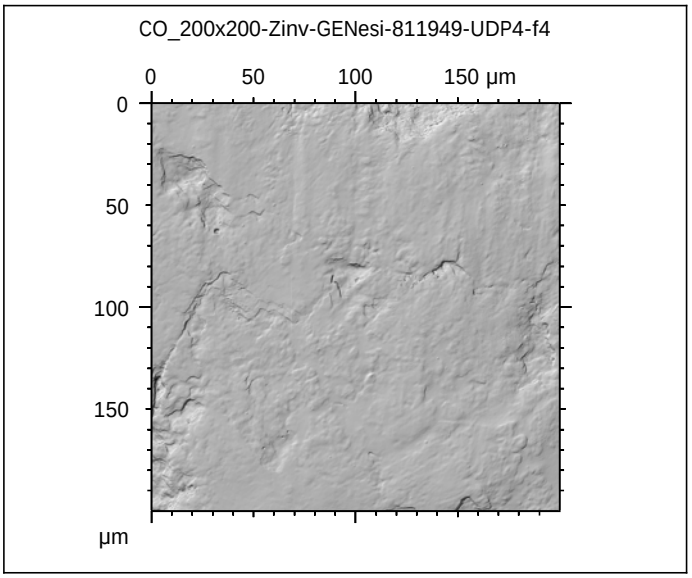
CO_200x200-Zinv-GENesi-811949-UDP4-f4
0
50
100
150 µm
0
50
100
150
µm

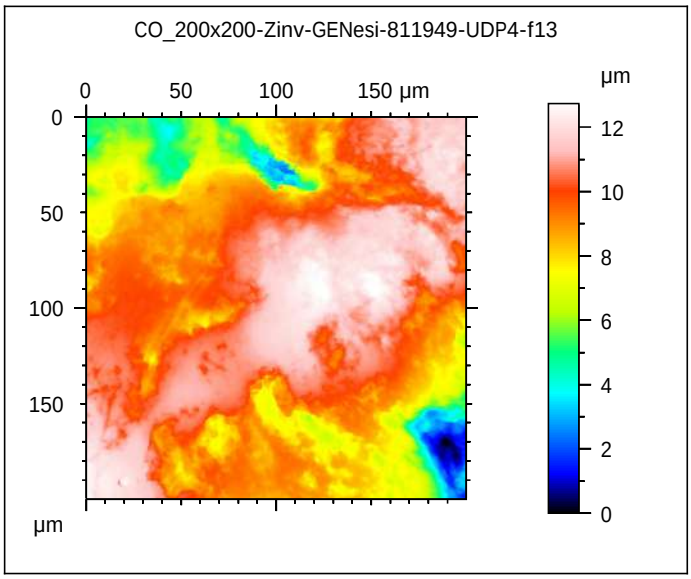
CO_200x200-Zinv-GENesi-811949-UDP4-f13
0
50
100
150 µm
µm
0
50
100
150
µm
12
10
8
6
4
2
0

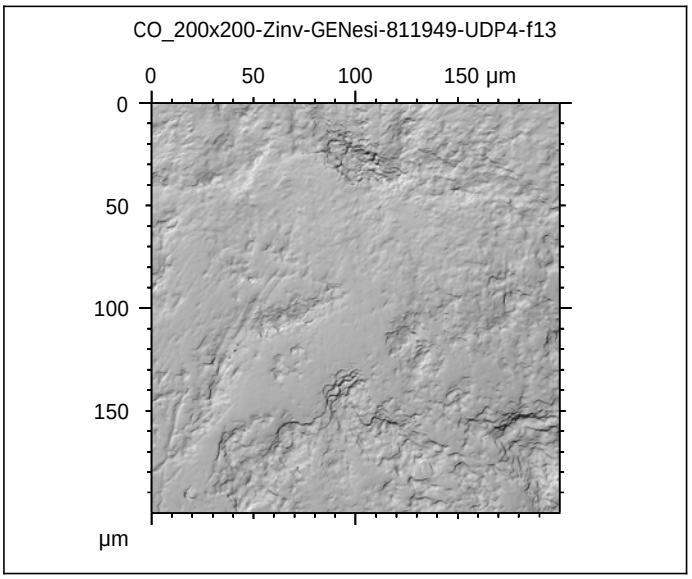
CO_200x200-Zinv-GENesi-811949-UDP4-f13
0
50
100
150 µm
0
50
100
150
µm

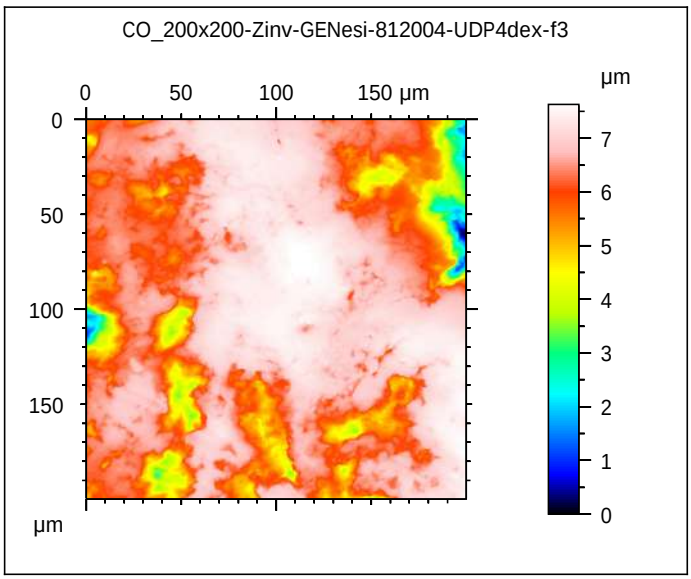
CO_200x200-Zinv-GENesi-812004-UDP4dex-f3
0
50
100
150 µm
µm
0
50
100
150
µm
7
6
5
4
3
2
1
0

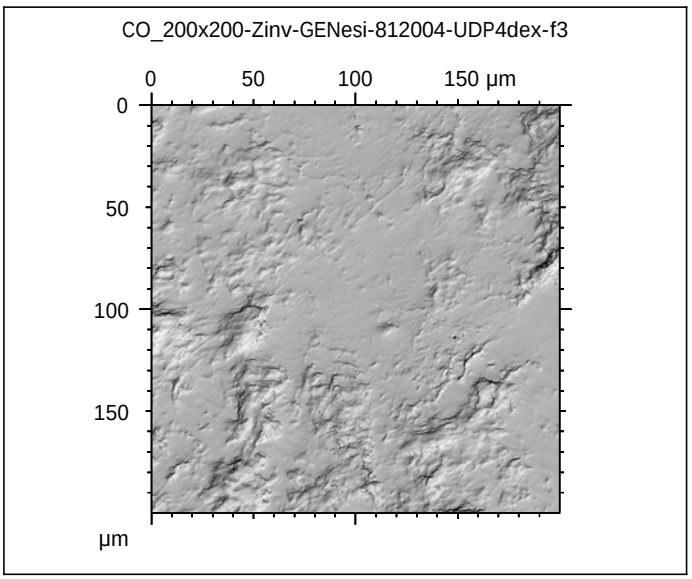
CO_200x200-Zinv-GENesi-812004-UDP4dex-f3
0
50
100
150 µm
0
50
100
150
µm

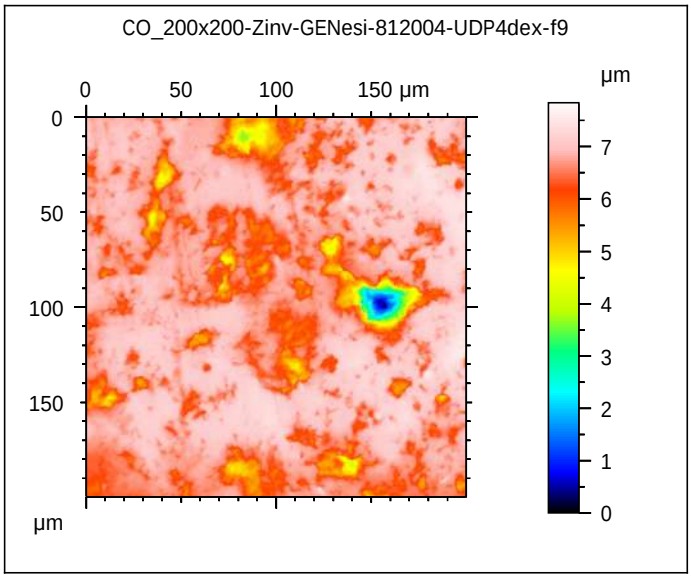
CO_200x200-Zinv-GENesi-812004-UDP4dex-f9
0
50
100
150 µm
µm
7
6
5
4
3
2
1
0

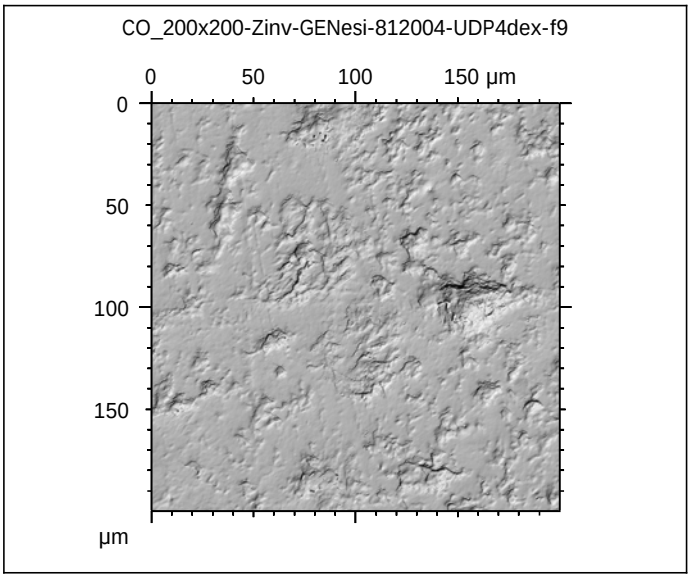
CO_200x200-Zinv-GENesi-812004-UDP4dex-f9
0
50
100
150 µm
µm

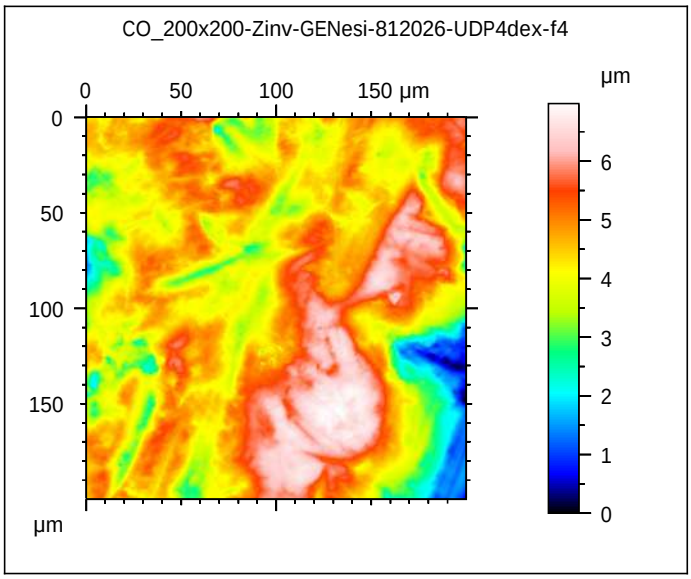
CO_200x200-Zinv-GENesi-812026-UDP4dex-f4
0
50
100
150 µm
µm
6
5
4
3
2
1
0

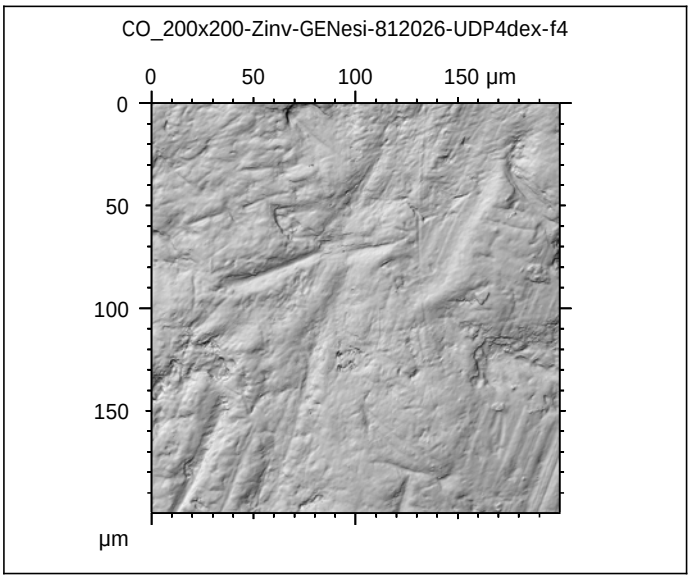
CO_200x200-Zinv-GENesi-812026-UDP4dex-f4
0
50
100
150 µm
µm

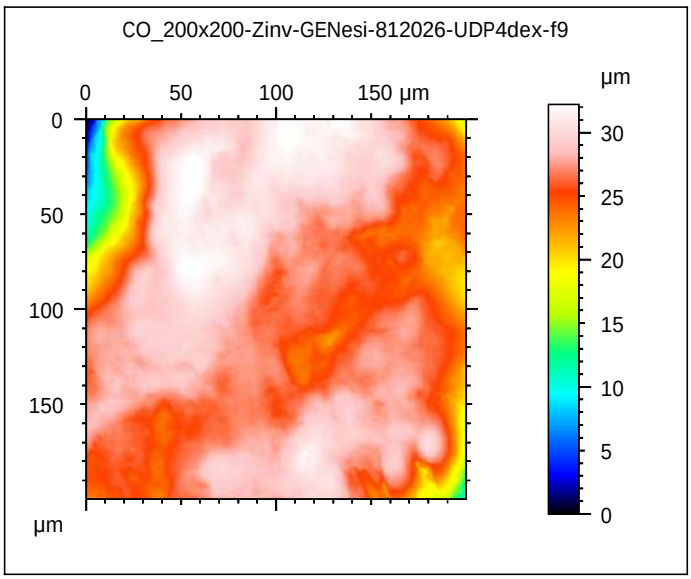
CO_200x200-Zinv-GENesi-812026-UDP4dex-f9
0
50
100
150 µm
µm
30
25
20
15
10
5
0

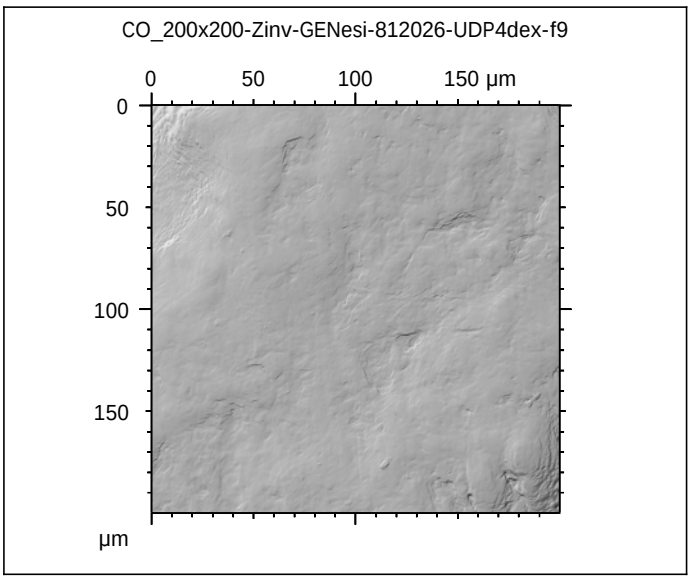
CO_200x200-Zinv-GENesi-812026-UDP4dex-f9
0
50
100
150 µm
µm

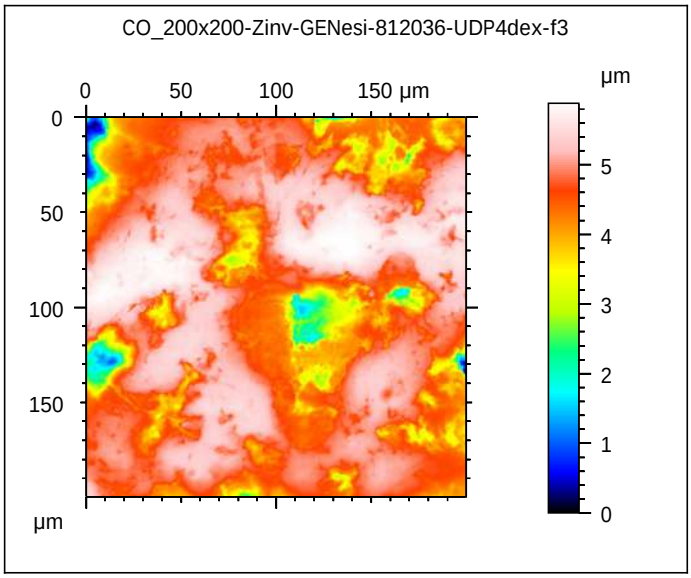
CO_200x200-Zinv-GENesi-812036-UDP4dex-f3
0
50
100
150 µm
µm
0
50
100
150
µm
5
4
3
2
1
0

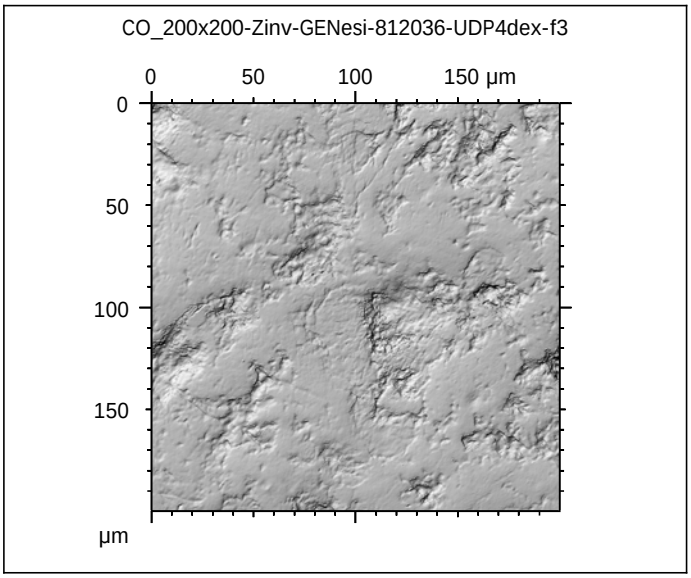
CO_200x200-Zinv-GENesi-812036-UDP4dex-f3
0
50
100
150 µm
0
50
100
150
µm

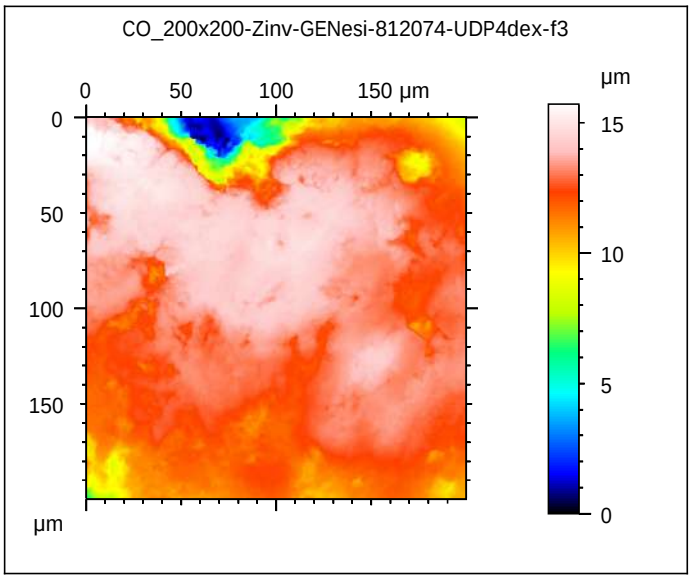
CO_200x200-Zinv-GENesi-812074-UDP4dex-f3
0
50
100
150 µm
µm
0
50
100
150
µm
15
10
5
0

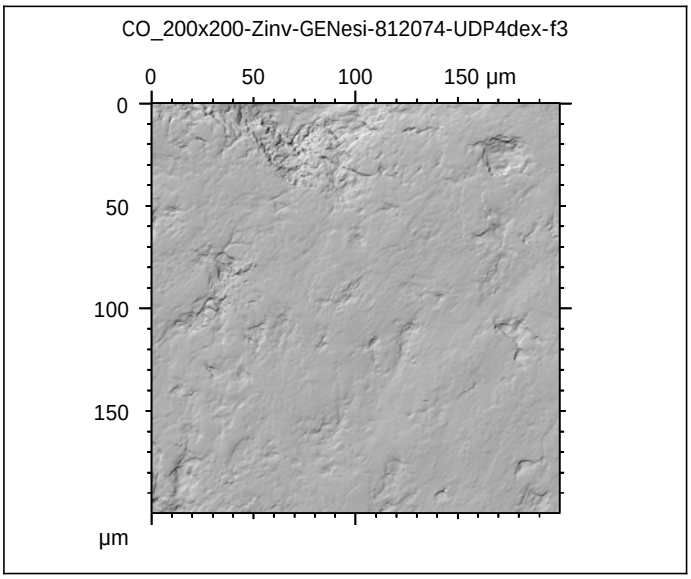
CO_200x200-Zinv-GENesi-812074-UDP4dex-f3
0
50
100
150 µm
0
50
100
150
µm

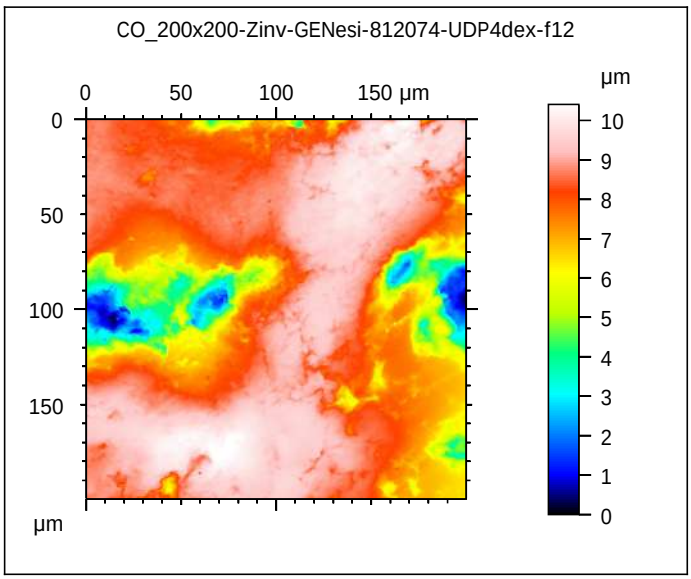
CO_200x200-Zinv-GENesi-812074-UDP4dex-f12
0
50
100
150 µm
µm
0
50
100
150
µm
10
9
8
7
6
5
4
3
2
1
0

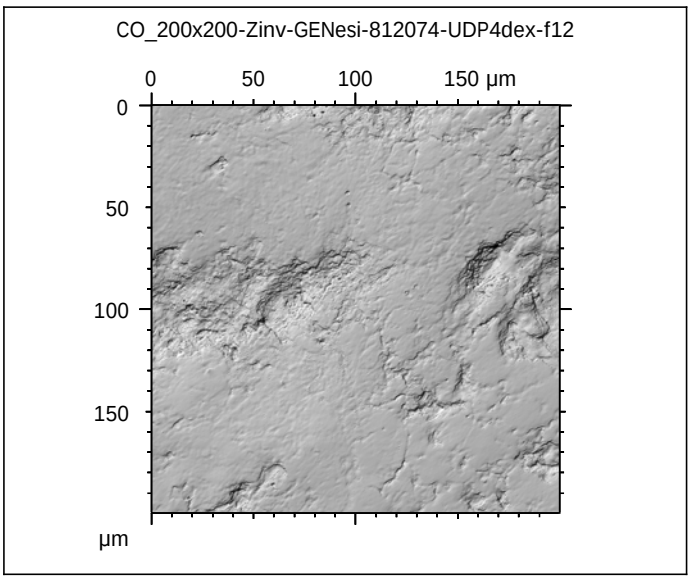
CO_200x200-Zinv-GENesi-812074-UDP4dex-f12
0
50
100
150 µm
0
50
100
150
µm

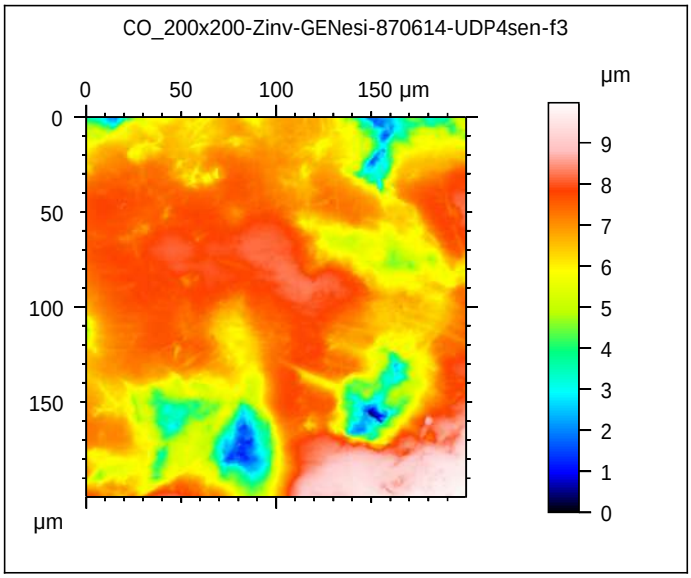
CO_200x200-Zinv-GENesi-870614-UDP4sen-f3
0
50
100
150 µm
µm
9
8
7
6
5
4
3
2
1
0

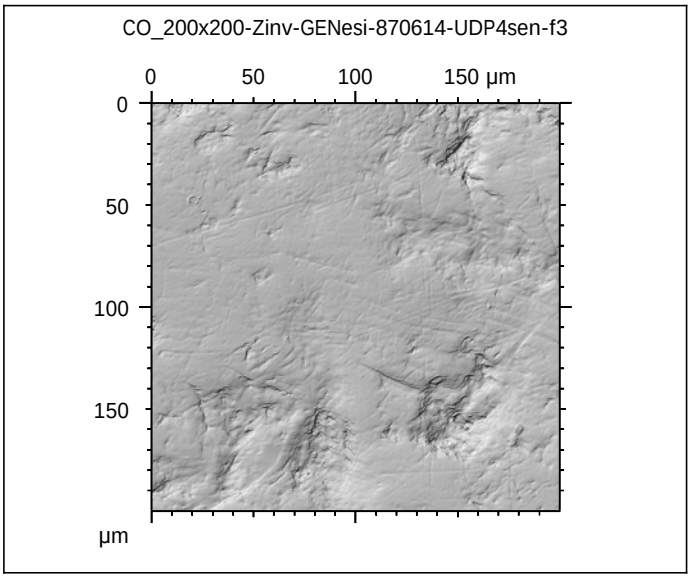
CO_200x200-Zinv-GENesi-870614-UDP4sen-f3
0
50
100
150 µm
µm

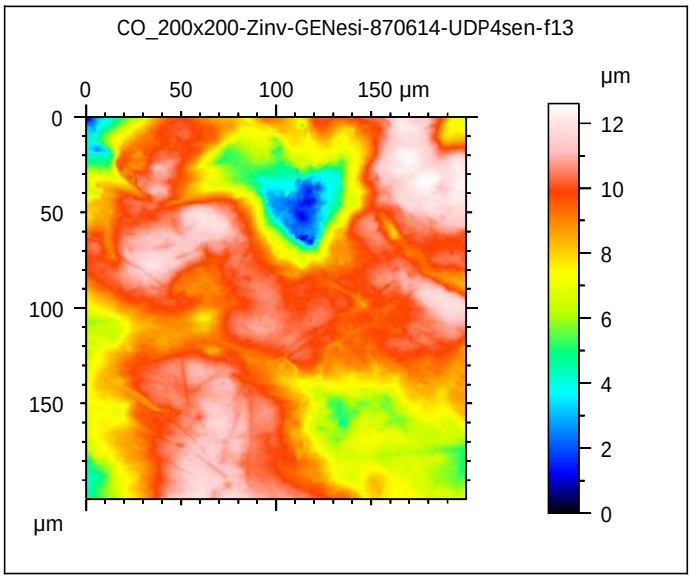
CO_200x200-Zinv-GENesi-870614-UDP4sen-f13
0
50
100
150 µm
µm
12
10
8
6
4
2
0

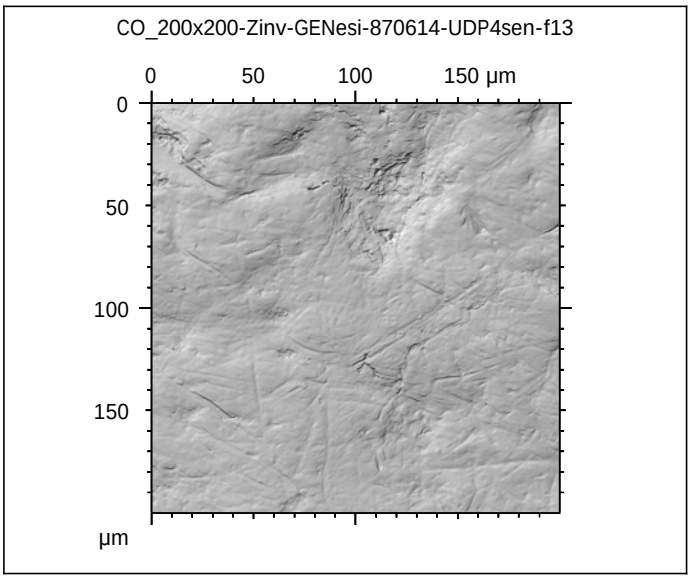
CO_200x200-Zinv-GENesi-870614-UDP4sen-f13
0
50
100
150 µm
µm

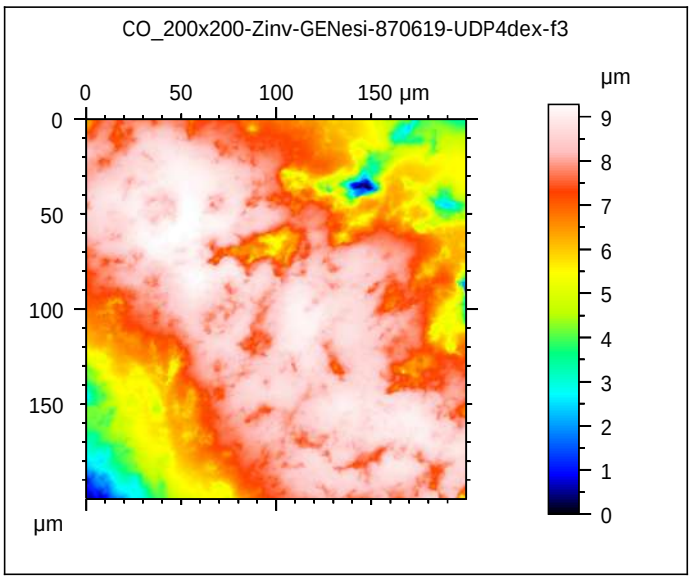
CO_200x200-Zinv-GENesi-870619-UDP4dex-f3
0
50
100
150 µm
µm
9
8
7
6
5
4
3
2
1
0

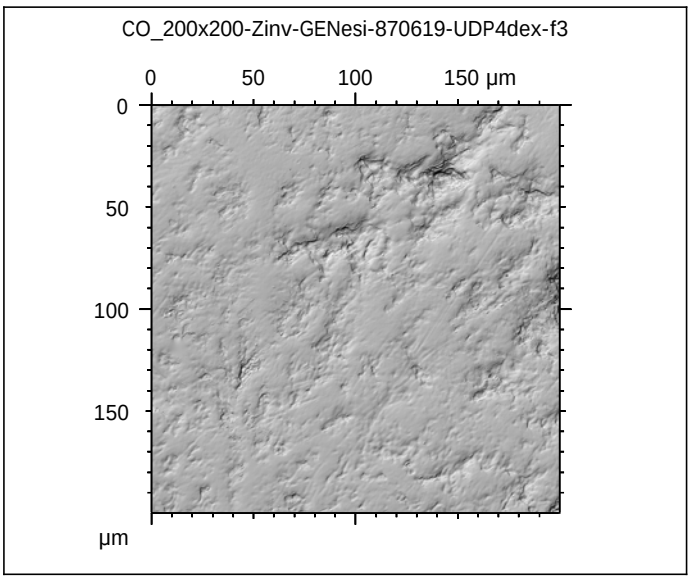
CO_200x200-Zinv-GENesi-870619-UDP4dex-f3
0
50
100
150 µm
µm

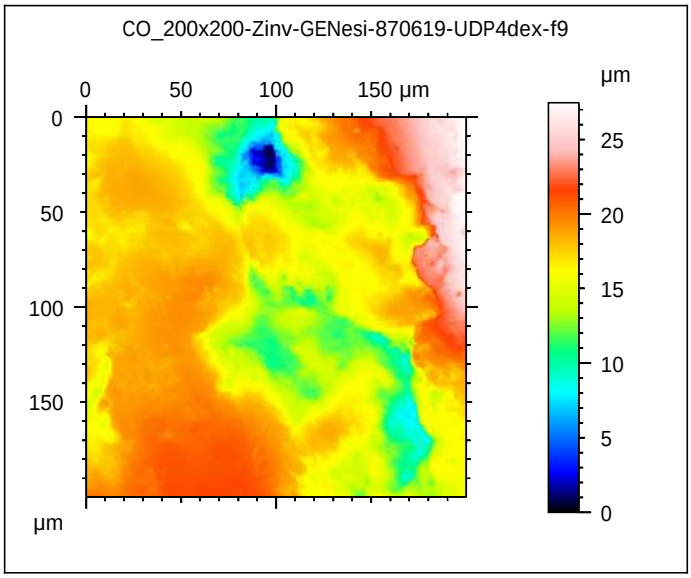
CO_200x200-Zinv-GENesi-870619-UDP4dex-f9
0
50
100
150 µm
µm
25
20
15
10
5
0

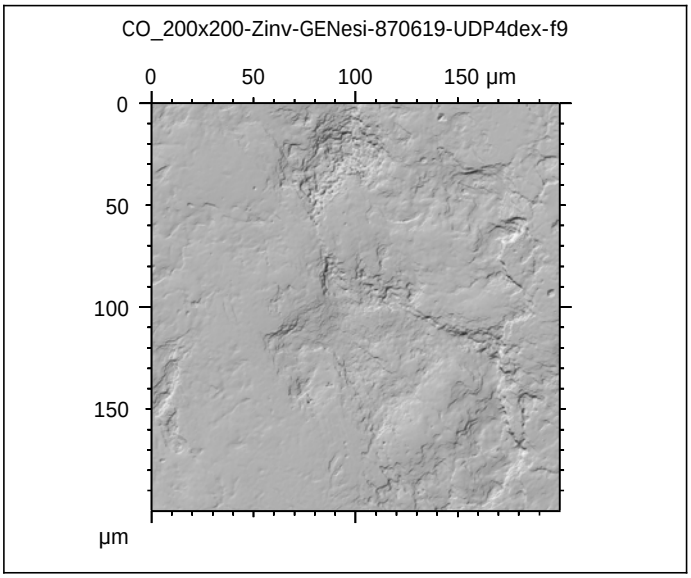
CO_200x200-Zinv-GENesi-870619-UDP4dex-f9
0
50
100
150 µm
µm

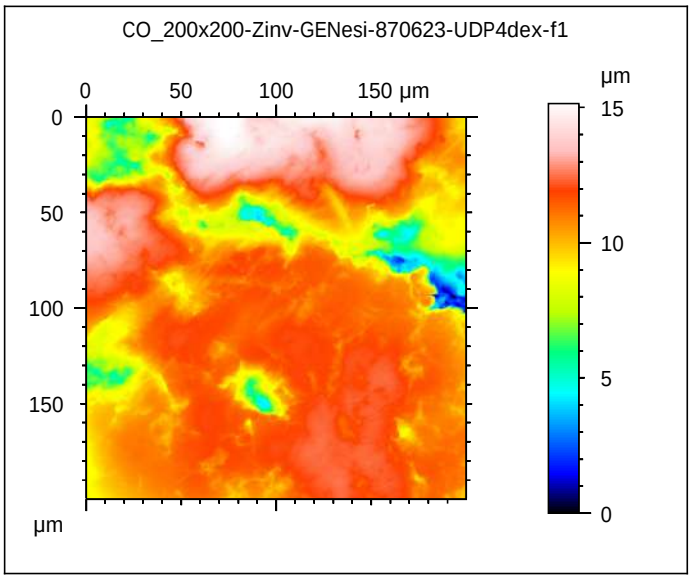
CO_200x200-Zinv-GENesi-870623-UDP4dex-f1
0
50
100
150 µm
µm
15
10
5
0

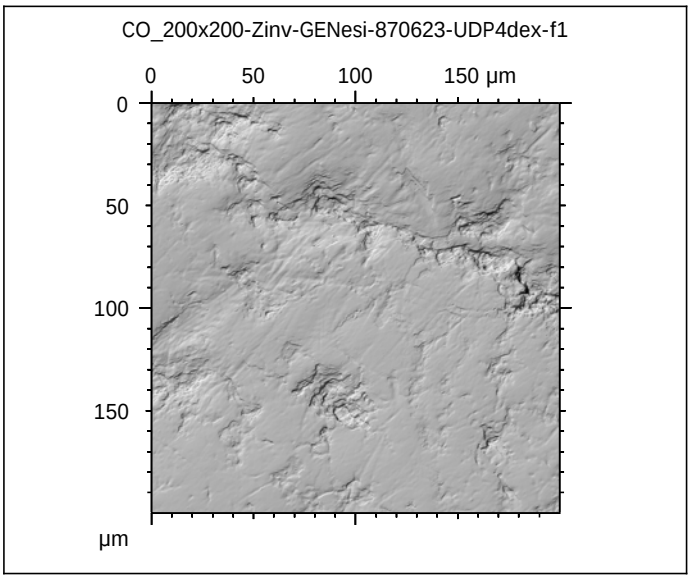
CO_200x200-Zinv-GENesi-870623-UDP4dex-f1
0
50
100
150 µm
µm

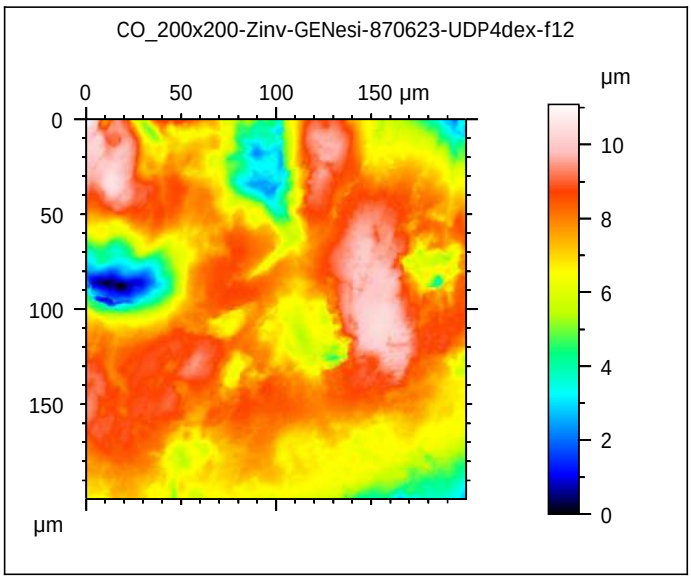
CO_200x200-Zinv-GENesi-870623-UDP4dex-f12
0
50
100
150 µm
µm
10
8
6
4
2
0

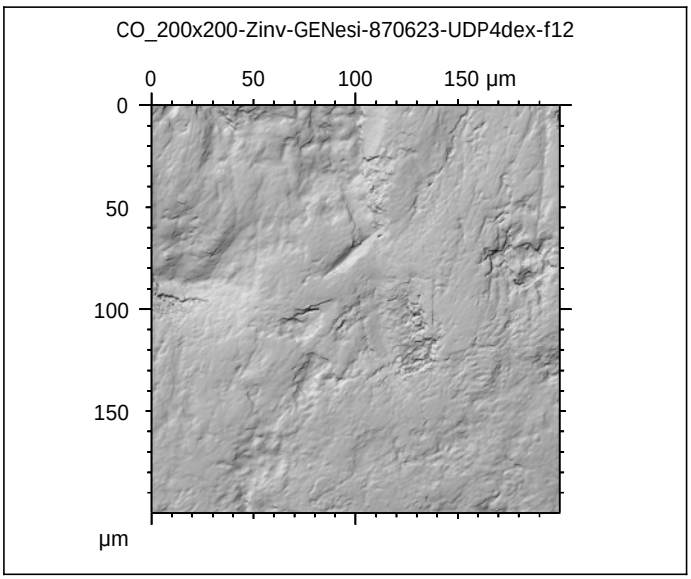
CO_200x200-Zinv-GENesi-870623-UDP4dex-f12
0
50
100
150 µm
µm

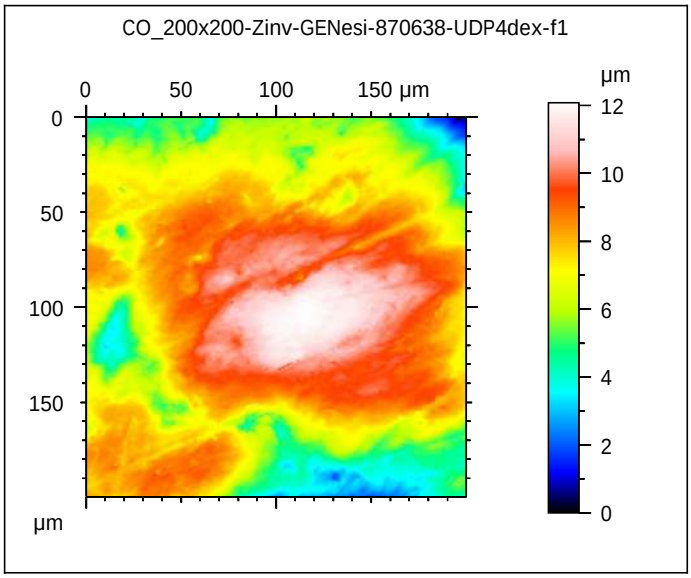
CO_200x200-Zinv-GENesi-870638-UDP4dex-f1
0
50
100
150 µm
µm
12
10
8
6
4
2
0

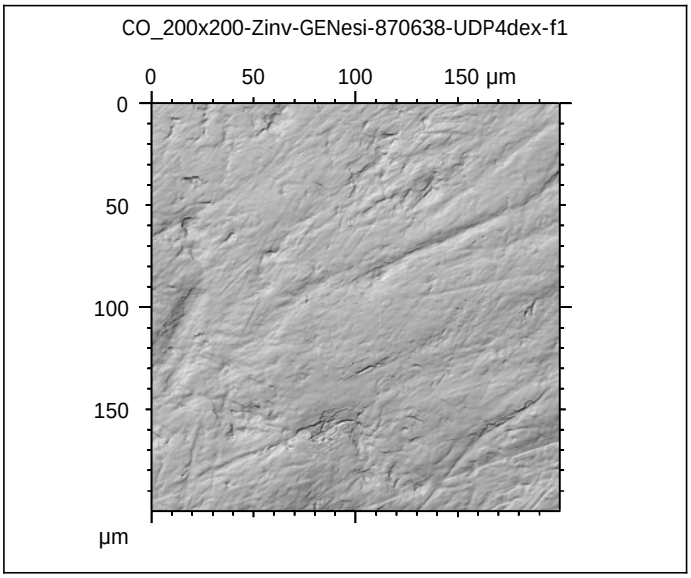
CO_200x200-Zinv-GENesi-870638-UDP4dex-f1
0
50
100
150 µm
µm

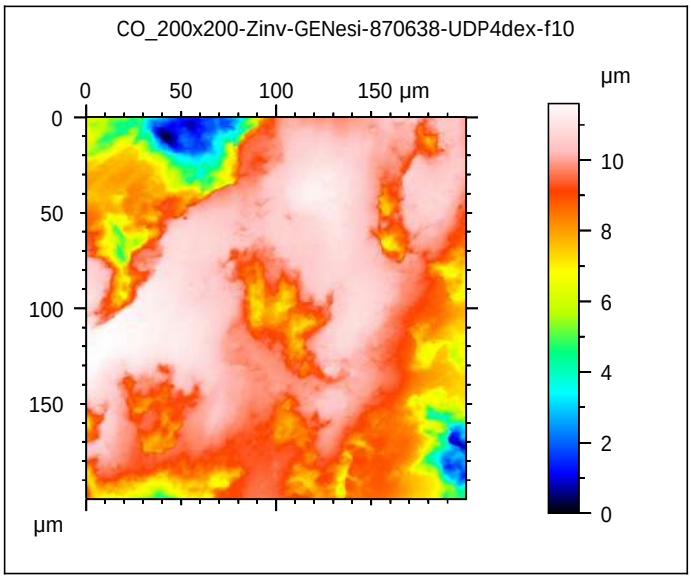
CO_200x200-Zinv-GENesi-870638-UDP4dex-f10
0
50
100
150 µm
µm
10
8
6
4
2
0

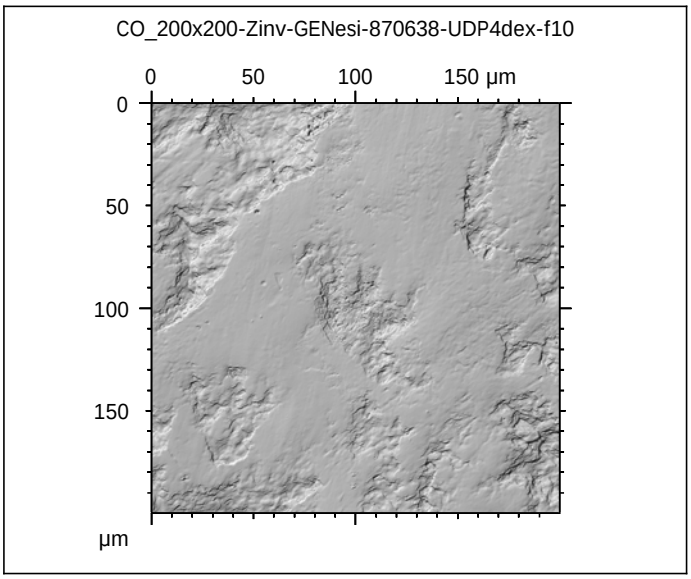
CO_200x200-Zinv-GENesi-870638-UDP4dex-f10
0
50
100
150 µm
µm

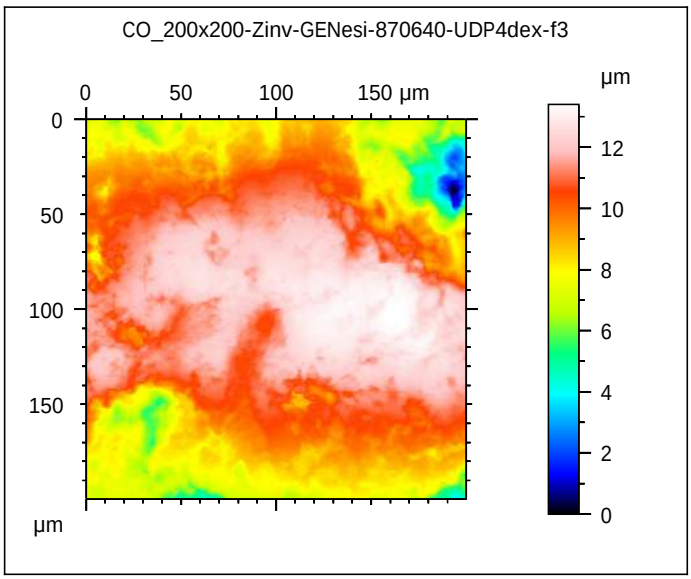
CO_200x200-Zinv-GENesi-870640-UDP4dex-f3
0
50
100
150 µm
µm
12
10
8
6
4
2
0

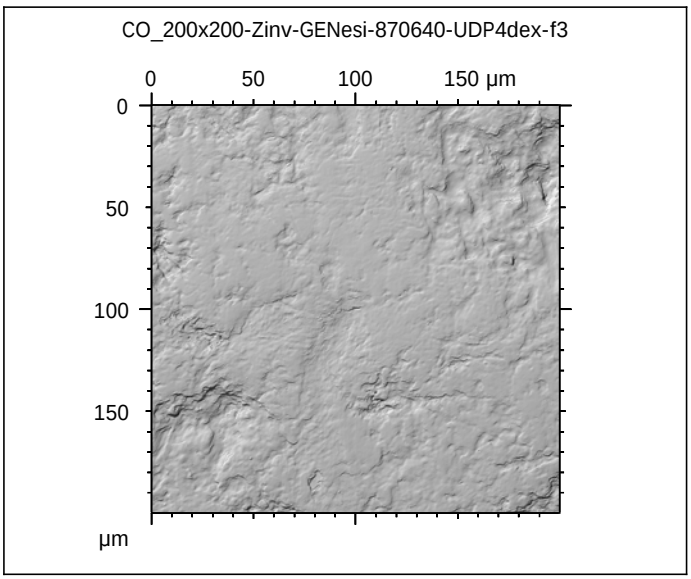
CO_200x200-Zinv-GENesi-870640-UDP4dex-f3
0
50
100
150 µm
µm

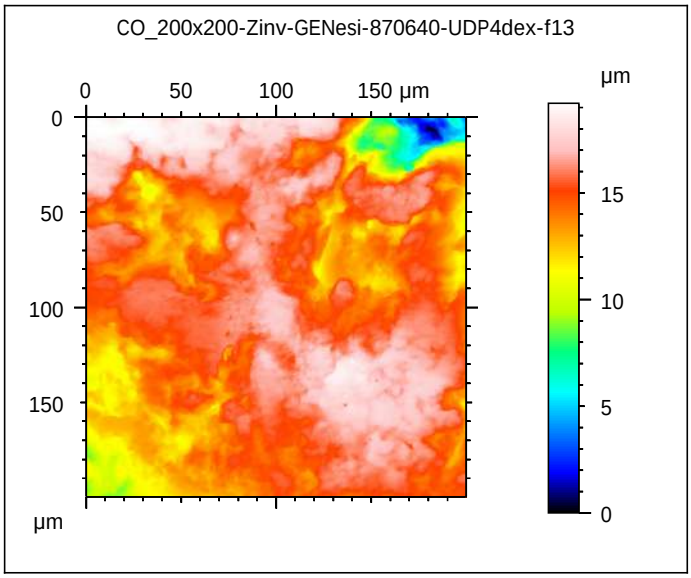
CO_200x200-Zinv-GENesi-870640-UDP4dex-f13
0
50
100
150 µm
µm
15
10
5
0

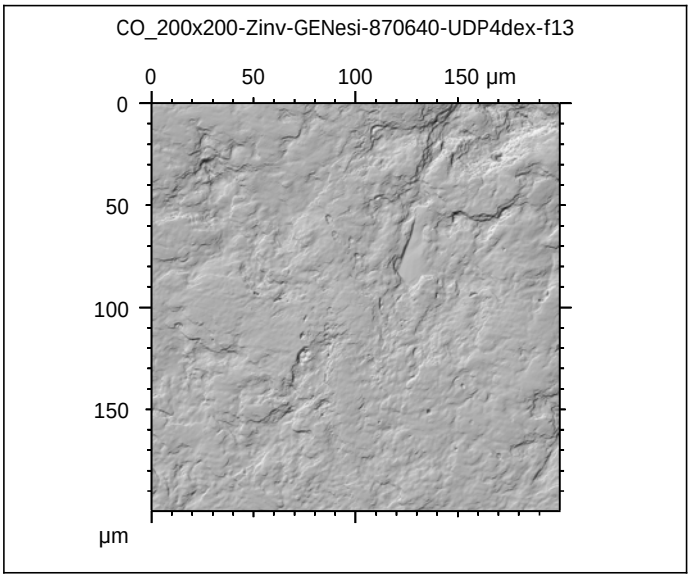
CO_200x200-Zinv-GENesi-870640-UDP4dex-f13
0
50
100
150 µm
µm

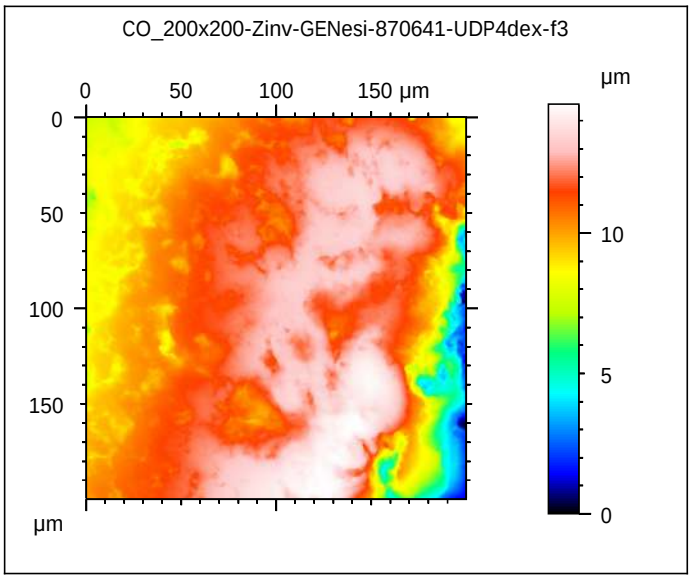
CO_200x200-Zinv-GENesi-870641-UDP4dex-f3
0
50
100
150 µm
µm
10
5
0

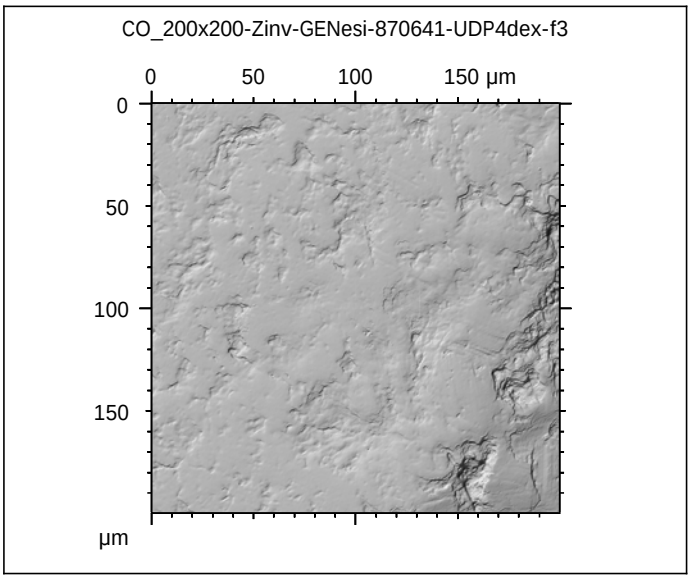
CO_200x200-Zinv-GENesi-870641-UDP4dex-f3
0
50
100
150 µm
µm

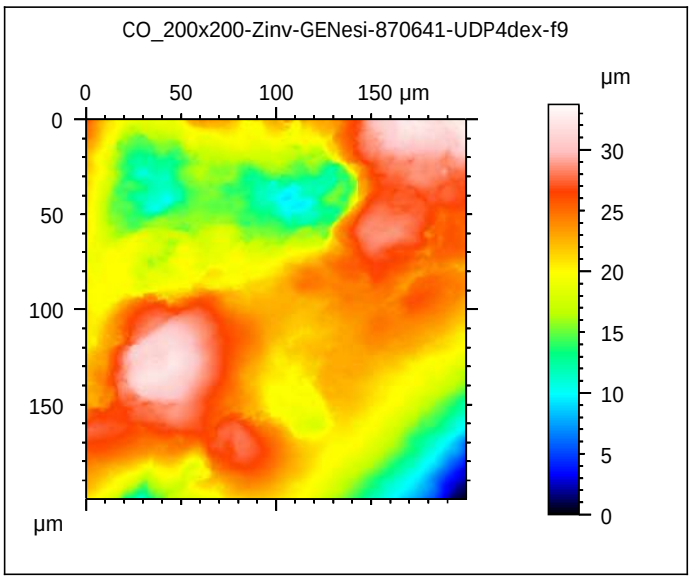
CO_200x200-Zinv-GENesi-870641-UDP4dex-f9
0
50
100
150 µm
µm
30
25
20
15
10
5
0

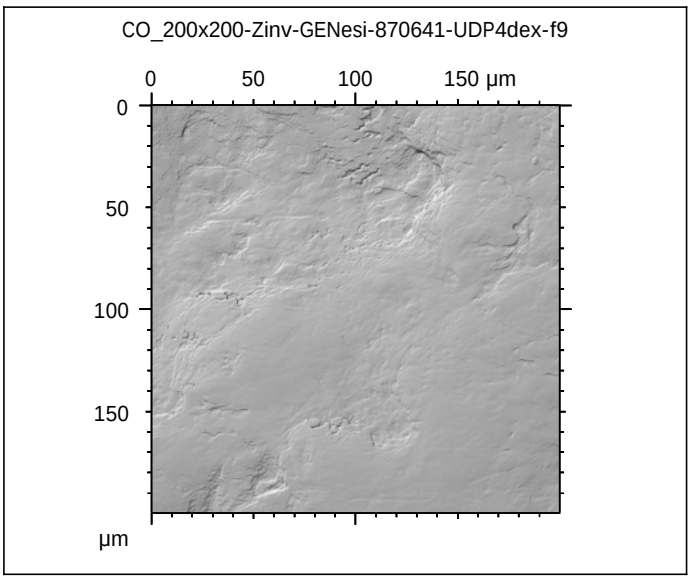
CO_200x200-Zinv-GENesi-870641-UDP4dex-f9
0
50
100
150 µm
µm

Photosimulations and false color elevation maps of scanned shearing and crushing facets on molars and deciduous premolars of the **barley group** (70% base diet + 30% barley seeds)

scanned at the PALEVOPRIM lab by M. Louail, University of Poitiers, France with "TRIDENT", white light confocal microscope Leica DCM8 - April 2020

ALIHOM Project (Région Nouvelle Aquitaine, France), ANR Diet-Scratches

ANR-17-CE27-0002

PIs: G. Merceron & S. Ferchaud

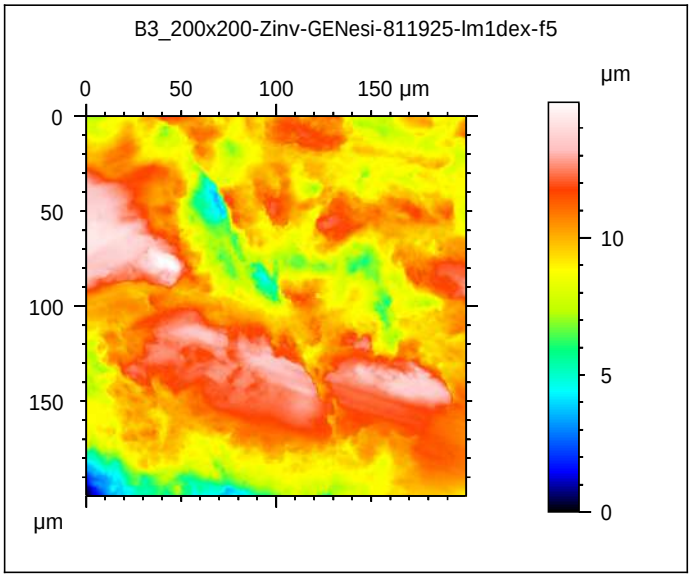

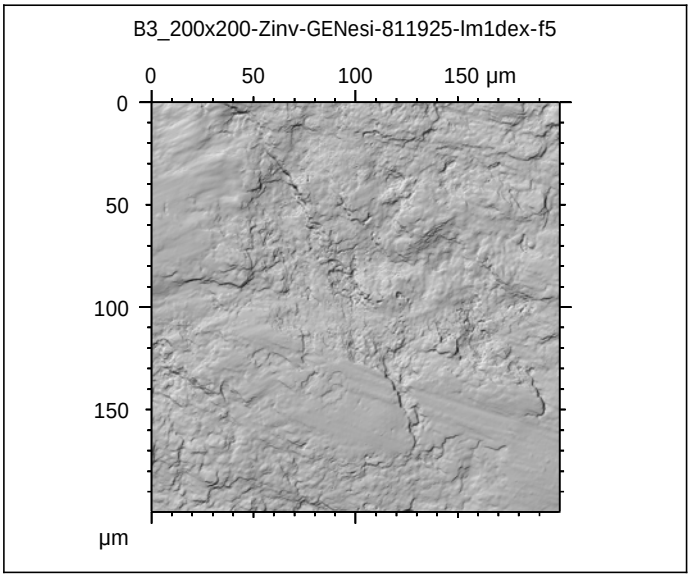

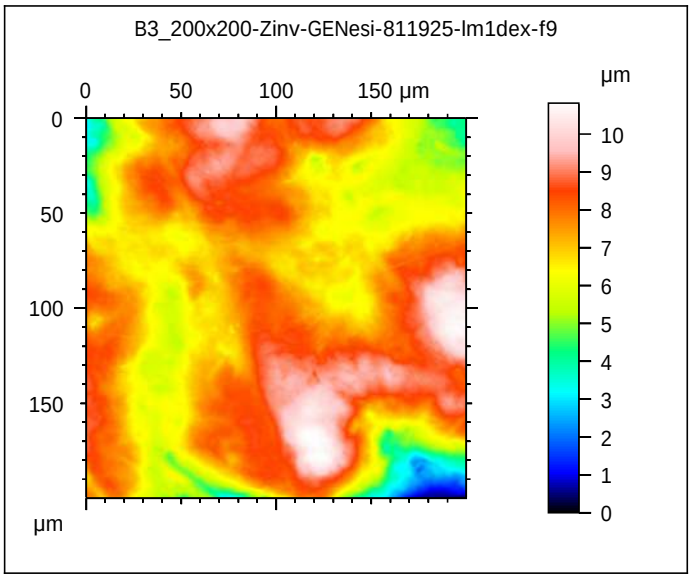

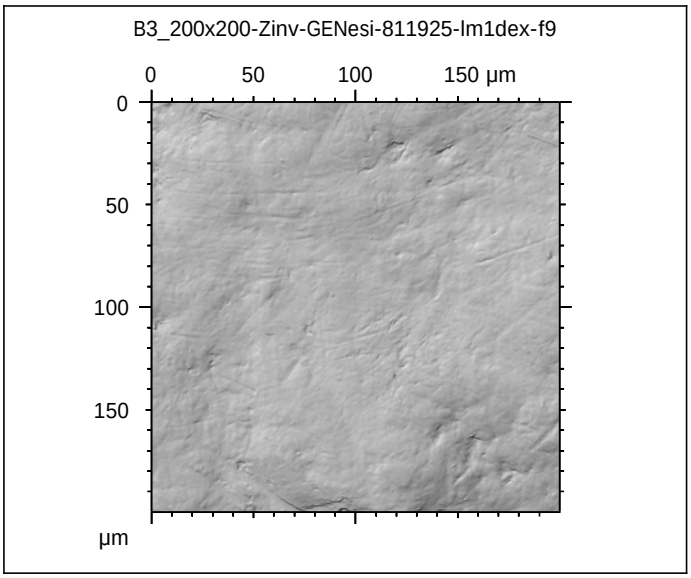

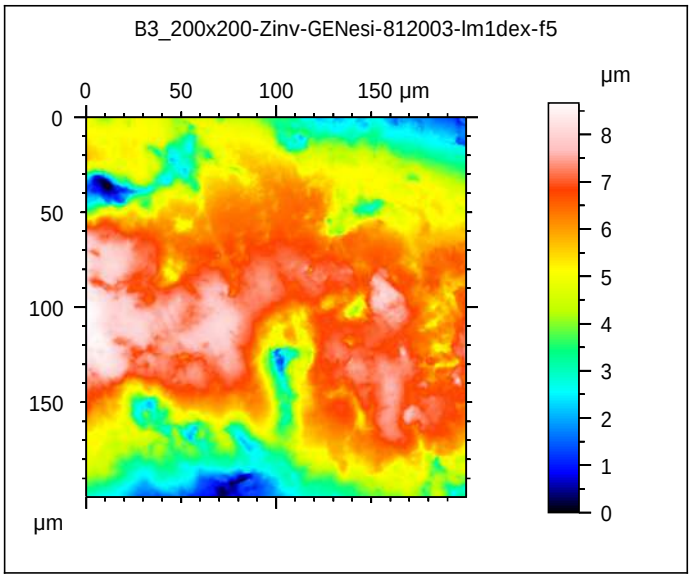

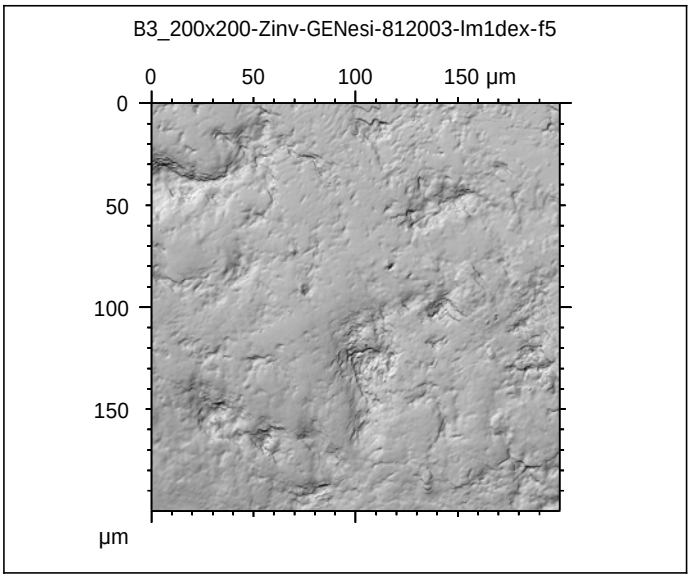

Leica Map Premium 8.0.9173

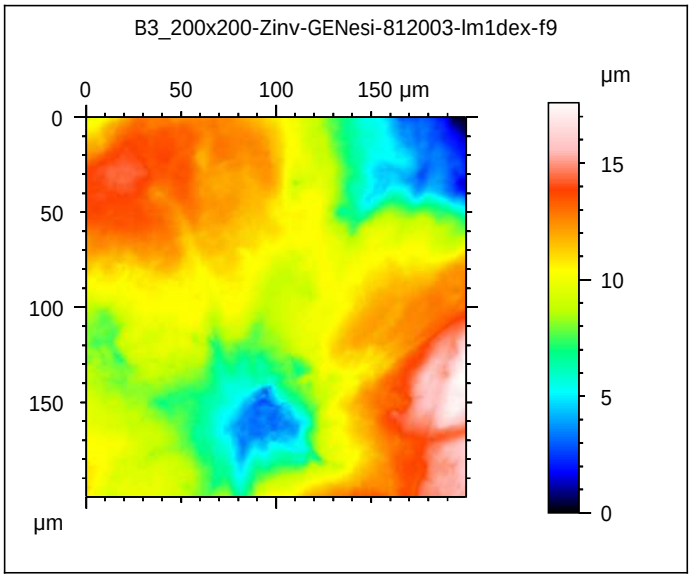
B3_200x200-Zinv-GENesi-812003-lm1dex-f9
0
50
100
150 µm
µm
15
10
5
0

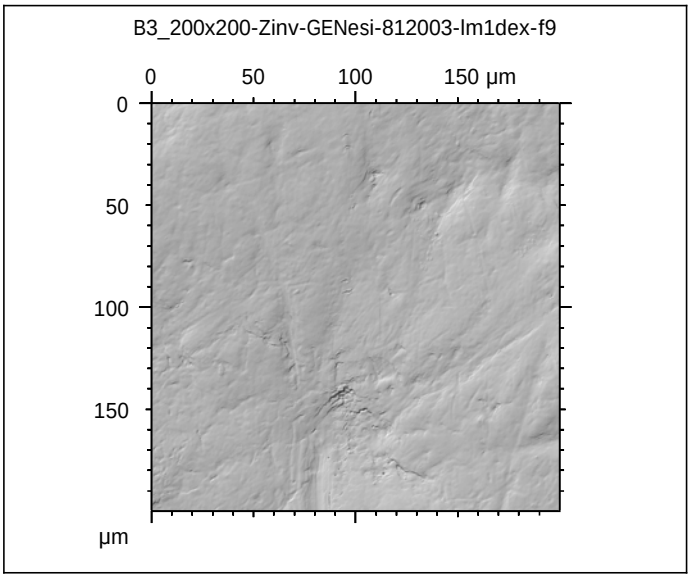
B3_200x200-Zinv-GENesi-812003-lm1dex-f9
0
50
100
150 µm
µm

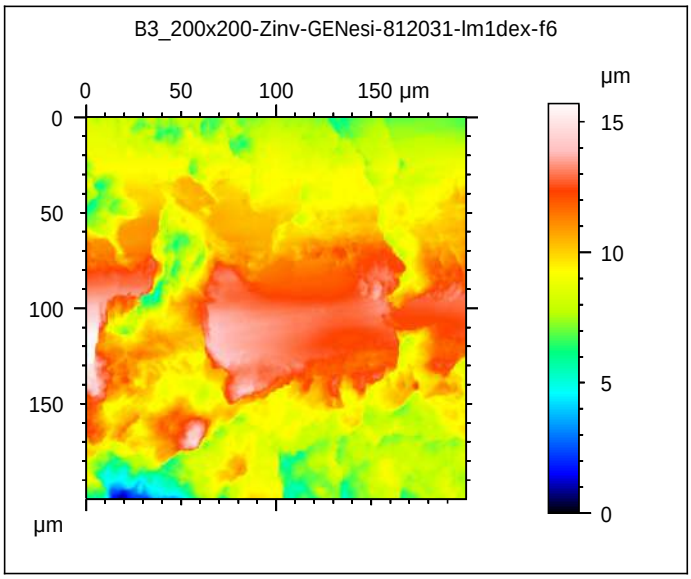
B3_200x200-Zinv-GENesi-812031-lm1dex-f6
0
50
100
150 µm
µm
15
10
5
0

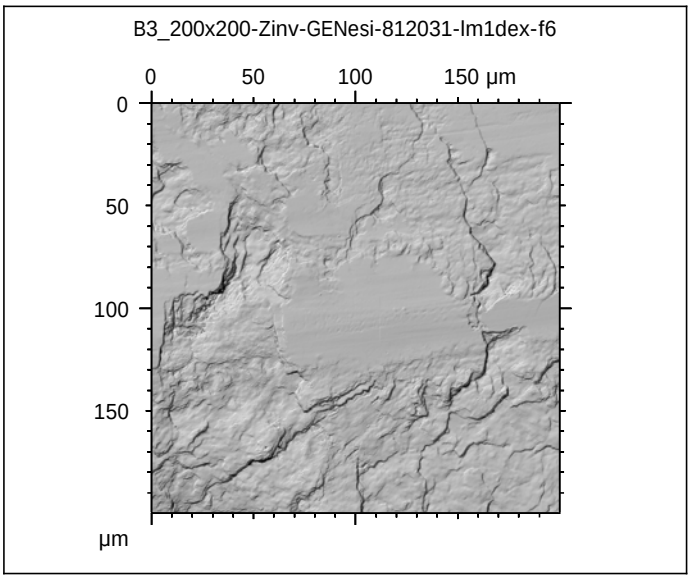
B3_200x200-Zinv-GENesi-812031-lm1dex-f6
0
50
100
150 µm
µm

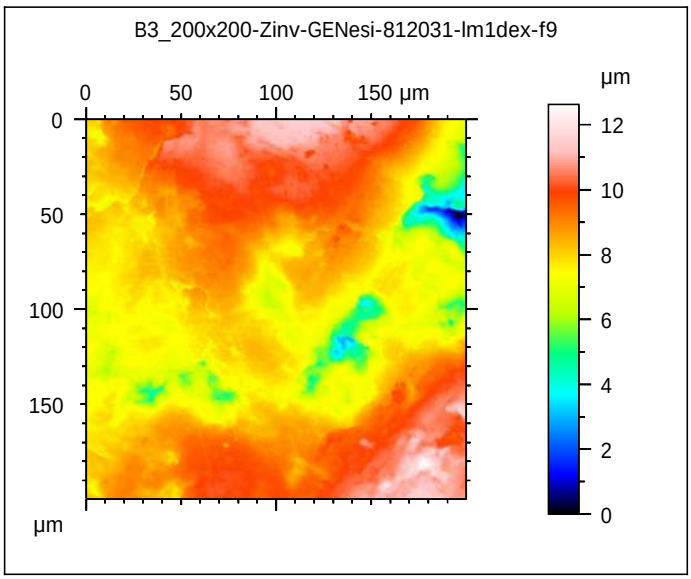
B3_200x200-Zinv-GENesi-812031-lm1dex-f9
0
50
100
150 µm
µm
12
10
8
6
4
2
0

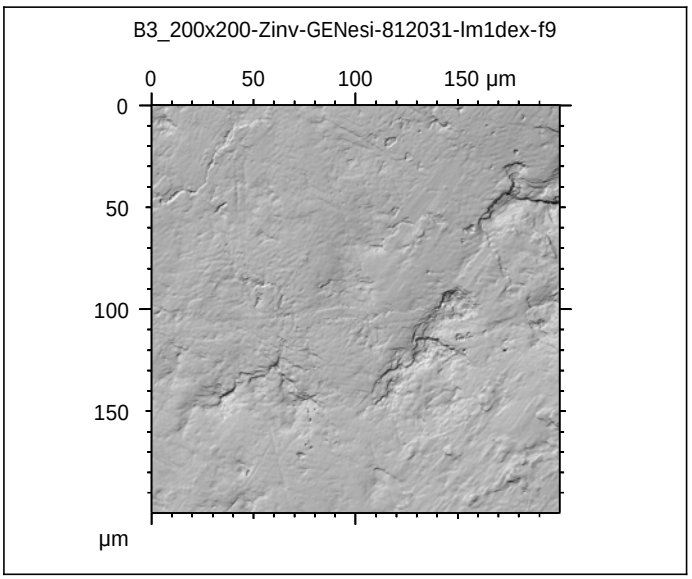
B3_200x200-Zinv-GENesi-812031-lm1dex-f9
0
50
100
150 µm
µm

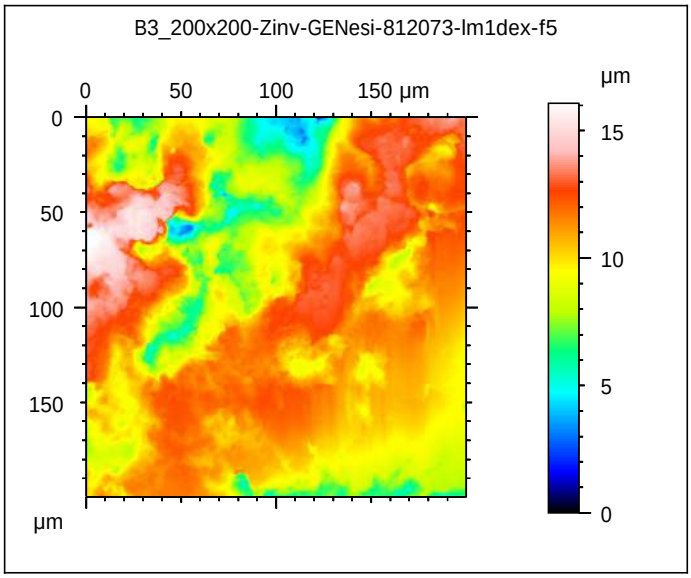
B3_200x200-Zinv-GENesi-812073-lm1dex-f5
0
50
100
150 µm
µm
15
10
5
0

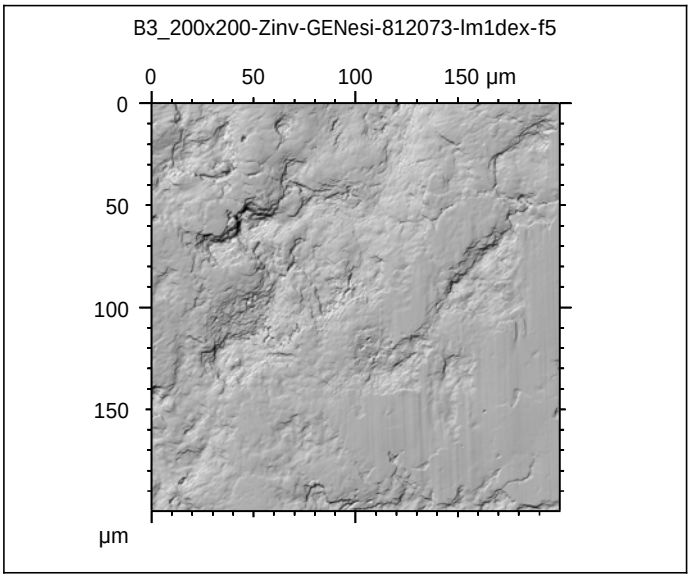
B3_200x200-Zinv-GENesi-812073-lm1dex-f5
0
50
100
150 µm
µm

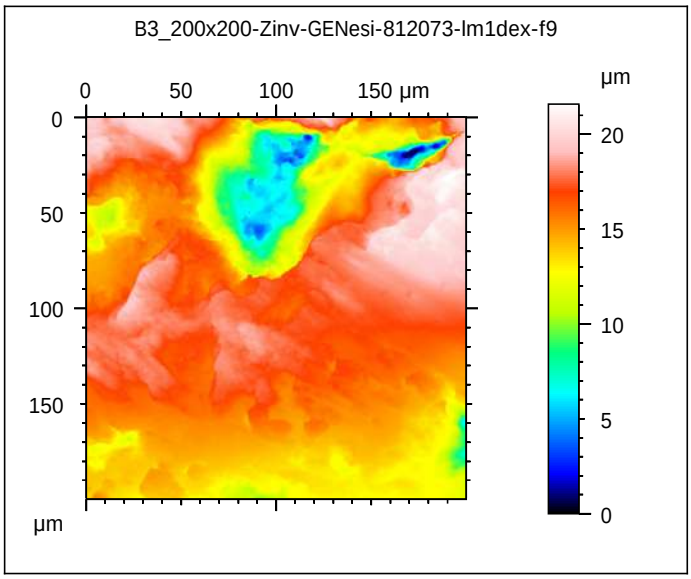
B3_200x200-Zinv-GENesi-812073-lm1dex-f9
0
50
100
150 µm
µm
20
15
10
5
0

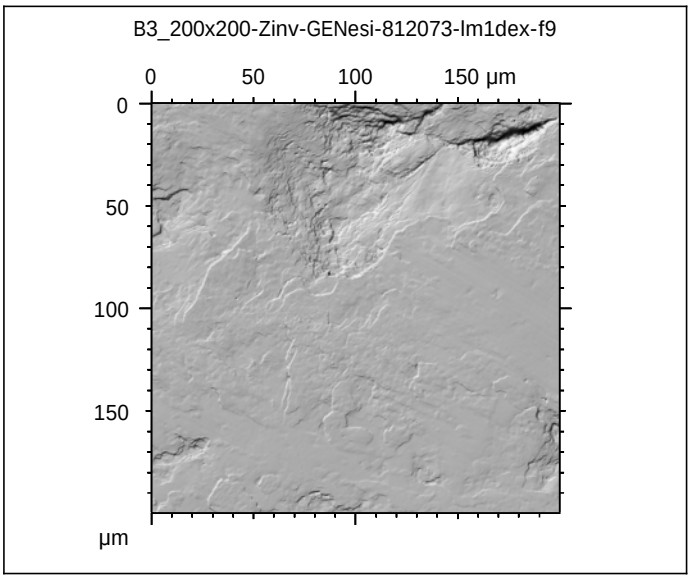
B3_200x200-Zinv-GENesi-812073-lm1dex-f9
0
50
100
150 µm
µm

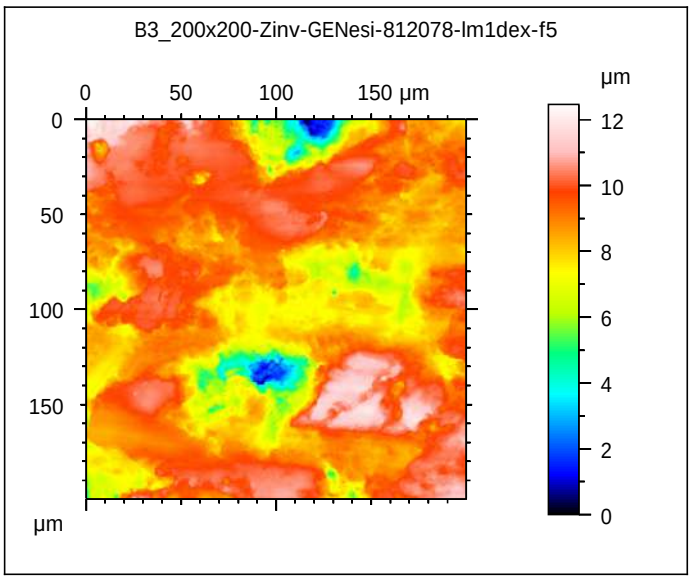
B3_200x200-Zinv-GENesi-812078-lm1dex-f5
0
50
100
150 µm
µm
12
10
8
6
4
2
0

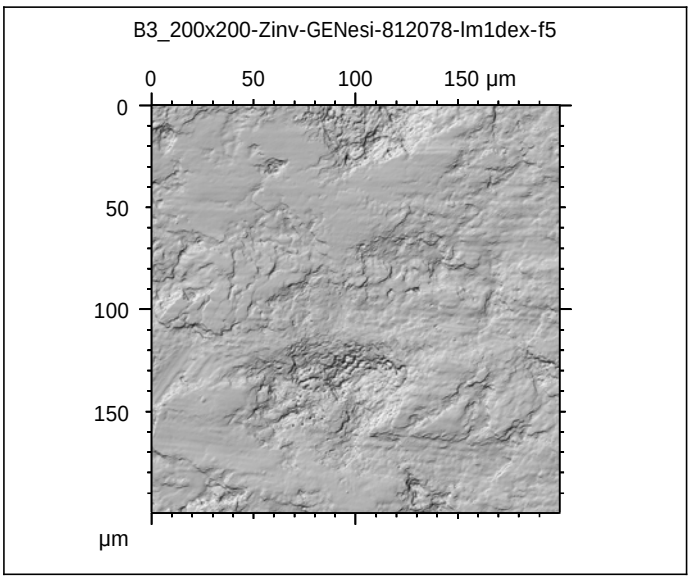
B3_200x200-Zinv-GENesi-812078-lm1dex-f5
0
50
100
150 µm
µm

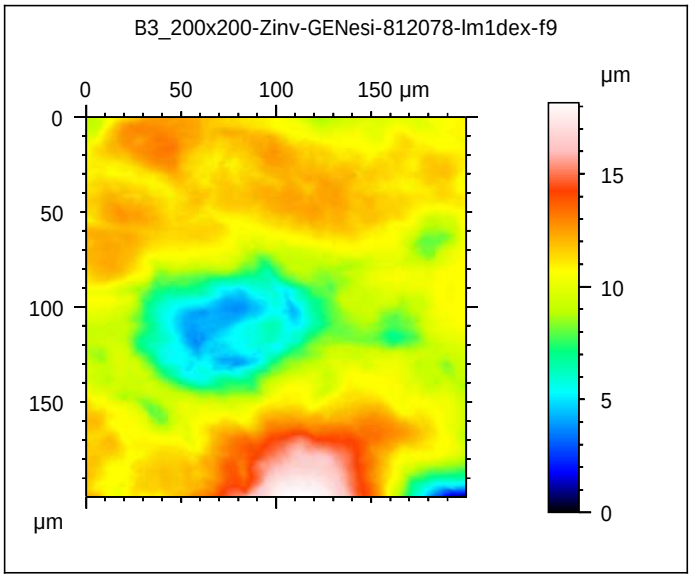
B3_200x200-Zinv-GENesi-812078-lm1dex-f9
0
50
100
150 µm
µm
15
10
5
0

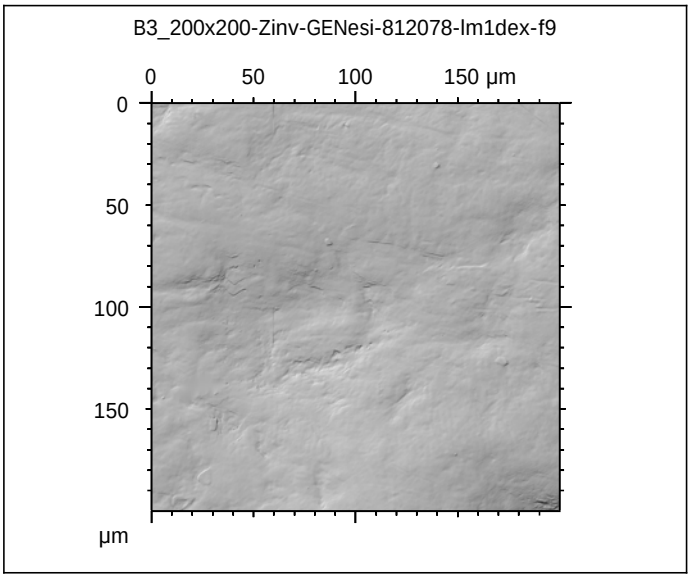
B3_200x200-Zinv-GENesi-812078-lm1dex-f9
0
50
100
150 µm
µm

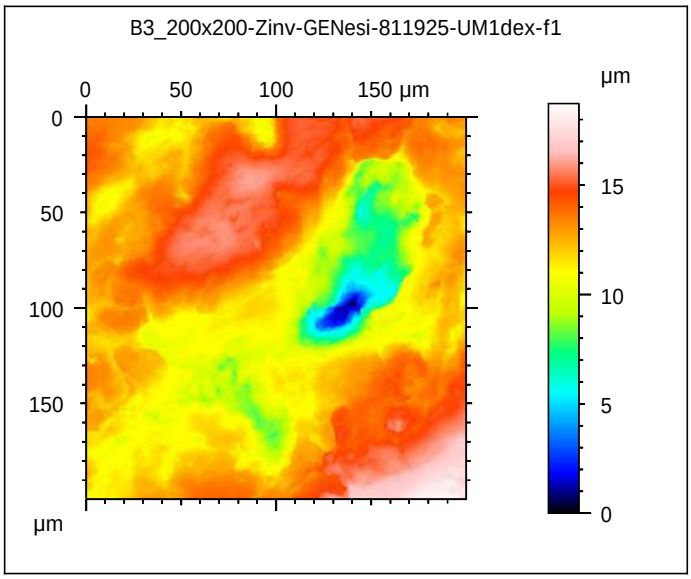
B3_200x200-Zinv-GENesi-811925-UM1dex-f1
0
50
100
150 µm
µm
15
10
5
0

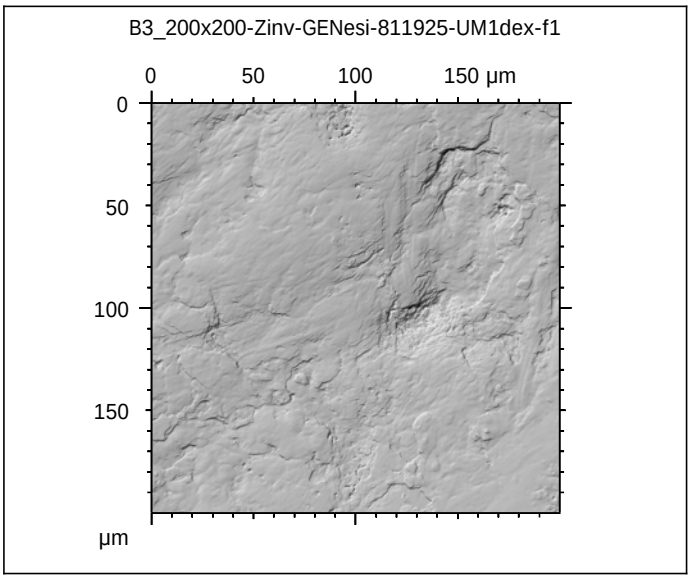
B3_200x200-Zinv-GENesi-811925-UM1dex-f1
0
50
100
150 µm
µm

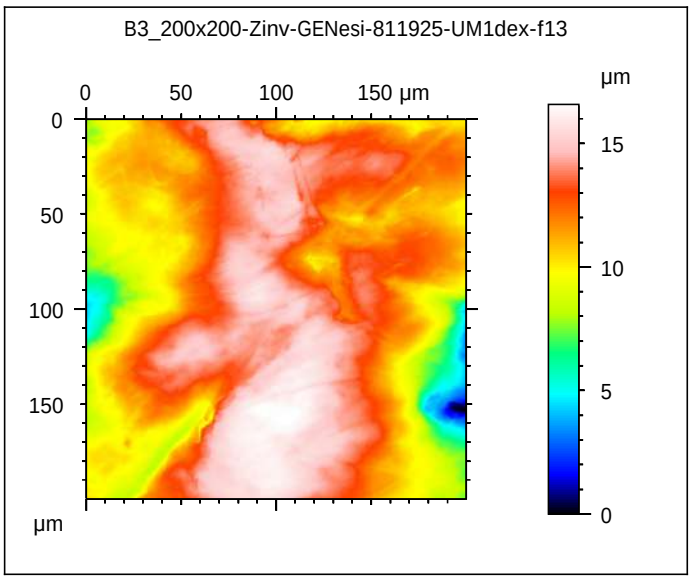
B3_200x200-Zinv-GENesi-811925-UM1dex-f13
0
50
100
150 µm
µm
15
10
5
0

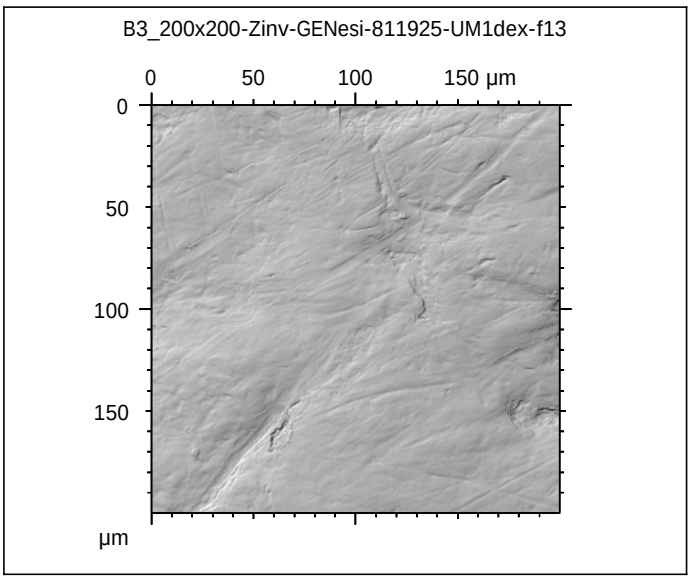
B3_200x200-Zinv-GENesi-811925-UM1dex-f13
0
50
100
150 µm
µm

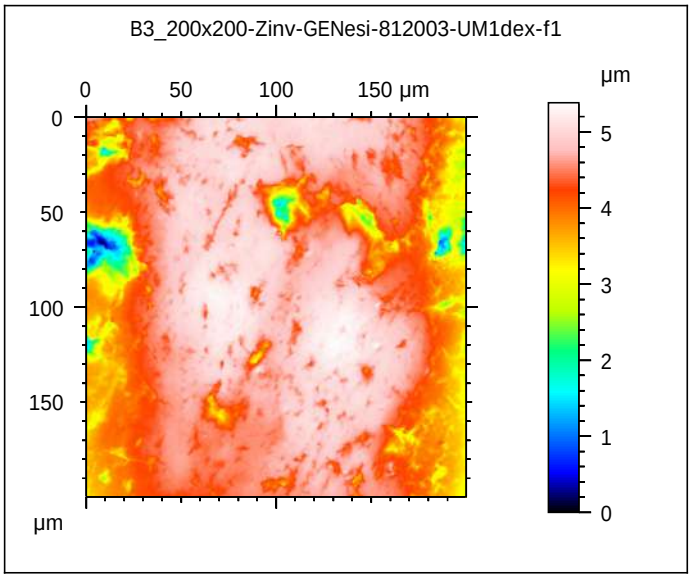
B3_200x200-Zinv-GENesi-812003-UM1dex-f1
0
50
100
150 µm
µm
0
50
100
150
µm
5
4
3
2
1
0

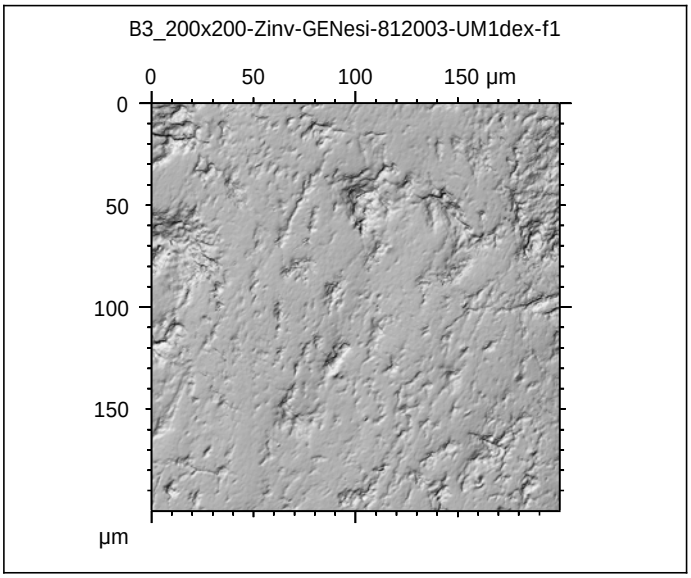
B3_200x200-Zinv-GENesi-812003-UM1dex-f1
0
50
100
150 µm
0
50
100
150
µm

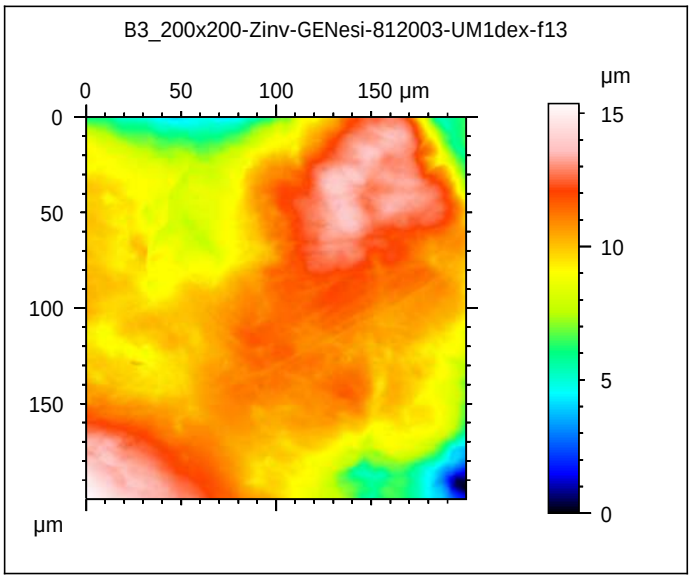
B3_200x200-Zinv-GENesi-812003-UM1dex-f13
0
50
100
150 µm
µm
0
50
100
150
µm
15
10
5
0

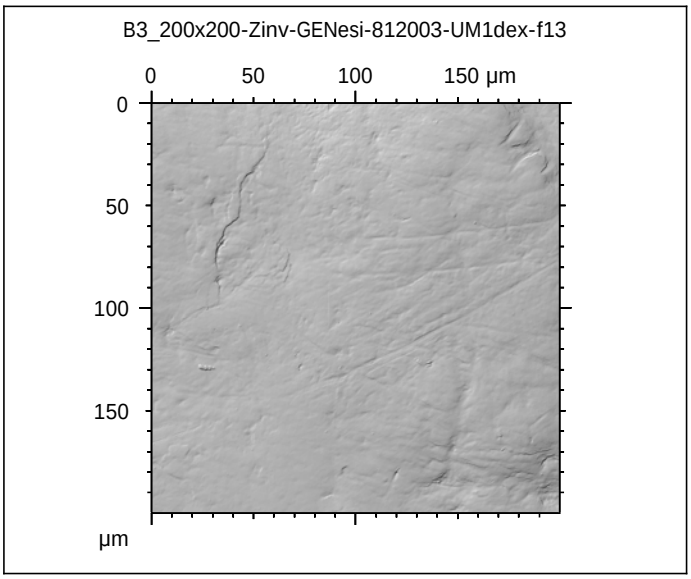
B3_200x200-Zinv-GENesi-812003-UM1dex-f13
0
50
100
150 µm
0
50
100
150
µm

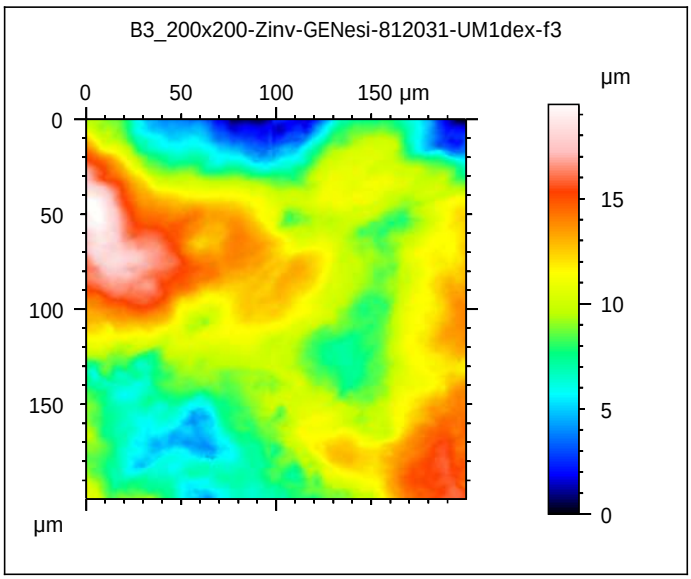
B3_200x200-Zinv-GENesi-812031-UM1dex-f3
0
50
100
150 µm
µm
0
50
100
150
µm
15
10
5
0

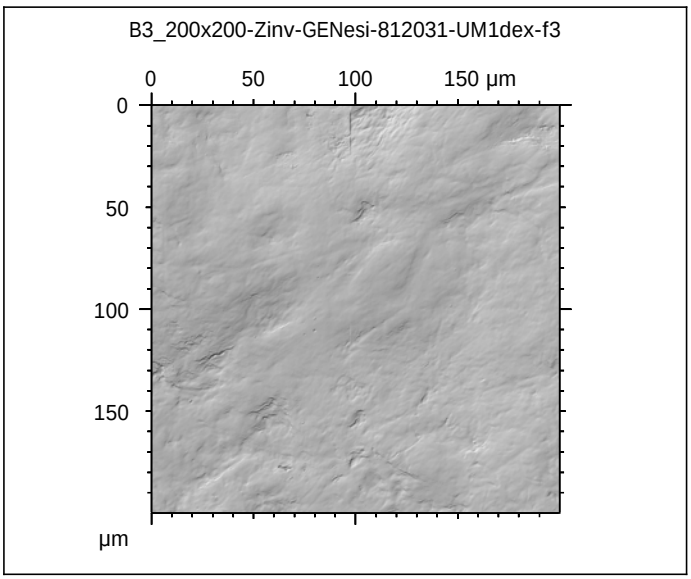
B3_200x200-Zinv-GENesi-812031-UM1dex-f3
0
50
100
150 µm
0
50
100
150
µm

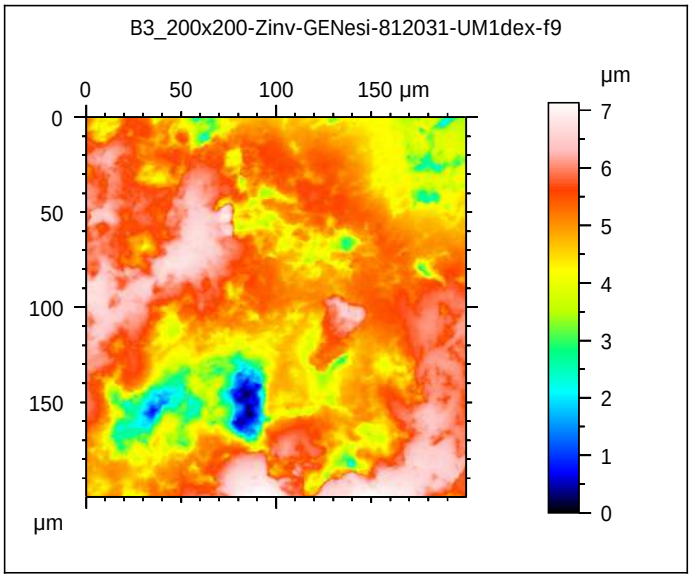
B3_200x200-Zinv-GENesi-812031-UM1dex-f9
0
50
100
150 µm
µm
7
6
5
4
3
2
1
0

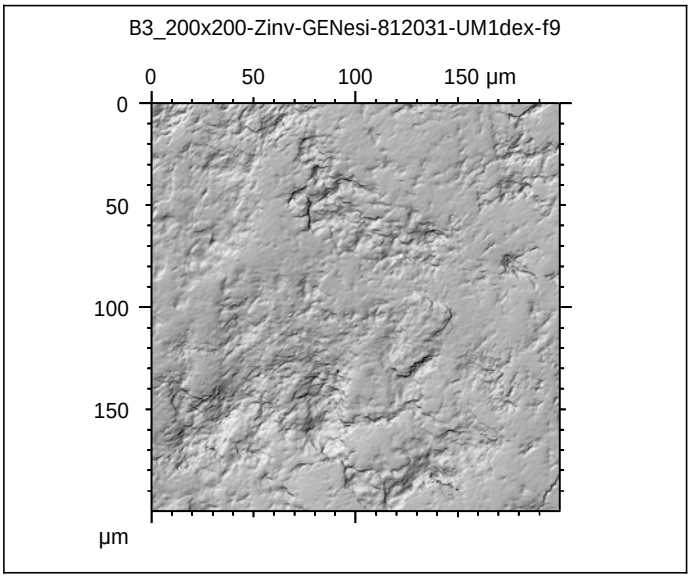
B3_200x200-Zinv-GENesi-812031-UM1dex-f9
0
50
100
150 µm
µm

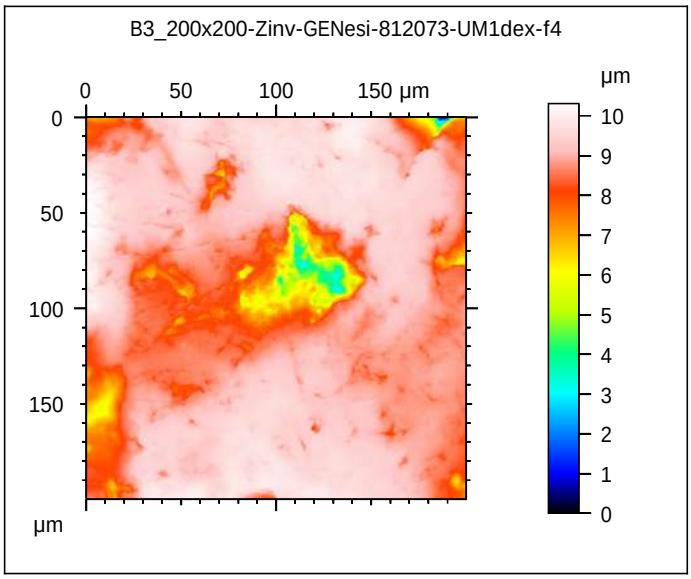
B3_200x200-Zinv-GENesi-812073-UM1dex-f4
0
50
100
150 µm
µm
10
9
8
7
6
5
4
3
2
1
0

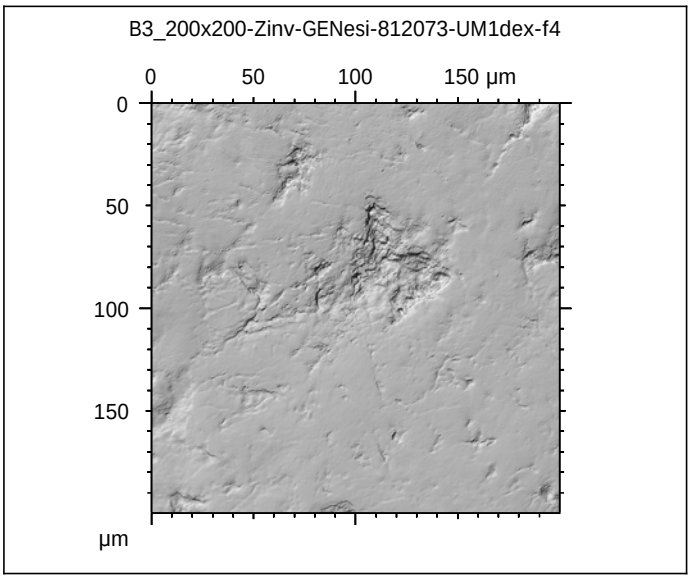
B3_200x200-Zinv-GENesi-812073-UM1dex-f4
0
50
100
150 µm
µm

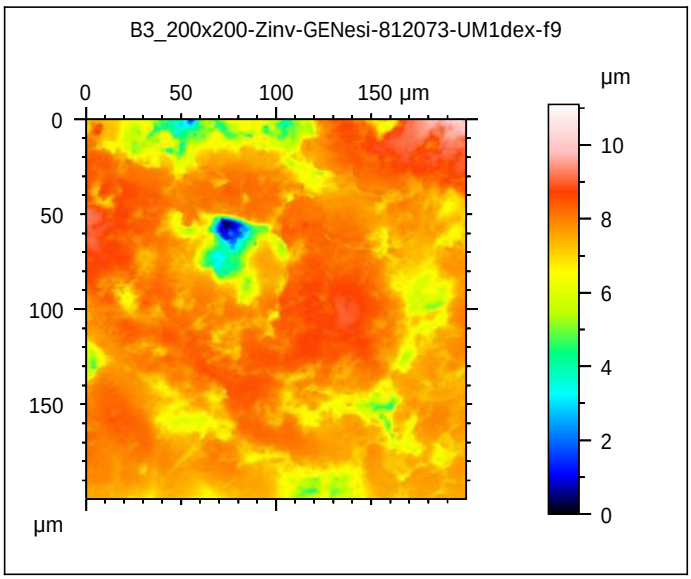
B3_200x200-Zinv-GENesi-812073-UM1dex-f9
0
50
100
150 µm
µm
10
8
6
4
2
0

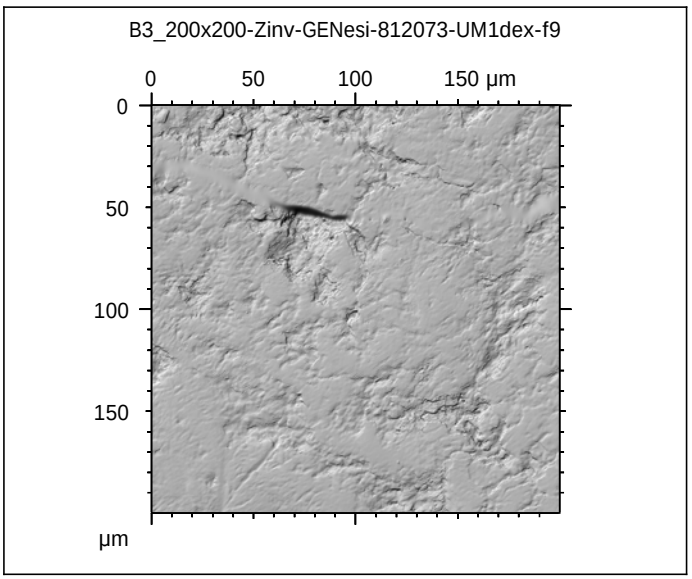
B3_200x200-Zinv-GENesi-812073-UM1dex-f9
0
50
100
150 µm
µm

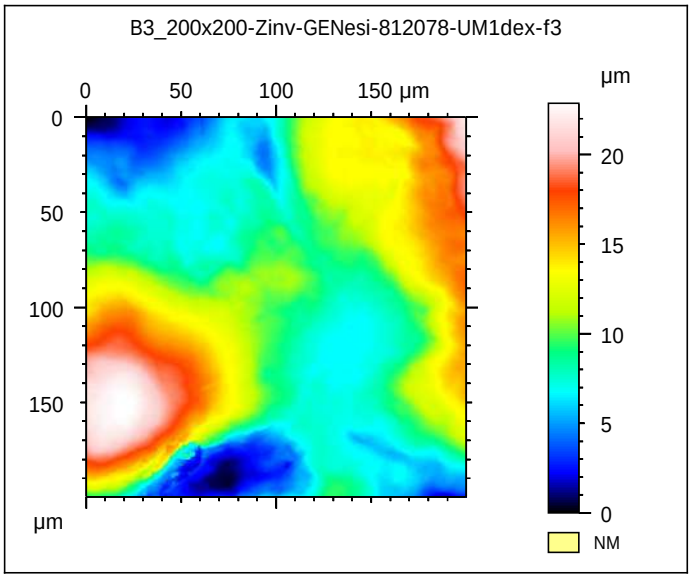
B3_200x200-Zinv-GENesi-812078-UM1dex-f3
0
50
100
150 µm
µm
20
15
10
5
0
NM

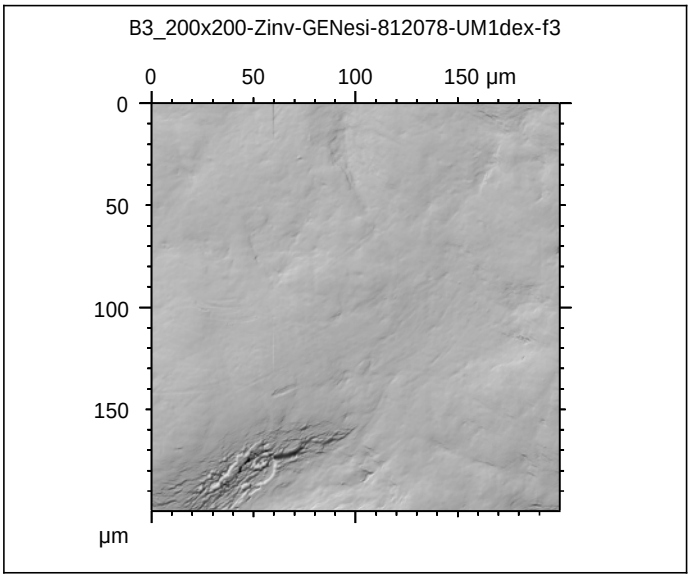
B3_200x200-Zinv-GENesi-812078-UM1dex-f3
0
50
100
150 µm
µm

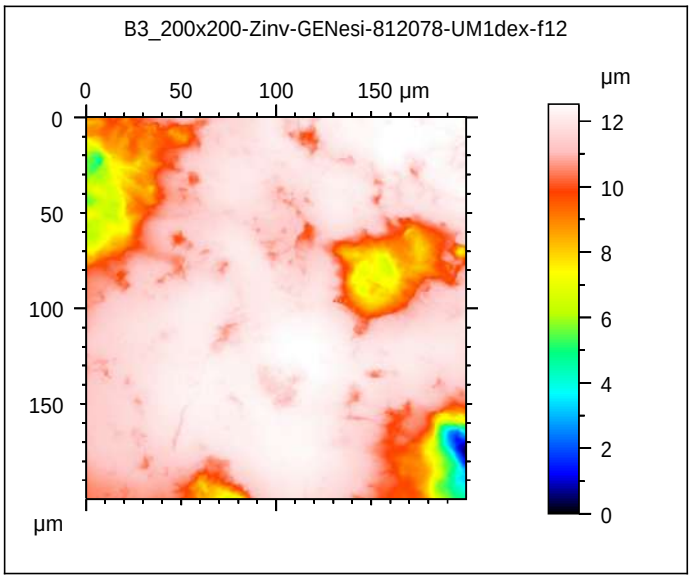
B3_200x200-Zinv-GENesi-812078-UM1dex-f12
0
50
100
150 µm
µm
12
10
8
6
4
2
0

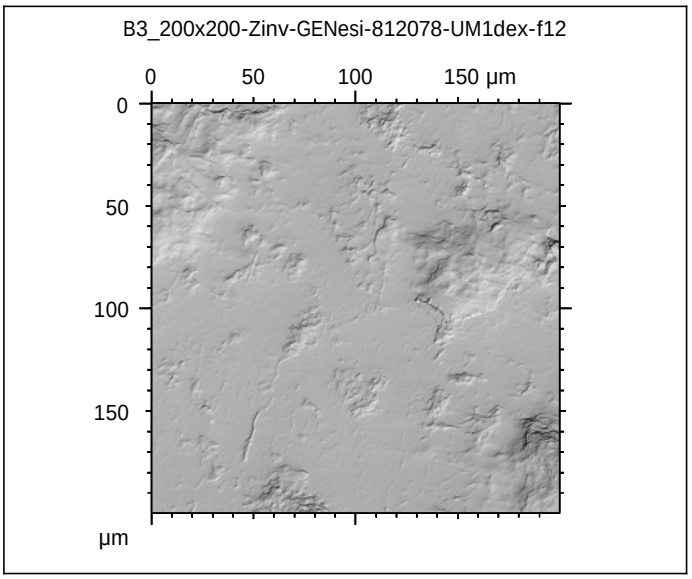
B3_200x200-Zinv-GENesi-812078-UM1dex-f12
0
50
100
150 µm
µm

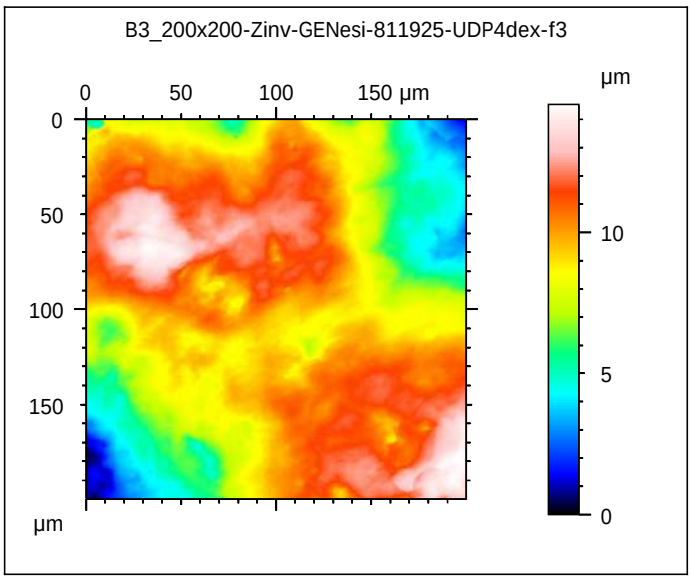
B3_200x200-Zinv-GENesi-811925-UDP4dex-f3
0
50
100
150 µm
µm
10
5
0

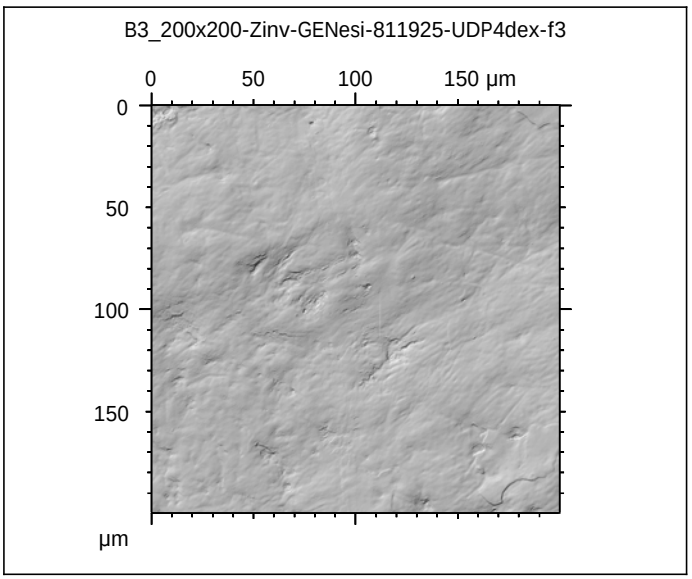
B3_200x200-Zinv-GENesi-811925-UDP4dex-f3
0
50
100
150 µm
µm

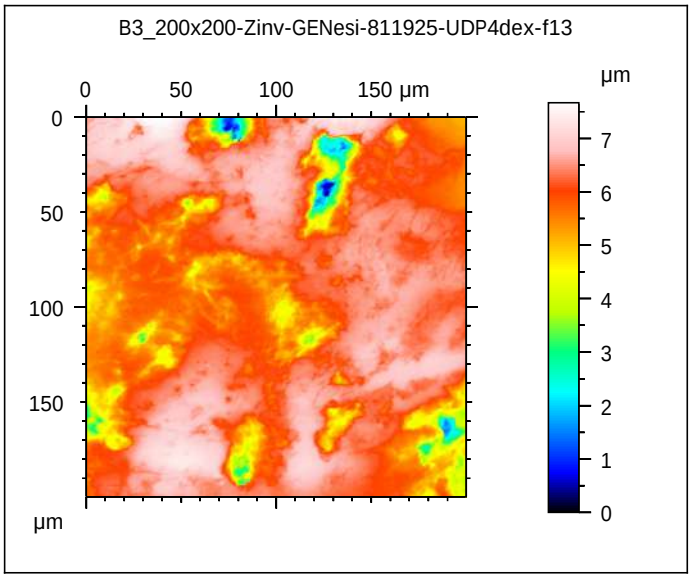
B3_200x200-Zinv-GENesi-811925-UDP4dex-f13
0
50
100
150 µm
µm
7
6
5
4
3
2
1
0

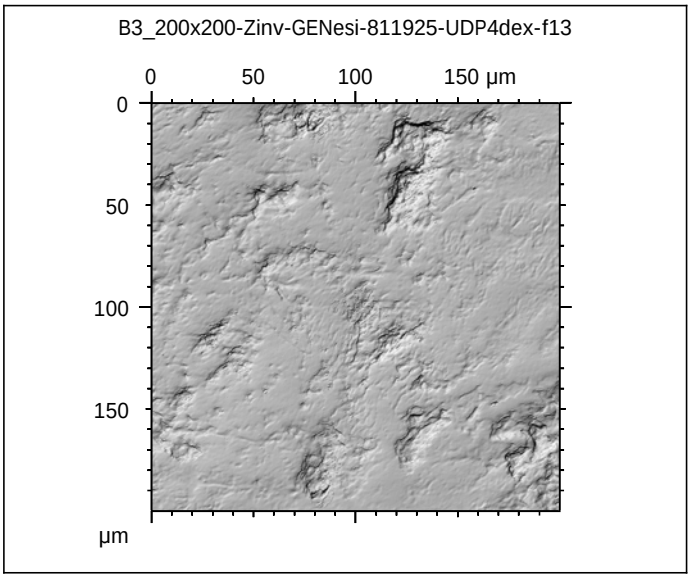
B3_200x200-Zinv-GENesi-811925-UDP4dex-f13
0
50
100
150 µm
µm

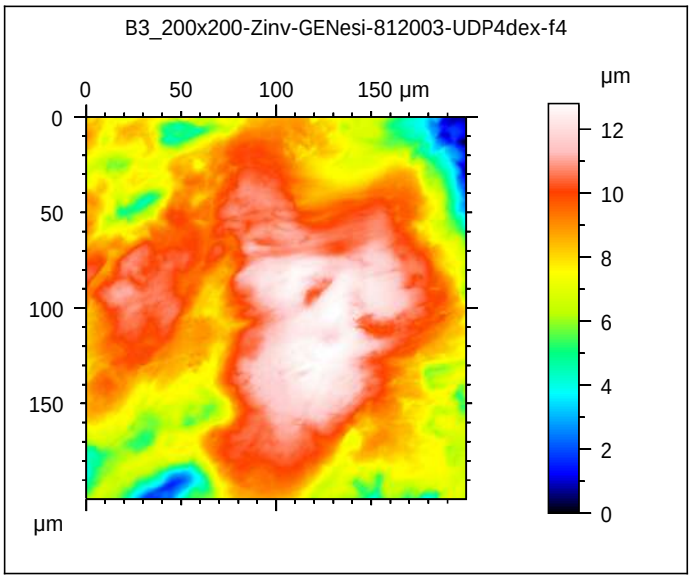
B3_200x200-Zinv-GENesi-812003-UDP4dex-f4
0
50
100
150 µm
µm
12
10
8
6
4
2
0

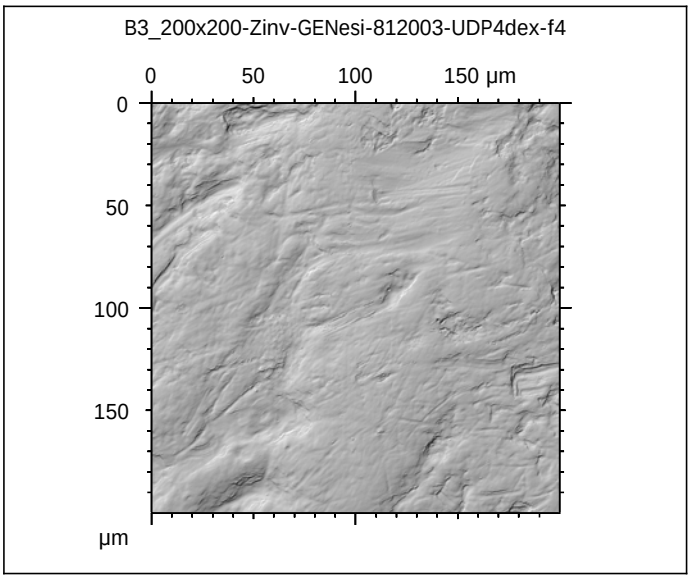
B3_200x200-Zinv-GENesi-812003-UDP4dex-f4
0
50
100
150 µm
µm

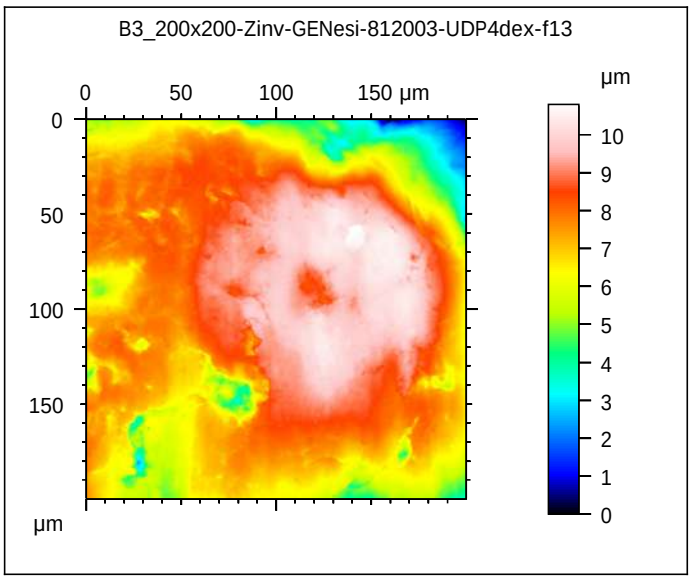
B3_200x200-Zinv-GENesi-812003-UDP4dex-f13
0
50
100
150 µm
µm
10
9
8
7
6
5
4
3
2
1
0

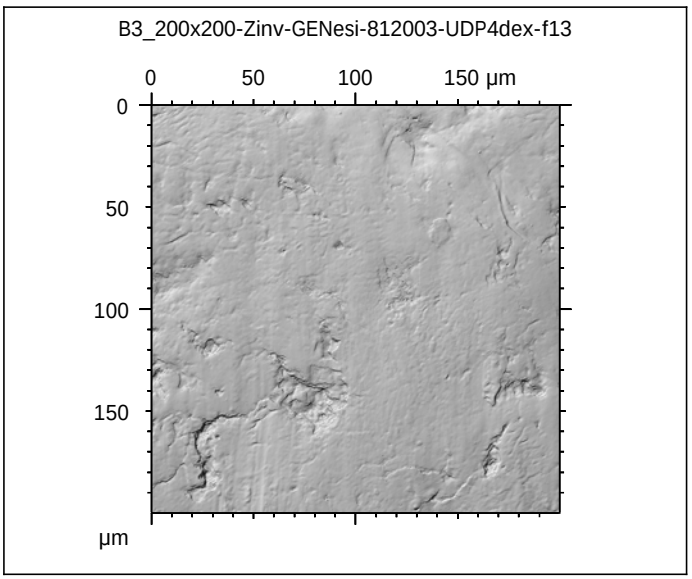
B3_200x200-Zinv-GENesi-812003-UDP4dex-f13
0
50
100
150 µm
µm

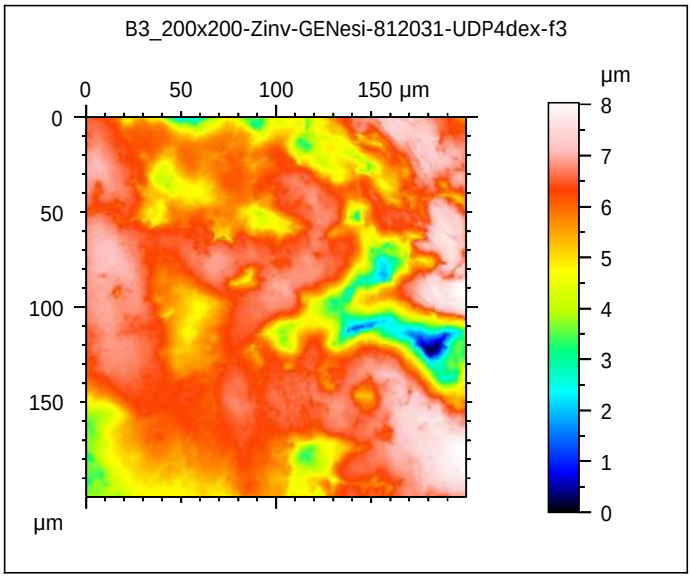
B3_200x200-Zinv-GENesi-812031-UDP4dex-f3
0
50
100
150 µm
µm
8
7
6
5
4
3
2
1
0

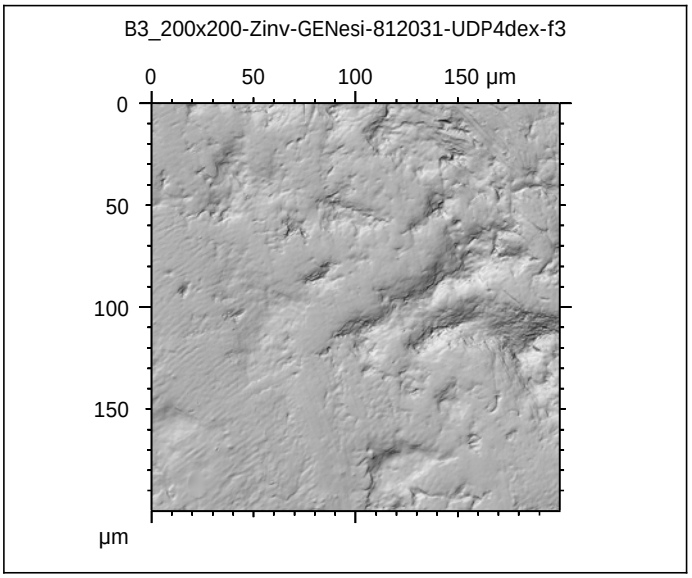
B3_200x200-Zinv-GENesi-812031-UDP4dex-f3
0
50
100
150 µm
µm

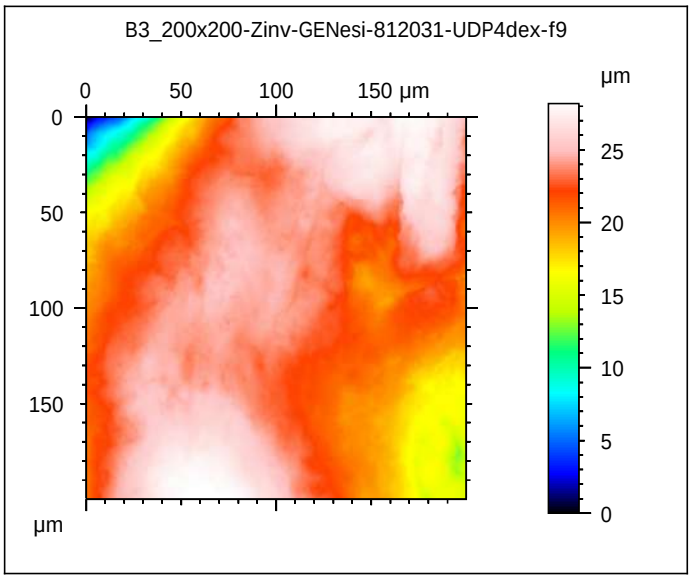
B3_200x200-Zinv-GENesi-812031-UDP4dex-f9
0
50
100
150 µm
µm
25
20
15
10
5
0

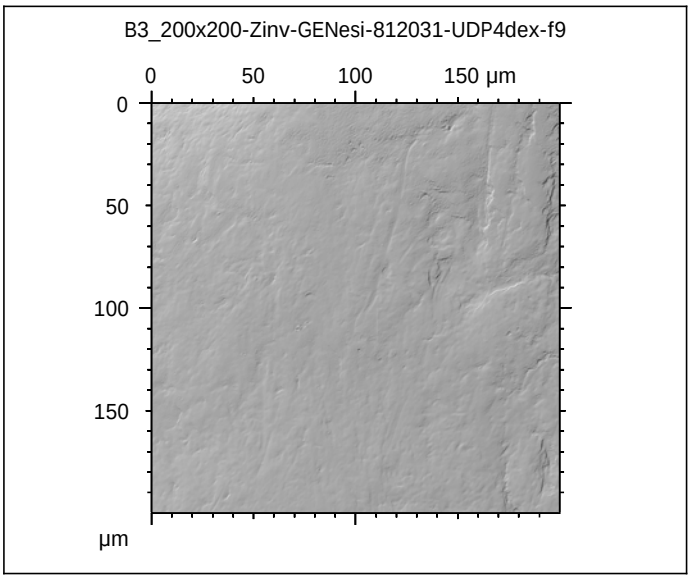
B3_200x200-Zinv-GENesi-812031-UDP4dex-f9
0
50
100
150 µm
µm

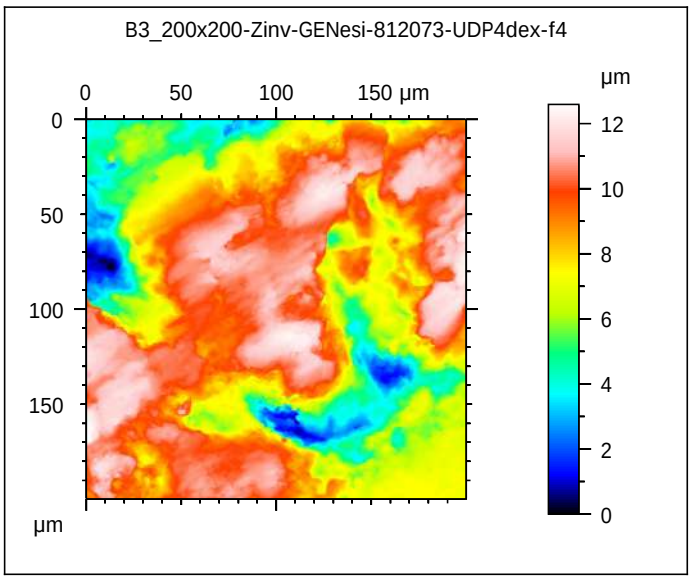
B3_200x200-Zinv-GENesi-812073-UDP4dex-f4
0
50
100
150 µm
µm
12
10
8
6
4
2
0

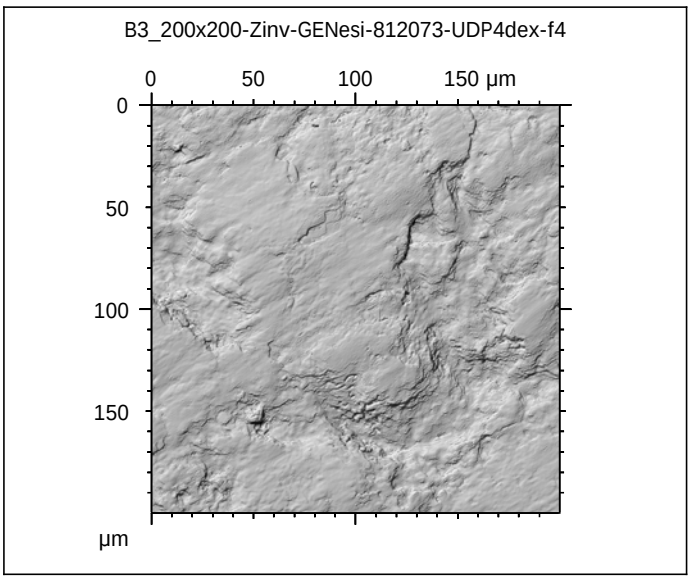
B3_200x200-Zinv-GENesi-812073-UDP4dex-f4
0
50
100
150 µm
µm

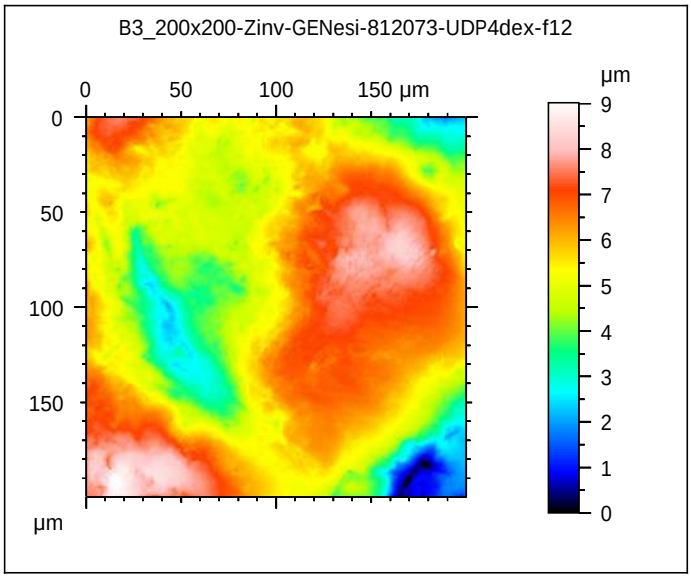
B3_200x200-Zinv-GENesi-812073-UDP4dex-f12
0
50
100
150 µm
µm
9
8
7
6
5
4
3
2
1
0

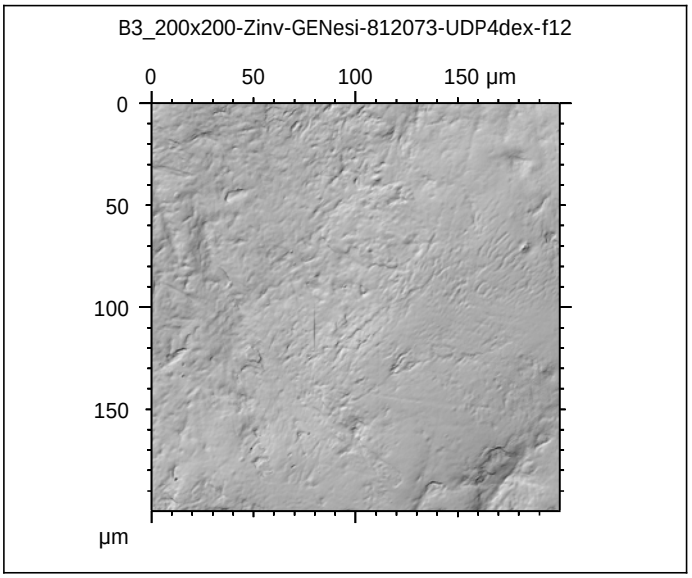
B3_200x200-Zinv-GENesi-812073-UDP4dex-f12
0
50
100
150 µm
µm

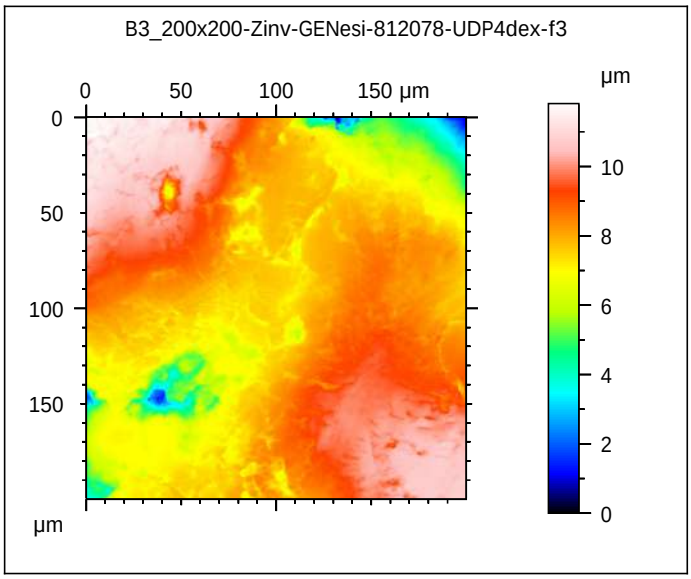
B3_200x200-Zinv-GENesi-812078-UDP4dex-f3
0
50
100
150 µm
µm
10
8
6
4
2
0

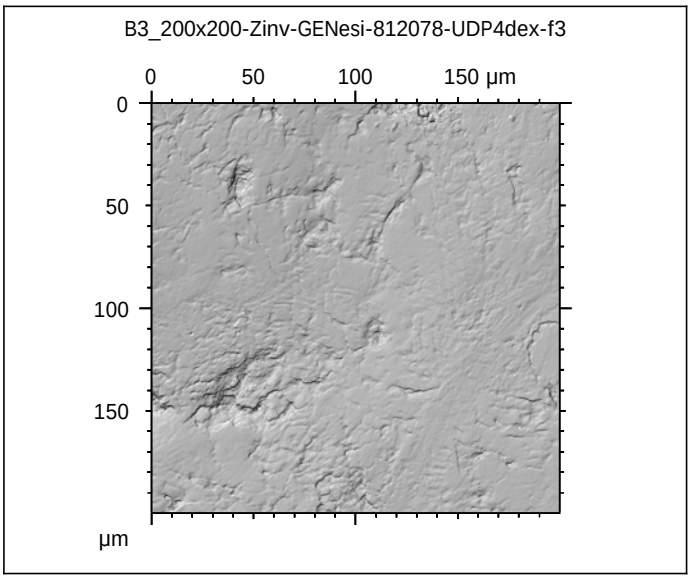
B3_200x200-Zinv-GENesi-812078-UDP4dex-f3
0
50
100
150 µm
µm

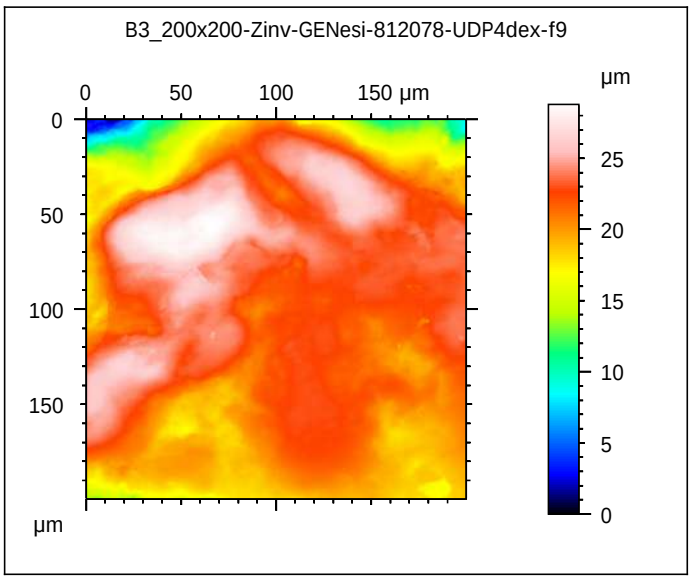
B3_200x200-Zinv-GENesi-812078-UDP4dex-f9
0
50
100
150 µm
µm
25
20
15
10
5
0

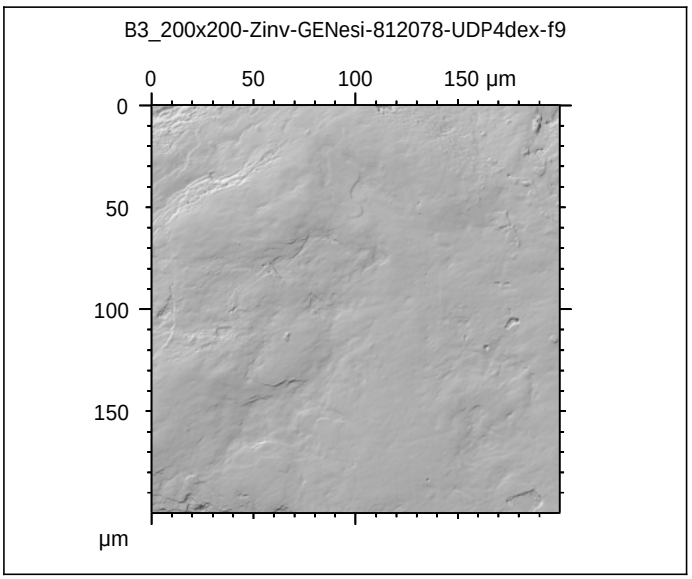
B3_200x200-Zinv-GENesi-812078-UDP4dex-f9
0
50
100
150 µm
µm

Photosimulations and false color elevation maps of scanned shearing and crushing facets on molars and deciduous premolars of the **corn group** (60% base diet + 20% corn flour + 20% corn kernels)

scanned at the PALEVOPRIM lab by M. Louail, University of Poitiers, France with "TRIDENT", white light confocal microscope Leica DCM8 - April 2020

ALIHOM Project (Région Nouvelle Aquitaine, France), ANR Diet-Scratches

ANR-17-CE27-0002

PIs: G. Merceron & S. Ferchaud

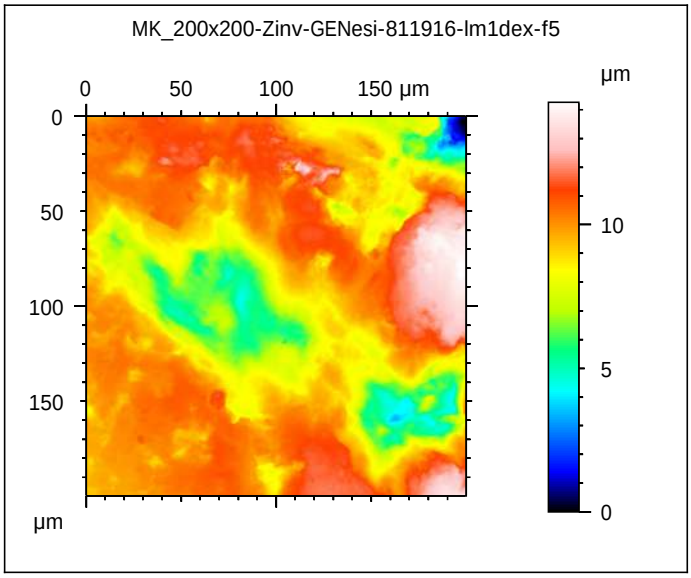

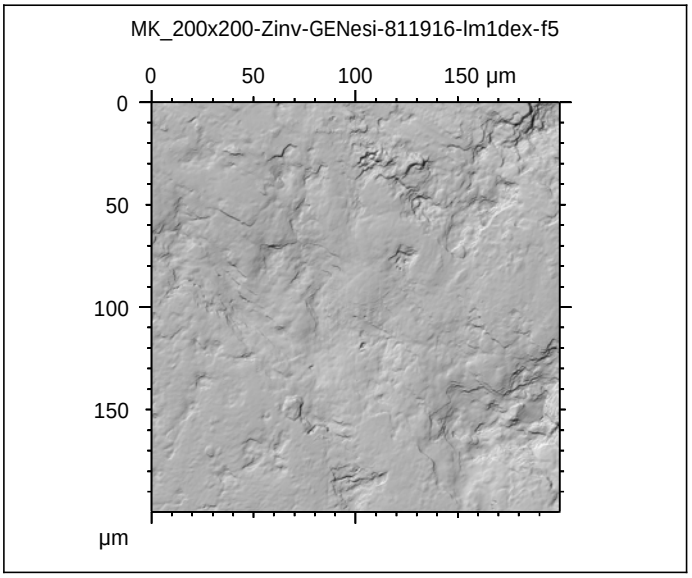

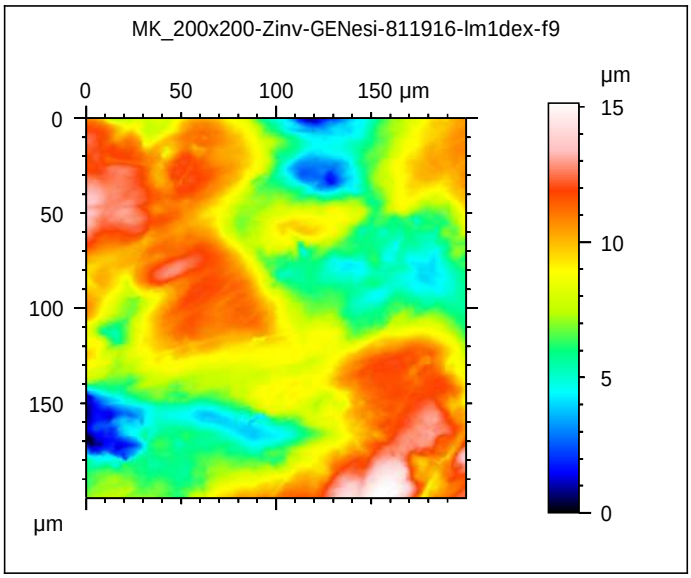

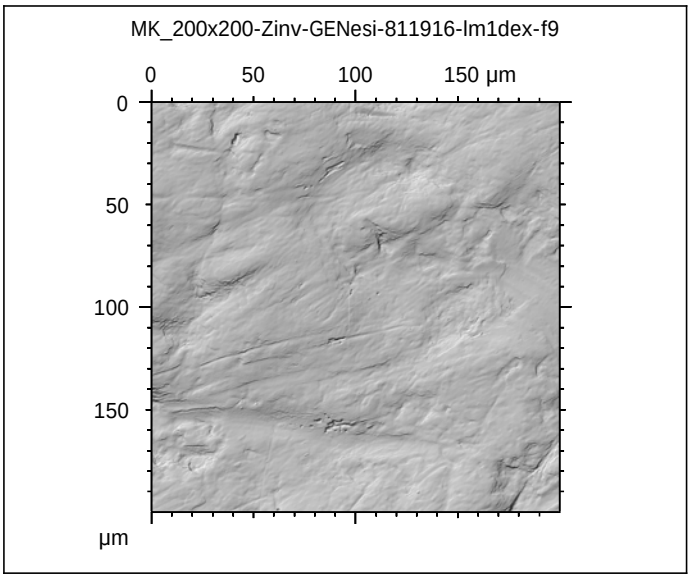

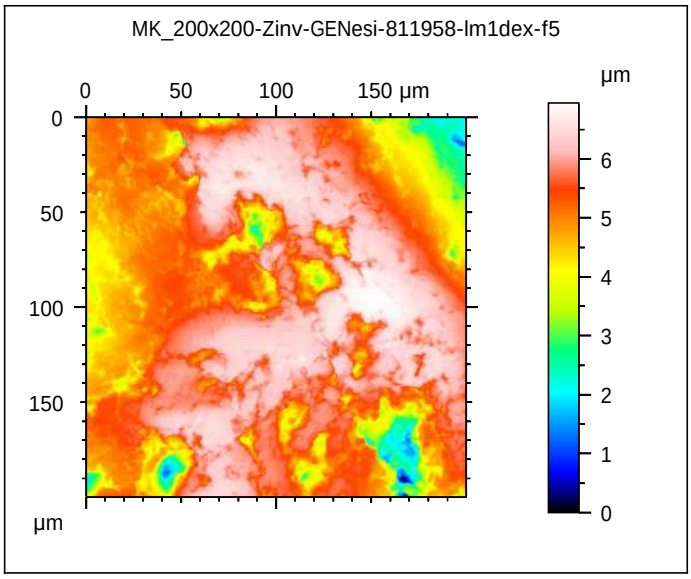

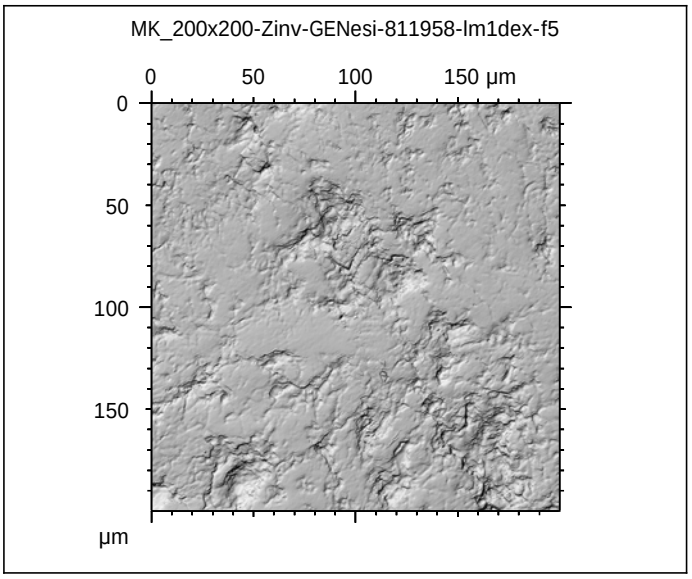

Leica Map Premium 8.0.9173

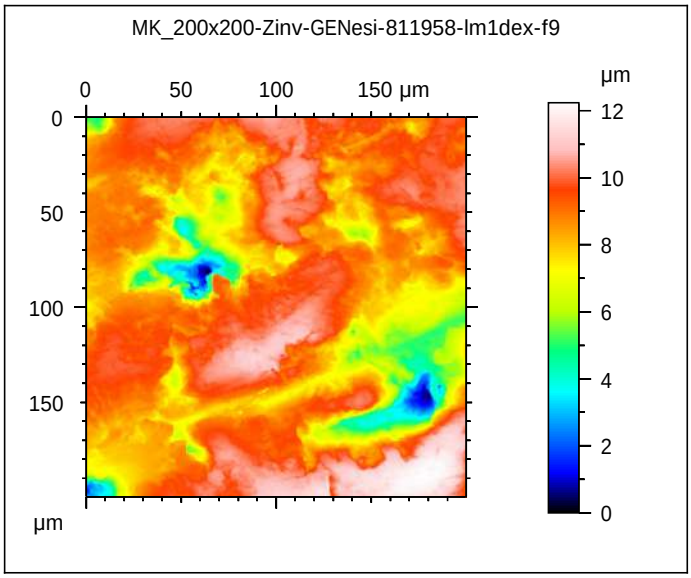
MK_200x200-Zinv-GENesi-811958-lm1dex-f9
0
50
100
150 µm
µm
12
10
8
6
4
2
0

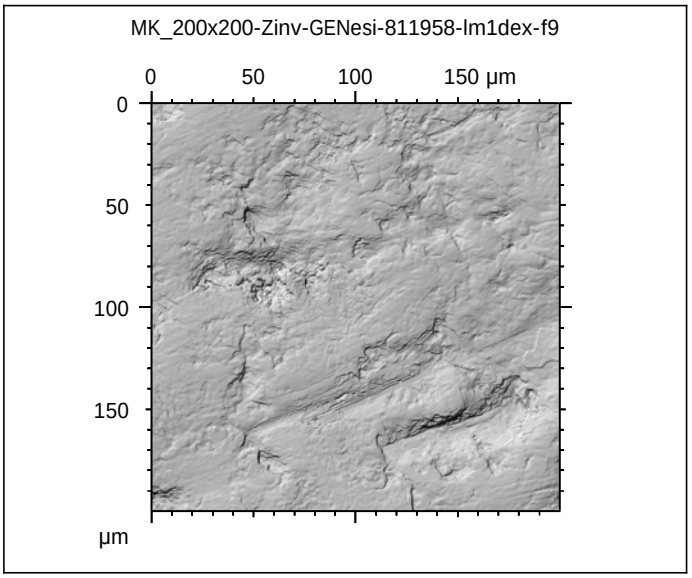
MK_200x200-Zinv-GENesi-811958-lm1dex-f9
0
50
100
150 µm
µm

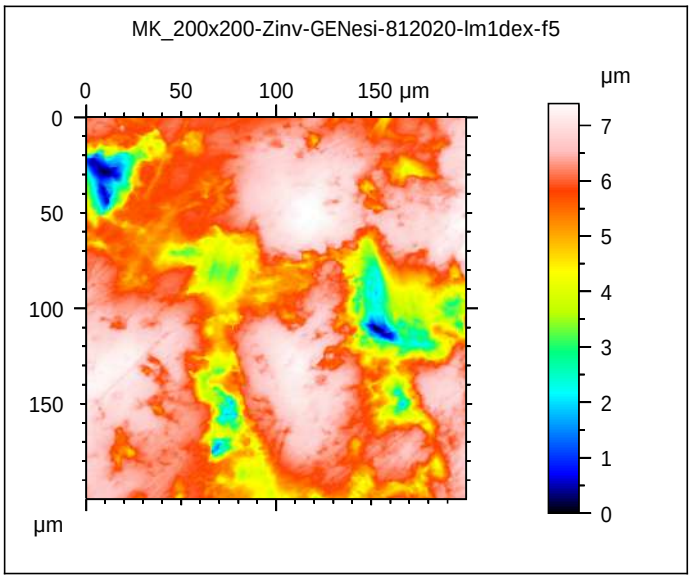
MK_200x200-Zinv-GENesi-812020-lm1dex-f5
0
50
100
150 µm
µm
7
6
5
4
3
2
1
0

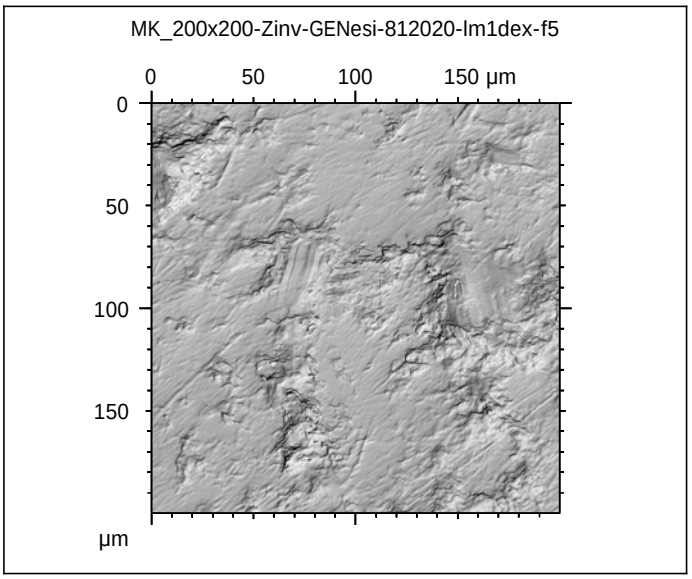
MK_200x200-Zinv-GENesi-812020-lm1dex-f5
0
50
100
150 µm
µm

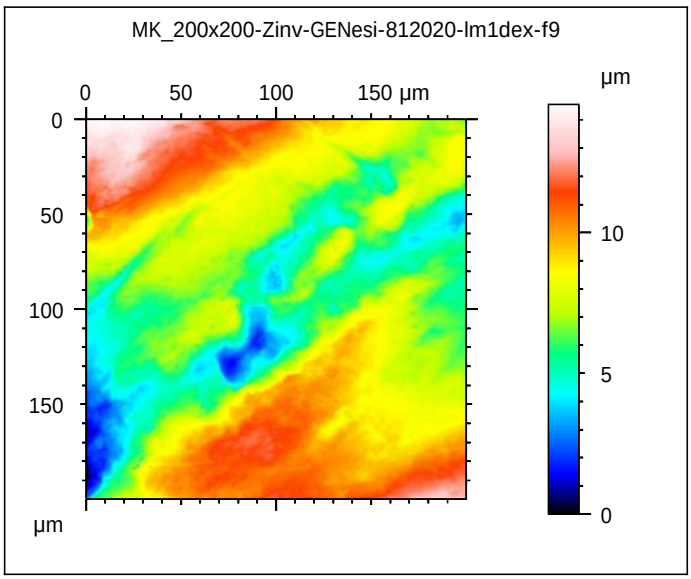
MK_200x200-Zinv-GENesi-812020-lm1dex-f9
0
50
100
150 µm
µm
10
5
0

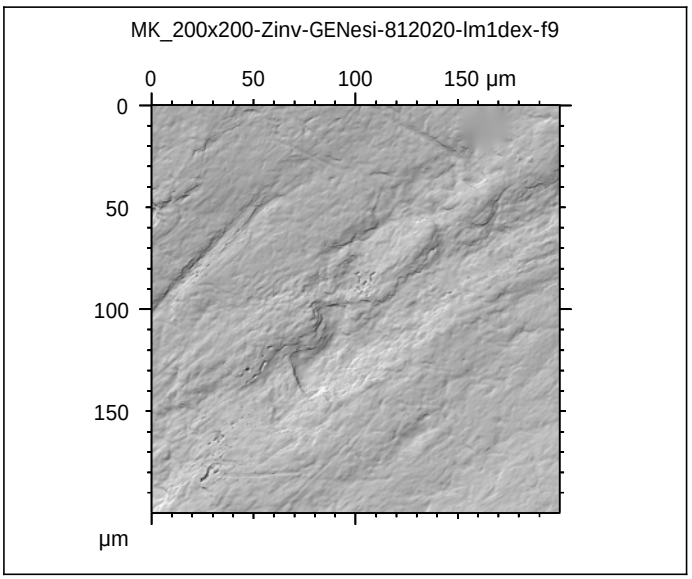
MK_200x200-Zinv-GENesi-812020-lm1dex-f9
0
50
100
150 µm
µm

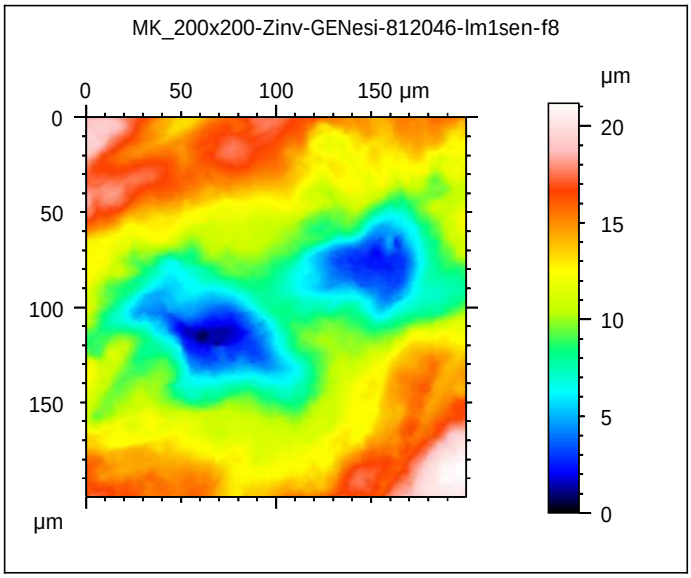
MK_200x200-Zinv-GENesi-812046-lm1sen-f8
0
50
100
150 µm
µm
20
15
10
5
0

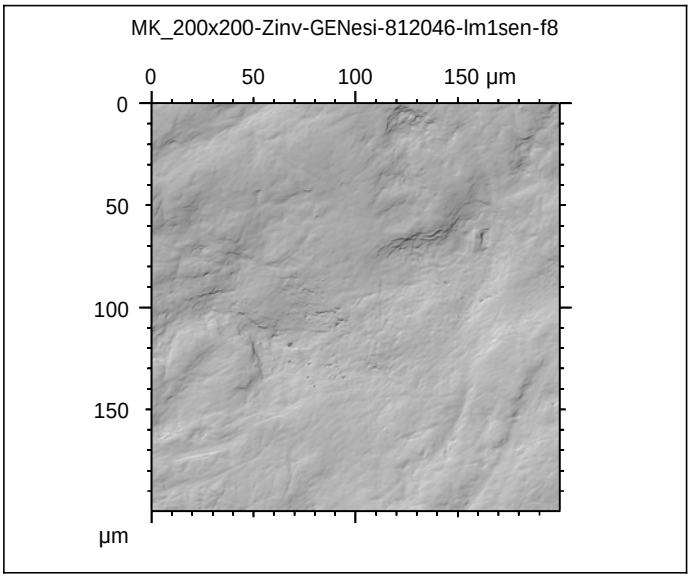
MK_200x200-Zinv-GENesi-812046-lm1sen-f8
0
50
100
150 µm
µm

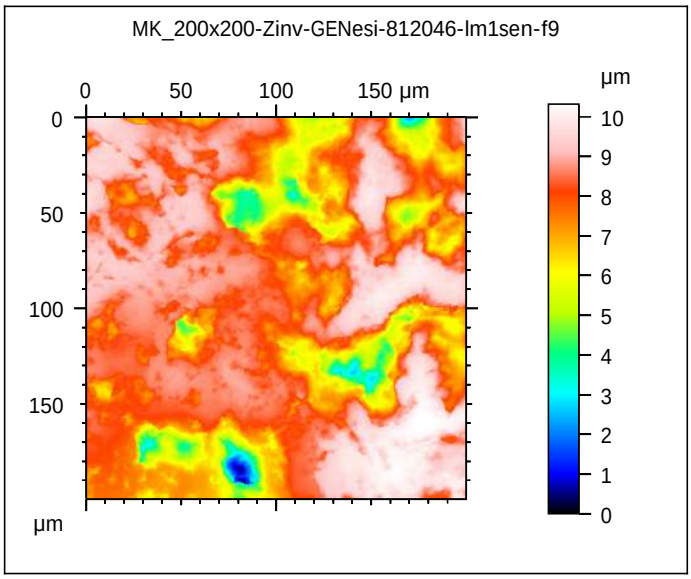
MK_200x200-Zinv-GENesi-812046-lm1sen-f9
0
50
100
150 µm
µm
10
9
8
7
6
5
4
3
2
1
0

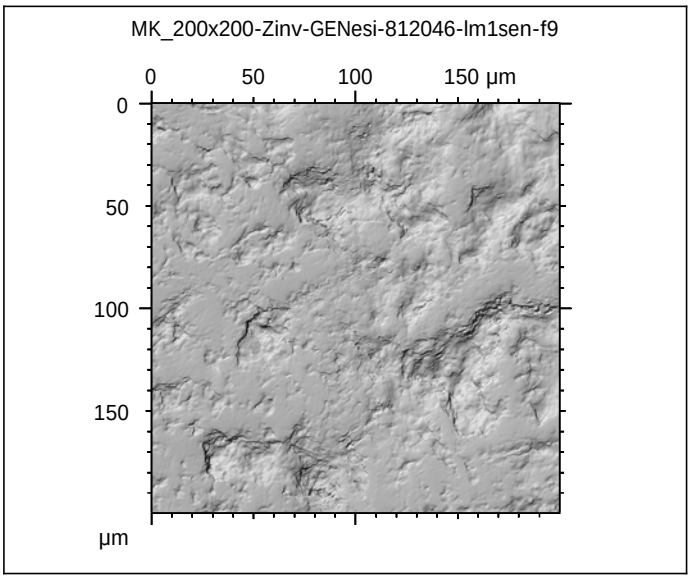
MK_200x200-Zinv-GENesi-812046-lm1sen-f9
0
50
100
150 µm
µm

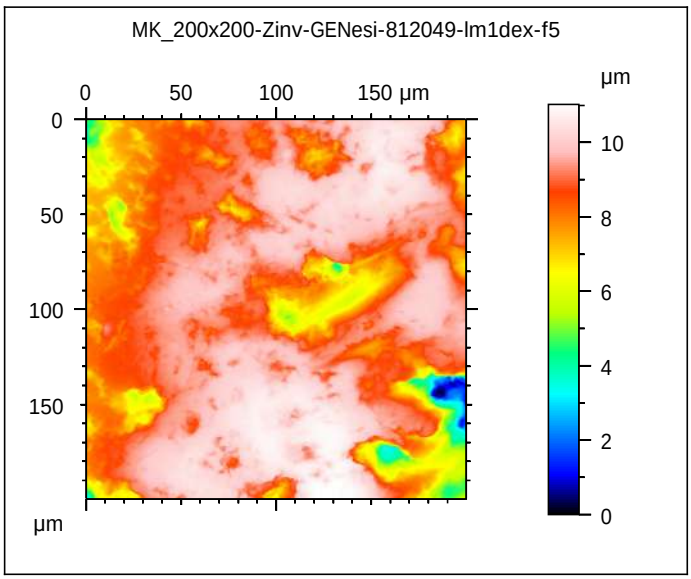
MK_200x200-Zinv-GENesi-812049-lm1dex-f5
0
50
100
150 µm
µm
10
8
6
4
2
0

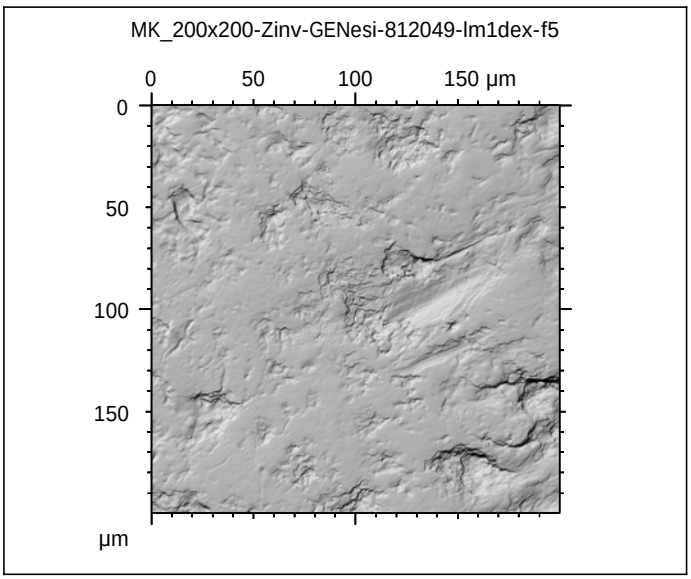
MK_200x200-Zinv-GENesi-812049-lm1dex-f5
0
50
100
150 µm
µm

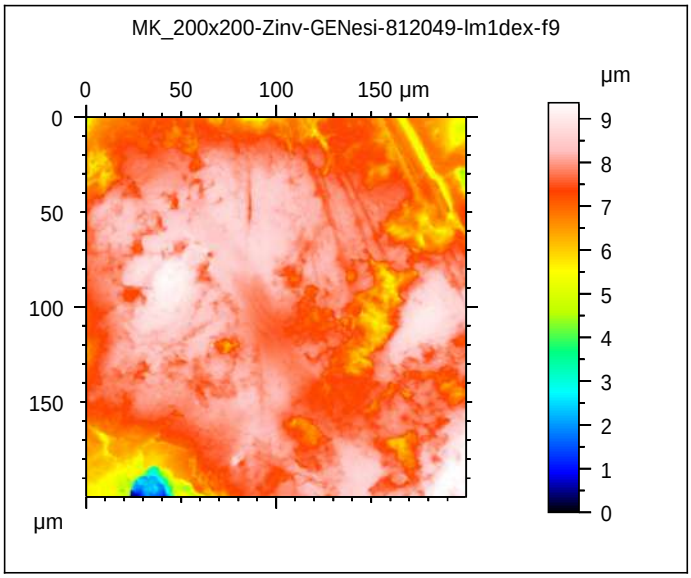
MK_200x200-Zinv-GENesi-812049-lm1dex-f9
0
50
100
150 µm
µm
9
8
7
6
5
4
3
2
1
0

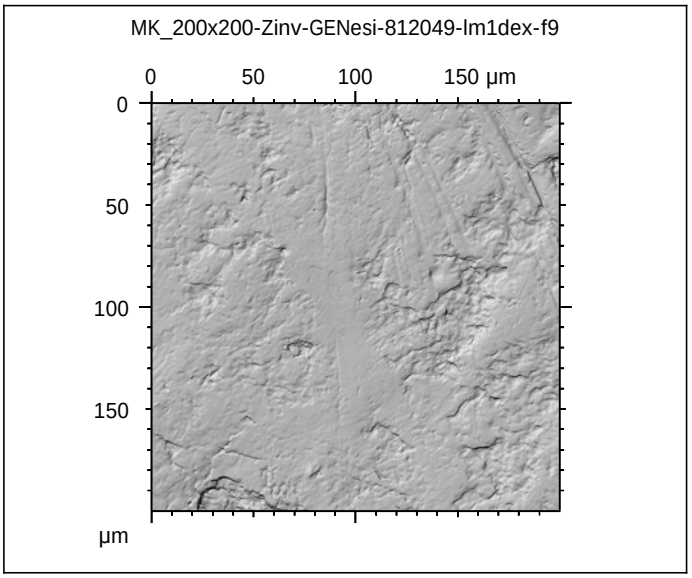
MK_200x200-Zinv-GENesi-812049-lm1dex-f9
0
50
100
150 µm
µm

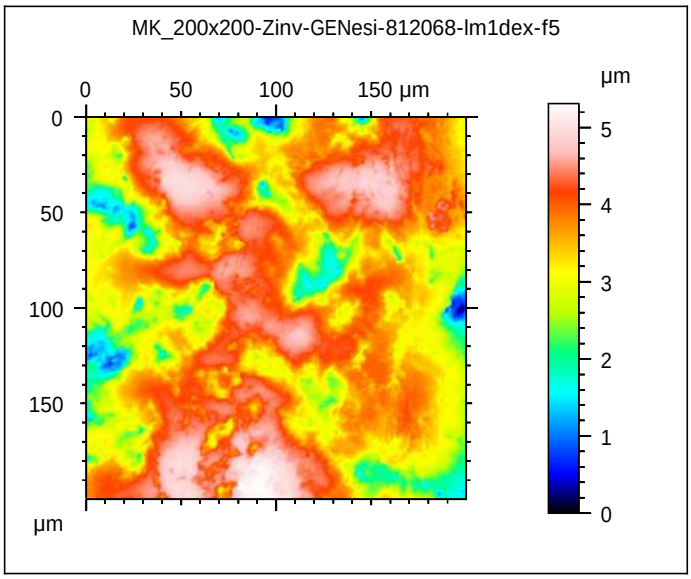
MK_200x200-Zinv-GENesi-812068-lm1dex-f5
0
50
100
150 µm
µm
5
4
3
2
1
0

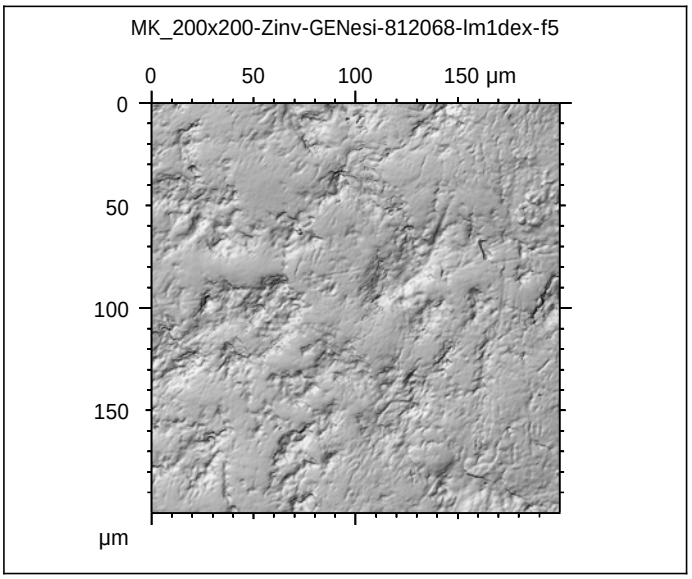
MK_200x200-Zinv-GENesi-812068-lm1dex-f5
0
50
100
150 µm
µm

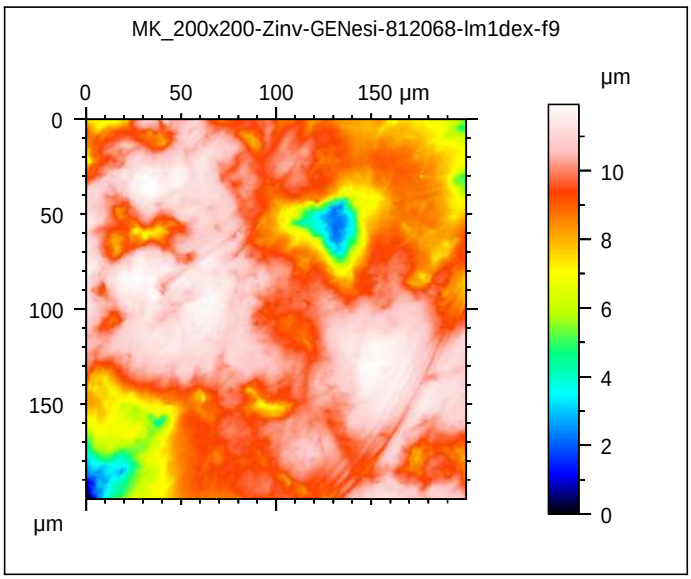
MK_200x200-Zinv-GENesi-812068-lm1dex-f9
0
50
100
150 µm
µm
10
8
6
4
2
0

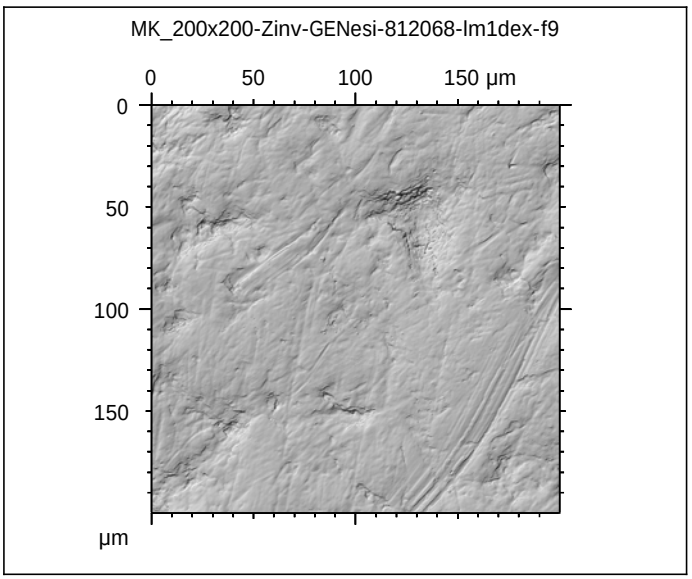
MK_200x200-Zinv-GENesi-812068-lm1dex-f9
0
50
100
150 µm
µm

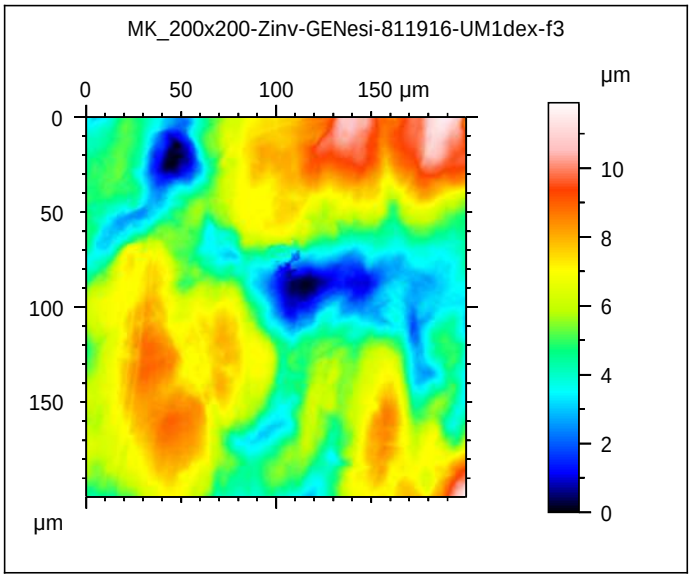
MK_200x200-Zinv-GENesi-811916-UM1dex-f3
0
50
100
150 µm
µm
0
50
100
150
µm
10
8
6
4
2
0

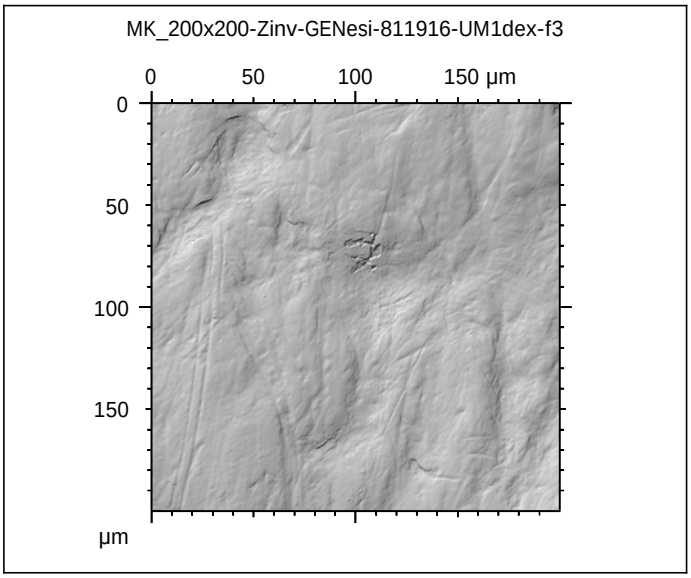
MK_200x200-Zinv-GENesi-811916-UM1dex-f3
0
50
100
150 µm
0
50
100
150
µm

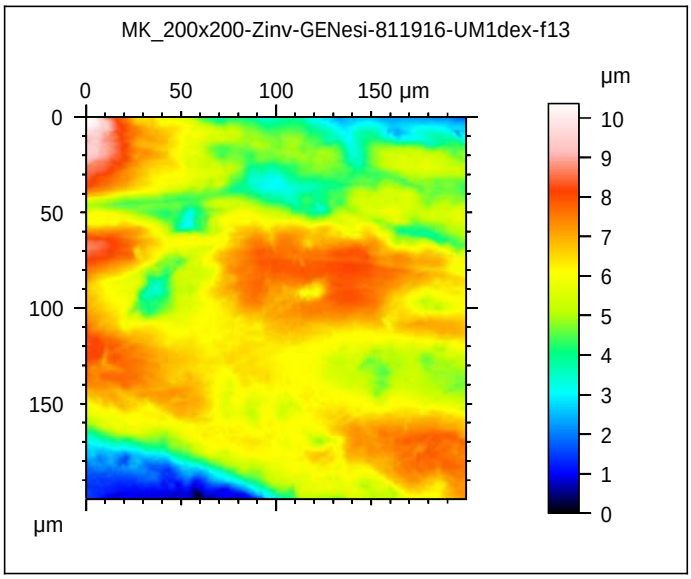
MK_200x200-Zinv-GENesi-811916-UM1dex-f13
0
50
100
150 µm
µm
0
50
100
150
µm
10
9
8
7
6
5
4
3
2
1
0

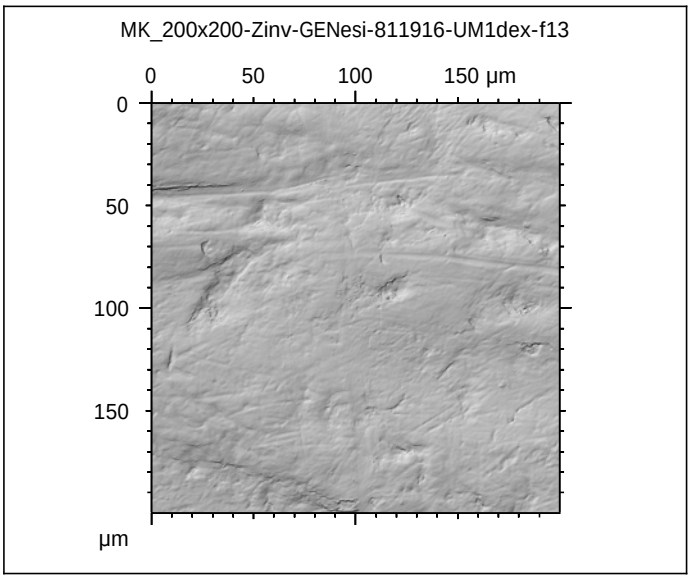
MK_200x200-Zinv-GENesi-811916-UM1dex-f13
0
50
100
150 µm
0
50
100
150
µm

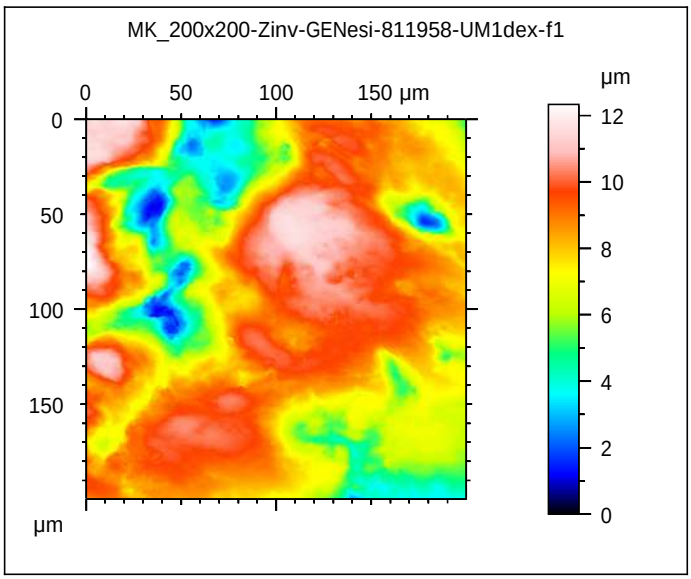
MK_200x200-Zinv-GENesi-811958-UM1dex-f1
0
50
100
150 µm
µm
0
50
100
150
µm
12
10
8
6
4
2
0

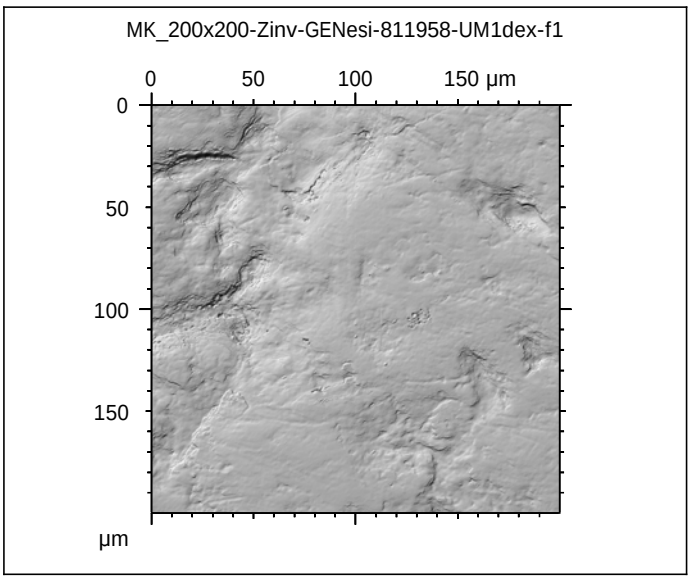
MK_200x200-Zinv-GENesi-811958-UM1dex-f1
0
50
100
150 µm
0
50
100
150
µm

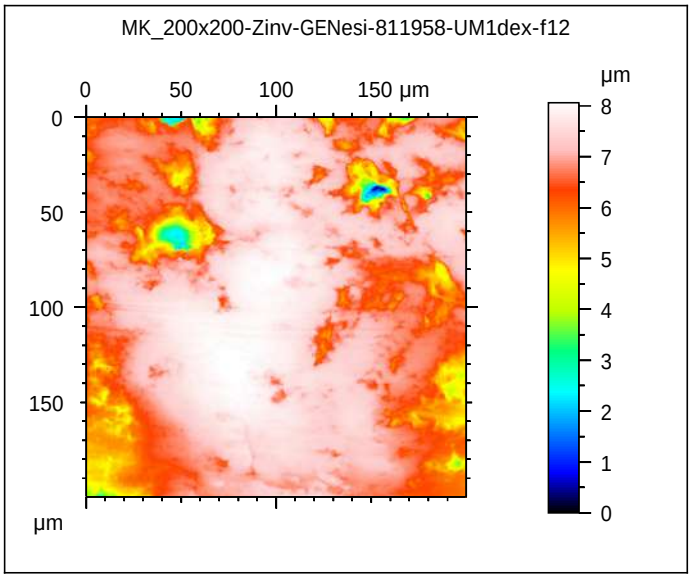
MK_200x200-Zinv-GENesi-811958-UM1dex-f12
0
50
100
150 µm
µm
8
7
6
5
4
3
2
1
0

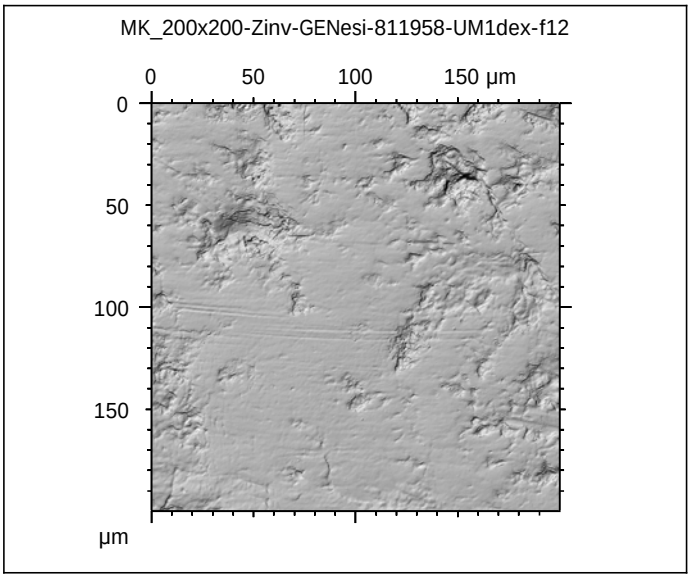
MK_200x200-Zinv-GENesi-811958-UM1dex-f12
0
50
100
150 µm
µm

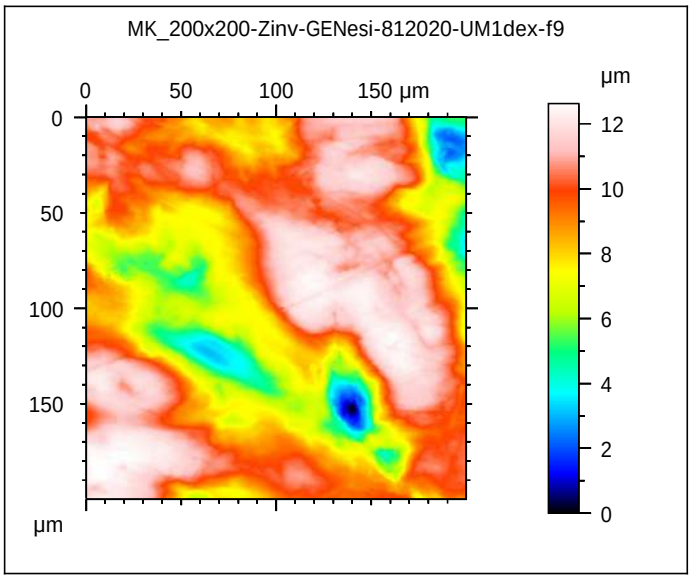
MK_200x200-Zinv-GENesi-812020-UM1dex-f9
0
50
100
150 µm
µm
12
10
8
6
4
2
0

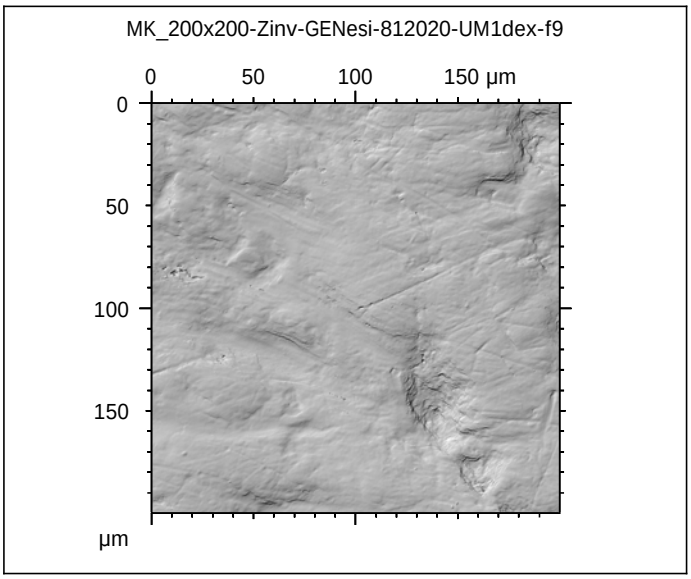
MK_200x200-Zinv-GENesi-812020-UM1dex-f9
0
50
100
150 µm
µm

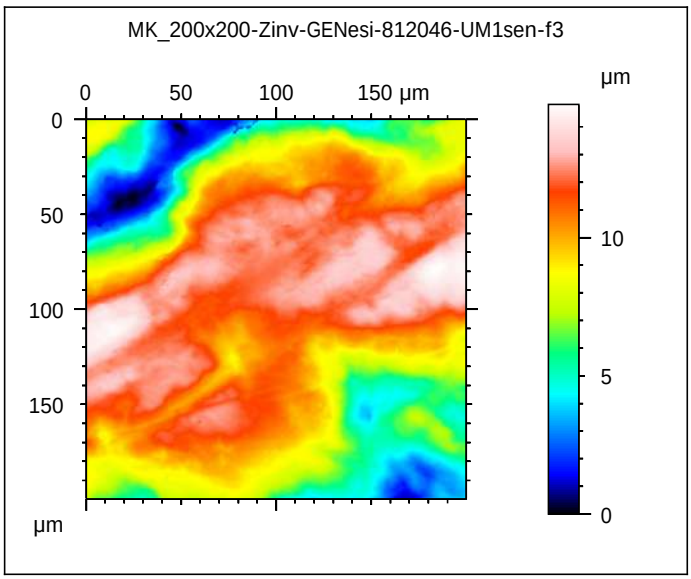
MK_200x200-Zinv-GENesi-812046-UM1sen-f3
0
50
100
150 µm
µm
10
5
0

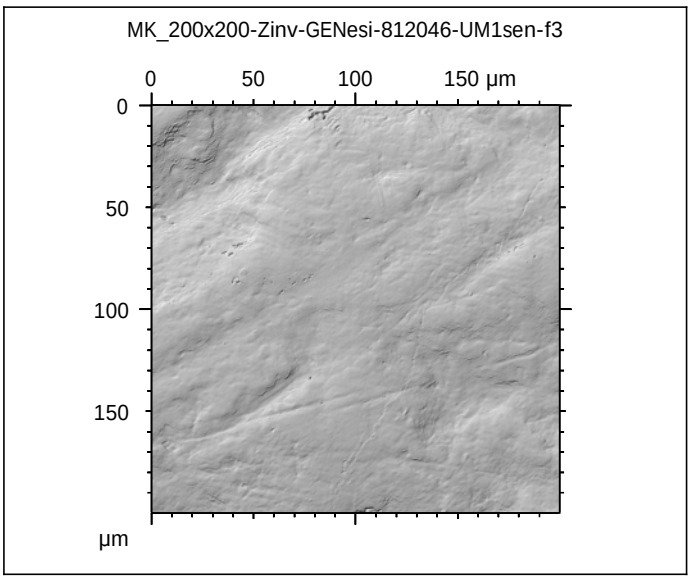
MK_200x200-Zinv-GENesi-812046-UM1sen-f3
0
50
100
150 µm
µm

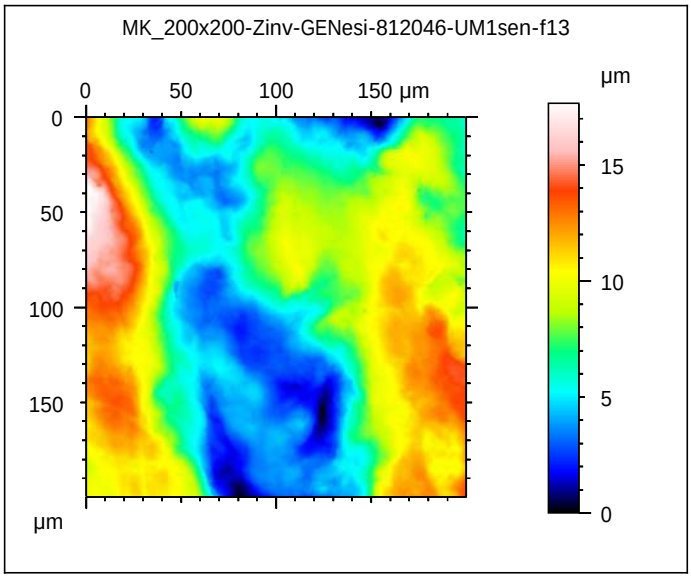
MK_200x200-Zinv-GENesi-812046-UM1sen-f13
0
50
100
150 µm
µm
15
10
5
0

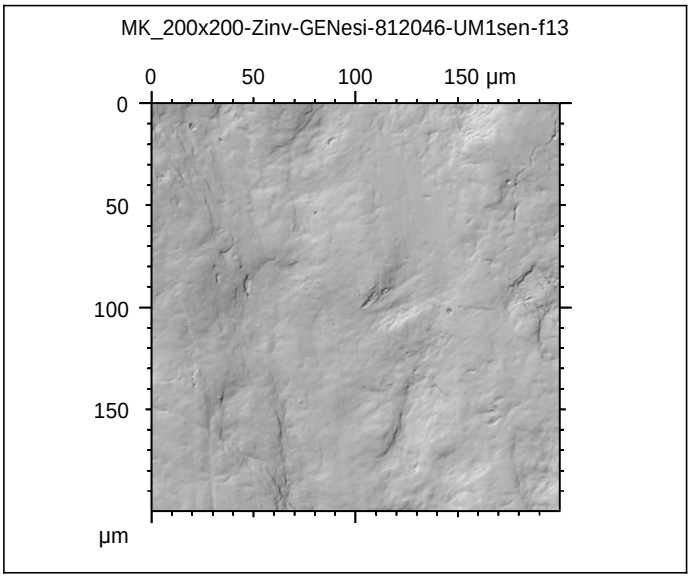
MK_200x200-Zinv-GENesi-812046-UM1sen-f13
0
50
100
150 µm
µm

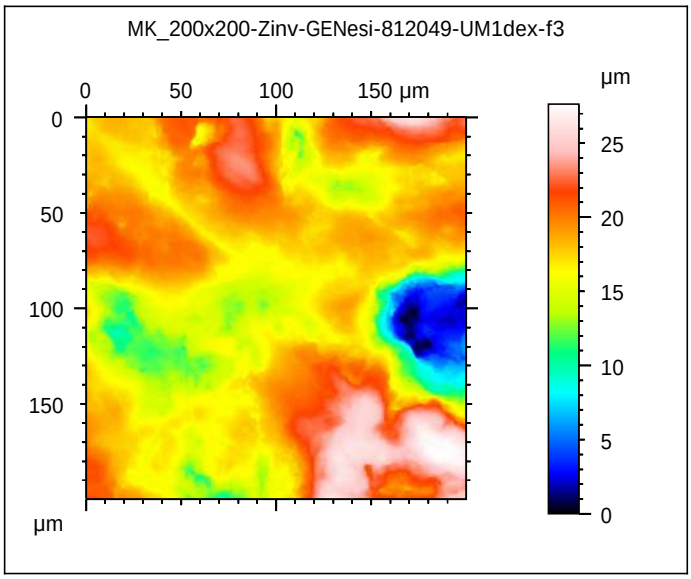
MK_200x200-Zinv-GENesi-812049-UM1dex-f3
0
50
100
150 µm
µm
25
20
15
10
5
0

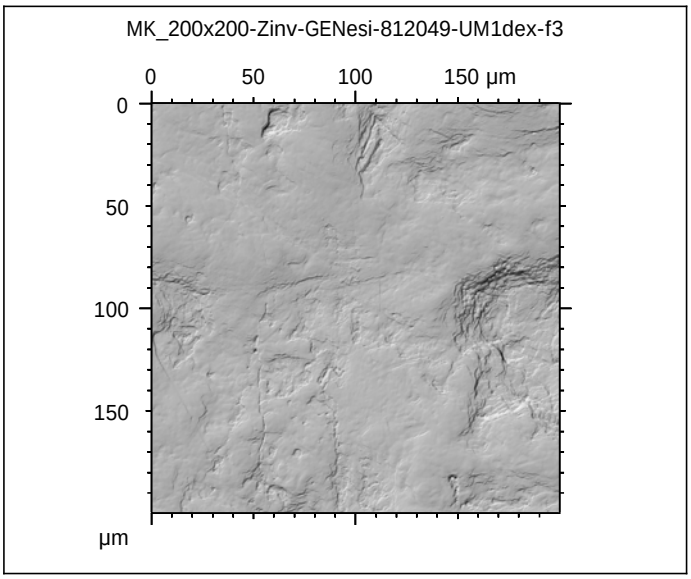
MK_200x200-Zinv-GENesi-812049-UM1dex-f3
0
50
100
150 µm
µm

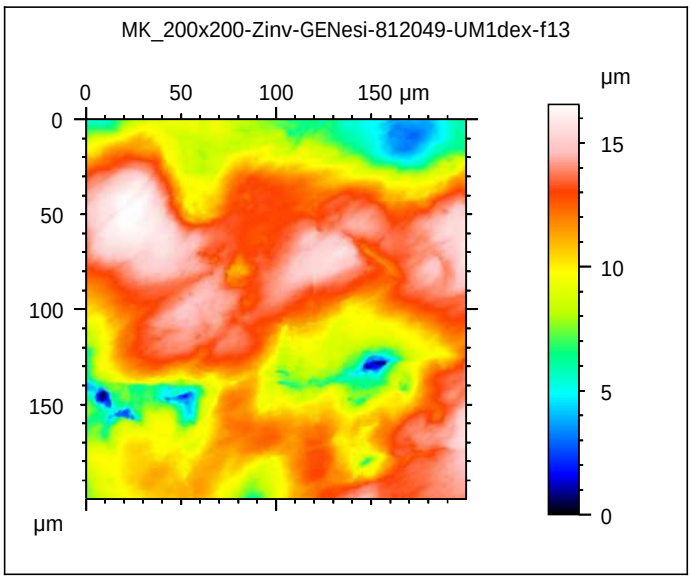
MK_200x200-Zinv-GENesi-812049-UM1dex-f13
0
50
100
150 µm
µm
15
10
5
0

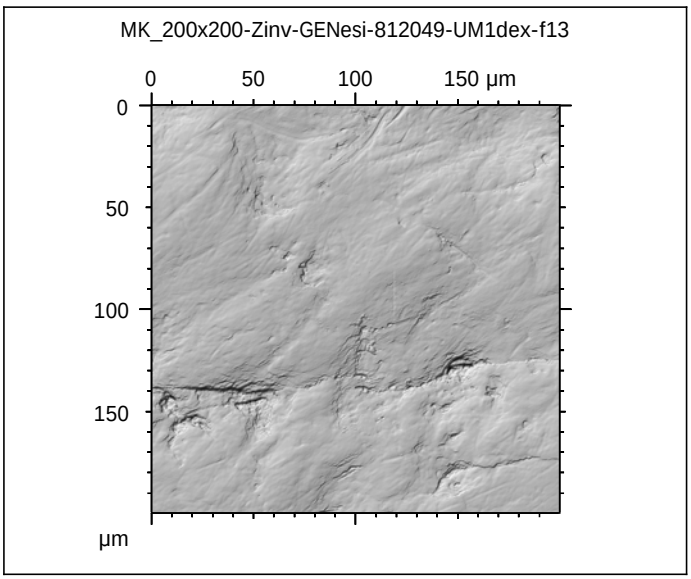
MK_200x200-Zinv-GENesi-812049-UM1dex-f13
0
50
100
150 µm
µm

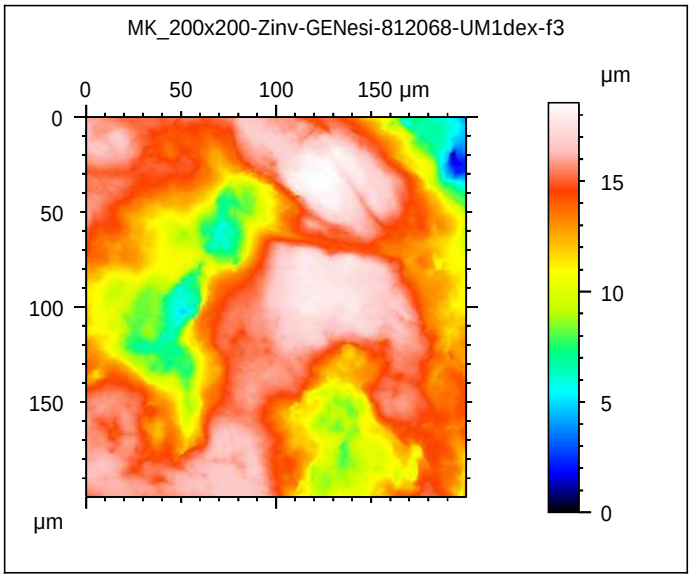
MK_200x200-Zinv-GENesi-812068-UM1dex-f3
0
50
100
150 µm
µm
15
10
5
0

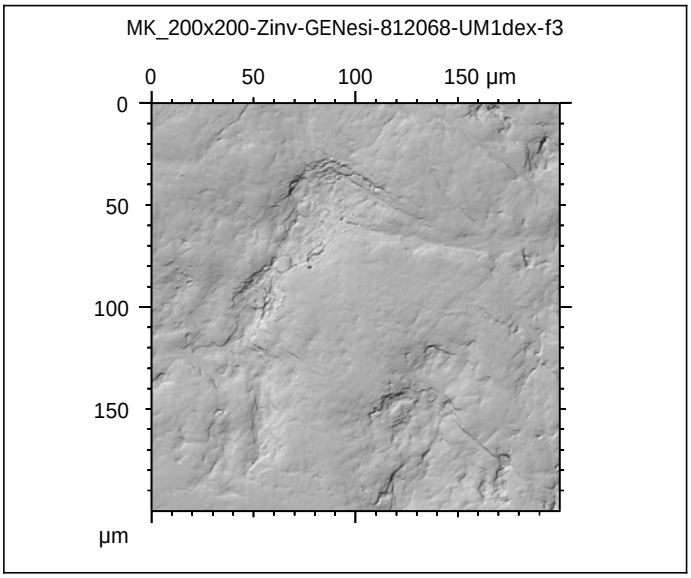
MK_200x200-Zinv-GENesi-812068-UM1dex-f3
0
50
100
150 µm
µm

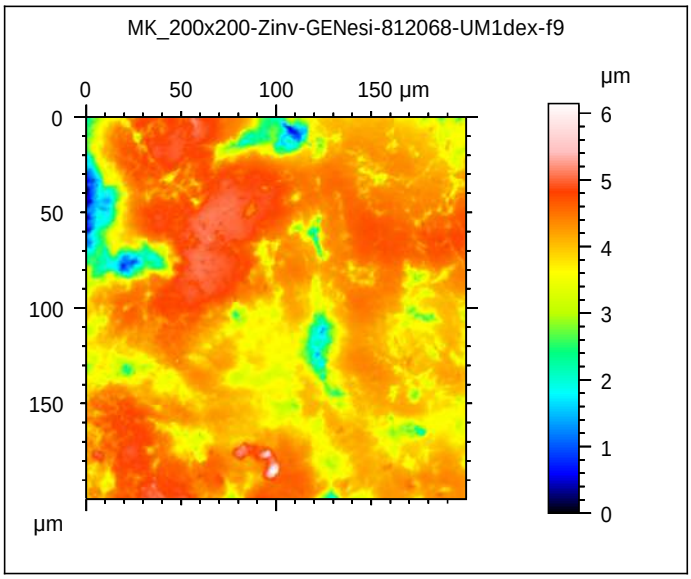
MK_200x200-Zinv-GENesi-812068-UM1dex-f9
0
50
100
150 µm
µm
6
5
4
3
2
1
0

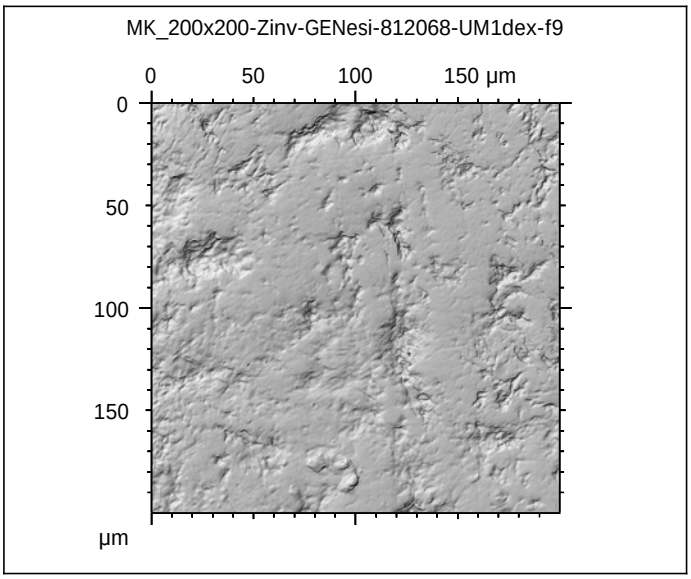
MK_200x200-Zinv-GENesi-812068-UM1dex-f9
0
50
100
150 µm
µm

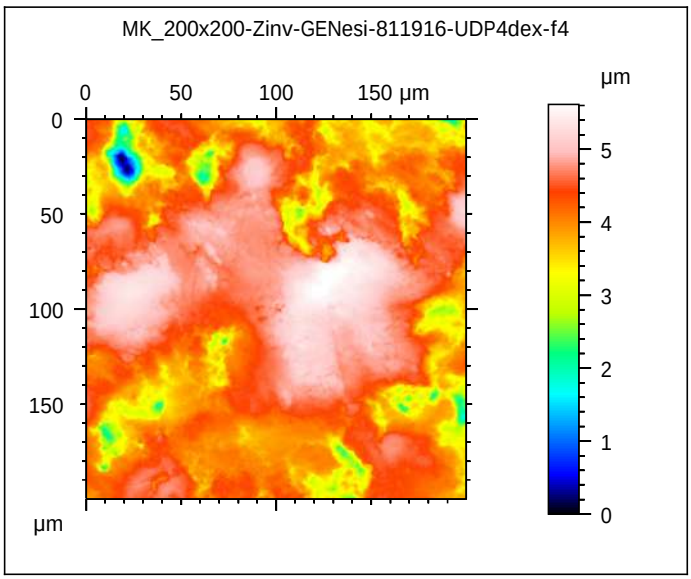
MK_200x200-Zinv-GENesi-811916-UDP4dex-f4
0
50
100
150 µm
µm
5
4
3
2
1
0

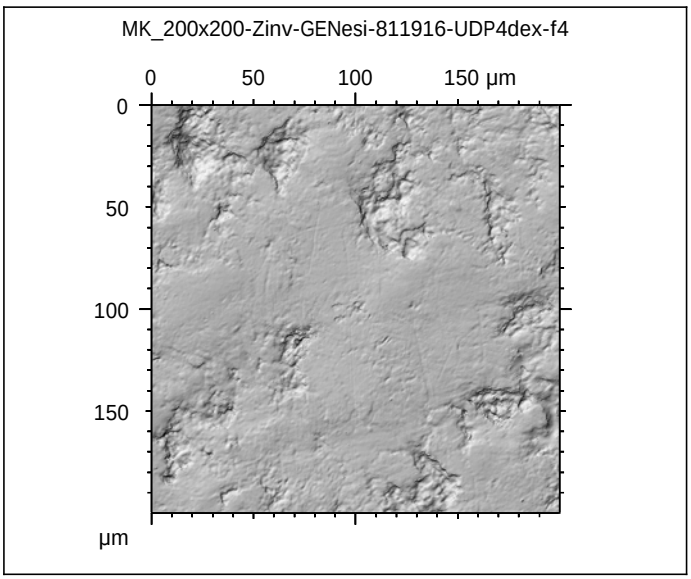
MK_200x200-Zinv-GENesi-811916-UDP4dex-f4
0
50
100
150 µm
µm

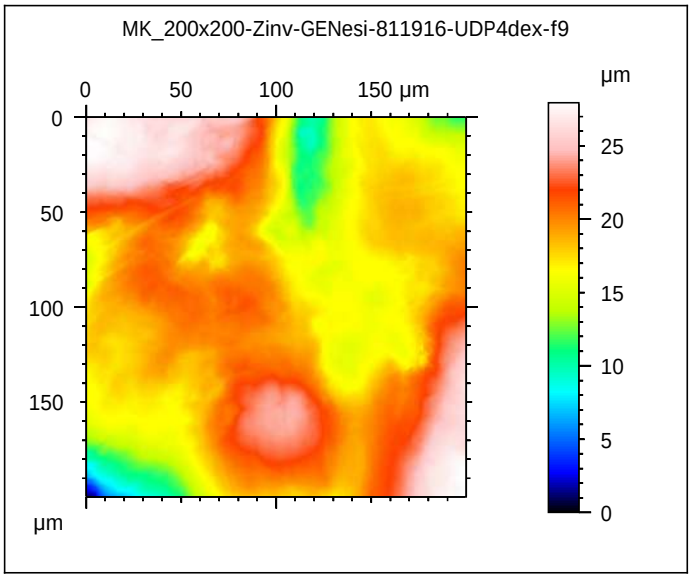
MK_200x200-Zinv-GENesi-811916-UDP4dex-f9
0
50
100
150 µm
µm
25
20
15
10
5
0

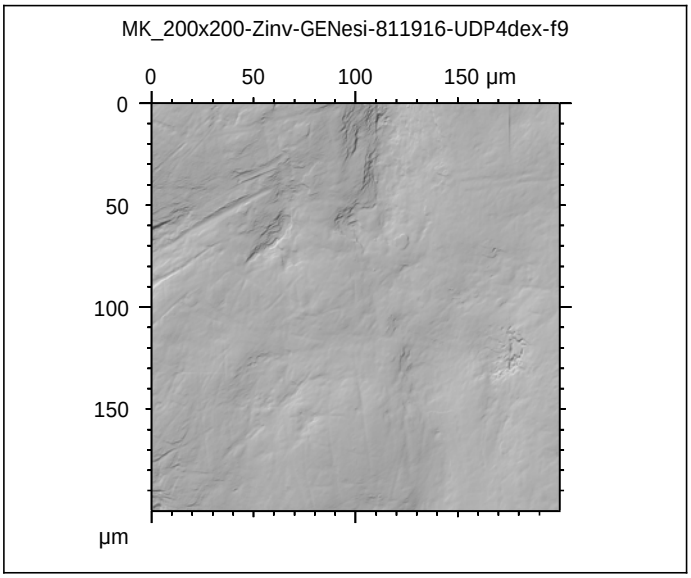
MK_200x200-Zinv-GENesi-811916-UDP4dex-f9
0
50
100
150 µm
µm

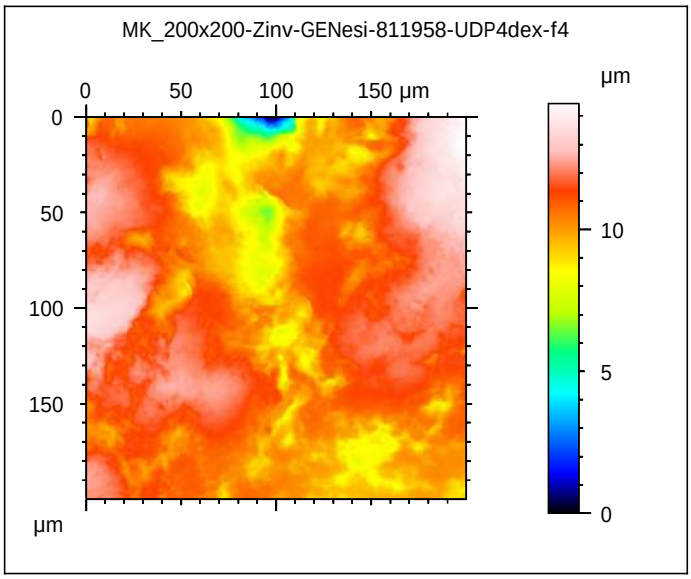
MK_200x200-Zinv-GENesi-811958-UDP4dex-f4
0
50
100
150 µm
µm
10
5
0

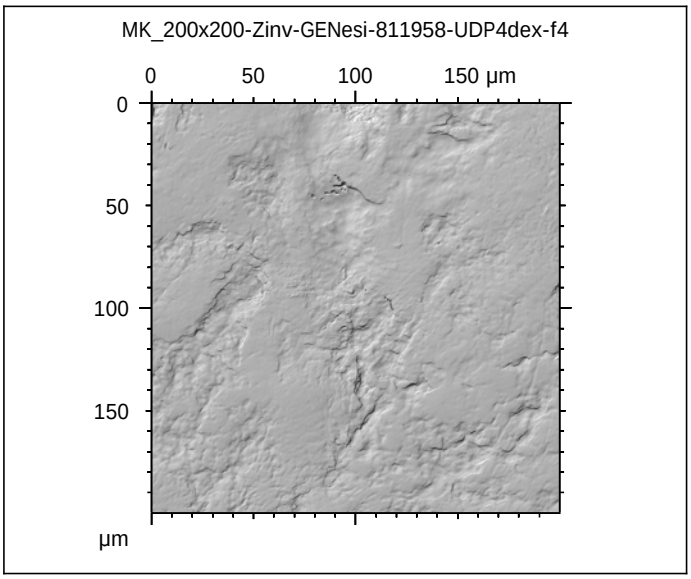
MK_200x200-Zinv-GENesi-811958-UDP4dex-f4
0
50
100
150 µm
µm

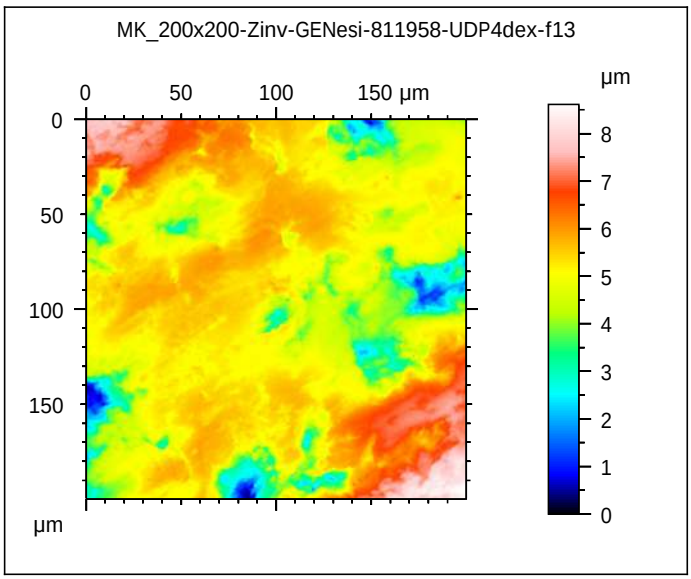
MK_200x200-Zinv-GENesi-811958-UDP4dex-f13
0
50
100
150 µm
µm
8
7
6
5
4
3
2
1
0

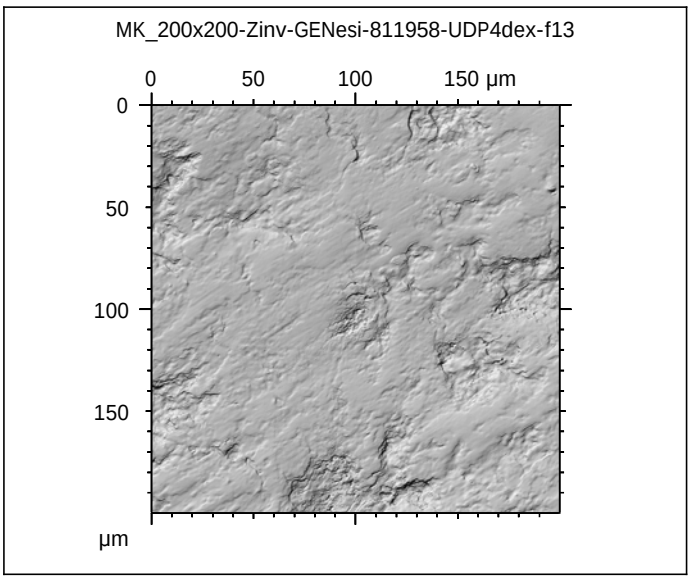
MK_200x200-Zinv-GENesi-811958-UDP4dex-f13
0
50
100
150 µm
µm

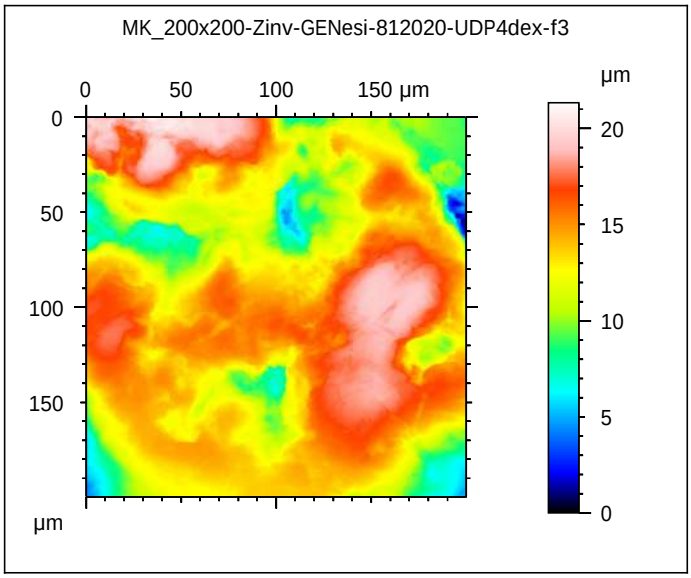
MK_200x200-Zinv-GENesi-812020-UDP4dex-f3
0
50
100
150 µm
µm
20
15
10
5
0

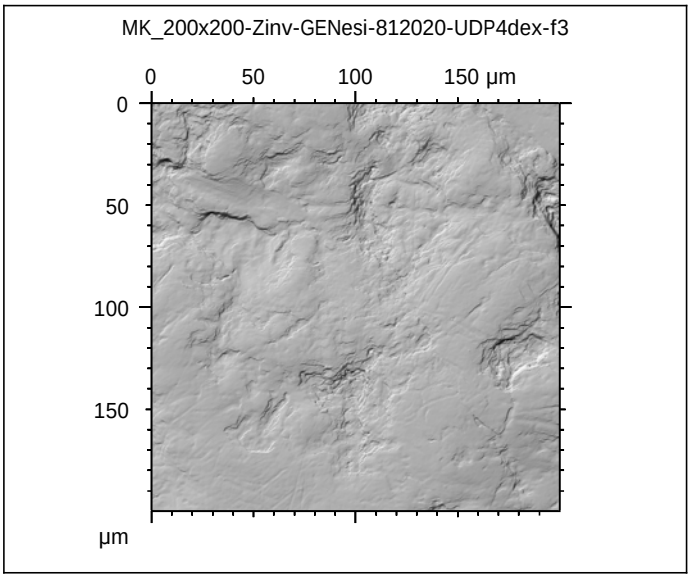
MK_200x200-Zinv-GENesi-812020-UDP4dex-f3
0
50
100
150 µm
µm

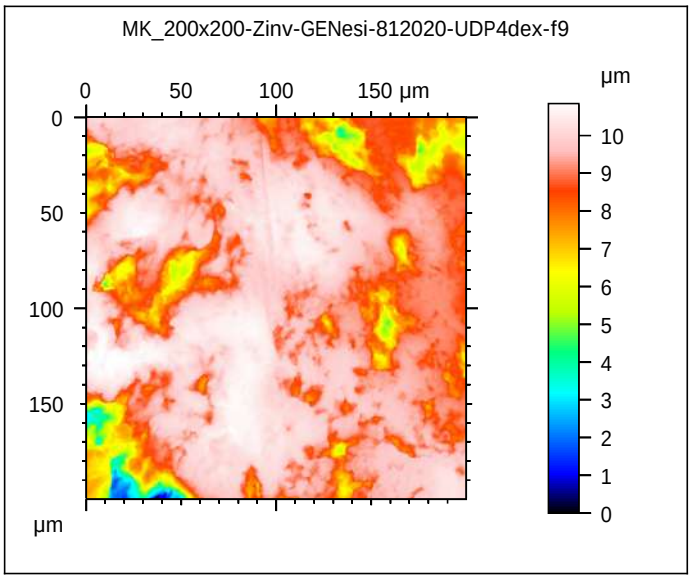
MK_200x200-Zinv-GENesi-812020-UDP4dex-f9
0
50
100
150 µm
µm
10
9
8
7
6
5
4
3
2
1
0

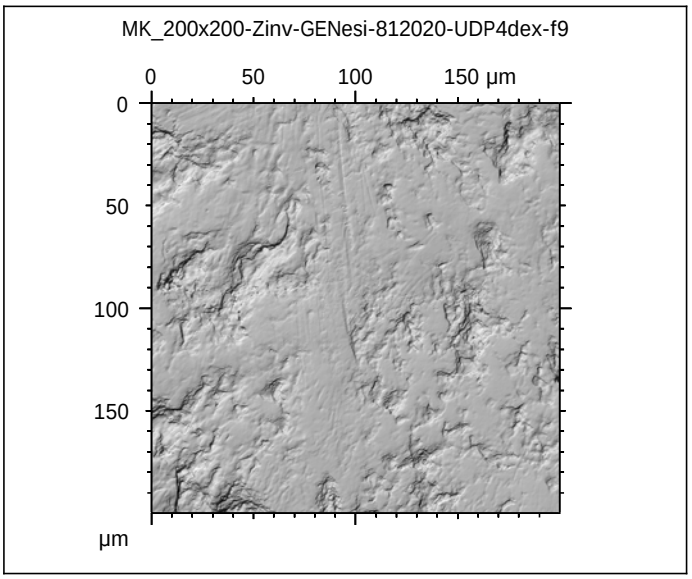
MK_200x200-Zinv-GENesi-812020-UDP4dex-f9
0
50
100
150 µm
µm

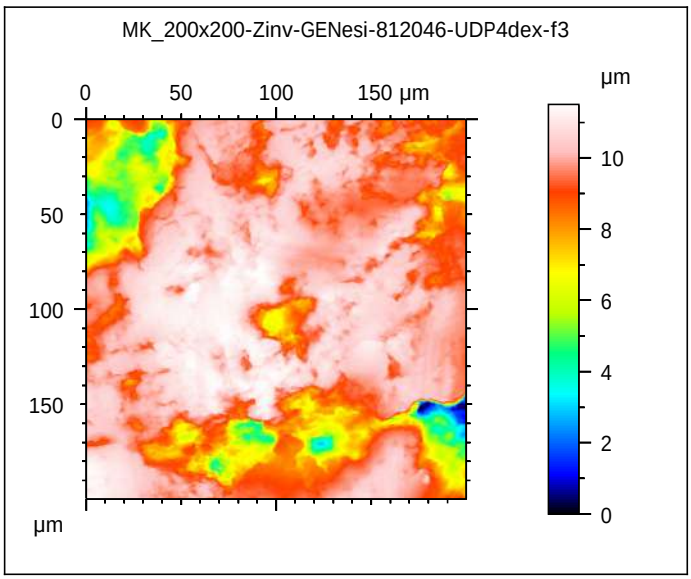
MK_200x200-Zinv-GENesi-812046-UDP4dex-f3
0
50
100
150 µm
µm
10
8
6
4
2
0

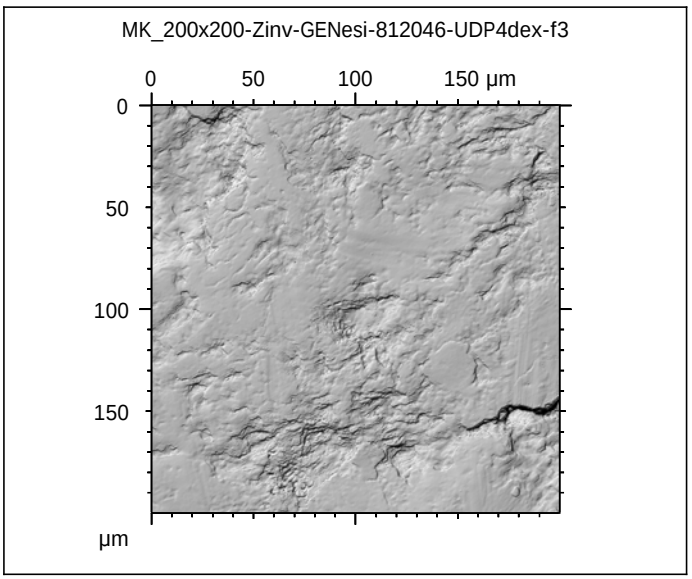
MK_200x200-Zinv-GENesi-812046-UDP4dex-f3
0
50
100
150 µm
µm

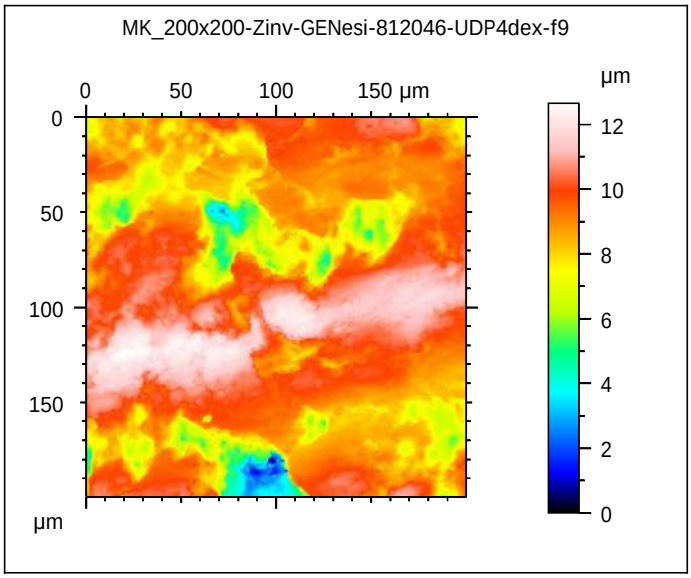
MK_200x200-Zinv-GENesi-812046-UDP4dex-f9
0
50
100
150 µm
µm
12
10
8
6
4
2
0

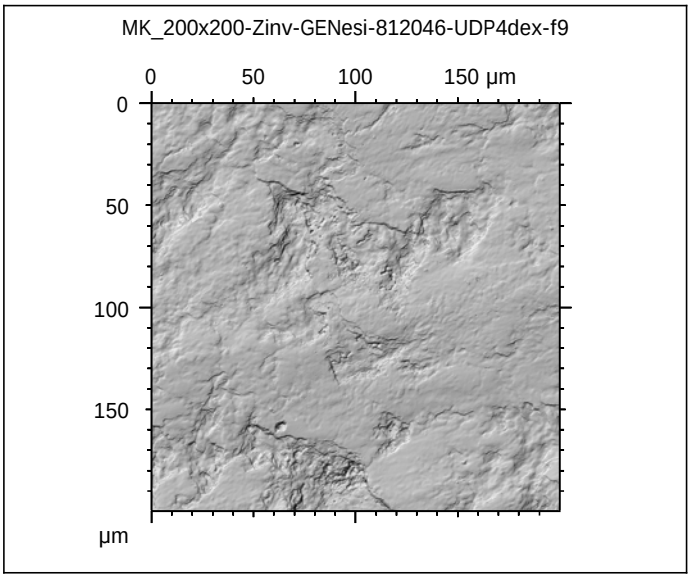
MK_200x200-Zinv-GENesi-812046-UDP4dex-f9
0
50
100
150 µm
µm

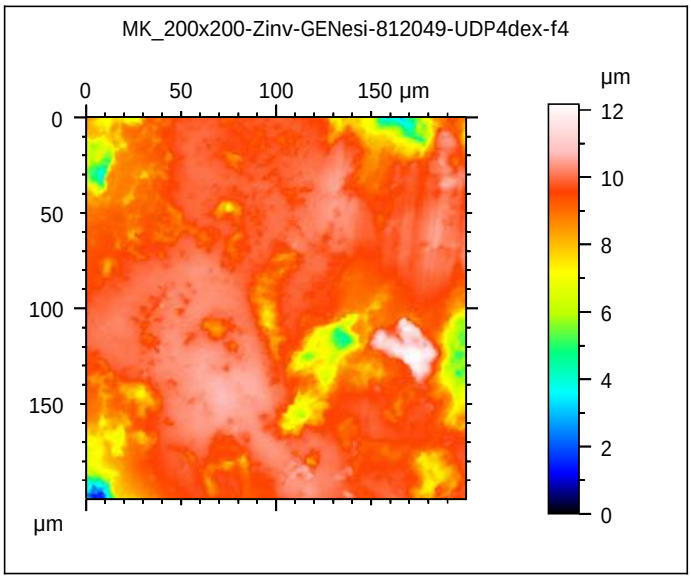
MK_200x200-Zinv-GENesi-812049-UDP4dex-f4
0
50
100
150 µm
µm
12
10
8
6
4
2
0

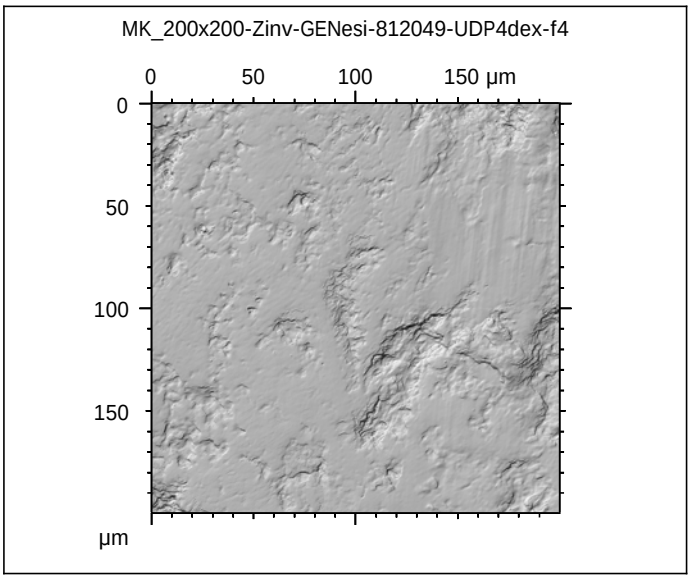
MK_200x200-Zinv-GENesi-812049-UDP4dex-f4
0
50
100
150 µm
µm

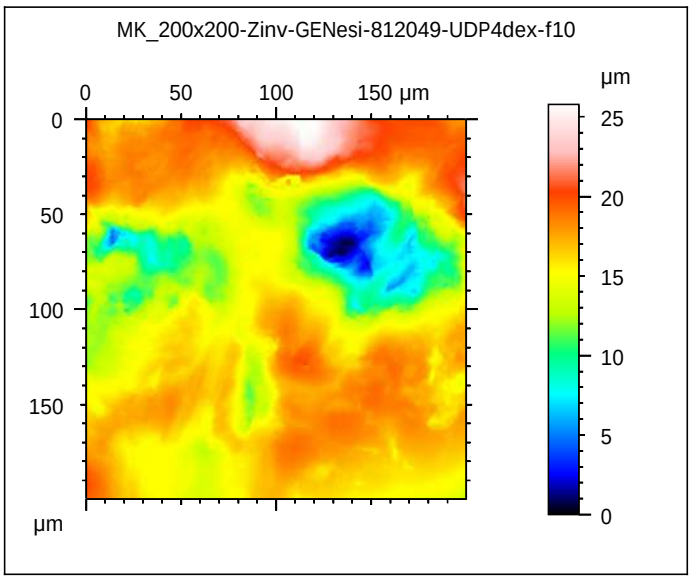
MK_200x200-Zinv-GENesi-812049-UDP4dex-f10
0
50
100
150 µm
µm
25
20
15
10
5
0

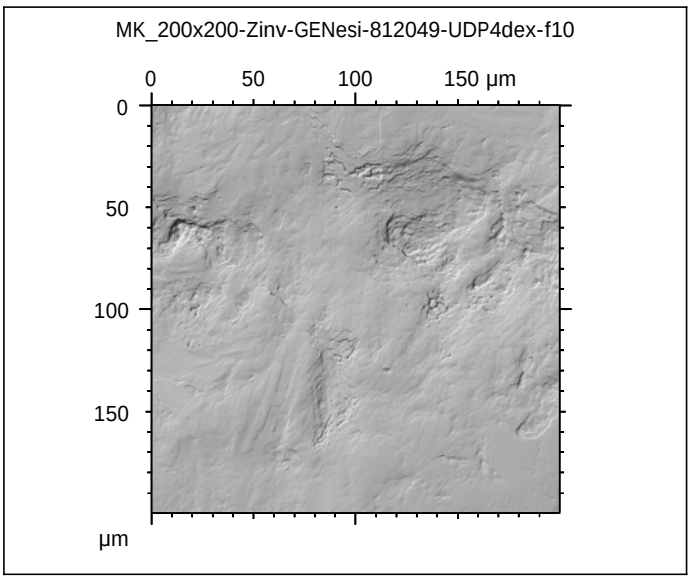
MK_200x200-Zinv-GENesi-812049-UDP4dex-f10
0
50
100
150 µm
µm

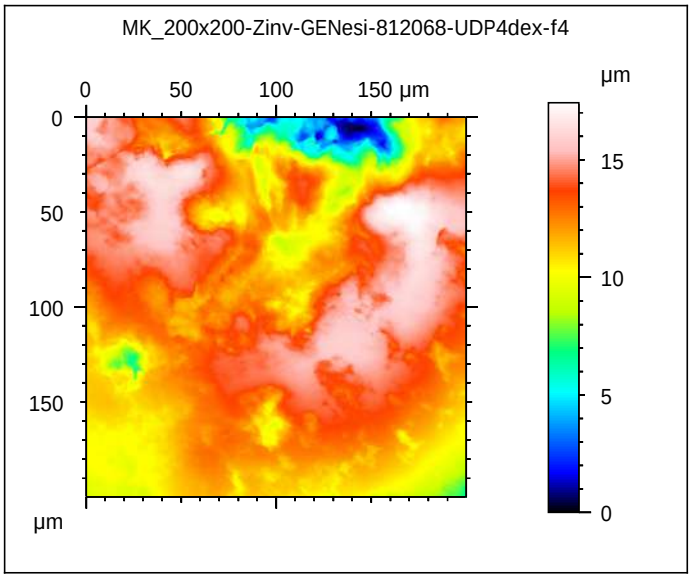
MK_200x200-Zinv-GENesi-812068-UDP4dex-f4
0
50
100
150 µm
µm
15
10
5
0

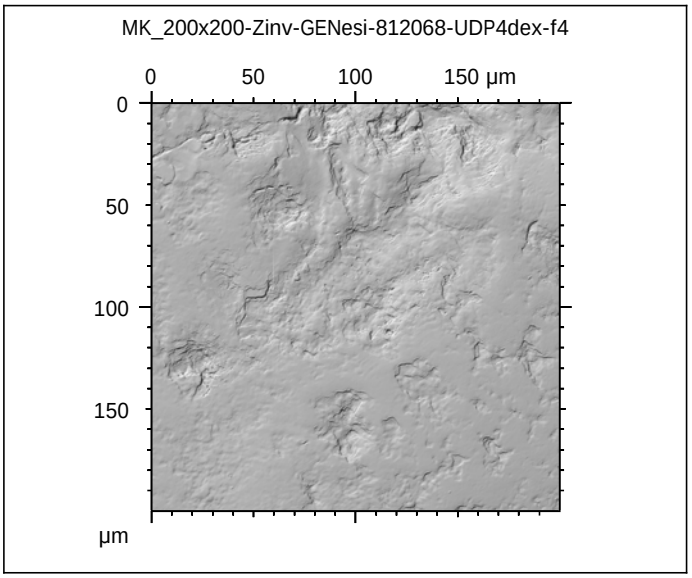
MK_200x200-Zinv-GENesi-812068-UDP4dex-f4
0
50
100
150 µm
µm

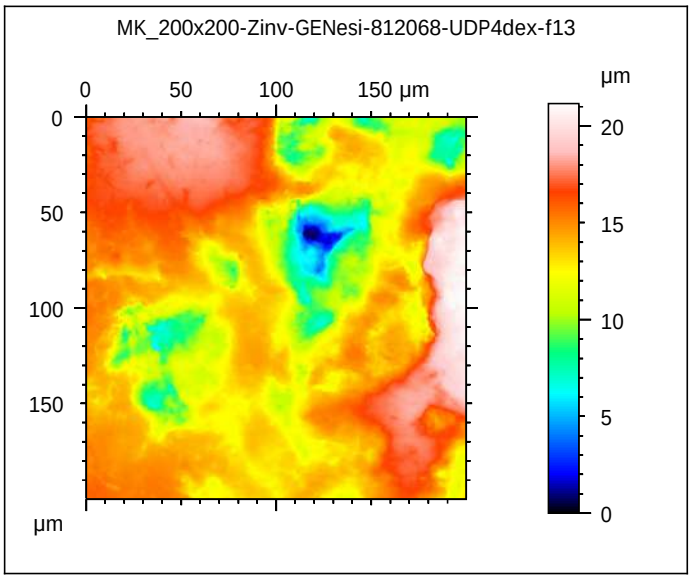
MK_200x200-Zinv-GENesi-812068-UDP4dex-f13
0
50
100
150 µm
µm
20
15
10
5
0

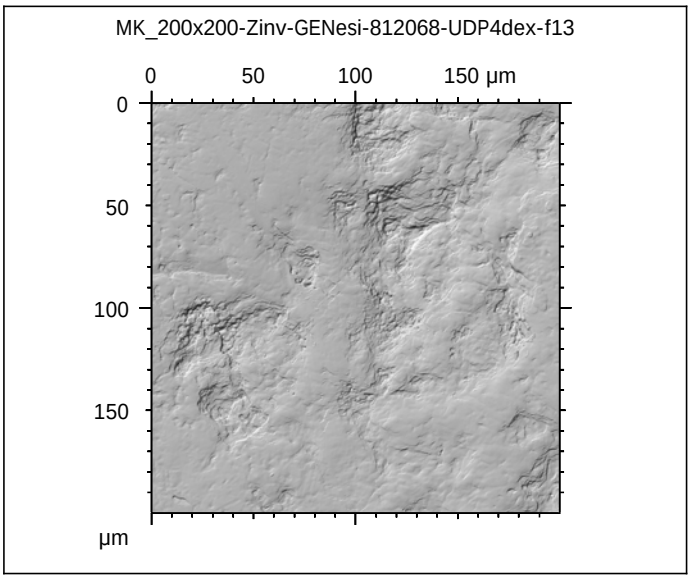
MK_200x200-Zinv-GENesi-812068-UDP4dex-f13
0
50
100
150 µm
µm

Photosimulations and false color elevation maps of scanned shearing and crushing facets on molars and deciduous premolars of the **hazelnut group** (100% base diet + 10 hazelnuts in shell per day)

scanned at the PALEVOPRIM lab by M. Louail, University of Poitiers, France with "TRIDENT", white light confocal microscope Leica DCM8 - April 2020

ALIHOM Project (Région Nouvelle Aquitaine, France), ANR Diet-Scratches

DIET-SCRATCHES

ANR-17-CE27-0002

PIs: G. Merceron & S. Ferchaud

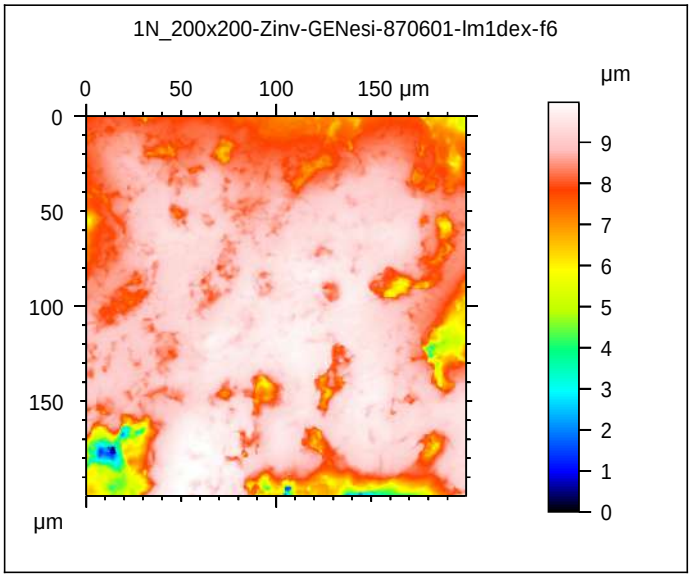

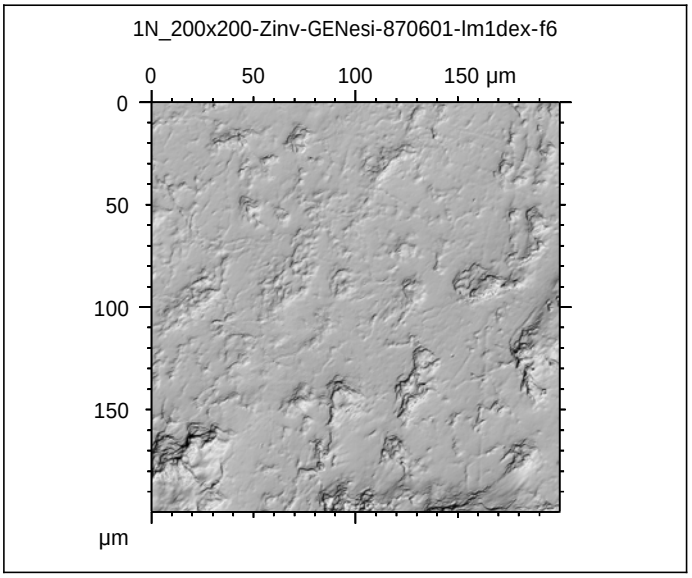

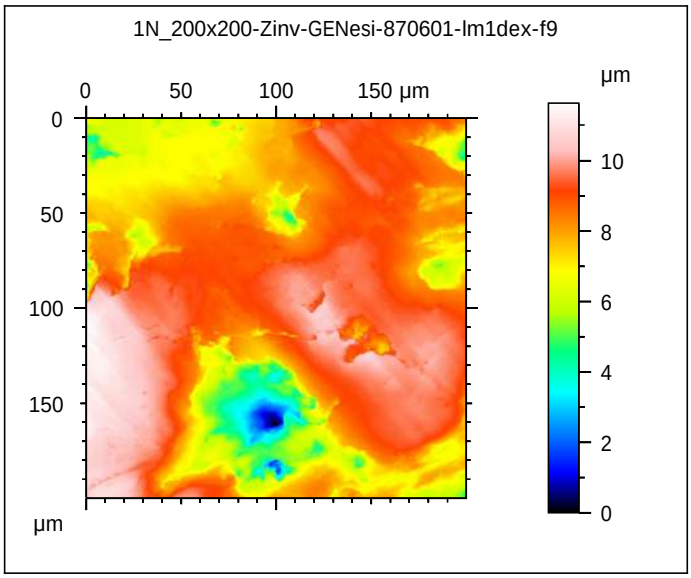

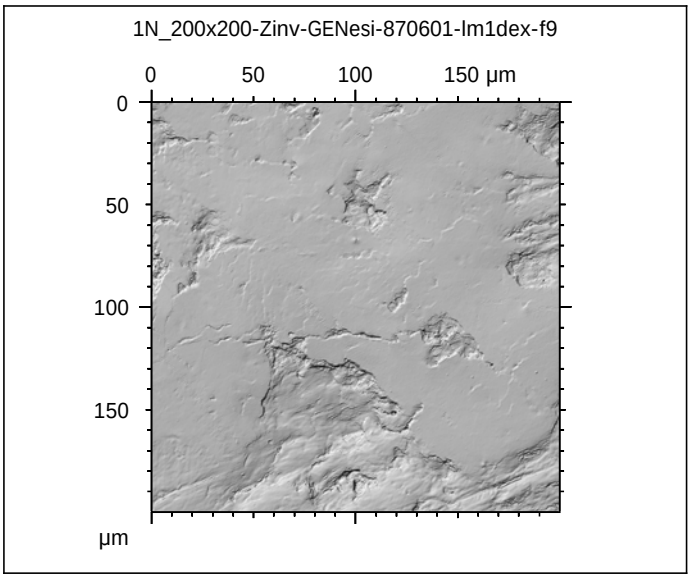

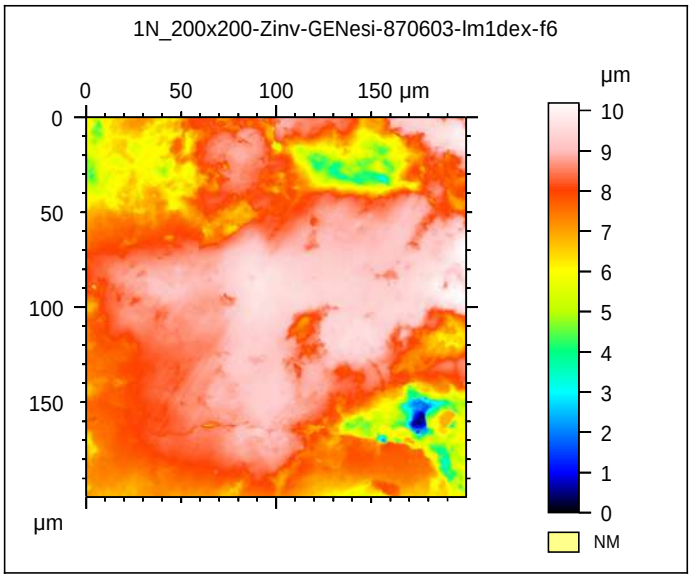

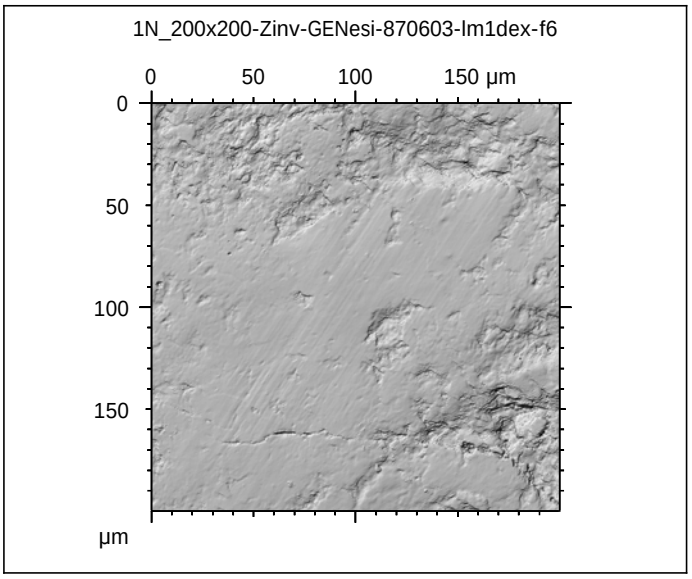

Leica Map Premium 8.0.9173

Photosimulations and false color elevation maps of scanned shearing and crushing facets on molars and deciduous premolars of the **hazelnut group** (100% base diet + 10 hazelnuts in shell per day)

scanned at the PALEVOPRIM lab by M. Louail, University of Poitiers, France with "TRIDENT", white light confocal microscope Leica DCM8 - April 2020

ALIHOM Project (Région Nouvelle Aquitaine, France), ANR Diet-Scratches

DIET-SCRATCHES

ANR-17-CE27-0002

PIs: G. Merceron & S. Ferchaud

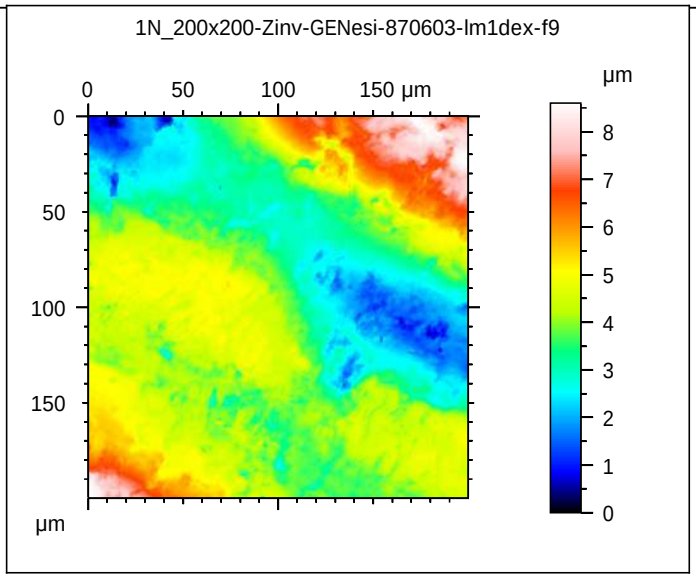

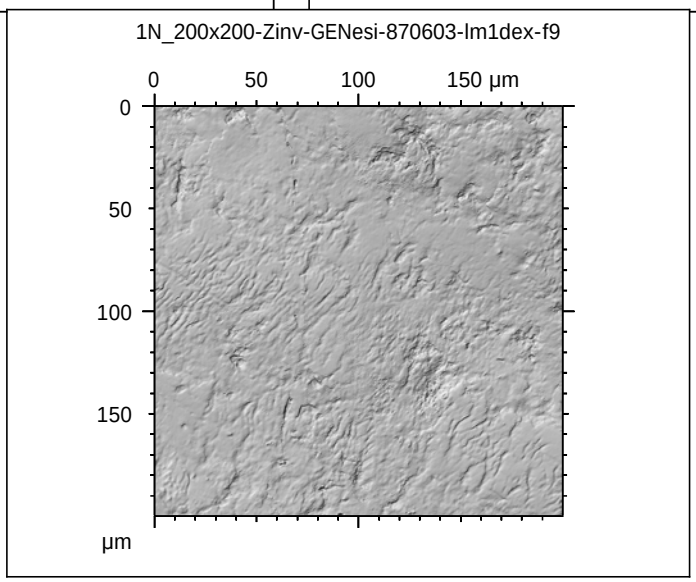

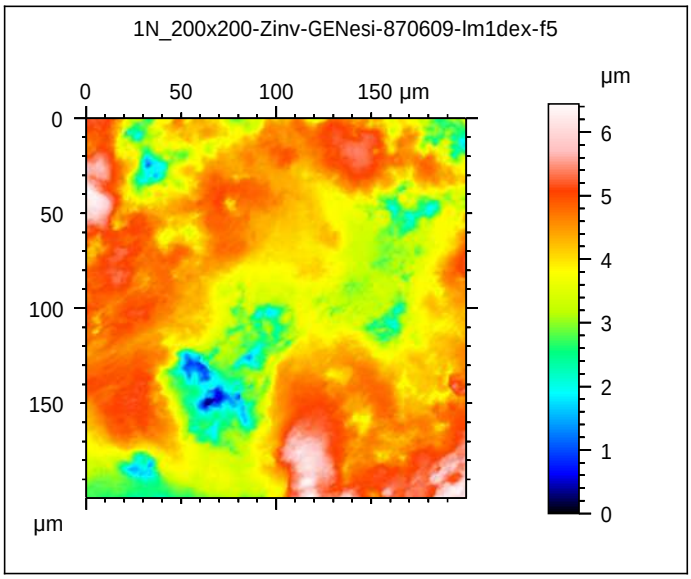

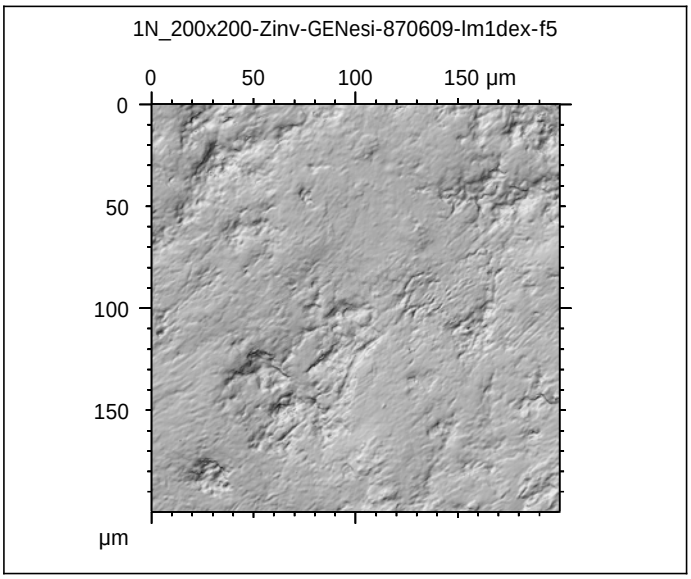

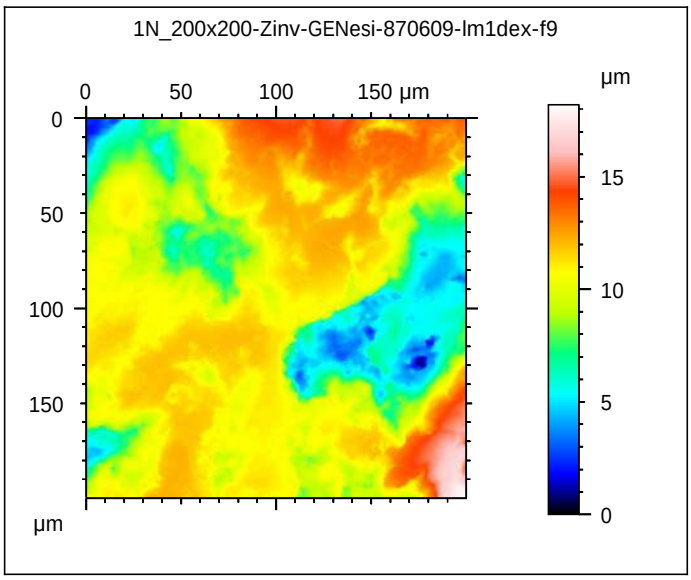

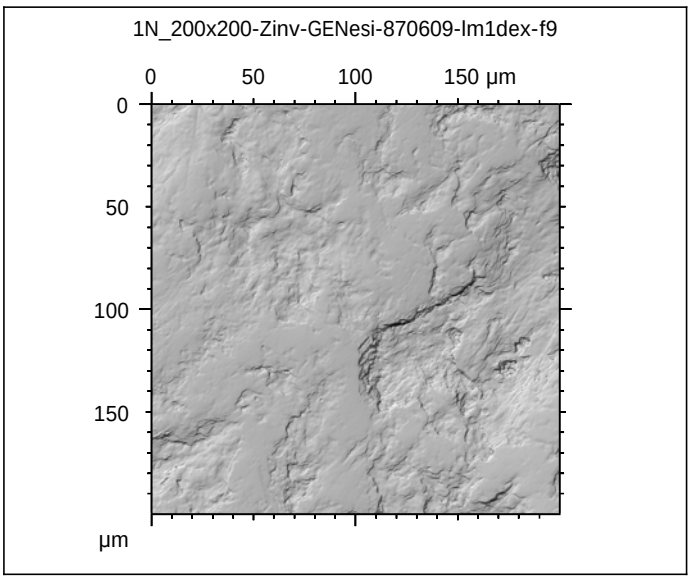

Leica Map Premium 8.0.9173

Photosimulations and false color elevation maps of scanned shearing and crushing facets on molars and deciduous premolars of the **hazelnut group** (100% base diet + 10 hazelnuts in shell per day)

scanned at the PALEVOPRIM lab by M. Louail, University of Poitiers, France with "TRIDENT", white light confocal microscope Leica DCM8 - April 2020

ALIHOM Project (Région Nouvelle Aquitaine, France), ANR Diet-Scratches

DIET-SCRATCHES

ANR-17-CE27-0002

PIs: G. Merceron & S. Ferchaud

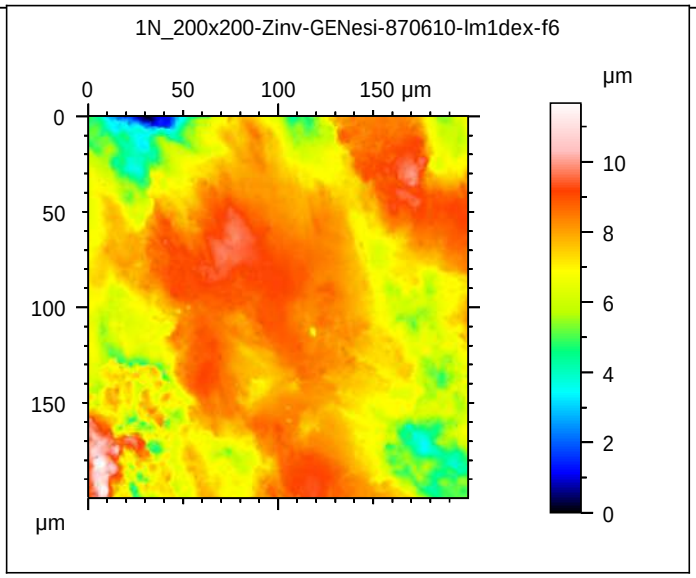

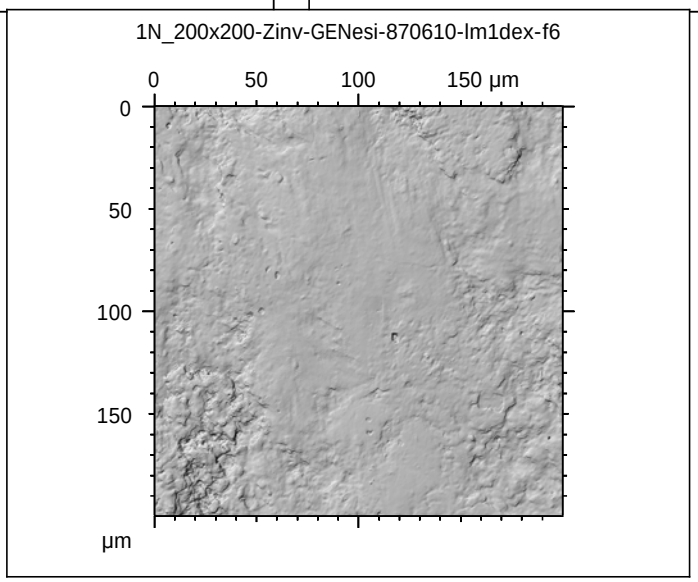

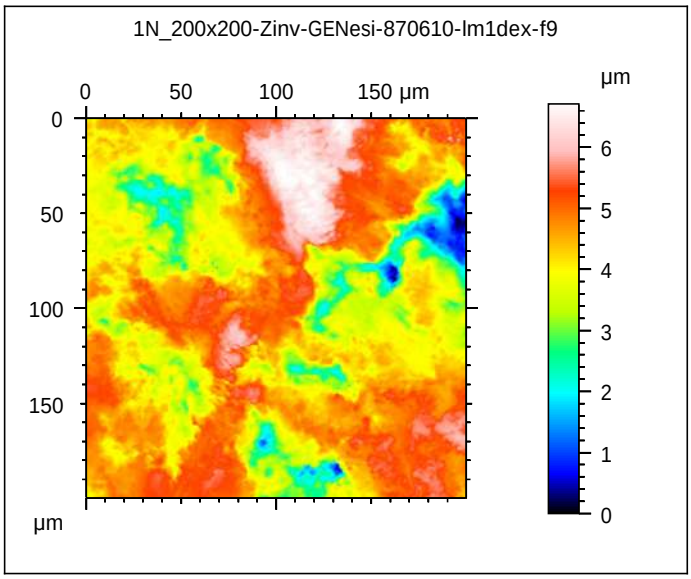

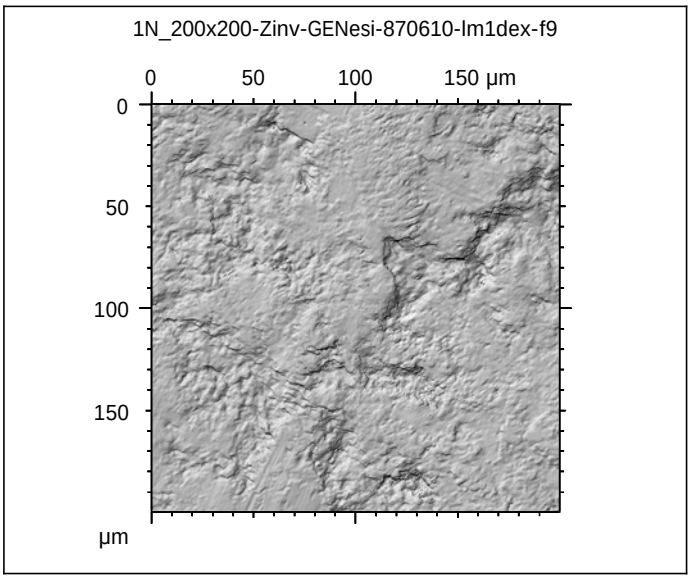

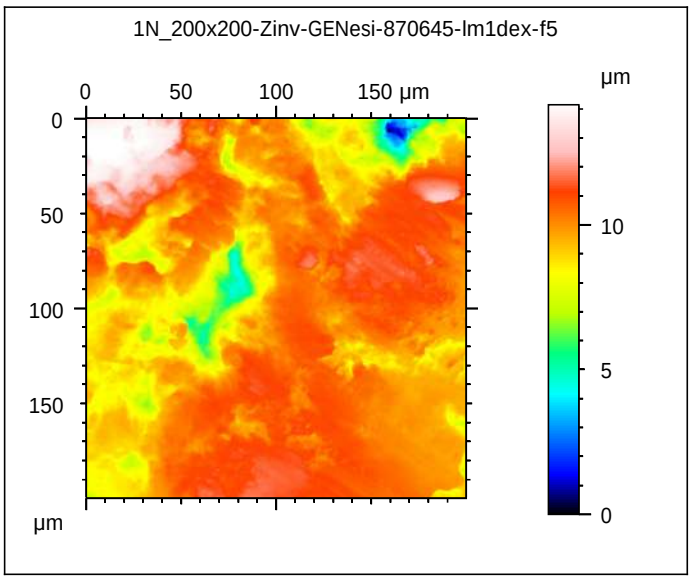

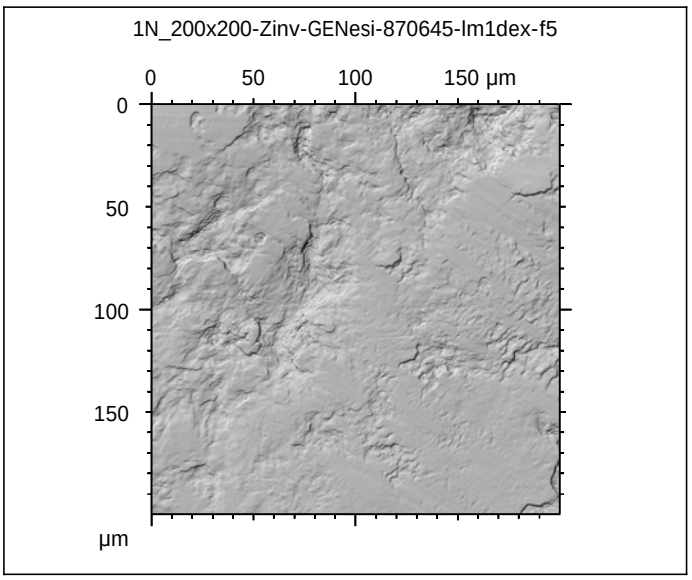

Leica Map Premium 8.0.9173

Photosimulations and false color elevation maps of scanned shearing and crushing facets on molars and deciduous premolars of the **hazelnut group** (100% base diet + 10 hazelnuts in shell per day)

scanned at the PALEVOPRIM lab by M. Louail, University of Poitiers, France with "TRIDENT", white light confocal microscope Leica DCM8 - April 2020

ALIHOM Project (Région Nouvelle Aquitaine, France), ANR Diet-Scratches

ANR-17-CE27-0002

PIs: G. Merceron & S. Ferchaud

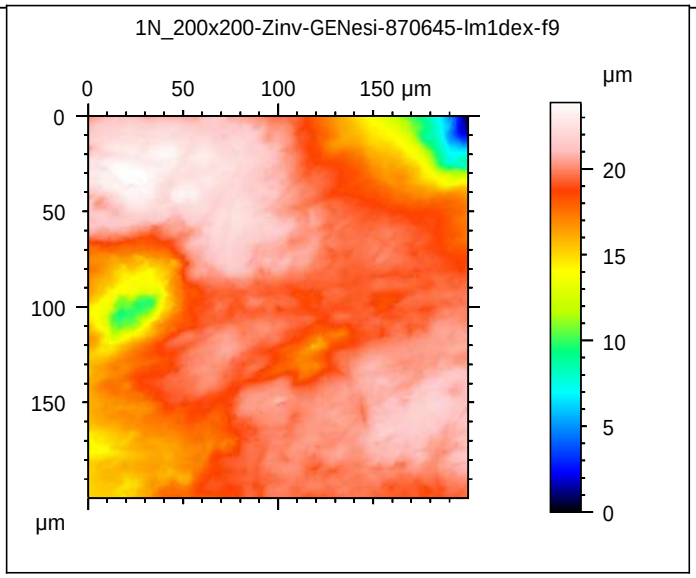

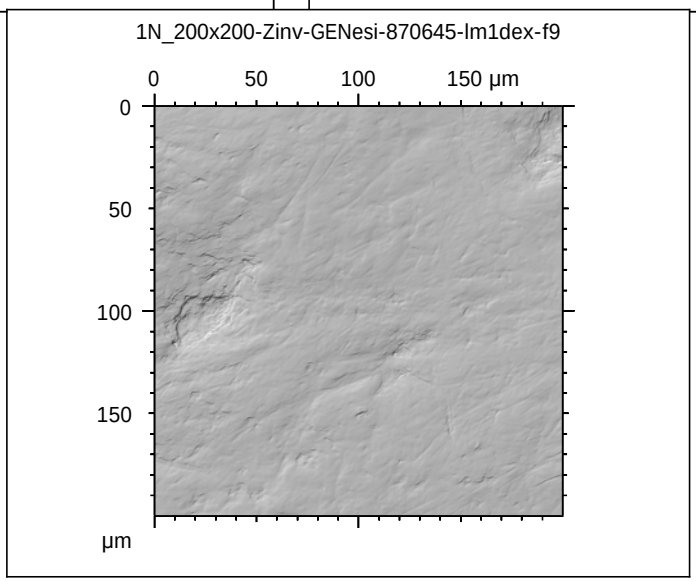

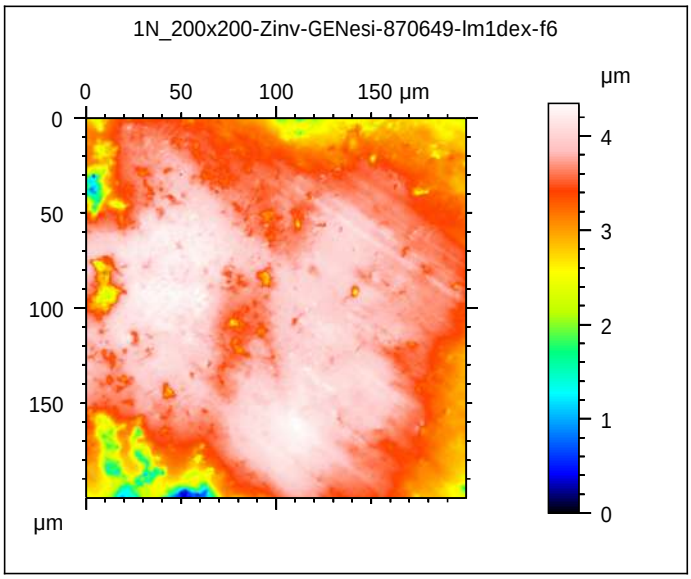

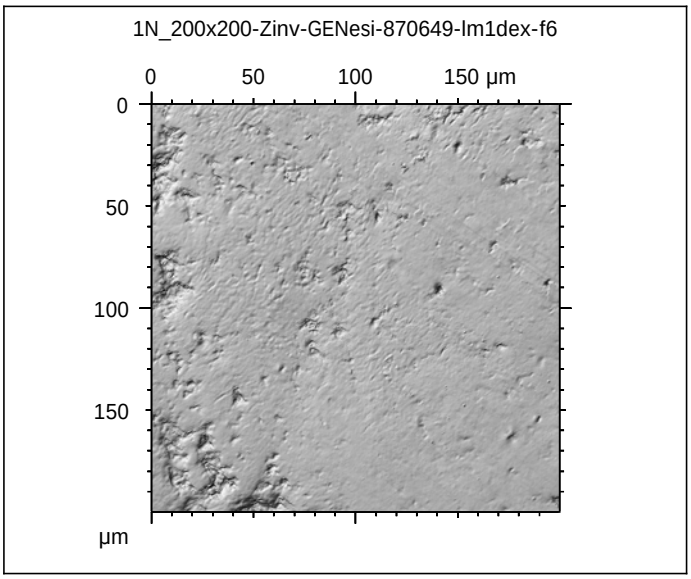

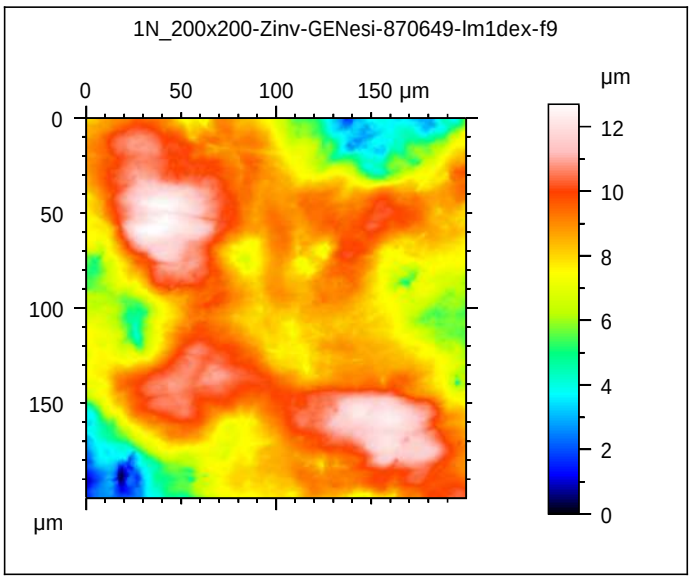

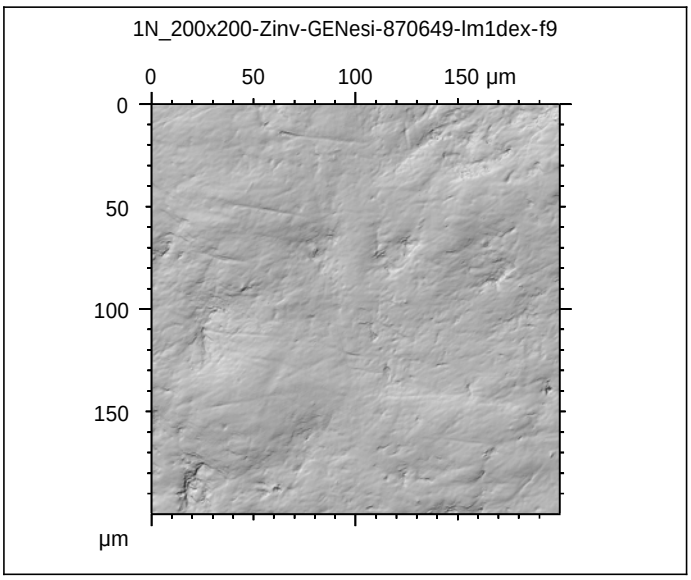

Leica Map Premium 8.0.9173

Photosimulations and false color elevation maps of scanned shearing and crushing facets on molars and deciduous premolars of the **hazelnut group** (100% base diet + 10 hazelnuts in shell per day)

scanned at the PALEVOPRIM lab by M. Louail, University of Poitiers, France with "TRIDENT", white light confocal microscope Leica DCM8 - April 2020

ALIHOM Project (Région Nouvelle Aquitaine, France), ANR Diet-Scratches

ANR-17-CE27-0002

PIs: G. Merceron & S. Ferchaud

1N_200x200-Zinv-GENesi-870601-UM1dex-f9

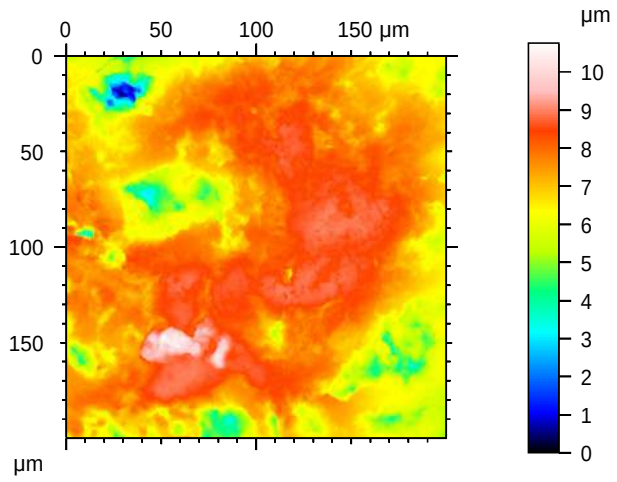

1N_200x200-Zinv-GENesi-870601-UM1dex-f9

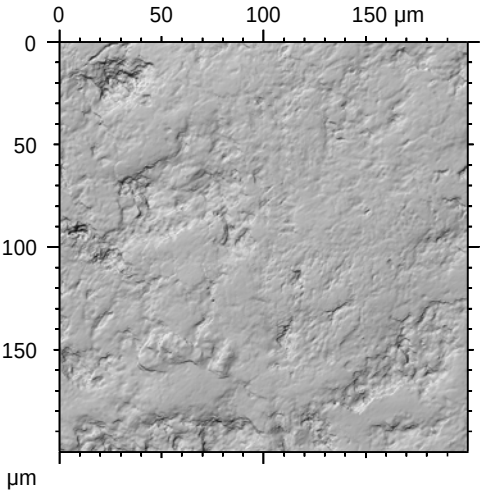

1N_200x200-Zinv-GENesi-870603-UM1dex-f3

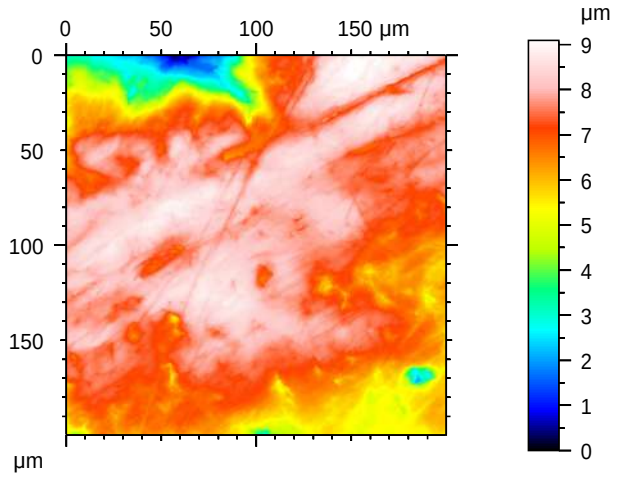

1N_200x200-Zinv-GENesi-870603-UM1dex-f3

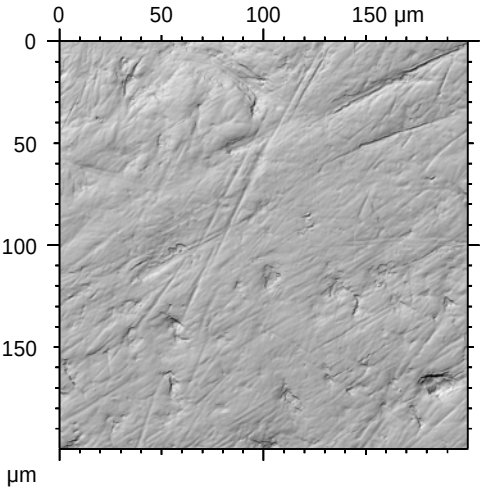

1N_200x200-Zinv-GENesi-870603-UM1dex-f9

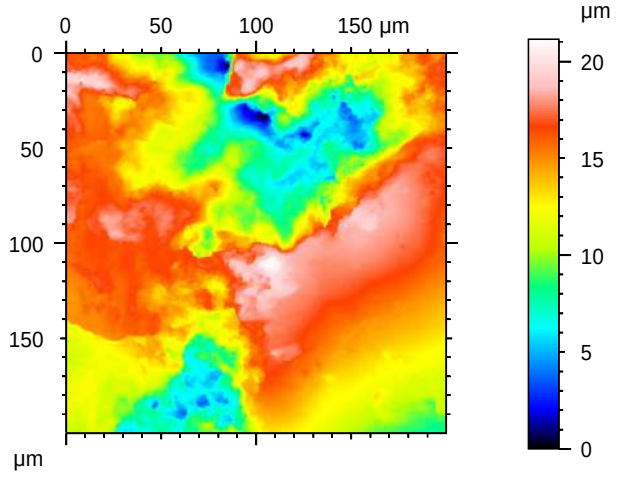

1N_200x200-Zinv-GENesi-870603-UM1dex-f9

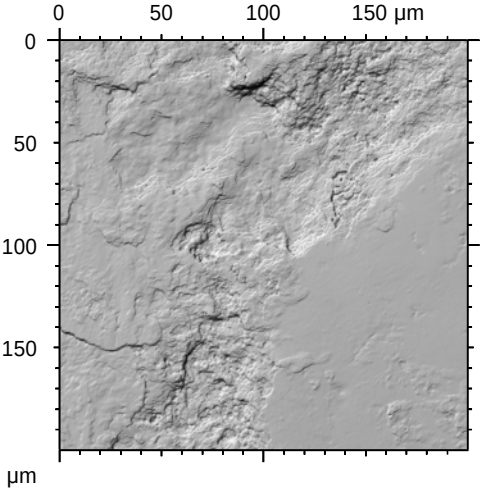

Leica Map Premium 8.0.9173

Photosimulations and false color elevation maps of scanned shearing and crushing facets on molars and deciduous premolars of the **hazelnut group** (100% base diet + 10 hazelnuts in shell per day)

scanned at the PALEVOPRIM lab by M. Louail, University of Poitiers, France with "TRIDENT", white light confocal microscope Leica DCM8 - April 2020

ALIHOM Project (Région Nouvelle Aquitaine, France), ANR Diet-Scratches

DIET-SCRATCHES

ANR-17-CE27-0002

PIs: G. Merceron & S. Ferchaud

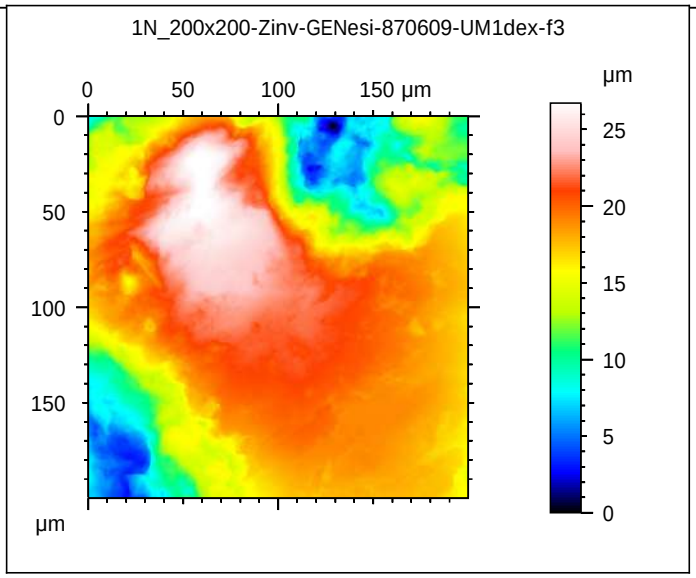

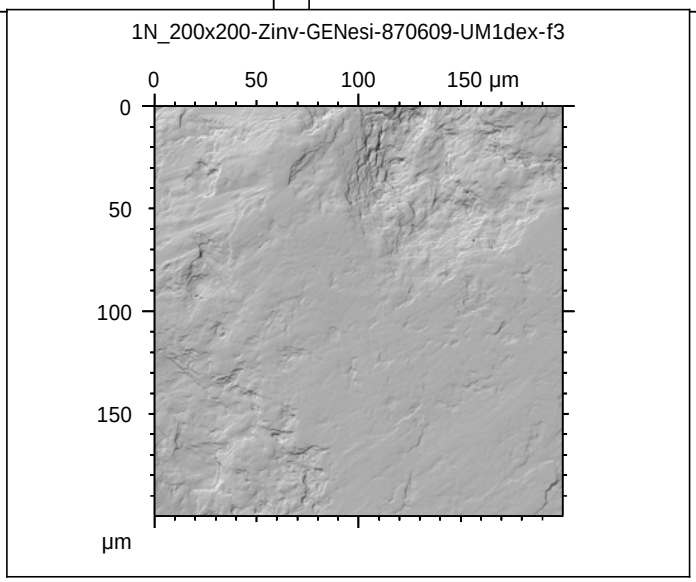

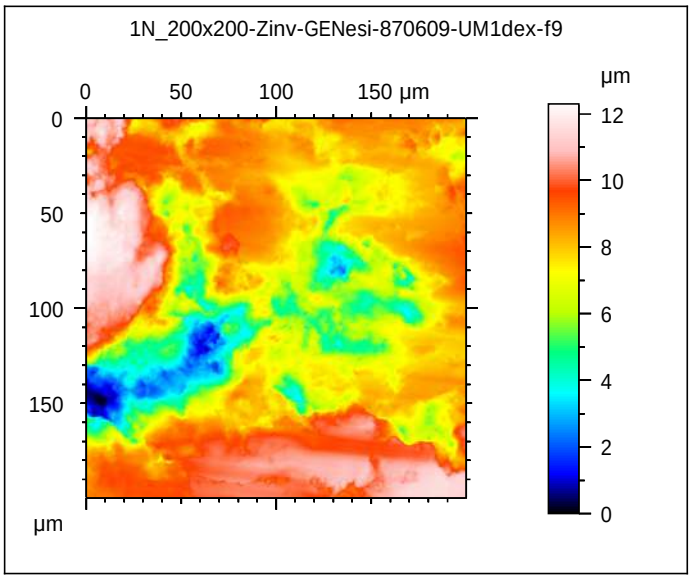

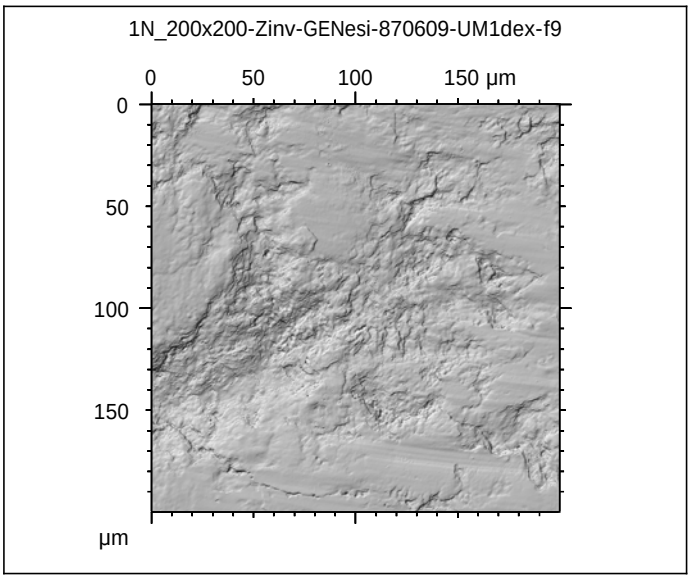

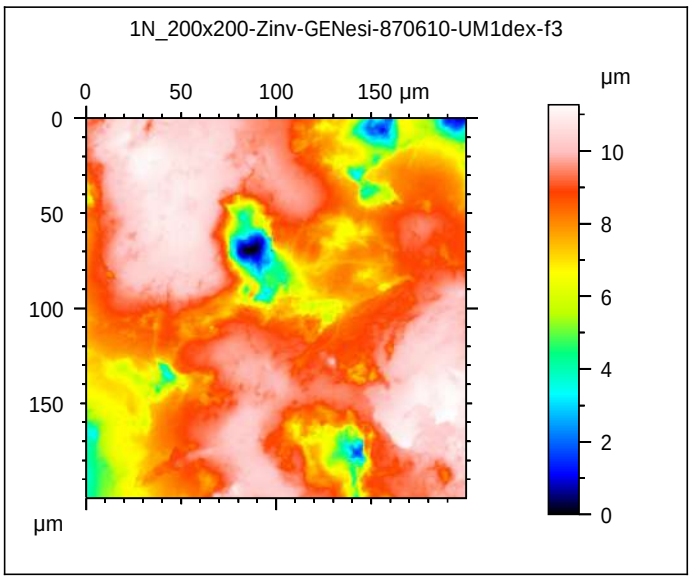

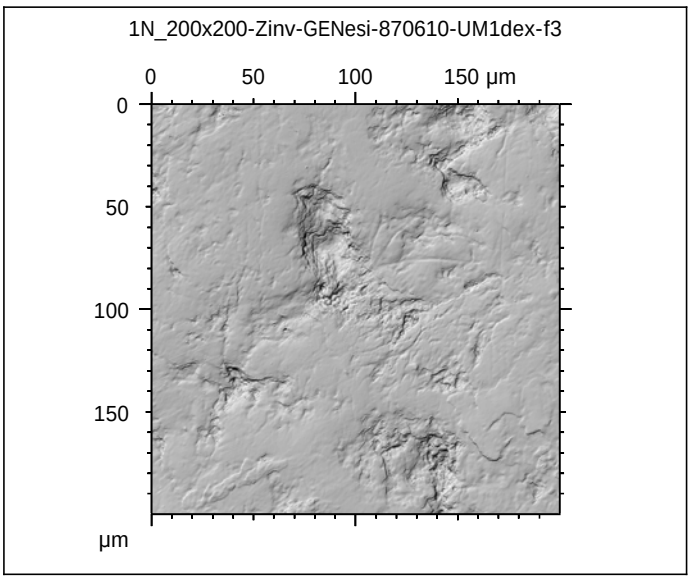

Leica Map Premium 8.0.9173

Photosimulations and false color elevation maps of scanned shearing and crushing facets on molars and deciduous premolars of the **hazelnut group** (100% base diet + 10 hazelnuts in shell per day)

scanned at the PALEVOPRIM lab by M. Louail, University of Poitiers, France with "TRIDENT", white light confocal microscope Leica DCM8 - April 2020

ALIHOM Project (Région Nouvelle Aquitaine, France), ANR Diet-Scratches

ANR-17-CE27-0002

PIs: G. Merceron & S. Ferchaud

1N_200x200-Zinv-GENesi-870610-UM1dex-f9

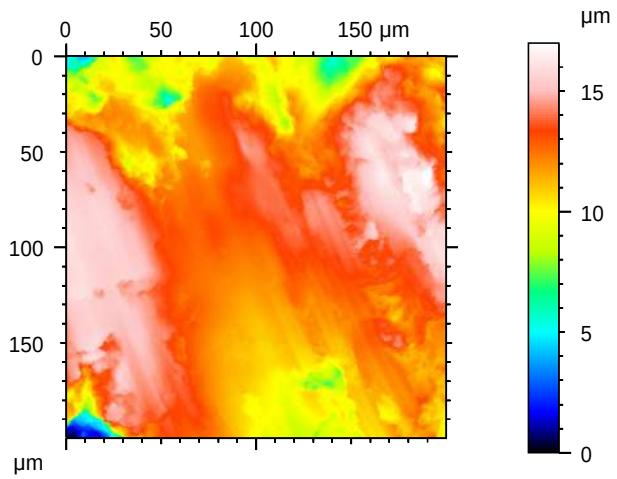

1N_200x200-Zinv-GENesi-870610-UM1dex-f9

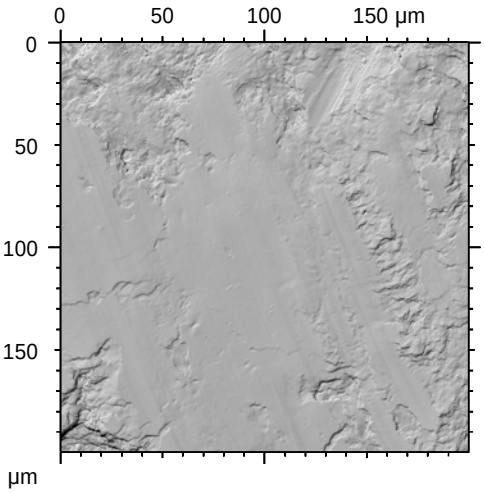

1N_200x200-Zinv-GENesi-870645-UM1dex-f4

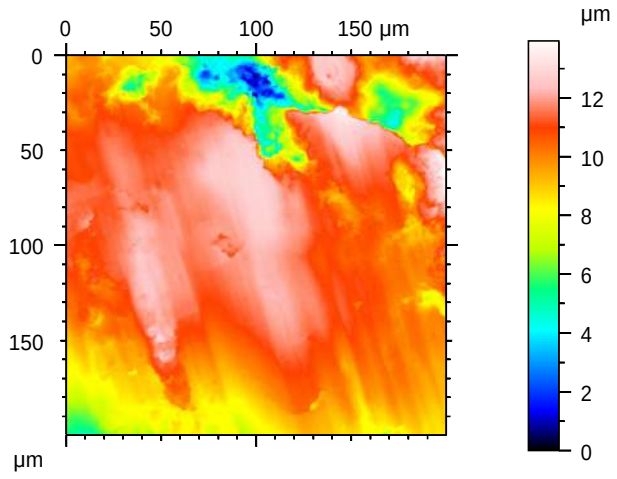

1N_200x200-Zinv-GENesi-870645-UM1dex-f4

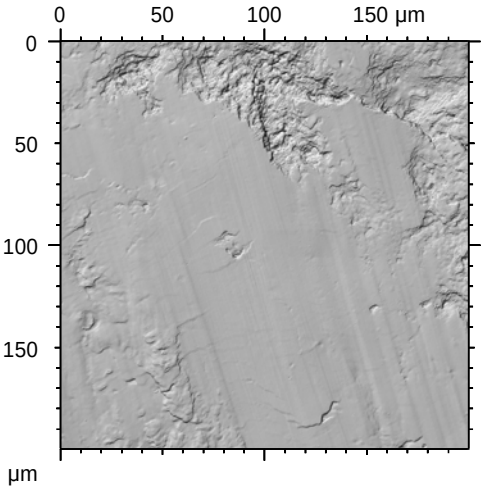

1N_200x200-Zinv-GENesi-870645-UM1dex-f9

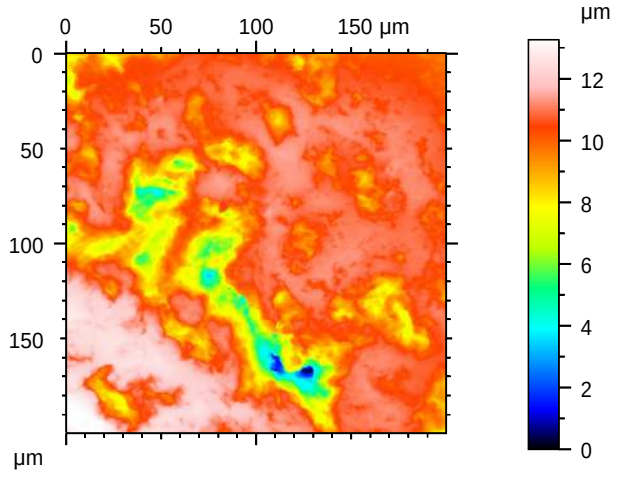

1N_200x200-Zinv-GENesi-870645-UM1dex-f9

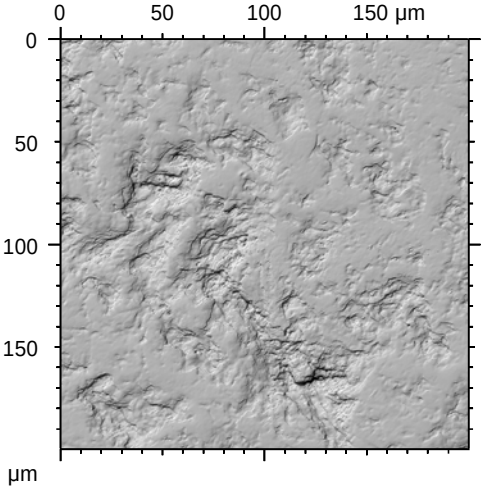

Leica Map Premium 8.0.9173

Photosimulations and false color elevation maps of scanned shearing and crushing facets on molars and deciduous premolars of the **hazelnut group** (100% base diet + 10 hazelnuts in shell per day)

scanned at the PALEVOPRIM lab by M. Louail, University of Poitiers, France with "TRIDENT", white light confocal microscope Leica DCM8 - April 2020

ALIHOM Project (Région Nouvelle Aquitaine, France), ANR Diet-Scratches

ANR-17-CE27-0002

PIs: G. Merceron & S. Ferchaud

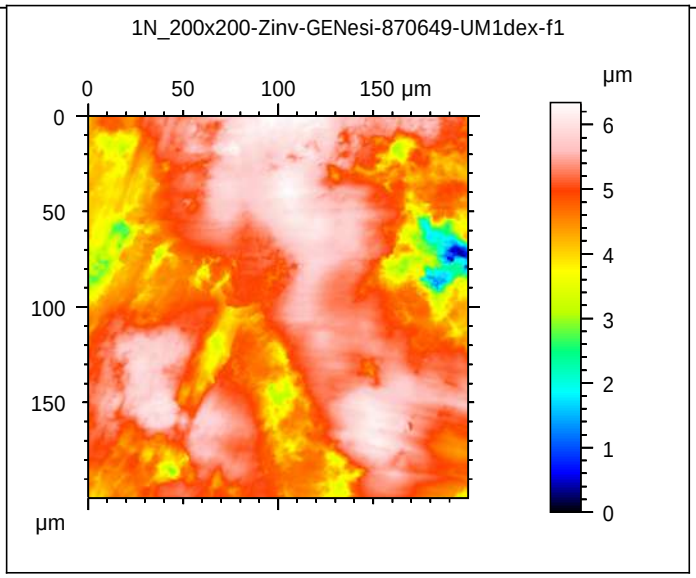

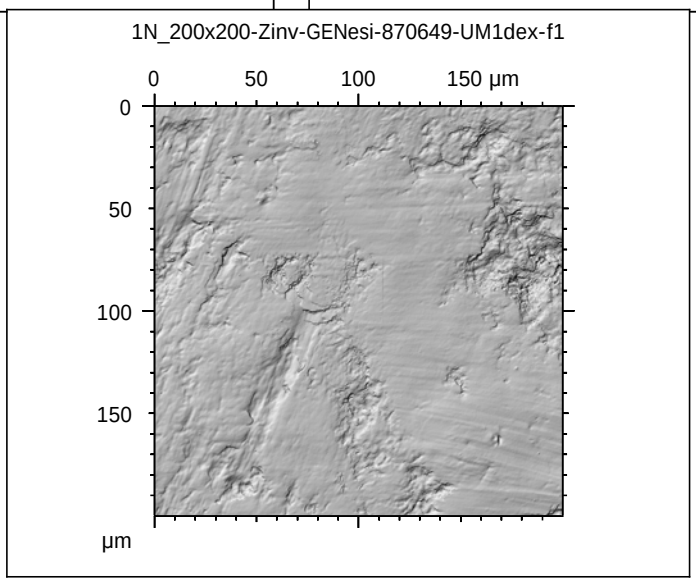

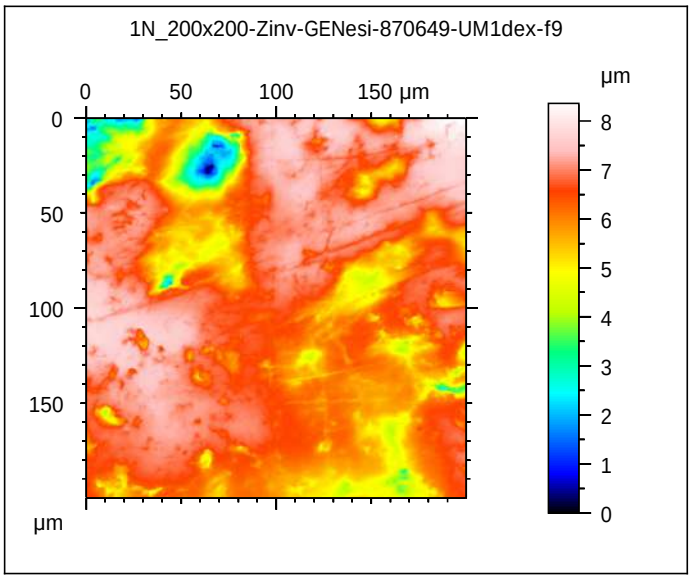

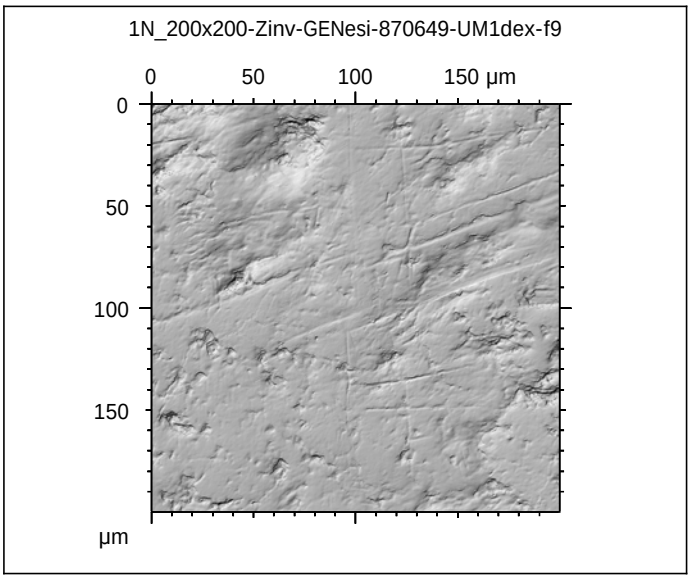

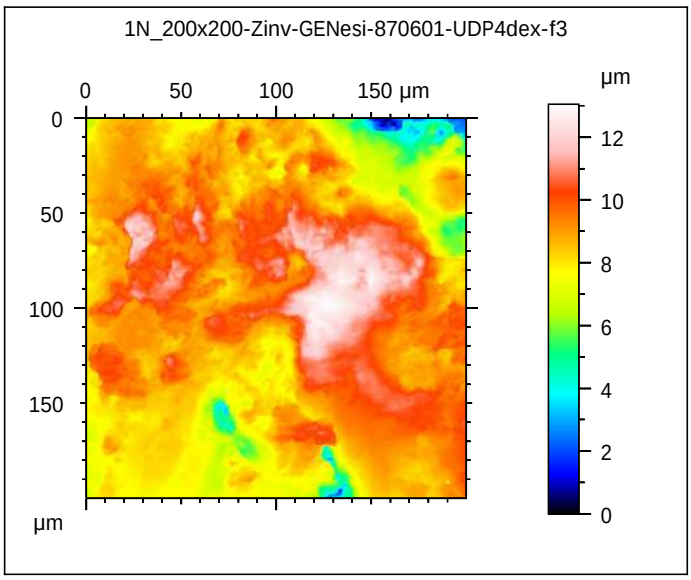

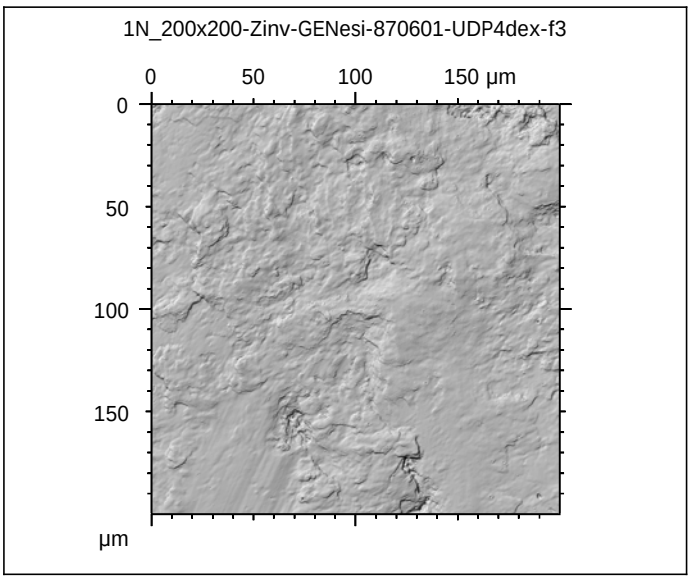

Leica Map Premium 8.0.9173

Photosimulations and false color elevation maps of scanned shearing and crushing facets on molars and deciduous premolars of the **hazelnut group** (100% base diet + 10 hazelnuts in shell per day)

scanned at the PALEVOPRIM lab by M. Louail, University of Poitiers, France with "TRIDENT", white light confocal microscope Leica DCM8 - April 2020

ALIHOM Project (Région Nouvelle Aquitaine, France), ANR Diet-Scratches

ANR-17-CE27-0002

PIs: G. Merceron & S. Ferchaud

1N_200x200-Zinv-GENesi-870601-UDP4dex-f9

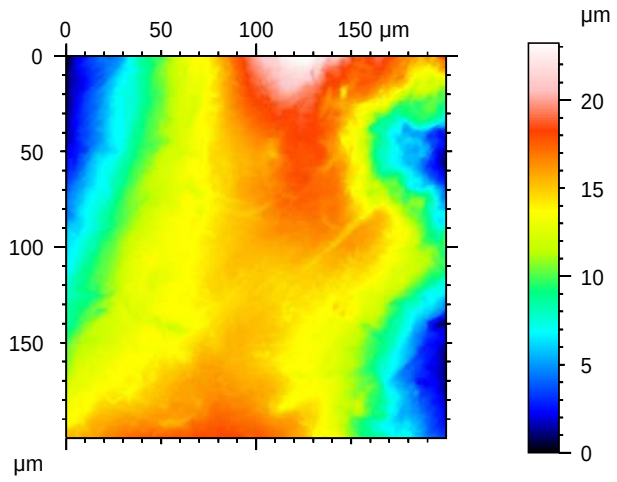

1N_200x200-Zinv-GENesi-870601-UDP4dex-f9

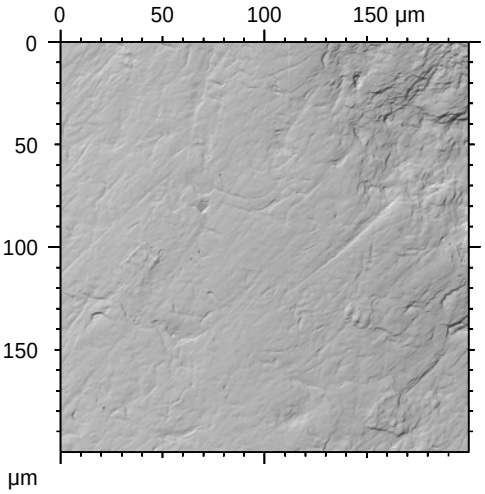

1N_200x200-Zinv-GENesi-870603-UDP4dex-f3

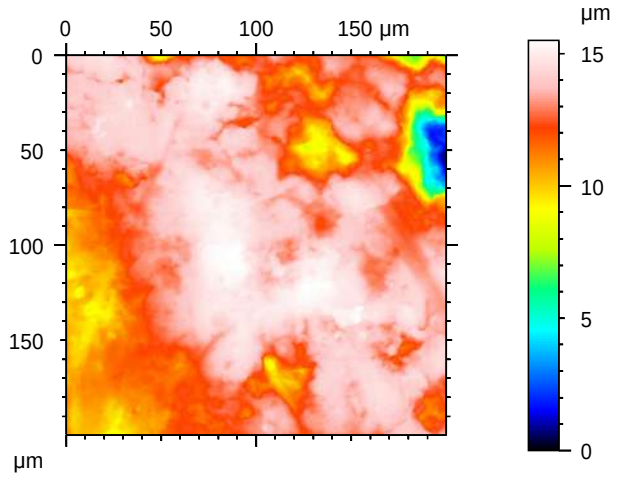

1N_200x200-Zinv-GENesi-870603-UDP4dex-f3

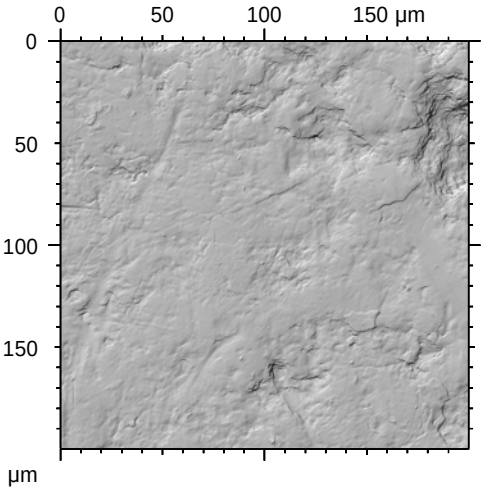

1N_200x200-Zinv-GENesi-870603-UDP4dex-f12

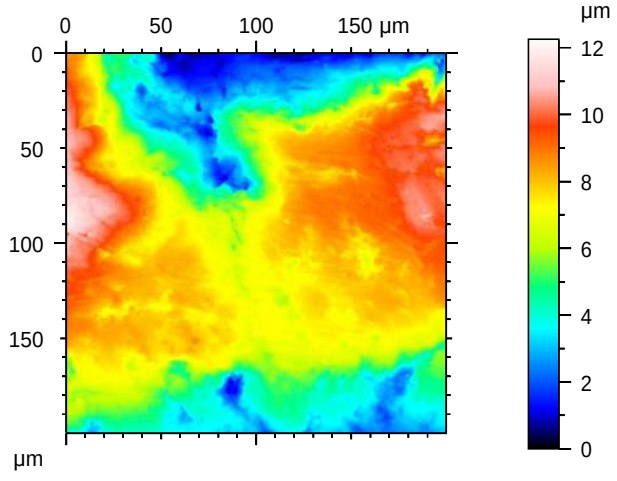

1N_200x200-Zinv-GENesi-870603-UDP4dex-f12

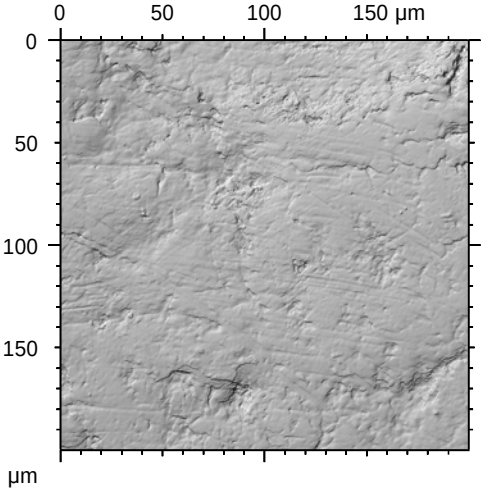

Leica Map Premium 8.0.9173

Photosimulations and false color elevation maps of scanned shearing and crushing facets on molars and deciduous premolars of the **hazelnut group** (100% base diet + 10 hazelnuts in shell per day)

scanned at the PALEVOPRIM lab by M. Louail, University of Poitiers, France with "TRIDENT", white light confocal microscope Leica DCM8 - April 2020

ALIHOM Project (Région Nouvelle Aquitaine, France), ANR Diet-Scratches

ANR-17-CE27-0002

PIs: G. Merceron & S. Ferchaud

1N_200x200-Zinv-GENesi-870609-UDP4dex-f3

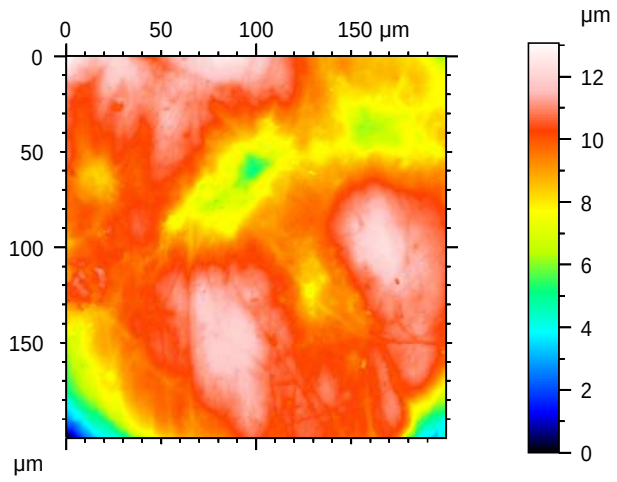

1N_200x200-Zinv-GENesi-870609-UDP4dex-f3

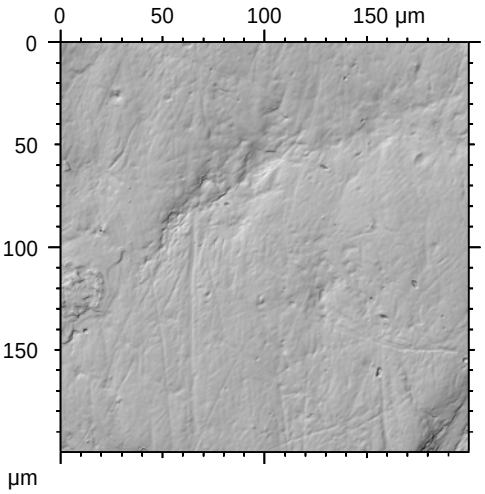

1N_200x200-Zinv-GENesi-870609-UDP4dex-f13

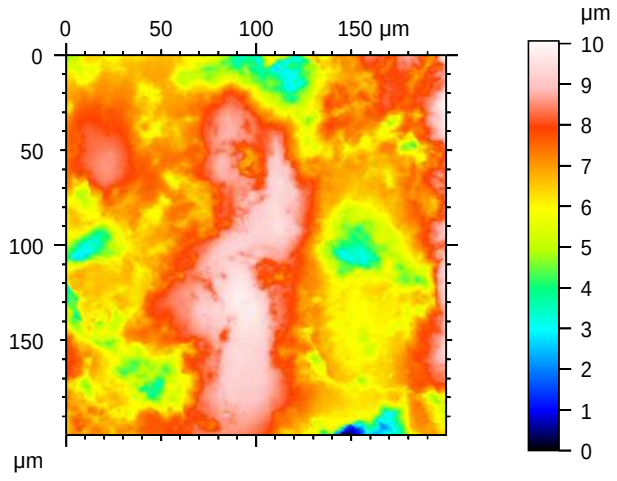

1N_200x200-Zinv-GENesi-870609-UDP4dex-f13

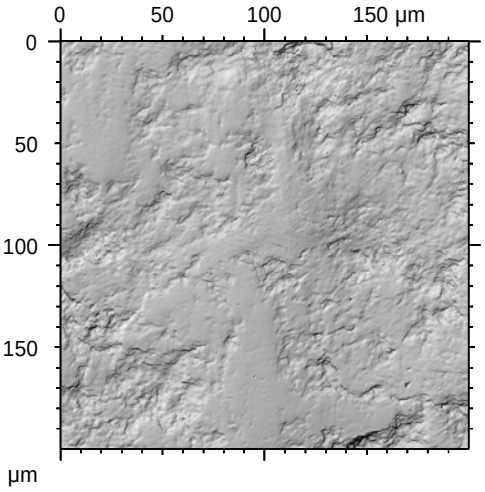

1N_200x200-Zinv-GENesi-870610-UDP4dex-f3

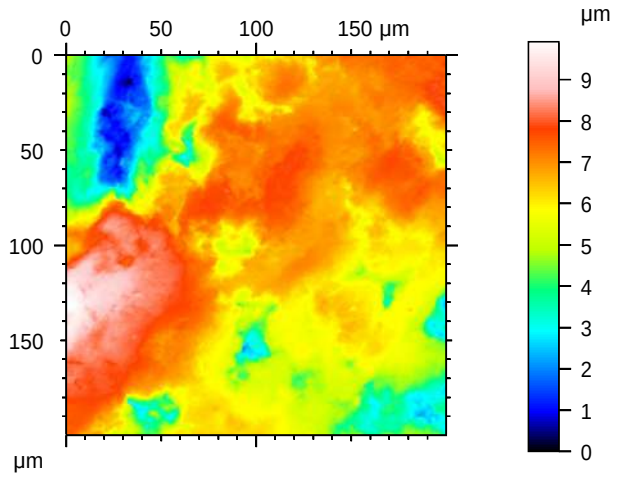

1N_200x200-Zinv-GENesi-870610-UDP4dex-f3

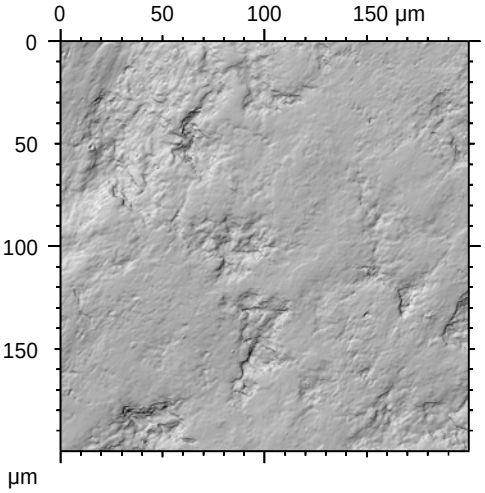

Leica Map Premium 8.0.9173

Photosimulations and false color elevation maps of scanned shearing and crushing facets on molars and deciduous premolars of the **hazelnut group** (100% base diet + 10 hazelnuts in shell per day)

scanned at the PALEVOPRIM lab by M. Louail, University of Poitiers, France with "TRIDENT", white light confocal microscope Leica DCM8 - April 2020

ALIHOM Project (Région Nouvelle Aquitaine, France), ANR Diet-Scratches

ANR-17-CE27-0002

PIs: G. Merceron & S. Ferchaud

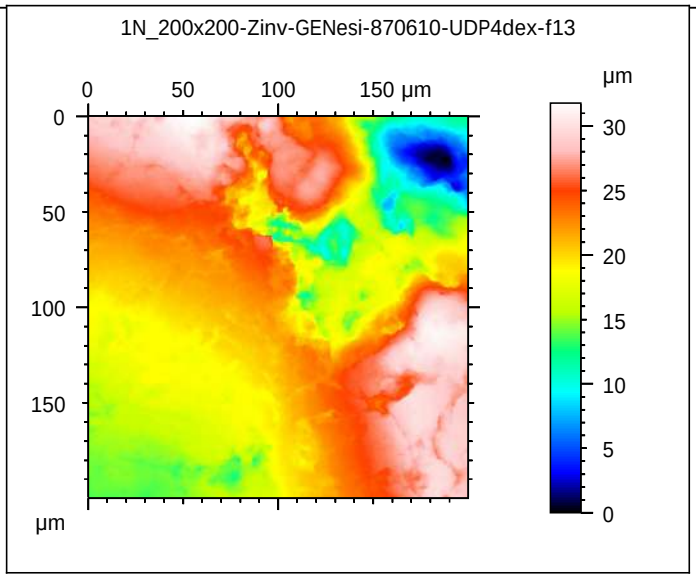

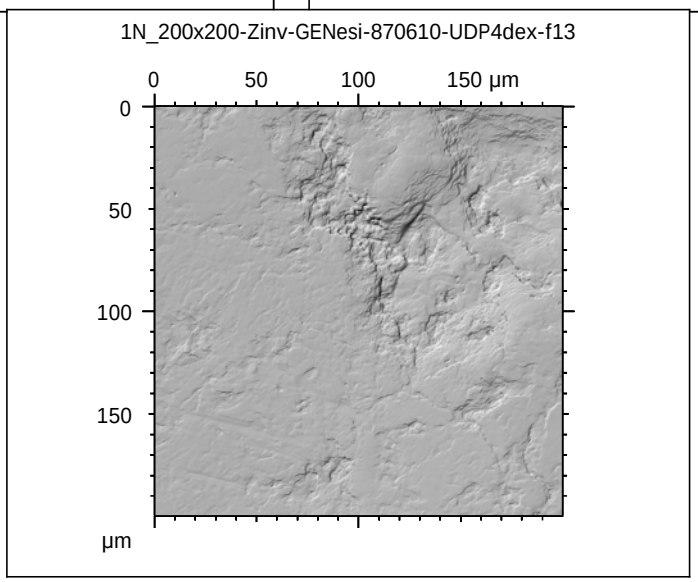

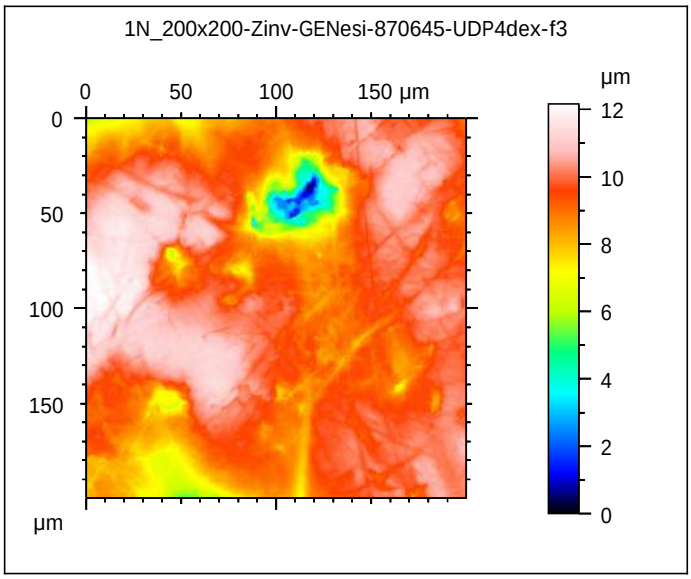

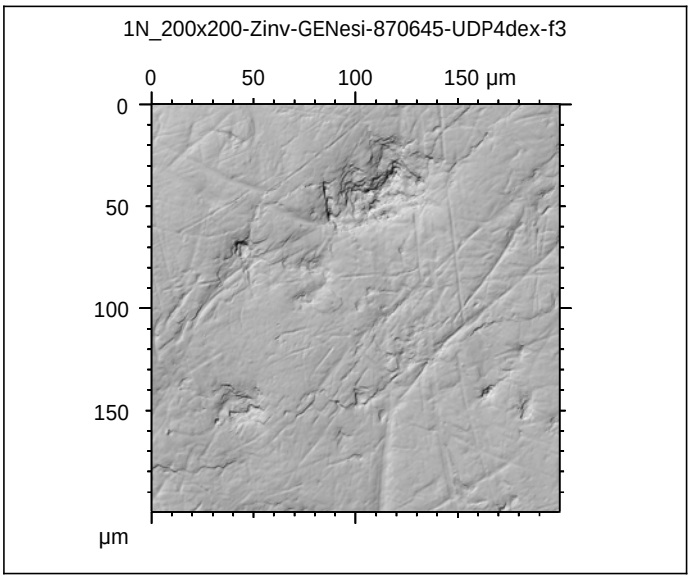

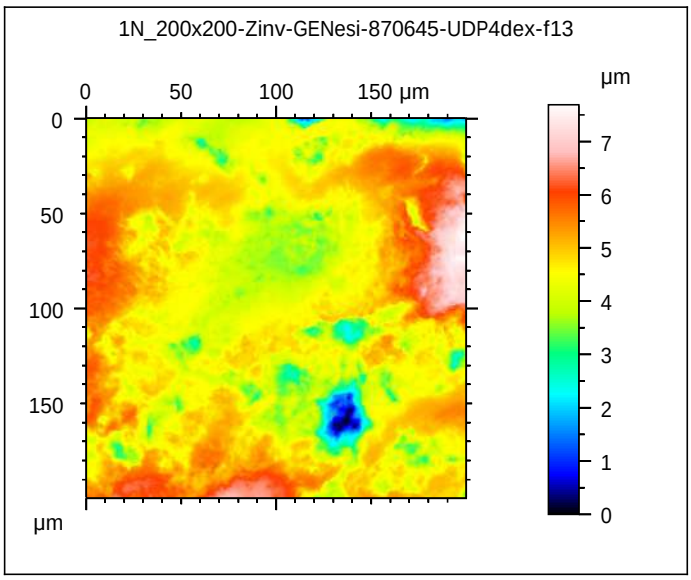

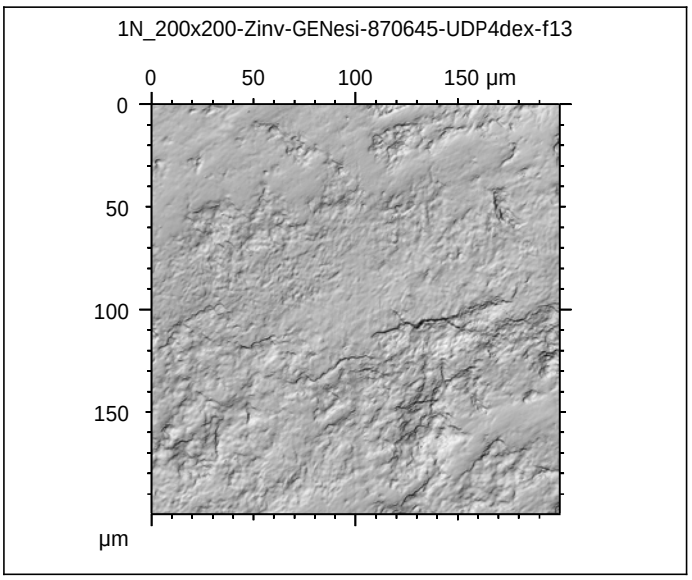

Leica Map Premium 8.0.9173

Photosimulations and false color elevation maps of scanned shearing and crushing facets on molars and deciduous premolars of the **hazelnut group** (100% base diet + 10 hazelnuts in shell per day)

scanned at the PALEVOPRIM lab by M. Louail, University of Poitiers, France with "TRIDENT", white light confocal microscope Leica DCM8 - April 2020

ALIHOM Project (Région Nouvelle Aquitaine, France), ANR Diet-Scratches

DIET-SCRATCHES

ANR-17-CE27-0002

PIs: G. Merceron & S. Ferchaud

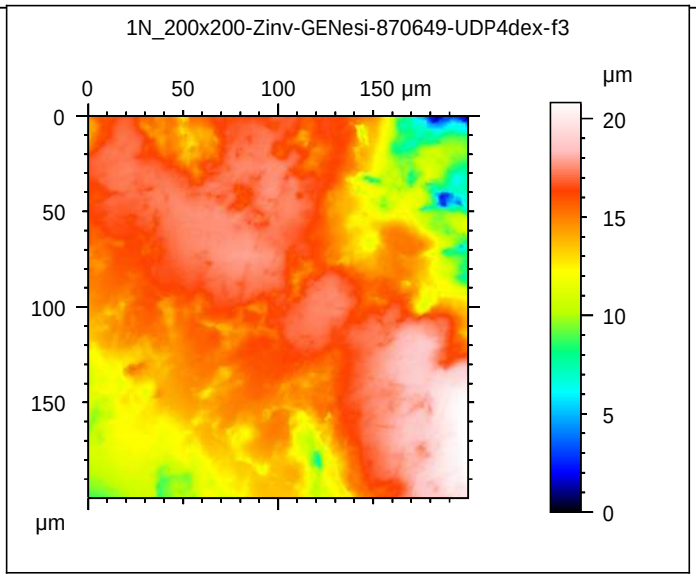

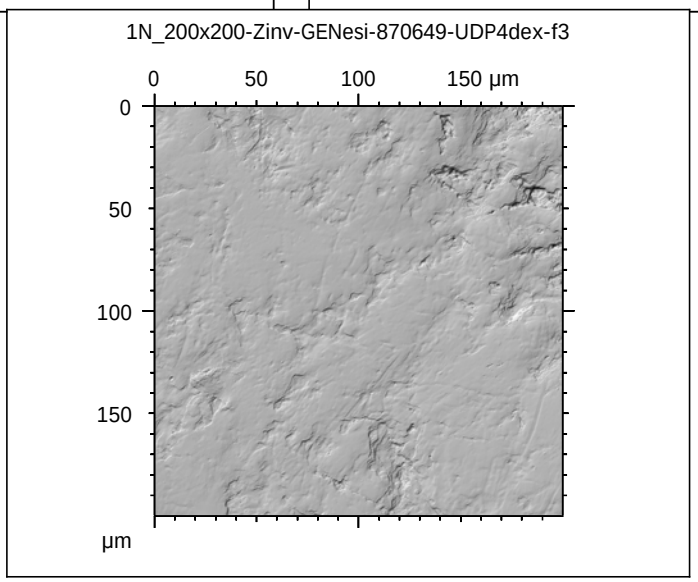

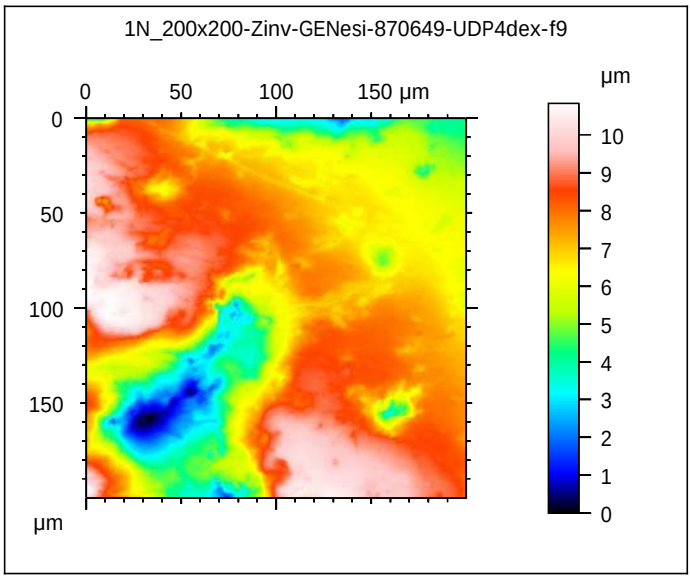

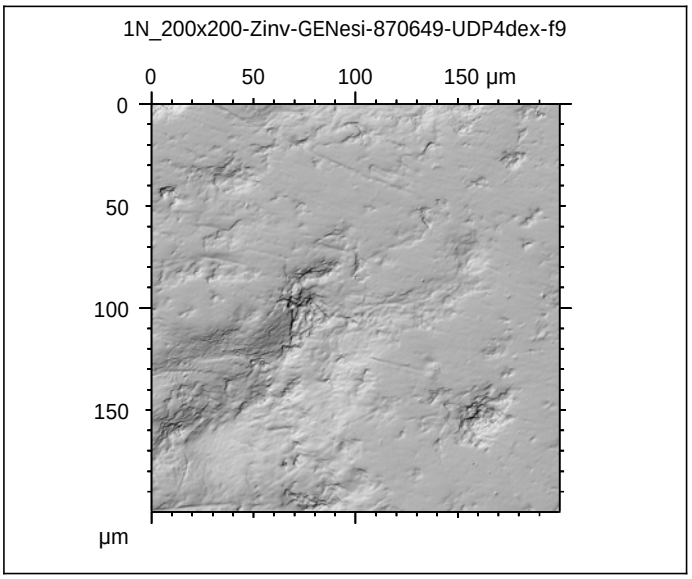

Leica Map Premium 8.0.9173